THÈSE DE DOCTORAT

de l'Université de recherche Paris Sciences et Lettres
PSL Research University

Préparée à MINES ParisTech

Elaboration et caractérisation de films d'hydrogel et de composites hydrogel-céramique pour les applications biomédicales

Design and characterization of hydrogel films and hydrogel-ceramic composites for biomedical applications

Ecole doctorale n°432

SCIENCES DES METIERS DE L'INGENIEUR

Spécialité Sciences et Génie des Matériaux

COMPOSITION DU JURY :

M. Philippe POULIN
CRPP, Université de Bordeaux,
Rapporteur

M. André STUDART
Complex Materials, ETH-Zürich,
Rapporteur

Mme. Ghislaine BERTRAND
CIRIMAT, ENSIACET-Toulouse,
Examinateur

M. Pierre WEISS
LIOAD, Université de Nantes,
Président du jury

M. Vincent GUIPONT
Centre des Matériaux, Mines Paristech, Paris
Examinateur

M. Laurent CORTÉ
Centre des Matériaux, Mines Paristech, Paris
Examinateur

Soutenue par **David MOREAU**
le 21 janvier 2016

Dirigée par
Laurent CORTÉ et Vincent GUIPONT

MINES ParisTech | PSL RESEARCH UNIVERSITY PARIS

À mon grand-père.

Remerciements

Je tiens à remercier tout d'abord mes directeurs de thèse, Laurent Corté et Vincent Guipont. Laurent a été un encadrant fantastique au cours de ces quatre années passées au Centre des Matériaux (CDM) de l'Ecole des Mines et au laboratoire Matière Molle et Chimie (MMC) de l'ESPCI. Son enthousiasme, son savoir et sa curiosité scientifique, sa rigueur et sa bienveillance m'ont permis d'aller au bout de cette belle aventure. Je remercie Vincent pour ses conseils avisés et nos riches discussions. J'ai pu bénéficier de sa grande expertise sur la projection thermique et de ses excellents conseils en matière de présentation. A leurs côtés, j'ai fait de nombreuses découvertes scientifiques, parfois inattendues, et je les remercie pour leur soutien et leur engagement sans faille tout au long de ma thèse (et ce n'est pas terminé!).

J'adresse mes remerciements à Jacques Besson, directeur du CDM et à Ludwik Leibler, directeur du MMC, pour m'avoir accueilli au sein de leur laboratoire et pour m'avoir donné accès à toutes les ressources nécessaires pour réaliser mes travaux de thèse.

Je remercie également l'ensemble de mon jury de thèse. Je suis reconnaissant envers Monsieur Philippe Poulin pour avoir accepté avec enthousiasme de rapporter mon travail et pour m'avoir fait part de commentaires très constructifs pendant et après la soutenance. As well, I would like to acknowledge very much André Studart to have reviewed my thesis very carefully and to have discussed my results with passion. Je tiens à remercier Monsieur Pierre Weiss pour m'avoir fait l'honneur de présider mon jury de thèse et à Madame Ghislaine Bertrand d'y avoir participé avec beaucoup d'engouement. Vos questions et vos remarques ont contribué à rendre ma soutenance vivante et inoubliable.

Une thèse dans le domaine des biomatériaux nécessite de nombreux savoir-faire, techniques et connaissances dans des domaines scientifiques variés, allant de la biologie

cellulaire à la caractérisation aux rayons X sur ligne synchrotron en passant par la chirurgie animale. Ces travaux sont par conséquent le fruit de nombreuses collaborations enrichissantes à la fois sur le plan humain et scientifique. J'adresse mes plus sincères remerciements à Hervé Petite, Didier Hannouche, Manon Bachy, Arthur Vilain, Morad Bensidhoum et Frédéric Baudin du laboratoire de Bioingénierie et Bioimagerie Ostéo-Articulaire de l'Université Paris-Diderot, pour les études *in vivo*. Je remercie également François Rannou, Caroline Chauvet, François Etienne, Jean-Maurice Petit et Lydia Tsagris de l'unité Inserm UMR-S 1124 «Pharmacologie, Toxicologie et Signalisation cellulaire» de l'Université Paris-Descartes pour les expériences originales et intenses d'encapsulation cellulaire. Je remercie chaleureusement Henry Proudhon qui a participé activement à la caractérisation aux rayons X de nos systèmes à la fois au laboratoire Navier de l'Ecole Nationale des Ponts et Chaussées appuyé par Nicolas Lenoir et au synchrotron SOLEIL épaulé par Sylvie Giraud et Christian Mocuta.

En plus des collaborations extérieures, les travaux de cette thèse n'auraient jamais abouti sans l'aide précieuse de nombreuses personnes du CDM et du MMC à qui j'adresse toute ma gratitude et que je remercie. Yann Auriac, pour tout son soutien et son ingéniosité absolument remarquable; François Borit avec qui nous avons réalisé toute la campagne d'essais coldspray; Maria Betbeder, Fabrice Gaslain, Anne Laurent et Nicole Dedave, pour la microscopie électronique et, plus spécifiquement, en mode 'low-vac'; Daniel Pachoutinsky, Sylvie Giraud, Henry Proudhon et Anthony Chesnaud pour les analyses aux rayons X; Jean-Christophe Tesseidre pour la corrélation d'image; Brigitte Raviard pour mes demandes de produits farfelus; Jean-Dominique Bartoux pour la granulométrie; Karine Vieillevigne pour les mesures ATG/ATD; Steve Duvinage pour ses conseils en photo; l'Atelier indispensable du CDM formé par René Cluzet, Jean-Pierre Etourneau, Christophe Meurin, Franck Bluzat et Georges Cassas pour leurs montages spécifiques et leurs coups de pouce divers et variés;

Corinne Soulié-Ziakovic pour les analyses IR; Gregory Sainte-Luce et Olivier Delhomme pour l'assistance informatique; Odile Adam pour la biblio et la documentation; Véronique Matos pour la logistique; Marie-France Boucher et Catherine Rouil pour leur assistance et le secrétariat chaleureux.

Une thèse c'est aussi des rencontres, des bons moments, des événements, des conférences. J'adresse un grand merci à: Nico la toupie, Victor, Erembert, Arina et Jia les occupants du bureau B108 pour l'avoir rendu aussi chaleureux; le bureau d'en face où règne une sacrée ambiance, grâce à une bande de joyeux lurons formée par Clém', Gui', Quentin, et Christophe (le grimpeur); David (aka DM, on finit ensemble!); François (stay cool ;)); Thibault (le perfectionniste); Samuel Forest et Anne-Françoise Gourgues pour leurs encouragements et leur bonne humeur; André Pineau et nos échanges sur les dispositifs médicaux dans les couloirs; PAP, mon partenaire de choc du trophée étudiant de golf; les doctorants et chercheurs du MMC qui m'ont accueilli à bras ouverts: Marie, Julien et André pour la bonne humeur quotidienne dans le bureau; le bureau (d'à côté) du bonheur formé par Coco, Technini, François la bonne affaire, Miki et Thibault (toujours le mot pour rire), auquel Jérémie se joignait presque quotidiennement; Lucie et Charlotte pour nos discussions tardives et le réconfort mutuel dans la rédaction; Raphael, Franz, Maddalena, Maïssa, Robi, Trystan, Max et Adrien pour l'ambiance du midi au PC café; Rémi et Michel pour nos discussions approfondies sur le PVA (entre autres); Fanny, Lise et Aurélie pour vos encouragements.

Et puis, il y a ceux qui m'ont toujours soutenu et encouragé dans la voie de la recherche. J'ai une pensée toute particulière pour Jean Woloszko, que je considère comme mon mentor depuis le début de mes études scientifiques. Je remercie également mes professeurs de l'Ecole Nationale d'Ingénieurs de Metz, Anne-Sophie Bonnet, Paul Lipinski, Emilie De-Brosses, Sylvain Philippon et Albert Tidu.

Enfin, je remercie ceux qui me soutiennent depuis longtemps et qui m'ont supporté pendant ces 3 années: mes parents, mon frère, mes grands-parents, Marine et mes amis de tous horizons. MERCI.

General introduction

In this thesis, I explore a particular class of polymers which are called hydrogels. Basically, hydrogels are three-dimensional cross-linked networks of hydrophilic polymer chains. These polymer networks can contain a quantity of water of several tens to thousands times their dry mass. In 1960, Wichterle and Lim[1] suggested that hydrogel-based materials could be of great interest for medical applications due to their water content and their structural, optical and mechanical properties that are close to those of living tissues. Since then, the progresses in medicine, biology and material sciences have led to multiple hydrogel-based inventions and to the development of commercial products for various biomedical applications, such as contact lenses,[2] wound dressings,[3,4] phantom tissues for medical imaging,[5] drug delivery systems,[6] tissue-engineered or non-degradable substitutes for organ and tissue repair,[7,8] diagnostic devices[9] or hygienic products.[10]

One particular application of hydrogels that could have a strong impact concerns the reconstruction of teared or diseased soft tissues of the osteoarticular system. Indeed, diseases and injuries of the osteo-articular system, such as osteoarthrisis (cartilage degeneration) or ligament tearing, have become today major health issues.[11] The occurrence of these problems is mostly attributed to the aging and to the intensification of sport in the general population. For instance osteoarthritis concerns 45 million people in the United States of America and costs about 2,600 $ per person per year.[12,13] Another example is the anterior cruciate ligament reconstruction, that is performed for instance on 35,000 people in France each year and represent a cost of about 7,000 € per patient.[14] One particular complication for the treatment of most damaged osteoarticular soft tissues is that they do not heal properly and cannot be healed by primary repair. As a result, the treatment often requires surgical reconstruction

using an auto or allograft. Autografts, which are sample tissues from the patient itself, are the gold standard, because they do not suffer from immune rejection. However the side effect caused by the donor site morbidity can be limiting. Allografts that come from other patients are used sometimes, but their availability and cost can be prohibited. Moreover the immune rejection of the graft implies that the patient takes heavy immunosuppressive treatments or that the graft is decellularized by methods that can alter the properties of the tissue. In this context, hydrogel-based substitutes are drawing a lot of attention as they could provide off-the-shelf alternate solutions.[15–18] Whether it be for ligament, cartilage or tendon replacement, such substitutes require a fine control of physicochemical properties to ensure the durability and the innocuousness, as well as an appropriate mechanical behavior that is appropriate to restore the physiological function. In particular, all these tissue substitutes are connected to bone. The anchoring is one of the major challenges in the design of these substitutes. Failures of anchoring can be dramatic and lead to failures or loosening of the implants. Indeed, anchoring points must resist to normal physiological cyclic loading, as well as punctual intense loads during the whole life of the patient. The general strategy to obtain a strong and durable anchoring to bone is to favor the creation of an intimate contact between the bone and the implant surface (osseointegration). This is usually achieved by functionalizing the implant surface. One functionalization strategy is to coat the surface of the hydrogel implant with a bioactive matter, such as bioceramics, drugs or even cells. The design and fabrication of such coatings is challenging: The coating process must produce adherent and cohesive coatings at the surface of the hydrogel substrates; It should preserve the properties of the substrate and also not compromise the bioactivity of the coating material; Lastly, it should be compatible with clinical practice requirements. In this work, I have studied processes to make ceramic coatings on hydrogel implants in the idea of improving the integration to bone tissue.

The hydrogels studied in this thesis are poly(vinyl alcohol) (PVA) hydrogels. PVA is a synthetic polymer which can form non-resorbable physically cross-linked hydrogels.[19] These PVA hydrogels have a good history with biocompatibility in numerous *in vivo* studies for the reconstruction of various soft tissues.[16] Nevertheless, cells adhere poorly to PVA hydrogels and a better control of the anchoring to bony tissues is still needed in several applications. According to the literature, one way to improve the osseointegration is the addition of a bio-ceramic coating, such as hydroxyapatite, might be an ideal option. Hydroxyapatite (HA) is the major mineral component of bone and has been shown to enhance osteoconduction.[20] It is already used as a bone substitute and as a coating for metallic prosthesis (*e.g.* hip prosthesis). For this research, I investigate two approaches to produce hydroxyapatite coatings on PVA substrates. The first approach is a soft method, based on dip-coating and physical cross-linking, which does not require strong energetic input. The second is a more energetic approach, based on thermal projection of hydroxyapatite particles using the cold spray process.

In more details, in the first soft approach, we explore how to produce composite hydrogel-ceramic coatings on a hydrogel substrate. With a process combining dip-coating with physical cross-linking of PVA, coatings of hydroxyapatite particles embedded in a non-degradable PVA hydrogel matrix are formed on hydrogel substrates. The fabrication of these coatings necessitates an appropriate choice of the composition and of the processing parameters. It is essential to determine how the solution composition governs the thickness, adherence and cohesion of the coating. In addition the PVA hydrogel matrix, containing the HA particles, is not degradable. Therefore, the process needs to be adjusted to ensure that HA must sufficiently exposed and accessible by cells. This approach is applied to produce coatings on PVA hydrogel ligament substitutes that have been recently developed at the Centre des Matériaux (CNRS UMR 7633) (Mines ParisTech) in collaboration with the

laboratory of Prof. David N. Ku at the University of GeorgiaTech.[21] Thanks to a close collaboration with the laboratory of "Bioingénierie et Bioimagerie Ostéo-Articulaire" (B2OA-UMR 7052) at Paris-Diderot University, we devised an *in vivo* study to assess their biocompatibility and their osteoconductivity. To carry out this study, we had to adapt the manufacturing process to sterile requirements and to produce coatings that are compatible with the animal model and surgical handling.

During the investigation of this first approach, I characterized in the parameters that govern the thickness of the coating and noted that it depends strongly on the swelling state of the hydrogel substrate. We studied how this phenomenon can be related to the peculiar ability of PVA solution to crosslink at high concentrations. This side study led to the discovery of a new method to produce hydrogel films, using the solvent depletion created at the surface of a swelling substrate. This swelling induced gelation method opens route to produce composite hydrogel-ceramic coatings without exterior action nor harsh treatment. We also wondered if sensitive matter, such as cells, can be encapsulated using this mild way to generate hydrogel films. In collaboration with the laboratory of "Toxicology Pharmacology and Cellular Signaling" (INSERM UMR-S 1124) at Paris-Descartes University, we investigated the process and devised encapsulation protocol that is compatible with cell culture requirements. With this first feasibility study, we aimed to understand how the cell viability depends on the different parameters of the process: the concentration of the solution, the swelling of the substrate and the temperature condition.

The second approach is a more energetic method, based on cold spray, which is a thermal spraying process. Usually thermal spraying is used, by way of plasma or high velocity oxy-fuel spraying, to coat metallic prosthesis with bioceramic particles. Here we exploit the relatively "mild" spraying conditions that cold spray process offers to produce hydroxyapatite coatings on thermo-sensitive PVA hydrogel substrates. Conversely to the first method, the

cold spray allows to form coatings of HA particles compactly stacked on hydrogel substrates without binder. However, the use of a thermal spraying process requires to define ranges of parameters for which it is possible to produce compact and adherent coatings of HA without deteriorating the hydrogel substrate. It is unlikely the PVA hydrogels can resist the temperature and pressure reached during spraying. However, an alternate approach consisting in firstly spraying onto dry PVA and secondly swelling the coated substrate might work. With a systematic study of the spraying parameters, we explore how to adapt the spraying process to produce a coating that is adherent and resist swelling. Microscopic investigations and temperature measurements during spraying help us understand what are the mechanisms involved in the coating formation. In a last very exploratory part of this work, I also studied how the composition and the microstructure of the sprayed particles influence coating thickness. Indeed, the temperatures used in cold spray do not melt the ceramic particles. Therefore, it is difficult to build a thick coating of pure ceramics. Here we approach this question by playing with the presence of synthesis residues that could act as a temporary binder to stack the sprayed particles.

This manuscript is organized in five sections as follows:

- Section 1 is a non-exhaustive literature review describing general properties of poly(vinyl alcohol) hydrogels, of hydroxyapatite and of PVA/HA hydrogel composites.
- Section 2 introduces the material used in this thesis, namely the PVA substrates and the hydroxyapatite particles.
- Section 3 presents the manufacturing process of the first approach, based on dip-coating, and the *in vivo* evaluation of the PVA hydrogel and hydroxyapatite composite coatings using a rabbit model of bone tunnel healing.

- Section 4 is dedicated to the understanding of the gelation mechanisms of PVA hydrogel film at the surface of a swelling polymer substrate and its application to cell encapsulation.
- Section 5 presents the energetic approach, based on cold spray to produce HA coatings on hydrogel substrates, as well as the exploratory study of the effect of powder composition on coating thickness.

Each section is introduced by a short paragraph giving the interests and the motivations of the study. The sections are divided in several chapters. Chapters 6 to 11 have been written in the form of an article. I chose this type of writing format, because it makes the reading easier due to the various and numerous topics treated in this thesis work. In particular, each chapter contains its specific introduction of state of the art and "Materials&Methods". In all of these chapters, a particular attention has been given not to repeat the same concepts and results. Some repetitions may still occur and I hope this will not make the reading too tedious.

References

1. Wichterle, O. & Lim, D. Hydrophilic gels for biological use. *Nature* **185,** 117–118 (1960).

2. Maldonado-Codina, C. & Efron, N. Hydrogel Lenses-Material and Manufacture: A Review. *Optom. Pract.* **4,** 101–115 (2003).

3. Intrasite®Gel. *Smith&Nephew* (2015). at <www.smith-nephew.com>

4. Aquasorb® Hydrogel Wound Dressing. *DeRoyal* (2015). at <www.deroyal.com>

5. Campbell, G. & Homblower, V. Tissue-mimicking phantom for prostate cancer brachytherapy. (2010) US 2010/0041005 A1

6. Chang, P. ., Meyrueix, R., Rivail, C. & Chateliier, J. Medusa: an Innovative Formulation Approach to Improve Pharmacokinetic & Safety Profiles of Biotherapeutics. *ONdrugDelivery* 4–6 (2011).

7. GelrinC. *Regentis Biomaterials* (2015). at <www.regentis.co.il>

8. Lifeline®. *Cytograft tissue engineering* (2015). at <www.cytograft.com>

9. Tokuda, T. *et al.* CMOS image sensor-based implantable glucose sensor using glucose-responsive fluorescent hydrogel. *Biomed. Opt. Express* **5,** 3859 (2014).

10. Pampers. *Procter&Gamble* (2015). at <www.pampers.com>

11. Hochberg, M. C. Osteoarthritis: new approaches. *Medicographia* **35,** 139 (2013).

12. Helmick, C. G. *et al.* Estimates of the prevalence of arthritis and other rheumatic conditions in the United States: Part I. *Arthritis Rheum.* **58,** 15–25 (2008).

13. Gabriel, S. ., Crowson, C. ., Champion, M. . & O'Fallon, W. . Direct medical costs unique to people with arthritis. *J. Rheumatol.* **24,** 719–725 (1997).

14. HAS. *Critères de suivi en rééducation et d'orientation en ambulatoire ou en SSR Après ligamentoplastie du croisé antérieur du genou*. (2008).

15. Sciarretta, F. V. 5 to 8 years follow-up of knee chondral defects treated by PVA-H hydrogel implants. *Eur. Rev. Med. Pharmacol. Sci.* **17,** 3031–3038 (2013).

16. Baker, M. I., Walsh, S. P., Schwartz, Z. & Boyan, B. D. A review of polyvinyl alcohol and its uses in cartilage and orthopedic applications. *J. Biomed. Mater. Res. B Appl. Biomater.* **100B,** 1451–1457 (2012).

17. Laurencin, C. T. & Freeman, J. W. Ligament tissue engineering: An evolutionary materials science approach. *Biomaterials* **26,** 7530–7536 (2005).

18. Kobayashi, M., Chang, Y.-S. & Oka, M. A two year in vivo study of polyvinyl alcohol-hydrogel (PVA-H) artificial meniscus. *Biomaterials* **26,** 3243–3248 (2005).

19. Hassan, C. M. & Peppas, N. A. in *Biopolymers· PVA Hydrogels, Anionic Polymerisation Nanocomposites* 37–65 (Springer, 2000).

20. Hench, L. L. Bioceramics: from concept to clinic. *J. Am. Ceram. Soc.* **74,** 1487–1510 (1991).

21. Bach, J. S. *et al.* Hydrogel fibers for ACL prosthesis: Design and mechanical evaluation of PVA and PVA/UHMWPE fiber constructs. *J. Biomech.* **46,** 1463–1470 (2013).

Section 1. Literature review

With this PhD research, I explore different ways of producing composite hydrogels in the perspective of biomedical applications. The literature review given in this section focuses on the existing knowledge about the main components studied in this work. It summarizes some basic knowledge on polymer hydrogels, in particular poly(vinyl alcohol) (PVA) hydrogels, on hydroxyapatite and on composites of PVA hydrogels/hydroxyapatite. A very large body of literature exists on these topics and this review does not pretend to be exhaustive.

Chapter 1 is a general introduction about hydrogels and more specifically about hydrogels of poly(vinyl alcohol). We evoke their chemical structure and how they are synthesized. The different processes of cross-linking are summarized. Some specific properties of PVA hydrogels are also described, in particular their swelling and mechanical characteristics as well as their use in biomedical applications. In chapter 2, hydroxyapatite is introduced. First, we give some details about its physical-chemical properties and manufacturing processes. Then its role and mechanism in bone formation are presented. In chapter 3, we present how PVA and hydroxyapatite can be processed together to form composites and we discuss about the in vitro and in vivo response of such systems.

Chapter 1. Poly(vinyl alcohol) hydrogels

1.1 What is a hydrogel?

Hydrogels are hydrophilic polymeric networks able to swell in water. Depending on their physic-chemical properties, they can absorb a quantity of water equivalent to a few times to thousands times their dry mass. Hydrogels remain solid in water because the macromolecules of the network are cross-linked and cannot dissolve. Crosslinking can be of chemical or physical nature. Chemical crosslinking involves permanent covalent bonds between polymer chains. Physical crosslinking forms reversible bonds, which can be hydrogen bonds, Van der Waals interactions, molecular chain entanglements, or hydrophobic forces.[1] The properties of hydrogels are defined by the polymer characteristics and the network structure. These properties can be tailored by the type of the polymer and the choice of the manufacturing process and its parameters.

Their high water content, their morphological characteristics, and mechanical properties close to that of biological tissues make them excellent candidates for biomedical uses.[2] Hydrogels motivate active researches soft tissue prosthesis,[3,4] tissue engineering scaffolds,[1,4] drug delivery systems,[5–7] contact lenses.[8] They are currently used clinically in applications, such as cartilage substitutes,[9] or contact lenses.[8,10] Hydrogels for biomedical applications can be obtained from natural[4] or synthetic polymers.[11] Natural hydrogels include polysaccharides like agarose, alginate, or chitosan, and proteins such as collagen or gelatin. Synthetic hydrogels include poly(ethylene glycol) (PEG), poly(vinyl alcohol) (PVA), poly(acrylic acid) (PAA), poly(hydroxyl ethyl methacrylate) (polyHEMA), or poly(vinyl pyrrolidone) (PVP). In this thesis, we will mainly focus on hydrogels of PVA, which are intensively studied in the biomedical field.[12]

1.2 Poly (vinyl alcohol) chemical structure and synthesis

Poly (vinyl alcohol) has a hydrocarbon backbone structure with -OH hydroxyl pendant groups. The hydroxyl groups provide polarity to the PVA chains, which makes them soluble in water. The synthesis of PVA is not achieved directly by polymerizing the corresponding monomer of vinyl alcohol. Figure 1 illustrates the reactions of PVA synthesis. First, PVA is obtained from the free radical polymerization of vinyl acetate monomer, which gives poly (vinyl acetate) (PVAc) ($C_4H_6O_2$).[13] Then PVAc is hydrolyzed to produce PVA (C_2H_4O). This hydrolysis reaction is realized in aqueous media in presence of caustic or acidic catalysts.[13]

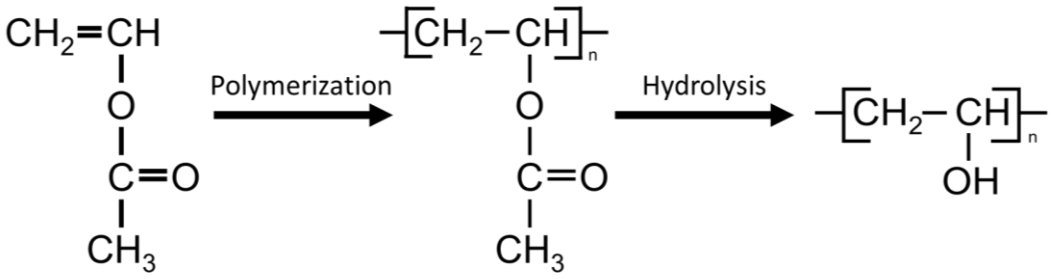

Figure 1 PVA synthesis: polymerization of vinyl acetate followed by a hydrolysis of poly(vinyl acetate).

This reaction of hydrolysis is not always complete, and PVA chains always contain a fraction of residual acetate groups. Depending on the process, the degree of hydrolysis can range from partial (~70%) to almost full hydrolysis (>99%).[14] It has been reported that the degree of hydrolysis has a strong impact on the solubility and crystallization of PVA. As shown in Figure 2, the solubility decreases strongly when the degree of hydrolysis reaches values superior to 97-98%.[12,13] This sensitivity to the degree of hydrolysis is explained by the fact that residual acetate groups weaken the inter- and intra-molecular bonding between hydroxyl groups of the polymer, due a steric hindrance, and make defects that hinder crystallization, making PVA more soluble.

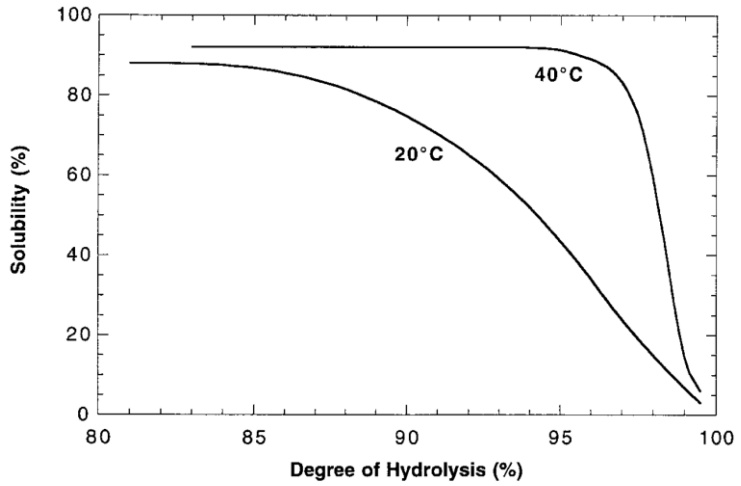

Figure 2 Solubility of PVA (M_w=77000 g/mol) as a function of degree of hydrolysis at dissolution temperature of 20 and 40°C.[13]

1.3 Crosslinking of PVA hydrogels

Chemical crosslinking

Chemical crosslinking of PVA is achieved by using crosslinking agents or by irradiation. Common crosslinking agents for PVA are formaldehyde, gluraldehyde and others aldehydes.[15] During chemical crosslinking, acetal bridges are formed between hydroxyl groups of pendant chains and the crosslinking agent in acidic environment, as shown in Figure 3.[16]

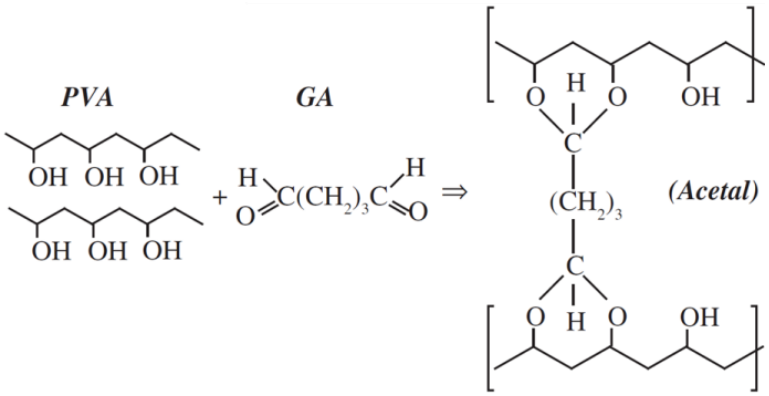

Figure 3 PVA and glutaraldehyde crosslinking in acidic environment.[16]

In the case of *in vivo* applications, these chemical crosslinking methods are usually not used because the cross-linking agents are often toxic and the processes require steps of washing to remove all unreacted crosslinking agents.[17] However recently, it has been shown that PVA/chitosan hydrogel chemically crosslinked with glutaraldehyde could be biocompatible. In a study of Mansur *et al.*,[18] cementoblast cells were seeded on PVA/chitosan hydrogel substrates with different glutaraldehyde content for 48 hours. Figure 4 presents MTT assays performed after 48 hours of culture. The absorbance relative values suggest a correct cellular viability on each substrate, containing 0%, 1% and 5% of glutaraldehyde.

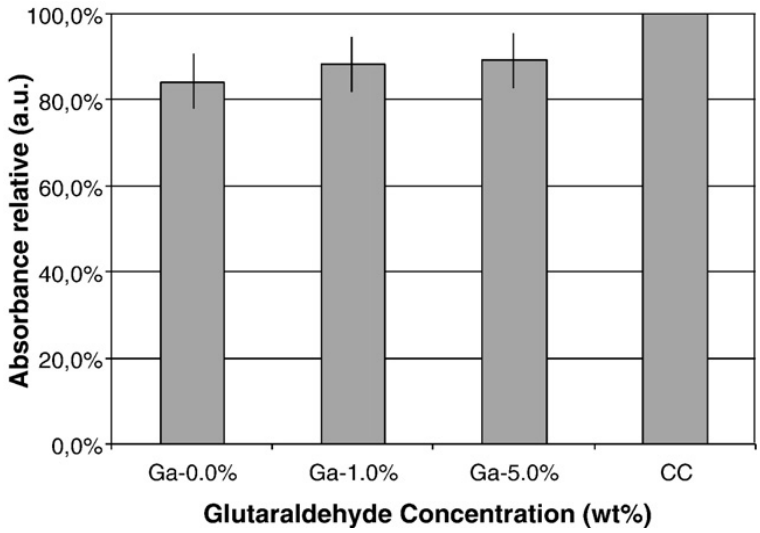

Figure 4 Viability of cementoblast cells seeded on Chi/PVA (1:3) with different network crosslinking densities (without GA, 1.0% and 5.0% GA) via MTT biocompatibility assay; Cellular control (CC) was used as reference.[18]

In other methods, chemical crosslinking is achieved by electron beam or gamma irradiation.[12,19–21] These methods do not require cross-linkers or initiators, which can be toxic and difficult to remove. They also have the advantages of cross-linking and sterilizing the PVA hydrogels in one step.[22] By varying the irradiation doses, hydrogel parameters (*e.g.* degree of crosslinking) can be tailored. Figure 5 shows the effect of irradiation dose on the crosslinking density for PVA aqueous solutions of 5, 10, 15 and 20 wt%.[23]

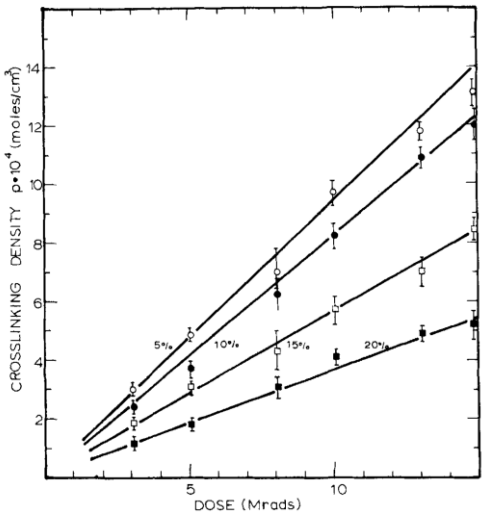

Figure 5 Variation of the crosslinking density p (mole/cms) of PVA networks with dose D, and initial concentration C, of aqueous PVA solutions. (Temperature of irradiation 30°C.) Bars represent standard error of the mean.[23]

Physical cross-linking

Interestingly, physical cross-linking can be performed with PVA as an alternative method to chemical cross-linking. This physical cross-linking uses the ability of PVA to create non-covalent cross-links between chains above a critical concentration.[24] Hydrogen bonds can formed between the hydroxyl pendant groups and several chains can assemble into crystallites, which act as cross-links to form three-dimensional network, as illustrated in Figure 6.[25]

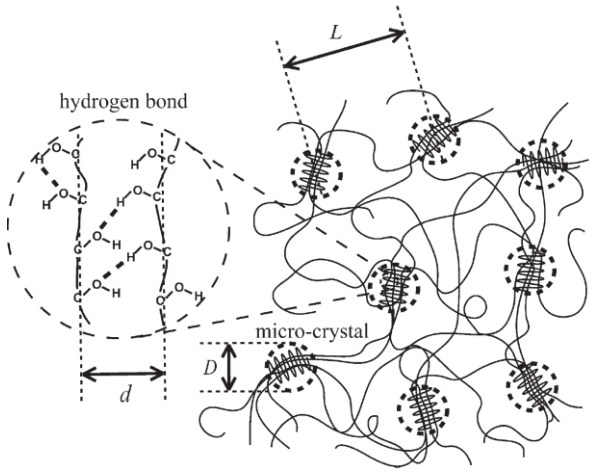

Figure 6 Schematic representation of the network structure of PVA gels crosslinked by microcrystals.[25]

The melting temperature of PVA crystallites depends on the degree of hydrolysis of PVA chains.[26] Figure 7 presents differential scanning calorimetry curves of PVA films produced by solvent casting of PVA solutions of different degree of hydrolysis (HD) and molecular weight (M_w).[27] PVA with higher HD (>99%) exhibit a higher melting temperature than PVA with lower HD (87-89%), with a difference of temperature of about 25-30°C. For highly hydrolyzed PVA chains, used in *in vivo* applications, PVA crystals melt at about 225°C. When immersed in water, physical PVA networks swell and form insoluble and stable hydrogels up to temperature of about 70-80°C.[12,28]

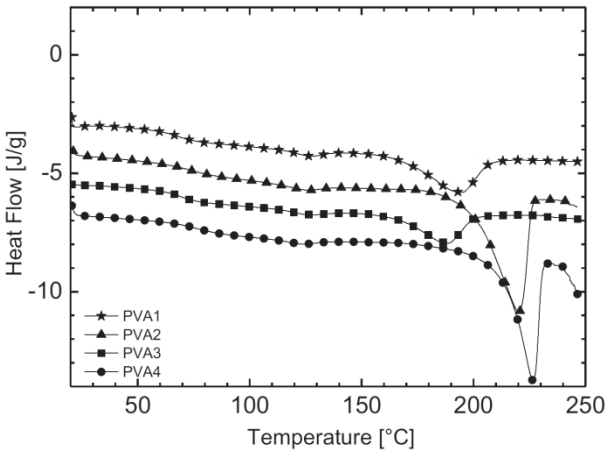

Figure 7 Differential scanning calometry curves of PVA films cross-linked by solvent casting and of different molecular weight (M_w, g/mol) and hydrolysis degree (HD, %). PVA1: M_w=31-50k, HD=87-89, PVA2: M_w=31-50k, HD=99, PVA1: M_w=146-186, HD=87-89, PVA1: M_w=146-186k, HD=99.[27]

Several methods have been explored to induce and increase PVA crystallization.[29] Certain methods require solvent casting,[25,30] freezing/thawing.[12,31] liquid-liquid phase separation (theta-gel formation),[32,33] or heat treatment.[34,35]

- Solvent casting:

PVA physical gels can be achieved from PVA solutions (aqueous or not) by slow dehydration.[24,25] Packter *et al.* have produced PVA films slow dehydration of concentrated PVA solution (20 wt%) cast on glass plates maintained over different pre-equilibrated metal salt hydrates, or other drying agents to induce different rates of evaporation. They showed that

the degree of crystallinity depends on the drying conditions, as shown on Figure 8.[24] Otsuka *et al.* produced dehydrated PVA films from 15 wt% PVA solution using the same process and obtained transparent films, as shown in Figure 9a. These films can be swollen in water and become stretchable hydrogels, as illustrated in Figure 9b.[25]

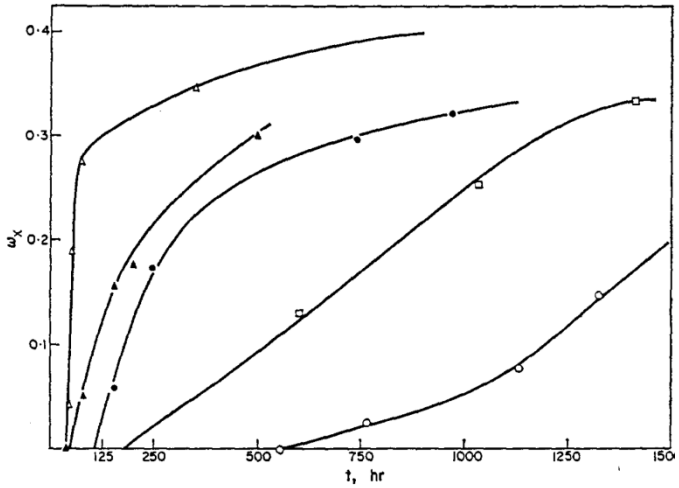

Figure 8 Degree of crystallinity (w_x) of PVA gel in function of drying time for different rate of evaporation depending on the nature of the drying agent (○ $K_2Cr_2O_7$ hydrate; □ KBr ●$Ca(N0_3)_2$ hydrate; ▲$MgCl_2$ hydrate ΔSiO_2).[24]

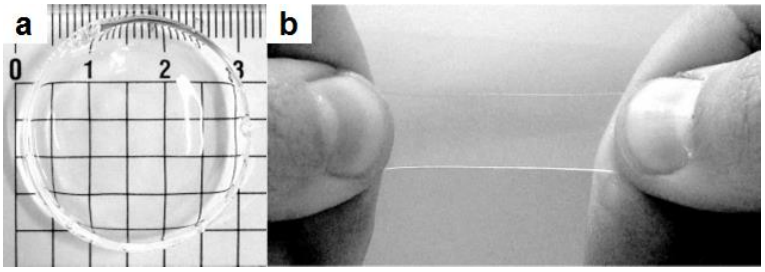

Figure 9 Pictures of the dehydrated sample (**a**) and the stretched swollen gel cut in a rectangle shape after repeated water exchange (**b**).[25]

- Freezing/Thawing gelation:

Another method is the freezing thawing technique. It has been introduced by Peppas in 1975.[36] In this process, the reticulation of PVA network is induced by a combination of three principal mechanisms: liquid-liquid phase separation, hydrogen bonding and crystallite formation.[37] During the freezing step of PVA aqueous solution (Figure 10a), phase separation occurs due to the formation of ice crystals which expel polymer PVA chains (Figure 10b),[38]

creating rich polymer and poor polymer regions by spinodal decomposition (Figure 11a).[37] In rich polymer region, PVA chains are concentrated enough to trigger hydrogen bonds (Figure 11b) and PVA chains arrange to form crystallites (Figure 11c). Then hydrogel are allowed to thaw for certain period, letting voids between crosslinked PVA regions (Figure 10c). Crosslinks formed during the freezing remain insoluble and a permanent hydrogel network is formed. The number of freezing/thawing cycles and the duration of freezing and thawing strongly influence the microstructure, the swelling and mechanical characteristics of the network. This last point will be discussed in the following.

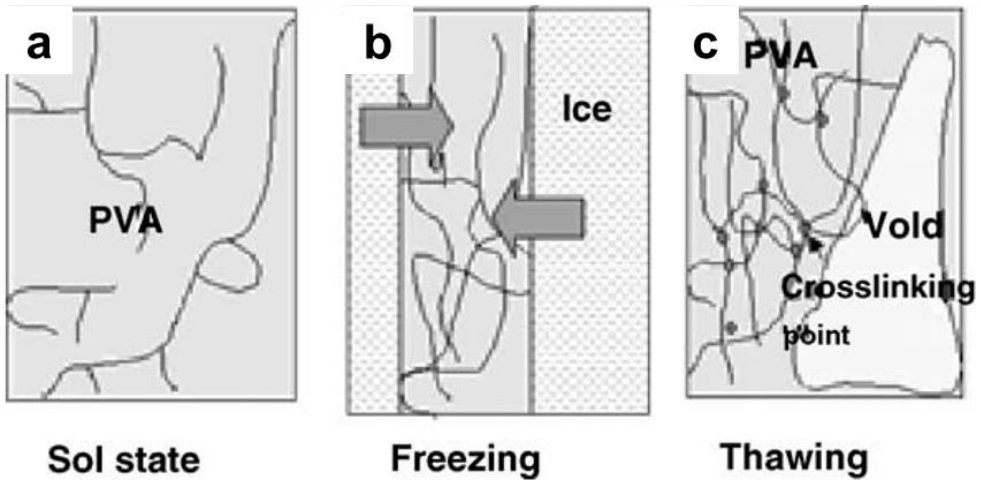

Figure 10 Schematic illustration of gel formation by freezing and thawing.[38]

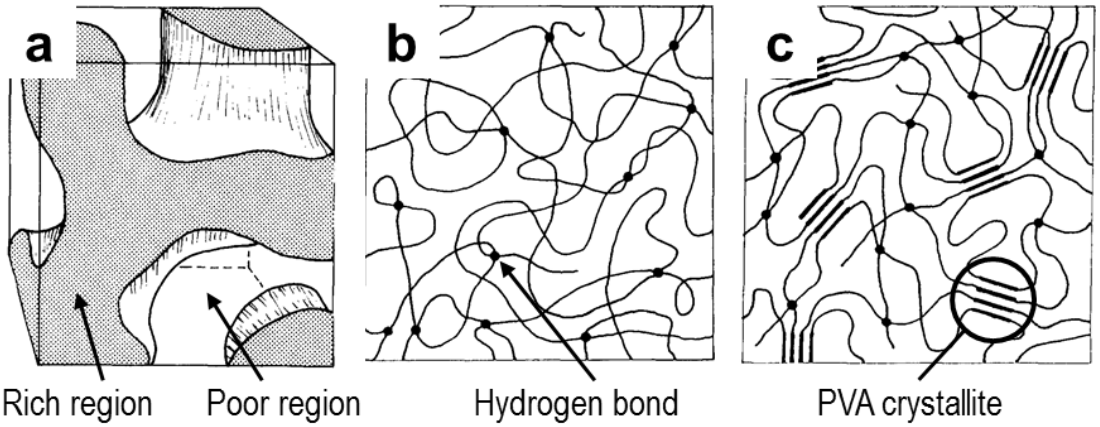

Figure 11 Schematic representations of: **a**) liquid-liquid phase separation, resulting in the development of an interconnected structure of polymer-rich and polymer-poor regions, **b**) a network formed by hydrogen bonding, **c**) PVA crystallite formation. (Modified from Kawanashi).[37]

- Theta-gel formation of PVA network:

The gelation of PVA hydrogels can be also be achieved by liquid-liquid demixing, using gelling agent.[32,33,39] The addition of a gelling agent like poly(ethylene glycol) (PEG) to PVA aqueous (or not) solution, decreases the solvent quality and imposes PVA to separate. This induces liquid-liquid demixing, creating PVA-rich phase, in which PVA chains crystallize, and PEG/water-rich phase, as illustrated in Figure 12.[33]

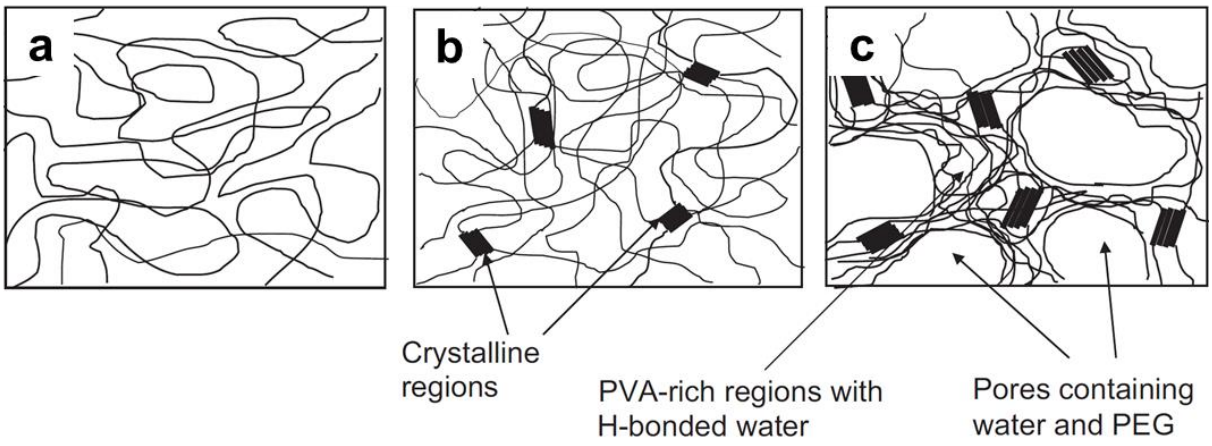

Figure 12 Schematic of a PVA theta-gel formation is shown here: **a**) PVA-PEG water mixture at 90 1C is a uniform solution; **b**) as the solution is cooled down phase separation begins and forces the PVA to form crystalline domains; **c**) with further cooling to near room temperature, phase separation results in the formation of pores containing water surrounded by PVA rich regions.[33]

- Annealing treatment:

Addition of an annealing treatment to PVA networks increase crystallization. Gonzalez and Alvarez have studied the effect of the annealing temperature on PVA hydrogels prepared by freezing/thawing. They showed that additional annealing treatment increase the crystallinity (Figure 13a) and reduce the water content M_t (Figure 13b) of the network. M_t was calculated as $M_t=M_f-M_i/M_i$, where M_f and M_i are the weights of the sample before and after immersion, respectively.

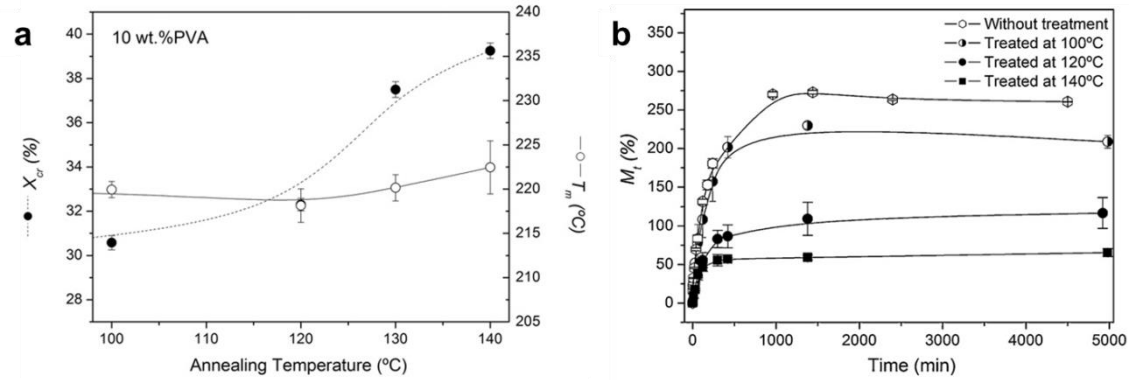

Figure 13 a) Crystallinity degree (Xcr%) and melting temperature (Tm) of hydrogels prepared from 10 wt.% PVA solution as a function of annealing temperature; **b**) Absorbed saline solution (%) at 37 ◦C as a function of time for untreated and annealed 5 wt.% hydrogels.[40]

Kobayashi et al. have studied PVA hydrogels applied for artificial meniscus.[35,41] They have produced PVA hydrogels by freezing/thawing followed by annealing treatment (Figure 14). Annealing treatment was performed to adjust the water content close to that of native meniscus. The final water content was 90 wt%.

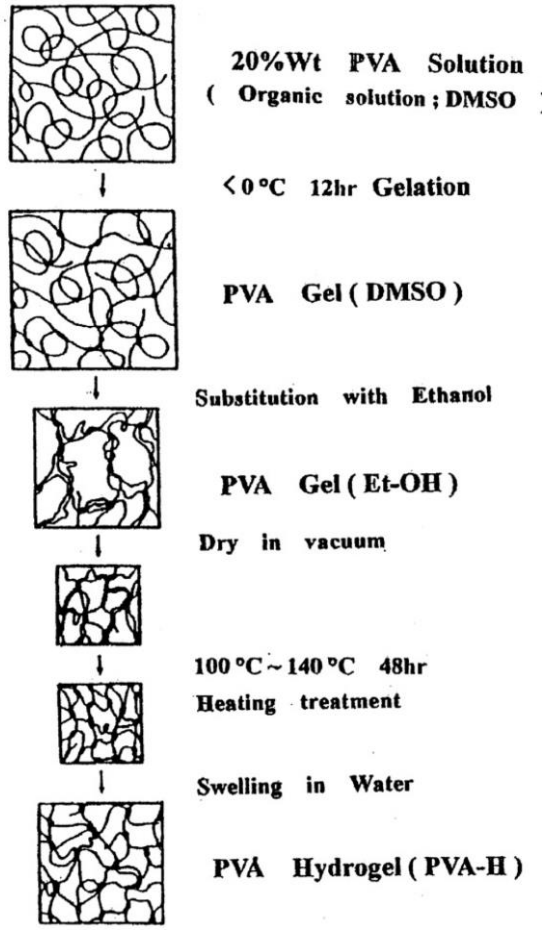

Figure 14 Steps of dehydration/annealing crosslinking method.[35,41]

1.4 Physical properties of PVA hydrogels

Microstructure of PVA hydrogels

The microstructure of PVA hydrogels depend on polymer characteristics (degree of polymerization, degree of hydrolysis, molecular weight), on the polymer concentration and on the type of gelation process and its parameters.

Different microstructures can be obtained depending on the properties of the initial polymer solution. Shi *et al.* have studied the microstructure of physical PVA/PVP (polyvinylpyrrolidone) hydrogels cross-linked by the freezing/thawing method. Here PVP was added to improve mechanical and tribological properties. They showed that the micro-pore size inside the hydrogel can be reduced by using PVA with a higher polymerization degree, as shown on Figure 15.[42] This effect is due to length of the PVA chains, which governs the number of cross-linking points. They also suggested that an increase in polymer concentration in the PVA solution reduced the size of the pore, as shown on Figure 16. An increase of the polymer concentration induces denser packing of polymer chains in the hydrogel network.

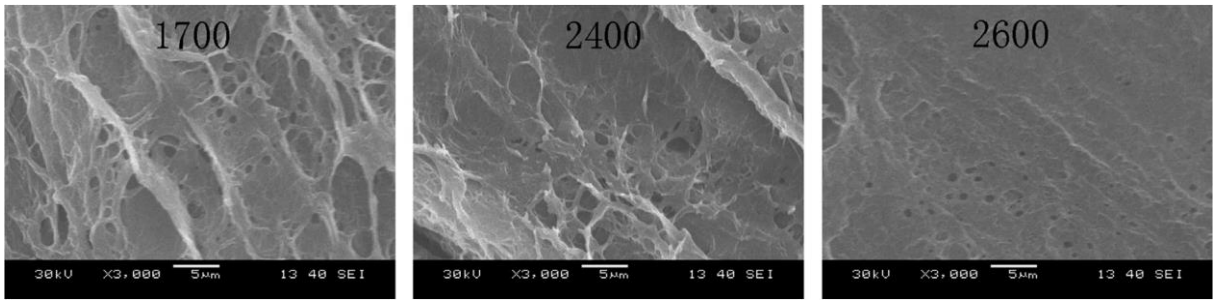

Figure 15 SEM micrographs of the cross-sections of PVA/PVP hydrogels (10%PVA/PVP) with polymerization degree of 1700, 2400 and 2600.[42]

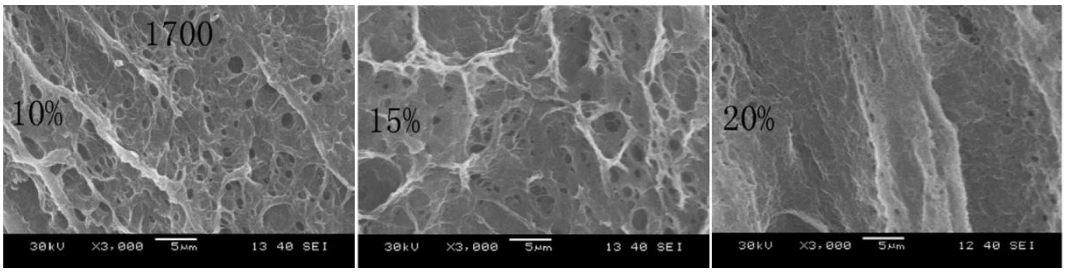

Figure 16 SEM micrographs of the cross-sections of PVA/PVP hydrogels, with polymer concentration solution of 10, 15 and 20 wt%.[42]

Different microstructures can be achieved by using various crosslinking processes. Holloway *et al.* have compared the microstructure of PVA hydrogel made through two different physical crosslinking processes: freezing/thawing (Figure 17) and aging (Figure 18).[43,44] Briefly, PVA hydrogels were produced from PVA solution of 10, 20, 30 and 35 wt% by applying several cycles of freezing/thawing or by pouring the solutions in closed containers and let it aged for 31 days at room temperature.

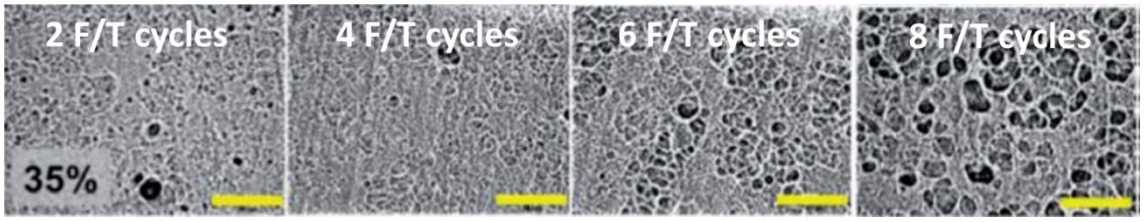

Figure 17 Micrographs of freeze-thawed PVA (35 wt% of PVA). Scale bar is 80 μm.[44]

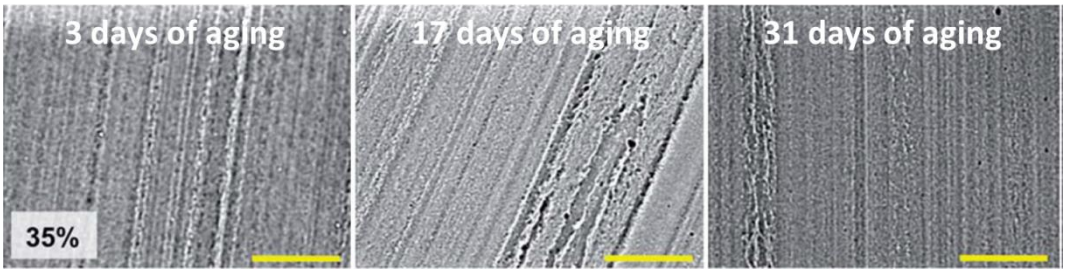

Figure 18 Micrographs of aged PVA hydrogels (35 wt% of PVA). Scale bar is 80 μm.[44]

They observed that the repetition of freezing thawing cycles tends to remodel the microstructure of the hydrogel network. An increase in the number of freezing thawing cycles induces an increase in the porosity of the network, as reported in Figure 19. As previously explained, during the freezing/thawing process phase separation occurs, which induces voids

filled with water and a small fraction of uncross-linked polymer (poor polymer regions). By repeating the number of cycles, the remaining uncross-linked polymer chains are expelled from these poor polymer regions to thicken the rich polymer regions. On the contrary, during aging process, no phase separation occurs. As a consequence, aged PVA hydrogels do not exhibit a high porosity level and do not show any microstructural changes with aging time, as shown in Figure 18. For instance, the porosity level was around 36% for a hydrogel obtained after 6 freezing/thawing cycles and 2.2% for 31 days aged hydrogel.[44]

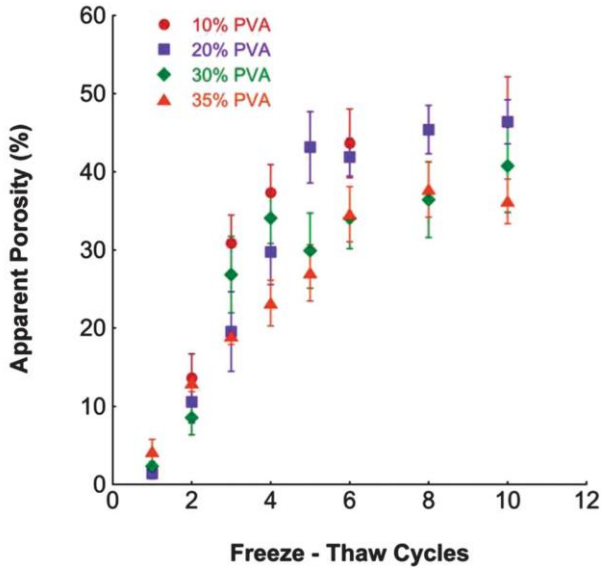

Figure 19 Apparent porosity of PVA hydrogels in function of number of freezing thawing cycles.[44]

Swelling of PVA hydrogels

A deep understanding of the swelling behavior of PVA hydrogels is fundamental to produce artificial substitutes that are able to mimic the behavior of living tissues. The swelling of a hydrogel is generally characterized by the degree of swelling Q. Q is calculated as follows: $Q=V_{eq}/V_{dry}$, where V_{eq} is the volume of the hydrogel at equilibrium and V_{dry} is the volume of the dry hydrogel. The swelling can also be characterized by its water content WC. WC is calculated as follows: $WC=(M_{eq}-M_{dry})/M_{eq}*100$, where M_{eq} is the weight of the hydrogel at equilibrium and M_{dry} is the weight of the dry hydrogel.

Like for all polymer gels, the swelling of PVA hydrogels are directly related to the cross-linking degree of the PVA network. The formation of crosslinks decreases polymer chain mobility. As a consequence, highly cross-linked hydrogels have a tighter structure and will swell less compared to hydrogels with lower crosslinking ratios, as shown in Figure 20.[45] This crosslinking degree is mostly governed by the on polymer characteristics, on the polymer concentration and on the type of gelation process and its parameters.

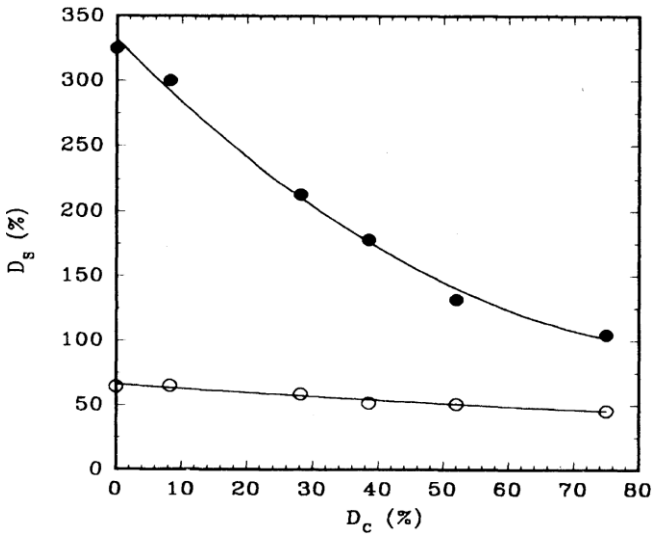

Figure 20 Swelling of chemically cross-linked PVA membrane as a function of the degree of crosslinking (● in water; ○ in ethanol).[45]

- Swelling as a function of the polymer characteristics

The polymer characteristics affect the swelling behavior of the hydrogel. The degrees of hydrolysis and of polymerization have an influence on the degree of swelling. Shi *et al.* have studied the effect of the polymerization degree of PVA and the polymer concentration of the solution, from which hydrogel are produced, on swelling behavior of physical PVA/PVP hydrogels cross-linked by the freezing/thawing method. They showed that the swelling ratio (calculated as $SR=W_s/W_d$, where W_s and W_d are the swelling equilibrium and dry weight of the samples respectively) decreases significantly when the degree of polymerization increases, as shown in Figure 21.[42] Longer PVA chains provide more cross-linking points that increases the crosslinking density of the hydrogel network, as previously mentioned.

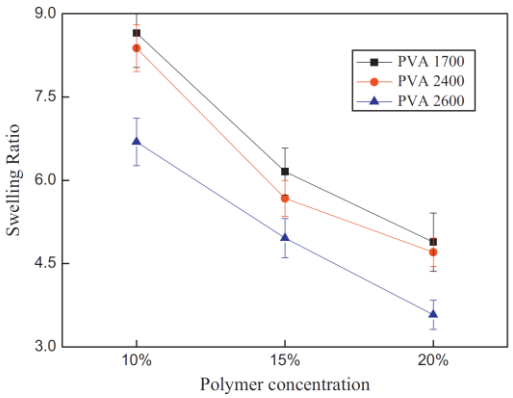

Figure 21 Swelling ratio as a function of polymerization degree and of polymer concentration for PVA hydrogels in phosphate buffer solution (PBS).[42]

- Swelling as a function of crosslinking process

For physically cross-linked PVA hydrogels, prepared by freezing/thawing method, the degree of swelling can be tuned by several parameter adjustments. Stauffer and Peppas have shown that the number of freezing/thawing cycles and the duration of the thawing time have an impact on the degree of swelling.[46] An increase in the number of cycles has been shown to decrease significantly the water uptake (calculated as $WU=W/W_0$, where W is the weight of the gel and W_0 is the initial frozen weight after the first freezing process), as shown in Figure 22.[46] Indeed, more and more crosslinks are created during each cycle, which is tightening the network and decreases the swelling ratio.[46–48]

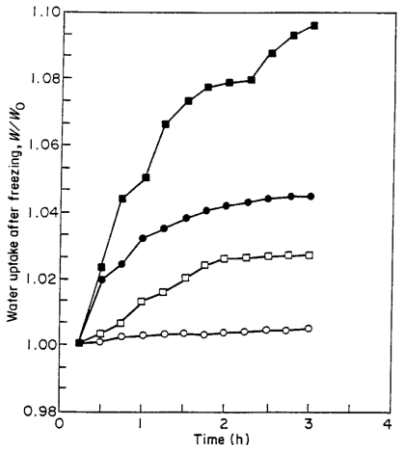

Figure 22 Swelling ratio in function of the thawing time and of the number of freezing/thawing cycles: ■ 2 cycles; ● 3 cycles; □ 4 cycles; ○ 5 cycles.[46]

In addition, the swelling ratio decreases with increasing PVA content of the initial aqueous solution. Several studies have shown that increase of PVA content induces an increase of crosslinking density.[21,42,46,47] This effect has been shown by Yang *et al.*, where they produced chemical PVA hydrogel by γ-irradiation with addition of 1 or 2 freezing/thawing cycles. Figure 23 shows that the degree of swelling (calculated as $DS=W_s/W_d$, where W_s and W_d are the swelling equilibrium and dry weight of the samples respectively) decreases in function of the PVA content (wt%).[21] Increasing of the PVA content improve the packing of the chains during the cross-linking.

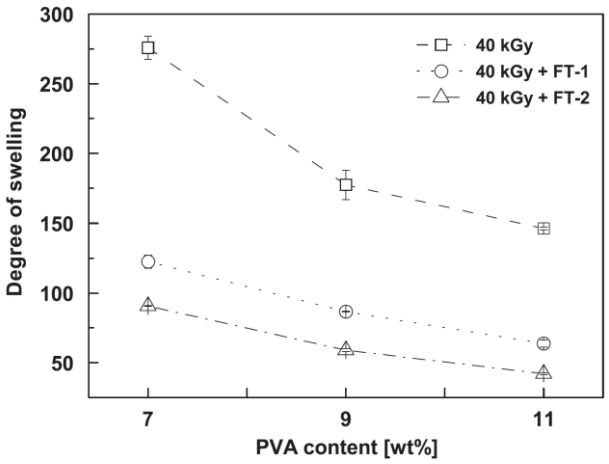

Figure 23 The degree of swelling as a function of PVA content.[21]

Mechanical properties of PVA hydrogels

The mechanical response of PVA hydrogels is important for many biomedical applications, such as orthopaedic soft tissue grafts, vascular grafts, or wound dressings. These systems should sustain physiological solicitations and remain intact through the implantation duration. PVA hydrogels are characterized by an elastic rubbery behaviour.[49] The mechanical behaviour of these hydrogels has been assessed by tensile, compressive, relaxation, creep test. Typical viscoelastic mechanical responses are shown by compressive stress-strain curves in Figure 24 and 25.[50,51] The curve in Figure 24 shows the compressive response of a physical PVA hydrogel cross-linked by freezing/thawing method. Same behaviour (Figure 25) is obtained with chemical PVA hydrogels cross-linked by inverse suspension polymerization[52]

with epichlorohydrin as cross-linking agent. These two compressive experiments show that PVA hydrogels can support large deformations of more than 60 % with dissipation.

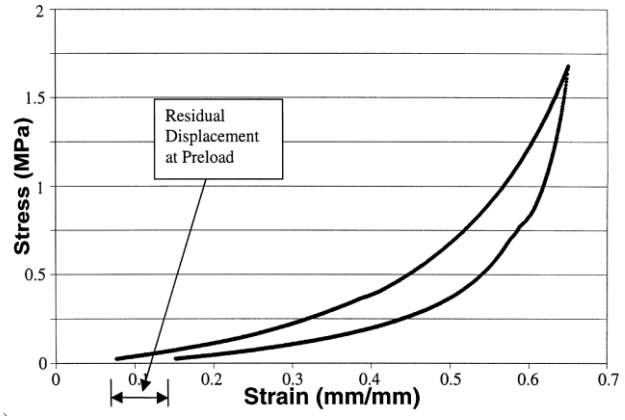

Figure 24 Compressive stress-strain curve of physically cross-linked PVA hydrogel.[50]

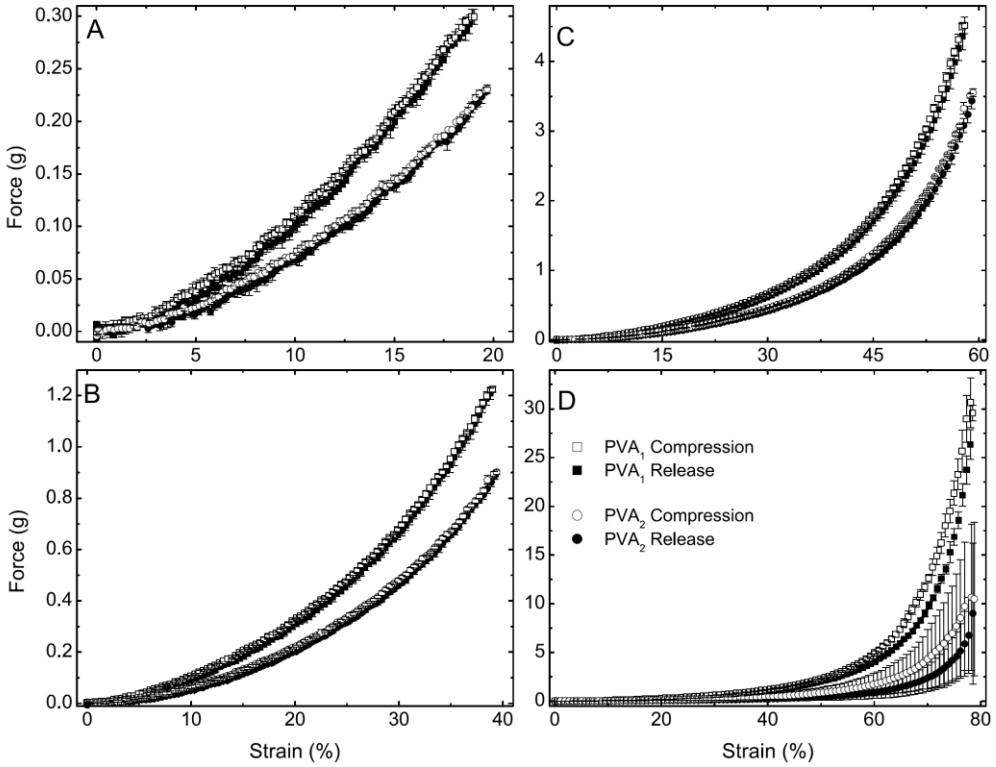

Figure 25 Typical force response profiles during a compression/release experiment performed on a PVA1 and PVA2 beads swollen in H2O. Beads were compressed to 20 (**A**), 40 (**B**), 60 (**C**), and 80% (**D**) strain (applied at 4% s-1).51

This non-linear rubbery behaviour has also been confirmed by tensile tests, performed on physically cross-linked PVA hydrogels by freezing/thawing technique for the construction

of a bioprosthetic heart valve stent by Wan *et al.*[53] Figure 26 presents the stress-strain curves for PVA hydrogels crosslinked by freezing/thawing cycles.

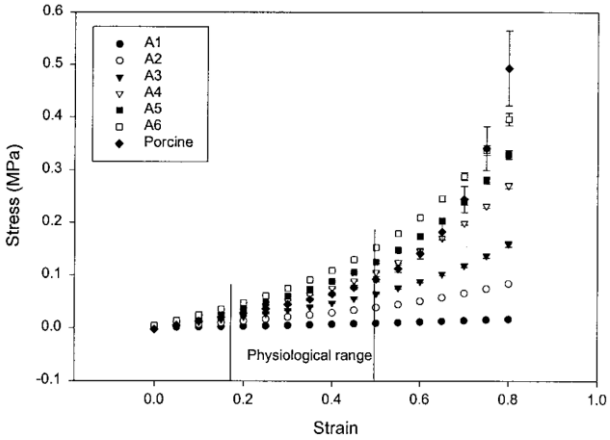

Figure 26 Stress–strain relationship of PVA hydrogel cross-linked by freezing/thawing method (1 to 6 cycles) compared to a porcine aortic root.[53]

Poisson's coefficient as also been evaluated. Since the living tissues are supposed to be uncompressible due to their high water content, it is important to obtain similar behaviour for PVA hydrogel.[54,55] Recently, Chen *et al.* have proposed a new method, based on optical flow technique, to evaluate the Poisson coefficient of physical PVA hydrogels cross-linked by freezing/thawing technique (4 cycles).[54] Figure 27 shows Poisson's ratio values for a series of images of PVA hydrogels under tensile tests. They obtained reasonable values of Poisson ratio of PVA hydrogels compared to others studies.[56] The mean value is 0.44±0.03.

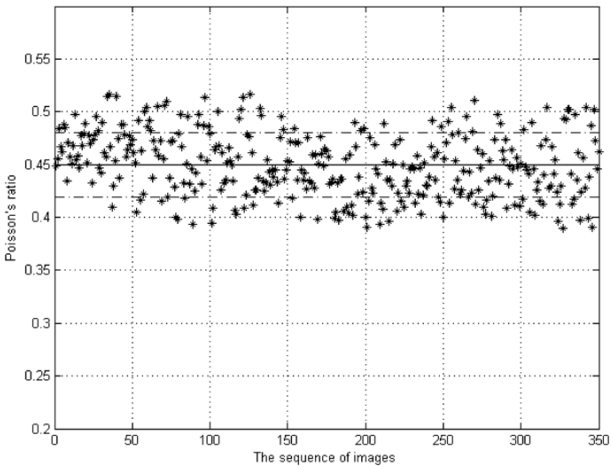

Figure 27 Poisson's ratio obtained from a series of images of PVA hydrogels.[54]

Like for the swelling ratio, the mechanical properties of PVA hydrogels can be modified by changing their crosslinking degree, which can be achieved by controlling the composition and the crosslinking process. Conversely to the swelling properties, an increase in the degree of crosslinking will strengthen the mechanical properties (strength, stiffness) of hydrogel.[57] For physical PVA hydrogels cross-linked by freezing thawing method, the PVA content, the molecular weight of the polymer, the number of freezing/thawing cycles and the duration and the rate of freezing and thawing are factors which affect the cross-linking density of PVA hydrogel networks and therefore have a significant effect on their mechanical properties.

It has been shown by Gupta *et al.* that the ultimate tensile strength of physical PVA hydrogels cross-linked by the freezing/thawing technique can be increased by increasing the polymer concentration, as shown on Figure 28a.[58] They related this phenomenon to the degree of crystallinity, which was also increased by increasing the polymer concentration, as shown on Figure 28b.

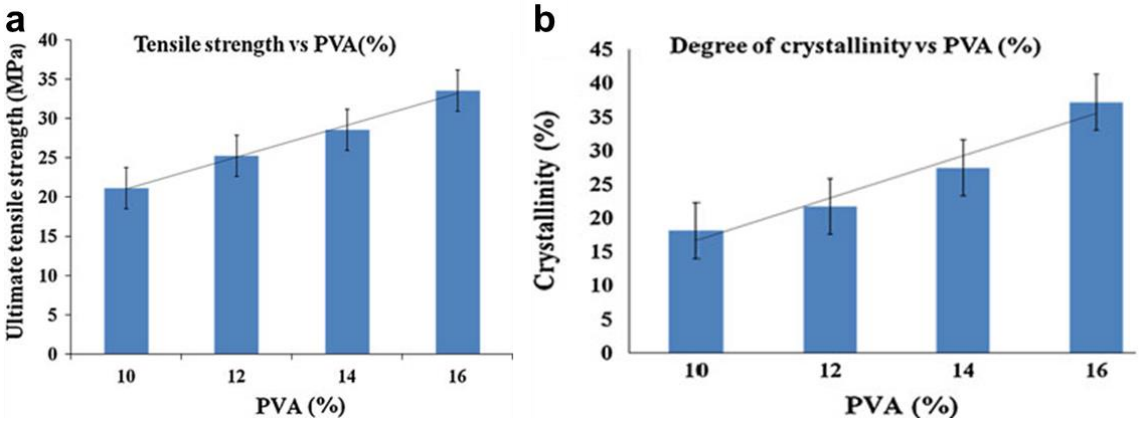

Figure 28 a) Ultimate tensile strength as a function of PVA concentration; **b**) Degree of crystallinity as a function of PVA concentration.[58]

Furthermore, it has been shown that the number of freezing/thawing cycles improves mechanical property.[59,60] In their experiments, Jiang *et al.* proceeded to uniaxial tensile strength tests on a cylindrical PVA hydrogel samples. They noted that the Young's modulus

increased with the number of cycles, as shown in Figure 29.[59] Previously, we evoked that the repetition of freezing/thawing cycle increases the formation of crystals between PVA chains. As a consequence, the increase of the crystallinity strengthens the hydrogel network.

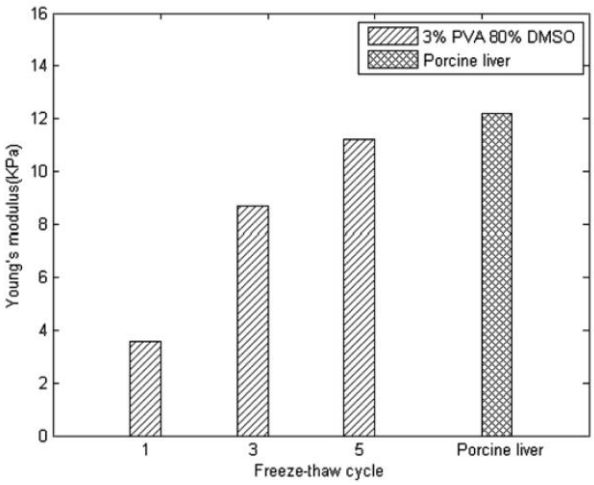

Figure 29 Young's modulus as a function of the number of Freezing/Thawing cycles.[59]

In their study, Stammen *et al.* explored the effect of water content on shear and compression properties of PVA hydrogels.[50] For the network with the lowest water content (75%), the mechanical properties were higher than for the network with the highest water content (80%), as seen in Table 1. Compressive and shear modulus of both hydrogels are in the range of human cartilage.

Material	Compressive modulus, E_{comp} (MPa)	Failure strain, ε_{ult} (%)	Failure stress, σ_{ult} (MPa)	Shear modulus, G (MPa)
Hydrogel formulation A (75% water)	1.1–18.4	60–62[b]	2.1[b]	0.17–0.43
Hydrogel formulation B (80% water)	0.7–6.8	45–47[b]	1.4[b]	0.10–0.40
Human articular cartilage	1.9–14.4[a]	30[c]	—	0.23[d]

Table 1 Comparison of compressive tangent modulus, failure stress and strain, and shear tangent modulus for both PVA hydrogel formulations and human articular cartilage.[50]

1.5 Biological applications of PVA hydrogels

In vivo studies

Thanks to their favourable characteristics such as high water content, mechanical strength, and a simple manufacturing process, PVA hydrogels have been intensively investigated for biomedical applications, in particular for soft tissue replacements. In several *in vivo* studies, PVA hydrogels have been shown to be biocompatible and well-tolerated. In particular, numerous systems based on PVA hydrogels have been suggested to restore articular cartilage defects.

In 1991, Noguchi *et al.* have investigated the biocompatibility of PVA hydrogels for the treatment of rabbit osteochondral defects in intra-articular capsule, as shown in Figure 30.[61] They observed a slight inflammatory response in the early stage of implantation (after 2 weeks), which disappeared completely later (after 52 weeks). In addition, no disturbances of the surrounding articular cartilage were noticed.

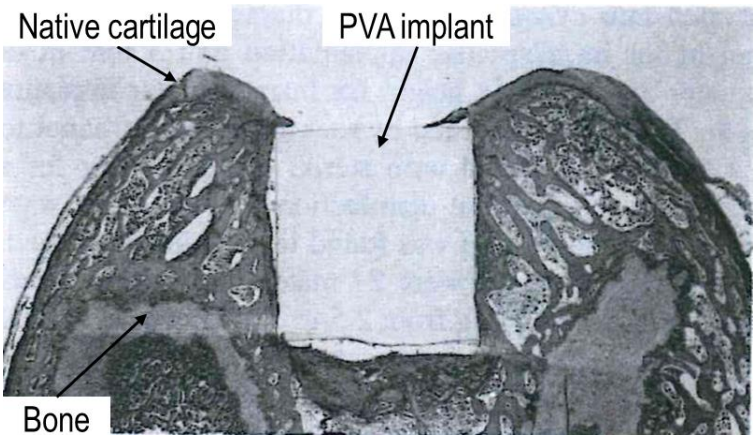

Figure 30 A photomicrograph at low magnification of a horizontal section of the distal femur showing the implant in place.[61]

In another rabbit model, Maher et al. have implanted PVA-PVP (poly vinylpyrrolidone) hydrogels in osteochondrodral defects and followed-up for 6 months.[62] No inflammation was reported as well as no bone osteolysis. However no intimate contact with

bone was noticed and implants were surrounded by a fibrous layer after 6 months of implantation, as shown in Figure 31.

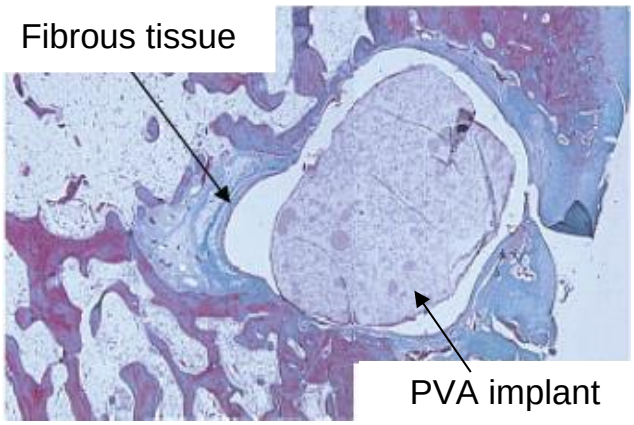

Figure 31 At 24 weeks the implant is completely encapsulated in fibrous tissue.[62]

PVA hydrogels have been also investigated as a material for meniscus replacement. A two-year *in vivo* study made by Kobayashi *et al.* showed that PVA hydrogels might be suitable for meniscus replacement due its appropriate mechanical behaviour close to that of native meniscus (Figure 32) and because no surrounding cartilage osteoarthrisis arose.[63]

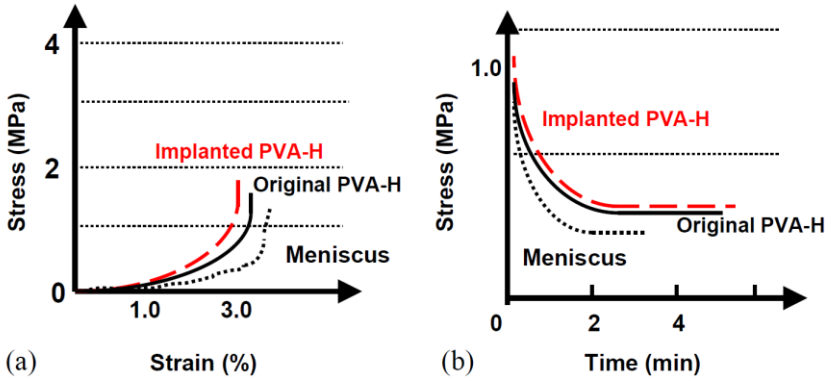

Figure 32 Mechanical properties of PVA-H artificial meniscus: (**a**) Stress–strain curves of the implanted and original PVA-H, and human natural meniscus in compression test. (**b**) Comparison of the stress–relaxation curves of the implanted and original PVA-H, and human natural meniscus.[63]

Allen *et al.* have investigated novel PVA hydrogel implants for the replacement of diseased nucleus pulposus.[64] Physical PVA hydrogel implants of 0.1 and 0.3 cm^3 (Figure 33a), obtained by the freezing/thawing technique, were inserted in discectomy defects created in intervertebral disc of 20 male baboons over 24 months. After 24 months of implantation,

PVA implants located within the nuclear cavity were intact and were surrounded by loose connective tissue, as shown in Figure 33b.

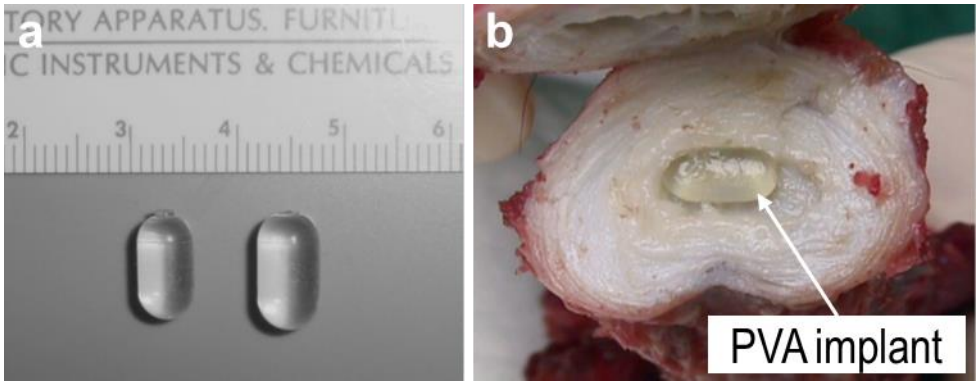

Figure 33 a) PVA implants used in the study; **b**) PVA implants that were located within the nuclear cavity were intact and surrounded by loose connective tissue.[64]

1.6 Clinical applications

In a review, Baker *et al.* report a clinical study on PVA cartilage implants made by Carticept Medical in which 15 patients were followed up for 30 months and 13 patients presented successful outcomes.[3] They indicate that no synovitis nor osteolysis in animal or clinical studies have been reported. In a follow-up review, it has been shown that PVA cartilage implants (Figure 34) could improve knee functionality and reduce pain for patients suffering from cartilage defects.[9]

Figure 34 10 and 15 mm synthetic cartilage implants.[9]

Several follow-ups have shown that those PVA implants are well anchored and have not been deteriorated after a long duration of implantation. This is suggested by MRI observations of PVA implants after 12 (Figure 35a) and 96 (Figure 35b) months of

implantation in a 50 year-old female patient. MRI at 96 months shows that the implant is fixed with no abnormalities. This patient recovered complete knee functionality and stability and was pain free.

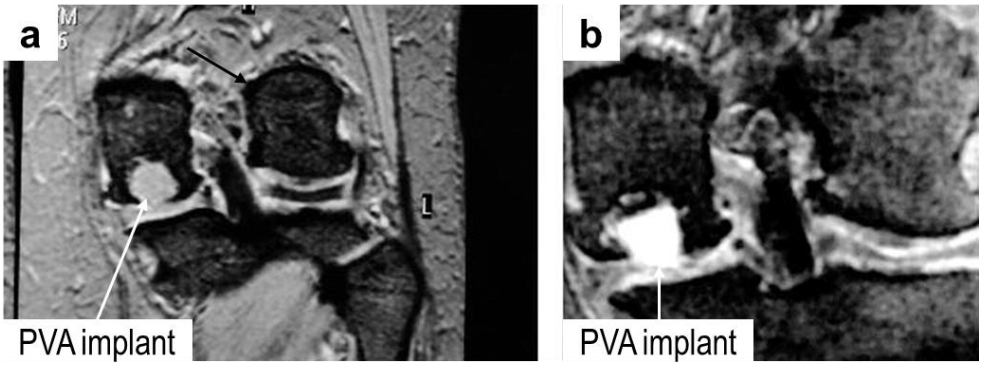

Figure 35 50 year-old woman with 10 mm defect on the weight bearing area of the left medial central condyle at 12 (**a**) and at 96 (**b**) months post-implantation.[9]

1.7 Perspectives and challenges related to PVA hydrogels for biomedical application

Strong efforts are accomplished to develop efficient synthetic substitutes to replace other types of soft tissue of the osteo-articular system, in particular ligament and tendon. Recently, Bach *et al.* have developed artificial ligaments for anterior cruciate ligament replacement (ACL). These construct are made of assemblies of PVA hydrogel fibres. They have shown that these systems reproduced closely the tensile response of human ACL, as shown in Figure 36.[65]

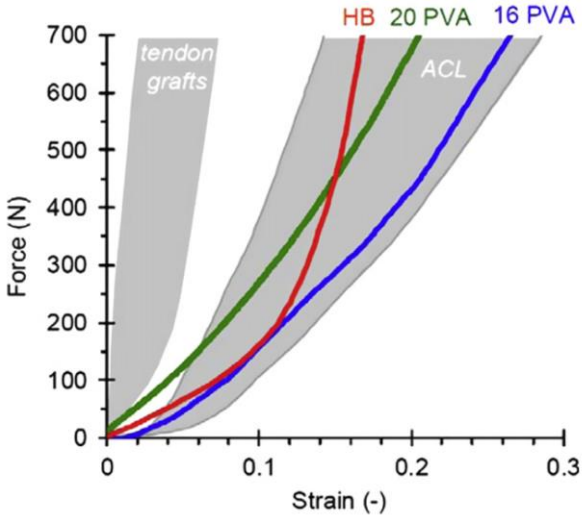

Figure 36 Tensile force versus strain for different PVA hydrogel fibre constructs (red, blue and green curves). Shaded regions show the typical ranges for the native ACL and tendons used for autografts.[65]

Regarding their *in vivo* performance, PVA hydrogels have been shown to be bio-inert, with a very poor ability for cell adhesion.[62,66,67] In particular, in the perspective of use for the replacement of soft osteoarticular tissues such as tendons, ligaments or cartilages, the implants need to be connected to surrounding bone tissue and a lack of affinity with the host bone tissue may lead to anchorage failures at the bone-implant interface. To address this question the surface of the implant can be functionalized by an osseoconductive coating. Such a coating can be obtained by the use of bioceramic particles like hydroxyapatite.

Chapter 2. Hydroxyapatite

2.1 Chemical composition and preparation

Hydroxyapatite (HA) is a mineral, which belongs to the calcium-phosphate materials. Its chemical formula is $Ca_{10}(PO_4)_6(OH)_2$. Hydroxyapatite crystallizes in the hexagonal system (Figure 37). Hydroxyapatite degrades at temperatures above 1400°C, where structural deterioration occurs, identified by a decrease in density and hardness.[68]

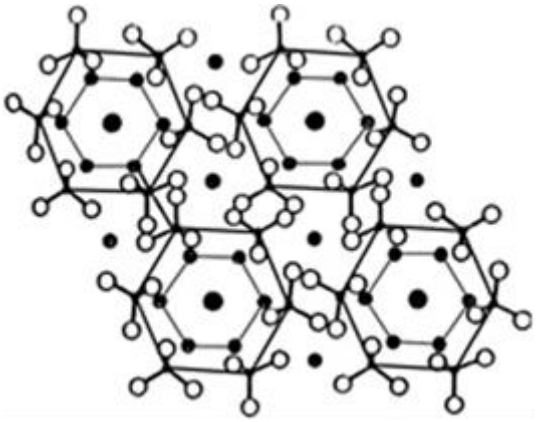

Figure 37 Hydroxyapatite structure [web.mit.edu]

This mineral is the main component of dentin and bone (65% of the mineral matter), and it has the closest Ca/P ratio to bone : Ca/P ratio of HA is 1.67 and bone ratio is 1.57-1.62.[69] Because of its excellent biocompatibility, it is widely used for implant coating and as a mineral scaffold for bone substitution.[69,70]

Concerning HA synthesis, several methods can be used: wet methods such as precipitation and hydrothermal techniques, sol-gel methods with emulsion techniques, and dry methods. One of the most popular techniques is the precipitation method. It is based on a wet method and consists in a reaction of precipitation between calcium hydroxide ($Ca(OH)_2$) and orthophosphoric acid (H_3PO_4) or ammonium phosphate ($(NH_4)_2HPO_4$).[71,72]

The size and the crystallinity of the particles created by this technique strongly depend on the pH of the solution and on the temperature. This technique is widely used because large amounts of HA can be produced at a reasonable cost and in absence of organic solvent.[71] Another popular technique is a sol-gel method, which allows a homogeneous molecular mixing, a low processing temperature and ability to generate various form of HA, such as nanocrystalline powder and thin films).[73] Dry methods of HA fabrication involve solid-state diffusion during calcination of mixtures containing appropriate amounts of Ca^{2+} and PO_4^{3-} ions. The calcination temperature ranges between 900 and 1300°C.[74] Hydroxyapatite can be available in different forms, like powders, rods, blocks, injectable pastes, as suggested in Figure 38.[75]

Figure 38 General appearance of various commercial calcium orthophosphate-based bone graft materials.[75]

2.2 Osteoconductive properties of HA

Hydroxyapatite is an osteoconductive material. Albrektsonn *et al.*[76] give this definition: "an osteoconductive surface is one that permits bone growth on its surface or down into pores, channels or pipes". Many *in vitro* studies have shown that implants containing HA particles enhance bone formation, including cell proliferation, adhesion, and an increase of osteocalcin level.[77] Dalby *et al.* have shown that addition of hydroxyapatite improves cells adhesion. They used poly-methylmethacrylate (PMMA) cement coated with 0%, 4,6%, 8,8%

of hydroxyapatite powder.[78] They isolated human osteoblast cells (HOB) from femoral head of a patient undergoing total joint replacement. Then HOB cells were cultured on the material for 1, 3, 7, 14 and 28 days at 37°C. Morphological investigation by SEM showed that the anchorage of HOB looks qualitatively more efficient on HA coated PMMA than on bare PMMA, as shown in Figure 39.

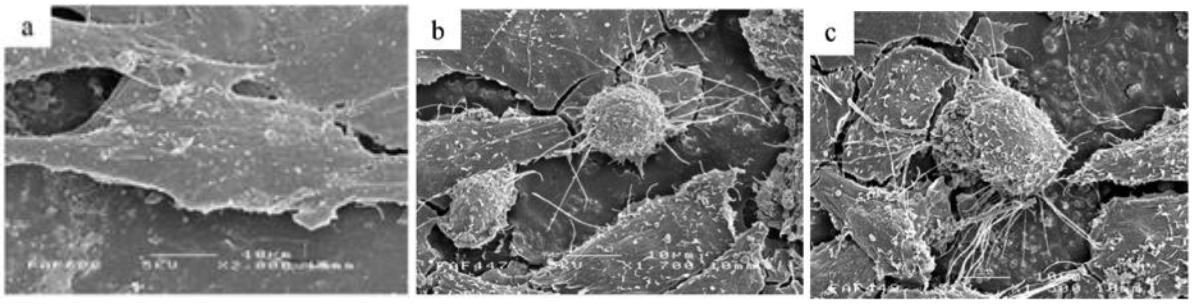

Figure 39 SEM observations of PMMA/HA scaffold a)PMMA without HA; b) PMMA+4,4%HA; c)PMMA+8,8%HA.[78]

A higher number of focal adhesion plaques, viewed by vinculin staining, was observed as HA incorporation into the cements increased, as shown in Figure 40b and c. Actin cytoskeleton organization was improved and many stress fibres appeared.

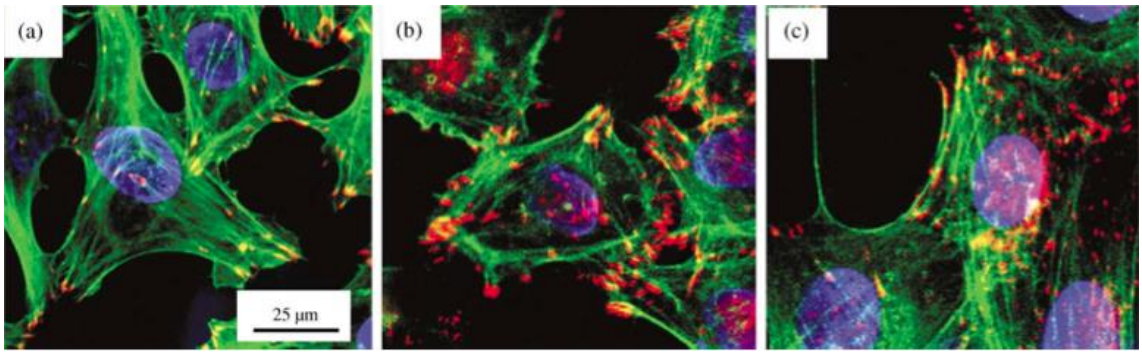

Figure 40 Confocal observations a) PMMA without HA ; b) PMMA+4,4%HA ; c) PMMA+8,8%HA Fibronectin proliferation.[78]

Many *in vivo* studies and reviews have also reported the osseoconductive ability of HA, used for osteointegration of medical implant or as bone substitutes.[70,77,79,80] In a study, Wang *et al.* have evaluated the osseointegration of Ti-6Al-4V implants with and without plasma sprayed HA coatings.[80] After 4 and 12 weeks of implantation, the amount of new bone was more important with the coated implant than with the bare implant, as shown in Figure

41a and b. In addition, a direct contact was noticed between the host tissue and the coated implant surface, whereas a fibrous tissue interface was found between the bare implant and the host bone tissue, as shown in Figure 41c and d.

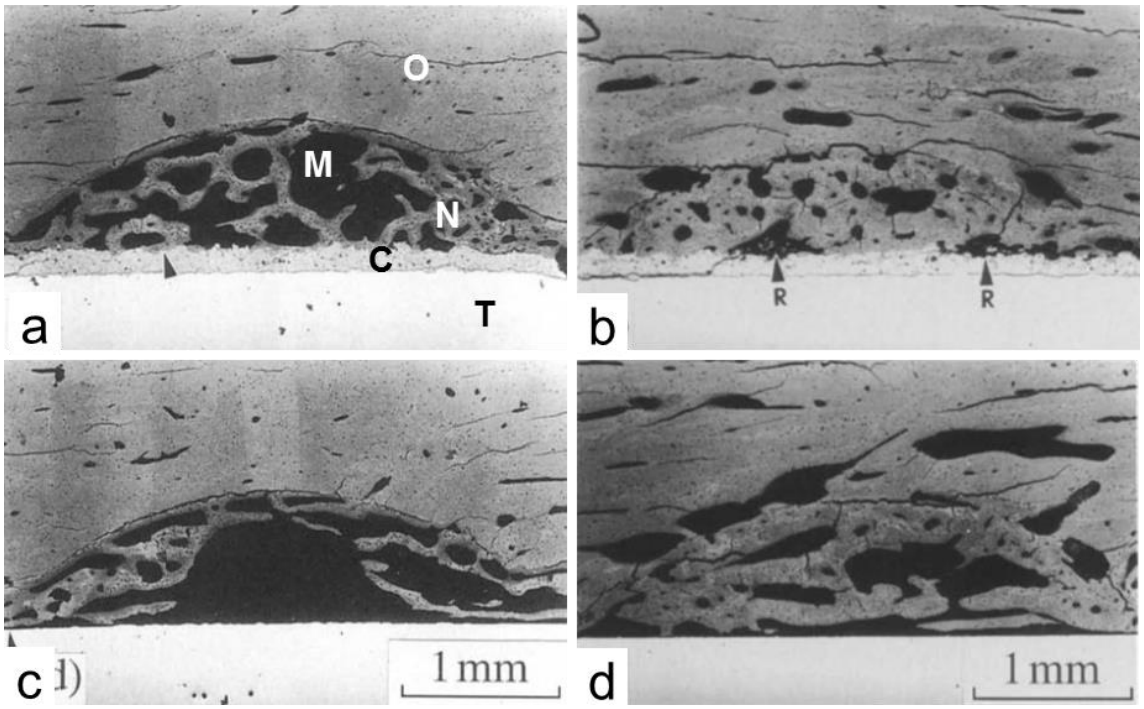

Figure 41 Scanning electron microscopy observations using backscattered electron detector of histological sections in defective bone regions: a-b) HA coated implant face at 4 and 12 weeks; c-d) Ti-6AI 4V at 4 and 12 weeks. O, original cortical bone; N, new bone; M, bone marrow; C, HA coating; T, Ti alloy.[80]

The interactions between HA and bone have not been clearly understood yet. Figure 42 shows a schematic representation of the mineralization process proposed by Bertazzo *et al.*[81] It appears that ion transfers happen at the interface between hydroxyapatite coating and bone surface (1, 2 and 3), followed by proteins adsorption (4) and cells adhesion and proliferation (5 and 6), and finally new bone is formed (7) and natural metabolism starts again (8).

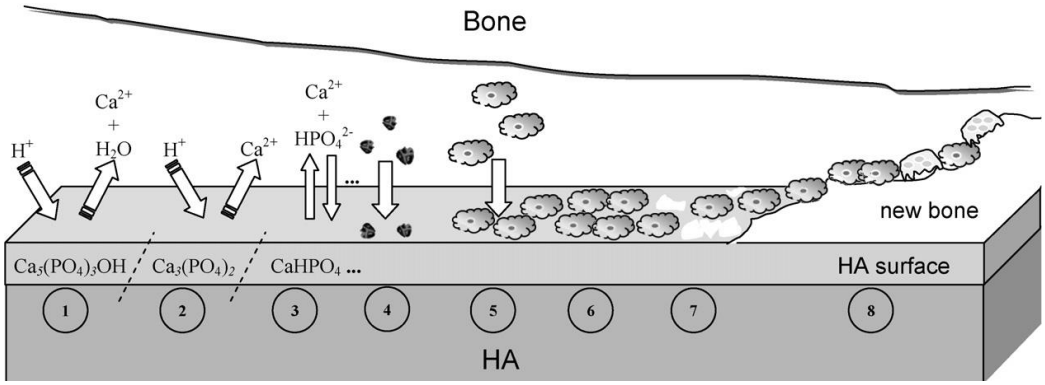

Figure 42 Schematic diagram representing the phenomena that occur on the surface of hydroxyapatite after implantation.[81]

The bioactivity of a bioceramic material depends on its biodegradation *in vivo*. This mechanism occurs with physicochemical dissolution and cellular activity, namely the bioresorption. The kinetics of this biodegradation depends on multiple factors: Ca/P ratio, phase purity, crystalline size, porosity, surface area and solubility (Table 2). Compared to other phosphocalcic ceramics, HA particles have generally a slower degradation.[75]

Ca/P molar ratio	Compounds and their typical abbreviations	Chemical formula	Solubility at 25 °C, −log K$_s$	Solubility at 25 °C, g/L	pH stability range in aqueous solutions at 25 °C
0.5	Monocalcium phosphate monohydrate (MCPM)	$Ca(H_2PO_4)_2·H_2O$	1.14	~18	0.0–2.0
0.5	Monocalcium phosphate anhydrous (MCPA or MCP)	$Ca(H_2PO_4)_2$	1.14	~17	[c]
1.0	Dicalcium phosphate dihydrate (DCPD), mineral brushite	$CaHPO_4·2H_2O$	6.59	~0.088	2.0–6.0
1.0	Dicalcium phosphate anhydrous (DCPA or DCP), mineral monetite	$CaHPO_4$	6.90	~0.048	[c]
1.33	Octacalcium phosphate (OCP)	$Ca_8(HPO_4)_2(PO_4)_4·5H_2O$	96.6	~0.0081	5.5–7.0
1.5	α-Tricalcium phosphate (α-TCP)	α-$Ca_3(PO_4)_2$	25.5	~0.0025	[a]
1.5	β-Tricalcium phosphate (β-TCP)	β-$Ca_3(PO_4)_2$	28.9	~0.0005	[a]
1.2–2.2	Amorphous calcium phosphates (ACP)	$Ca_xH_y(PO_4)_z·nH_2O$, n = 3 − 4.5; 15%–20% H_2O	[b]	[b]	~5–12 [d]
1.5–1.67	Calcium-deficient hydroxyapatite (CDHA or Ca-def HA) [e]	$Ca_{10-x}(HPO_4)_x(PO_4)_{6-x}(OH)_{2-x}$ ($0 < x < 1$)	~85	~0.0094	6.5–9.5
1.67	Hydroxyapatite (HA, HAp or OHAp)	$Ca_{10}(PO_4)_6(OH)_2$	116.8	~0.0003	9.5–12
1.67	Fluorapatite (FA or FAp)	$Ca_{10}(PO_4)_6F_2$	120.0	~0.0002	7–12
1.67	Oxyapatite (OA, OAp or OXA) [f]	$Ca_{10}(PO_4)_6O$	~69	~0.087	[a]
2.0	Tetracalcium phosphate (TTCP or TetCP), mineral hilgenstockite	$Ca_4(PO_4)_2O$	38–44	~0.0007	[a]

Table 2 Existing calcium orthophosphates and their major properties.[75]

2.3 Biological response to HA particles

In this thesis, we mainly used HA micro-particles with spherical shape. Regarding the cellular inflammatory response to this type of HA particles, Laquerierre *et al.* have shown

that spherical HA particles are expected to initiate less inflammatory response than irregular and needle-like particles.[82] Other *in vitro* studies by Laquerriere *et al.* have shown that large non-phagocytable particles (10-70 µm) do not provoke a strong inflammatory response. For smaller sizes in the range 1-30 µm, they find that some cellular response and inflammatory activity occur and depend also on the shape of the particles.[83,84] An *in vitro* and *in vivo* study by Malard *et al.* has shown that small particles with diameters ranging from 10 to 20 µm induce more inflammatory response than larger ones.[85] These studies suggest that the *in vivo* inflammatory response of HA particles is mostly governed by their shape and their size. A proper combination of different sizes of HA particles could be used for the fabrication of composite implants. The efficiency of HA particles in terms of osteoconduction is also govern by the size of HA particles. Hulsart-Billström et al. have tested HA hydrogel composites with different sizes and shapes of HA particles. They implanted several compositions of such hydrogel compositesin the quadriceps of rats and observed the implant after 4 weeks following implantation. As shown in Figure 43, it appears that nanoHA particles having a mean size of 400 nm facilitate the formation of denser bone compare to other type of HA particles.[86]

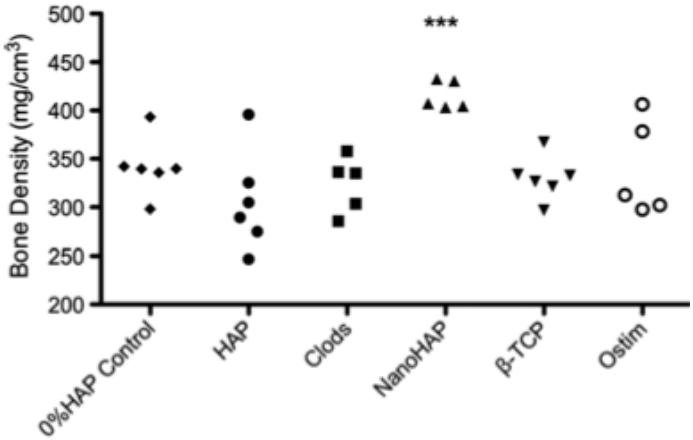

Figure 43 Bone density in function of HAp size.[86]

Chapter 3. Composites of PVA/HA

In this thesis, we are particularly interested in composites of PVA hydrogels and hydroxyapatite. In this last part of the bibliographic review, we will firstly focus on the different processes to produce such composites and their physical properties. Then we will discuss their biological integration, through examples of *in vitro* and *in vivo* studies.

3.1 Fabrication processes and physical properties

Multiple methods to produce composites of PVA hydrogel and HA particles have been investigated. The most common method consists in physical blending of a HA powder in a PVA solution, as shown in Figure 44a.[48,66,87–90] HA particles can also be directly produced via *in situ* precipitation in PVA solutions, as observed in Figure 44b.[91–94] In general, *in situ* HA is formed through the reaction of a solution of calcium hydroxide added to a solution of phosphoric acid. The temperature and pH of the reaction need to be controlled, in order to achieve the intended characteristics. An another method consists in an alternate soaking of PVA hydrogels into a calcium solution and a phosphate solution until apatite formation occurs at the surface of the hydrogel, as shown in Figure 44c.[95,96] Pulsed laser deposition can also be used to deposit a thin layer of HA of hundreds of nanometers on a substrate, as shown in Figure 44d.[67] However this pulsed laser deposition generates only thin and amorphous coatings, which would necessitate additional heat treatments to increase the crystallinity.

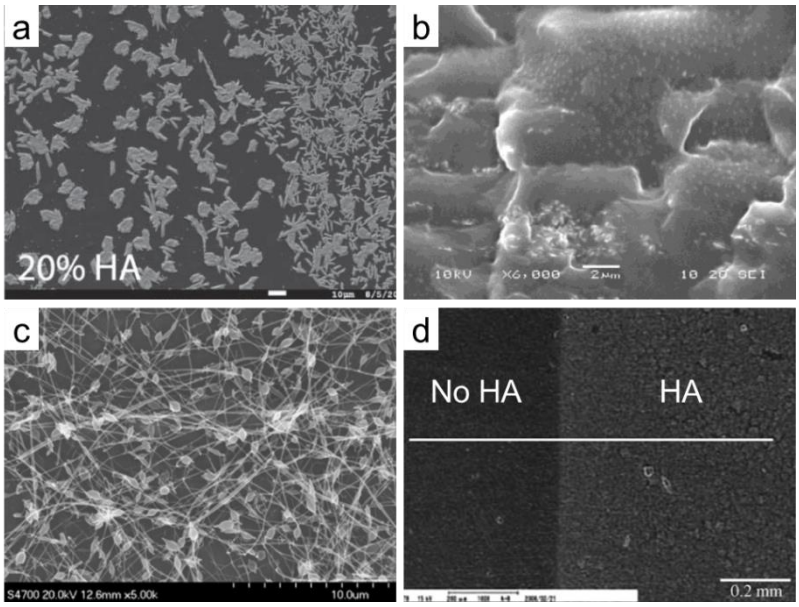

Figure 44 Scanning electron microscopy observations of: **a**) PVA/HA composite membrane, made by blending of PVA solution with HA (20wt%) and crosslinked by drying;[88] **b**) PVA/nanoHA composite, made by *in situ* formation of HA (3wt%) in a PVA solution and crosslinked by freezing/thawing;[93] **c**) PVA/HA nanofiber scaffold, made by alternate soaking of an electrospun PVA fiber scaffold in calcium and phosphate baths;[96] **d**) Surface of PVA hydrogel coated with HA by pulsed laser deposition.[67]

Like for many hydrogel composites with inorganic particles, the addition of HA particles affects the mechanical properties of PVA hydrogels.[97] Hydrogels reinforced with HA particles exhibit higher mechanical properties, in particular stiffness, toughness and strength. Wu *et al.* have tested a 15%wt PVA hydrogel mixed with DMSO/water solvent and two amounts of HA particules, 2% and 5%.[98] These hydrogel samples were obtained by the freezing-thawing method. Samples were immerged in simulated body fluid for 1, 3, 5, 9 et 14 day at a temperature of 37°C. They performed compressive test on these samples and found that the Young's modulus was increasing with the amount of HA particles, as shown on Figure 45.

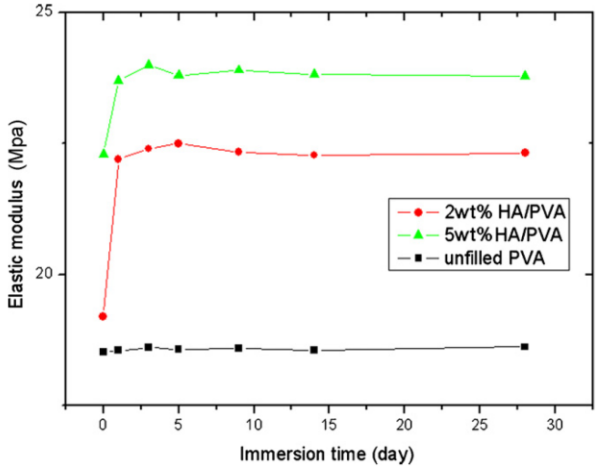

Figure 45 Effect of HA content on the Young's modulus of PVA/HA composite hydrogels.[98]

Addition of HA particles also decreases the water-swelling ratio. In a study of Pan *et al.*, a PVA/HA solution made by co-precipitation was used to manufacture hydrogel composites using the freezing/thawing technique.[47] In their experiment, swelling was evaluated by weighing dried samples and then by letting them swell in different media. The addition of HA nanoparticles to PVA matrix was found to decrease the swelling ratio, as shown on Figure 46.

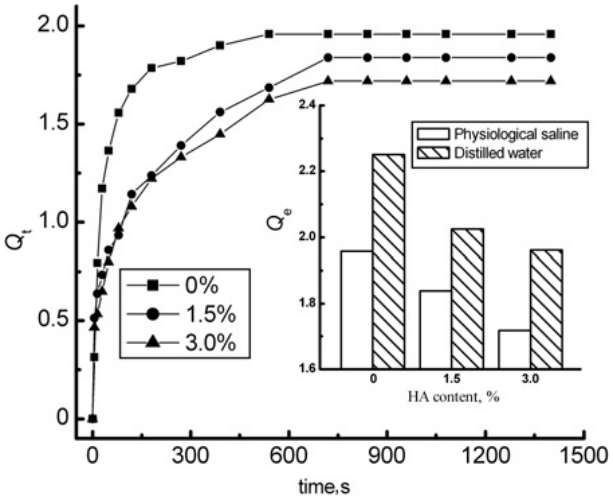

Figure 46 Effect of nano-HA content on the swelling behaviour of PVA/HA gel composites.[47]

The addition of HA particles in PVA hydrogels affects their mechanical and swelling behaviour, because it increases the degree of crosslinking of the network. Particles act like crosslinks between PVA chains and tend to increase the polymer network density.[99,100] This

phenomenon is particularly interesting to tailor the mechanical and swelling characteristics of hydrogel composites. In particular, for bone anchorage of soft tissue substitutes, mechanical properties have to be similar to the host bone to improve mechanical sustainment.

3.2 Biological studies of PVA/HA composites

Composites of PVA/HA have already shown some promising results *in vitro* and *in vivo*. In their *in vitro* studies Hou *et al.*[66] et Hayami *et al.*[67] have clearly shown that HA particles enhance cell adhesion to PVA hydrogels. Figure 47 shows human osteoblasts seeded on PVA substrates (a), and PVA substrates coated with HA nano particles (c). After 13 days (b and d), cells have proliferated on substrates coated with HA particles while no cellular proliferation is seen on the pure PVA substrate.

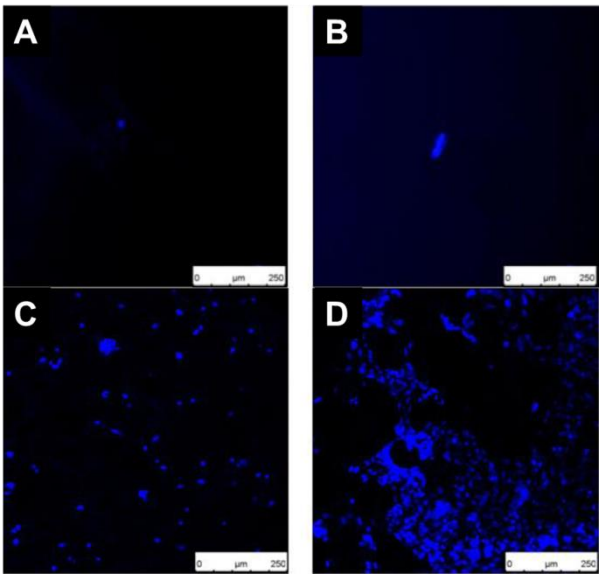

Figure 47 Confocal fluorescence images of human osteoblasts seeded on PVA (**a** and **b**) and nHAP/PVA (**c** and **d**) hydrogels. Scale bar is 250 μm.[66]

Matsumura *et al.* have coated PVA hydrogels with HA via pulsed laser deposition.[101] An amorphous HA coating of 300 nm was produced. Measures of osteocalcin secretion (OCN) of mouse osteoblasts cultured on this substrate are shown on Figure 48. The level of

OCN is higher after 3 weeks for PVA hydrogel coated with HA than PVA hydrogel without coating. It proves that HA coating contributes to enhance cell adhesion, proliferation, and osteoblastic differentiation.

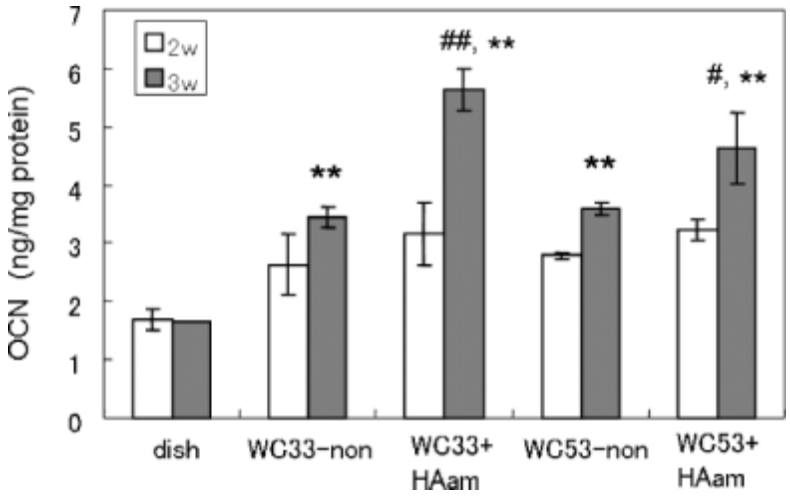

Figure 48 Osteocalcin secretion of MC3T3-E1 cells on various surfaces (WC33 and WC53 are PVA hydrogels with 33 and 53 wt% of water content respectively).[101]

Very few *in vivo* studies on PVA/HA composites are available.[102,103] An *in* vivo study of Wang *et al.* reports the good *in vivo* tolerance of PVA/HA/gelatin disc implants (4x4x1.5 mm^3) in a subcutaneous murine model.[102] After 12 weeks, they noticed tissue ingrowth at the surface and inside the implant. This tissue resembled the surrounding original tissue and few inflammatory cells were found near the surface implant.

Conclusion

As presented in the literature review, PVA hydrogels are relevant candidates for biomedical applications. They present specific properties close to living tissue, in terms of structure, swelling and mechanical properties. Their morphology, swelling ability, and mechanical behavior can be adjusted to obtain proper functional characteristics for a particular use. We have seen that PVA hydrogel are studied for soft tissue implants, but they do not show strong affinity with host tissue, in particular with bone. This is the reason why osteoconductive material, such as HA, can be added to solve these adhesion and anchoring issues. *In vitro* and *in vivo* studies on HA particles have shown that the type of particles influences the response of the cells and of the host tissues. Spherical particles with a diameter ranges from 10 to 100 µm are recommended for *in vivo* application. We have seen that blends of PVA hydrogel and HA particles enhanced adhesion of bone cells to PVA/HA hydrogels and could be used for improvement of anchoring of soft tissue implants. Furthermore, addition of HA seems to strengthen the mechanical properties of PVA hydrogels at the expense of swelling capacity. However little is described in the literature about the *in vivo* response of PVA/HA composites. In addition the physicochemical and structural requirements of such composites, like the accessibility of cells to the particles, are not well described and discussed in the literature.

References

1. Hoffman, A. S. Hydrogels for biomedical applications. *Adv. Drug Deliv. Rev.* **64,** 18–23 (2012).

2. Wichterle, O. & Lim, D. Hydrophilic gels for biological use. *Nature* **185,** 117–118 (1960).

3. Baker, M. I., Walsh, S. P., Schwartz, Z. & Boyan, B. D. A review of polyvinyl alcohol and its uses in cartilage and orthopedic applications. *J. Biomed. Mater. Res. B Appl. Biomater.* **100B,** 1451–1457 (2012).

4. Drury, J. L. & Mooney, D. J. Hydrogels for tissue engineering: scaffold design variables and applications. *Biomaterials* **24,** 4337–4351 (2003).

5. Peppas, N. A. & Colombo, P. Analysis of drug release behavior from swellable polymer carriers using the dimensionality index. *J. Controlled Release* **45,** 35–40 (1997).

6. Peppas, N. A., Hilt, J. Z., Khademhosseini, A. & Langer, R. Hydrogels in Biology and Medicine: From Molecular Principles to Bionanotechnology. *Adv. Mater.* **18,** 1345–1360 (2006).

7. Hoare, T. R. & Kohane, D. S. Hydrogels in drug delivery: Progress and challenges. *Polymer* **49,** 1993–2007 (2008).

8. Nicolson, P. C. & Vogt, J. Soft contact lens polymers: an evolution. *Biomaterials* **22,** 3273–3283 (2001).

9. Sciarretta, F. V. 5 to 8 years follow-up of knee chondral defects treated by PVA-H hydrogel implants. *Eur. Rev. Med. Pharmacol. Sci.* **17,** 3031–3038 (2013).

10. Maldonado-Codina, C. & Efron, N. Hydrogel Lenses-Material and Manufacture: A Review. *Optom. Pract.* **4,** 101–115 (2003).

11. Gibas, I. & Janik, H. Review: synthetic polymer hydrogels for biomedical applications. (2010).

12. Hassan, C. M. & Peppas, N. A. in *Biopolymers· PVA Hydrogels, Anionic Polymerisation Nanocomposites* 37–65 (Springer, 2000).

13. *Polyvinyl Alcohol--Developments, 2nd Edition*. (C.A. Finch, 1992).

14. Chiellini, E., Corti, A., D'Antone, S. & Solaro, R. Biodegradation of poly (vinyl alcohol) based materials. *Prog. Polym. Sci.* **28,** 963–1014 (2003).

15. Mansur, H. S., Sadahira, C. M., Souza, A. N. & Mansur, A. A. P. FTIR spectroscopy characterization of poly (vinyl alcohol) hydrogel with different hydrolysis degree and chemically crosslinked with glutaraldehyde. *Mater. Sci. Eng. C* **28,** 539–548 (2008).

16. Reis, E. F. dos *et al.* Synthesis and characterization of poly (vinyl alcohol) hydrogels and hybrids for rMPB70 protein adsorption. *Mater. Res.* **9,** 185–191 (2006).

17. Sun, H. W., Feigal, R. J. & Messer, H. H. Cytotoxicity of glutaraldehyde and formaldehyde in relation to time of exposure and concentration. *Pediatr Dent* **12,** 303–7 (1990).

18. Mansur, H. S., de S. Costa, E., Mansur, A. A. P. & Barbosa-Stancioli, E. F. Cytocompatibility evaluation in cell-culture systems of chemically crosslinked chitosan/PVA hydrogels. *Mater. Sci. Eng. C* **29,** 1574–1583 (2009).

19. Peppas, N. A. & Merrill, E. W. Poly (vinyl alcohol) hydrogels: Reinforcement of radiation-crosslinked networks by crystallization. *J. Polym. Sci. Polym. Chem. Ed.* **14,** 441–457 (1976).

20. Yang, X., Liu, Q., Chen, X., Yu, F. & Zhu, Z. Investigation of PVA/ws-chitosan hydrogels prepared by combined γ-irradiation and freeze-thawing. *Carbohydr. Polym.* **73,** 401–408 (2008).

21. Yang, X., Zhu, Z., Liu, Q., Chen, X. & Ma, M. Effects of PVA, agar contents, and irradiation doses on properties of PVA/ws-chitosan/glycerol hydrogels made by γ-irradiation followed by freeze-thawing. *Radiat. Phys. Chem.* **77,** 954–960 (2008).

22. Assadi, H., Gärtner, F., Stoltenhoff, T. & Kreye, H. Bonding mechanism in cold gas spraying. *Acta Mater*. **51,** 4379–4394 (2003).

23. Peppas, N. A. & Merrill, E. W. Development of semicrystalline poly (vinyl alcohol) hydrogels for biomedical applications. *J. Biomed. Mater. Res.* **11,** 423–434 (1977).

24. Packter, A. & Nerurkar, M. Crystallization in films of polar vinyl polymers-I. Crystallinity of polyvinyl alcohol films prepared by evaporation of aqueous solutions. *Eur. Polym. J.* **4,** 685–693 (1968).

25. Otsuka, E. & Suzuki, A. A simple method to obtain a swollen PVA gel crosslinked by hydrogen bonds. *J. Appl. Polym. Sci.* **114,** 10–16 (2009).

26. Maria, T. M. C., de Carvalho, R. A., Sobral, P. J. A., Habitante, A. M. B. Q. & Solorza-Feria, J. The effect of the degree of hydrolysis of the PVA and the plasticizer concentration on the color, opacity, and thermal and mechanical properties of films based on PVA and gelatin blends. *J. Food Eng.* **87,** 191–199 (2008).

27. Van Etten, E. A. *et al.* Insulating characteristics of polyvinyl alcohol for integrated electronics. *Thin Solid Films* **568,** 111–116 (2014).

28. Lozinsky, V. I., Domotenko, L. V., Vainerman, E. S., Mamtsis, A. M. & Rogozhin, S. V. On the possibility of mechanodestruction of poly (vinyl alcohol) molecules under moderate freezing of its concentrated water solutions. *Polym. Bull.* **15,** 333–340 (1986).

29. Bolto, B., Tran, T., Hoang, M. & Xie, Z. Crosslinked poly(vinyl alcohol) membranes. *Prog. Polym. Sci.* **34,** 969–981 (2009).

30. Peppas, N. A. Crystallization of polyvinyl alcohol-water films by slow dehydration. *Eur. Polym. J.* **18,** 495–498 (1976).

31. Hassan, C. M., Ward, J. H. & Peppas, N. A. Modeling of crystal dissolution of poly (vinyl alcohol) gels produced by freezing/thawing processes. *Polymer* **41,** 6729–6739 (2000).

32. Inamura, I. Liquid-liquid phase separation and gelation in the poly(vinyl alcohol)-poly(ethylene glycol)–water system. Dependence on molecular weight of poly(ethylene glycol). *Polym. J.* **18,** 269–272 (1986).

33. Bodugoz-Senturk, H. *et al.* The effect of polyethylene glycol on the stability of pores in polyvinyl alcohol hydrogels during annealing. *Biomaterials* **29,** 141–149 (2008).

34. Katz, M. G. & Wydeven, T. Selective permeability of PVA membranes. II. Heat-treated membranes. *J. Appl. Polym. Sci.* **27,** 79–87 (1982).

35. Kobayashi, M., Toguchida, J. & Oka, M. Preliminary study of polyvinyl alcohol-hydrogel (PVA-H) artificial meniscus. *Biomaterials* **24,** 639–647 (2003).

36. Peppas, N. A. Turbidimetric studies of aqueous poly (vinyl alcohol) solutions. *Makromol. Chem.* **176,** 3433–3440 (1975).

37. Kawanishi, K., Komatsu, M. & Inoue, T. Thermodynamic consideration of the sol-gel transition in polymer solutions. *Polymer* **28,** 980–984 (1987).

38. Hatakeyema, T., Uno, J., Yamada, C., Kishi, A. & Hatakeyama, H. Gel–sol transition of poly(vinyl alcohol) hydrogels formed by freezing and thawing. *Thermochim. Acta* **431,** 144–148 (2005).

39. Nijenhuis, K. in *Thermoreversible Networks Viscoelastic Properties and Structure of Gels* **130,** 37–66 (Springer Berlin Heidelberg, 1997).

40. Gonzalez, J. S. & Alvarez, V. A. The effect of the annealing on the poly(vinyl alcohol) obtained by freezing–thawing. *Thermochim. Acta* **521,** 184–190 (2011).

41. Kobayashi, M., Toguchida, J. & Oka, M. Development of an artificial meniscus using polyvinyl alcohol-hydrogel for early return to, and continuance of, athletic life in sportspersons with severe meniscus injury. I: mechanical evaluation. *The Knee* **10,** 47–51 (2003).

42. Shi, P., Teh, T. K. H., Toh, S. L. & Goh, J. C. H. Variation of the effect of calcium phosphate enhancement of implanted silk fibroin ligament bone integration. *Biomaterials* **34,** 5947–5957 (2013).

43. Holloway, J. L., Spiller, K. L., Lowman, A. M. & Palmese, G. R. Analysis of the in vitro swelling behavior of poly(vinyl alcohol) hydrogels in osmotic pressure solution for soft tissue replacement. *Acta Biomater.* **7,** 2477–2482 (2011).

44. Holloway, J. L., Lowman, A. M. & Palmese, G. R. The role of crystallization and phase separation in the formation of physically cross-linked PVA hydrogels. *Soft Matter* **9,** 826–833 (2013).

45. Kim, K.-J., Lee, S.-B. & Han, N. W. Effects of the degree of crosslinking on properties of poly(vinyl alcohol) membranes. *Polym. J.* **25,** 1295–1302 (1993).

46. Stauffer, S. R. & Peppas, N. A. Poly(vinyl alcohol) hydrogels prepared by freezing-thawing cyclic processing. *Polymer* **33,** 3932–3936 (1992).

47. Pan, Y. Swelling properties of nano-hydroxyapatite reinforced poly(vinyl alcohol) gel biocomposites. *Micro Nano Lett.* **5,** 237 (2010).

48. Song, W., Markel, D. C., Jin, X., Shi, T. & Ren, W. Poly(vinyl alcohol)/collagen/hydroxyapatite hydrogel: Properties and *in vitro* cellular response. *J. Biomed. Mater. Res. A* **100A,** 3071–3079 (2012).

49. Peppas, N. A. & Merrill, E. W. Crosslinked poly(vinyl alcohol) hydrogels as swollen elastic networks. *J. Appl. Polym. Sci.* **21,** 1763–1770 (1977).

50. Stammen, J. A., Williams, S., Ku, D. N. & Guldberg, R. E. Mechanical properties of a novel PVA hydrogel in shear and unconfined compression. *Biomaterials* **22,** 799–806 (2001).

51. Gauthier, M. A. *et al.* Degree of crosslinking and mechanical properties of crosslinked poly(vinyl alcohol) beads for use in solid-phase organic synthesis. *Polymer* **45,** 8201–8210 (2004).

52. Wan, Y., Huang, W., Wang, Z. & Zhu, X. X. Preparation and characterization of high loading porous crosslinked poly(vinyl alcohol) resins. *Polymer* **45,** 71–77 (2004).

53. Wan, W. K., Campbell, G., Zhang, Z. F., Hui, A. J. & Boughner, D. R. Optimizing the tensile properties of polyvinyl alcohol hydrogel for the construction of a bioprosthetic heart valve stent. *J. Biomed. Mater. Res.* **63,** 854–861 (2002).

54. Chen, F., Kang, D.-J. & Park, J.-H. New measurement method of Poisson's ratio of PVA hydrogels using an optical flow analysis for a digital imaging system. *Meas. Sci. Technol.* **24,** 55602 (2013).

55. Cloyd, J. M. *et al.* Material properties in unconfined compression of human nucleus pulposus, injectable hyaluronic acid-based hydrogels and tissue engineering scaffolds. *Eur. Spine J.* **16,** 1892–1898 (2007).

56. Urayama, K., Takigawa, T. & Masuda, T. Poisson's ratio of poly(vinyl alcohol) gels. *Macromolecules* **26,** 3092–3096 (1993).

57. Anseth, K. S., Bowman, C. N. & Brannon-Peppas, L. Mechanical properties of hydrogels and their experimental determination. *Biomaterials* **17,** 1674–1657 (1996).

58. Gupta, S., Webster, T. J. & Sinha, A. Evolution of PVA gels prepared without crosslinking agents as a cell adhesive surface. *J. Mater. Sci. Mater. Med.* **22,** 1763–1772 (2011).

59. Jiang, S., Liu, S. & Feng, W. PVA hydrogel properties for biomedical application. *J. Mech. Behav. Biomed. Mater.* **4,** 1228–1233 (2011).

60. Mori, Y., Tokura, H. & Yoshikawa, M. Properties of hydrogels synthesized by freezing and thawing aqueous polyvinyl alcohol solutions and their applications. *J. Mater. Sci.* **32,** 491–496 (1997).

61. Noguchi, T. *et al.* Poly(vinyl alcohol) hydrogel as an artificial articular cartilage: evaluation of biocompatibility. *J. Appl. Biomater.* **2,** 101–107 (1991).

62. Maher, S. A. *et al.* Nondegradable hydrogels for the treatment of focal cartilage defects. *J. Biomed. Mater. Res. A* **83A,** 145–155 (2007).

63. Kobayashi, M., Chang, Y.-S. & Oka, M. A two year in vivo study of polyvinyl alcohol-hydrogel (PVA-H) artificial meniscus. *Biomaterials* **26,** 3243–3248 (2005).

64. Allen, M. J. *et al.* Preclinical evaluation of a poly (vinyl alcohol) hydrogel implant as a replacement for the nucleus pulposus. *Spine* **29,** 515–523 (2004).

65. Bach, J. S. *et al.* Hydrogel fibers for ACL prosthesis: Design and mechanical evaluation of PVA and PVA/UHMWPE fiber constructs. *J. Biomech.* **46,** 1463–1470 (2013).

66. Hou, R. *et al.* Magnetic nanohydroxyapatite/PVA composite hydrogels for promoted osteoblast adhesion and proliferation. *Colloids Surf. B Biointerfaces* **103,** 318–325 (2013).

67. Hayami, T., Matsumura, K., Kusunoki, M., Nishikawa, H. & Hontsu, S. Imparting cell adhesion to poly(vinyl alcohol) hydrogel by coating with hydroxyapatite thin film. *Mater. Lett.* **61,** 2667–2670 (2007).

68. Ou, S.-F., Chiou, S.-Y. & Ou, K.-L. Phase transformation on hydroxyapatite decomposition. *Ceram. Int.* **39,** 3809–3816 (2013).

69. Dorozhkin, S. V. Calcium orthophosphates. *J. Mater. Sci.* **42,** 1061–1095 (2007).

70. Hench, L. L. Bioceramics: from concept to clinic. *J. Am. Ceram. Soc.* **74,** 1487–1510 (1991).

71. Nayak, A. K. Hydroxyapatite synthesis methodologies: an overview. *Int. J. ChemTech Res.* **2,** 903–907 (2010).

72. Santos, M. H., Oliveira, M. de, Souza, L. P. de F., Mansur, H. S. & Vasconcelos, W. L. Synthesis control and characterization of hydroxyapatite prepared by wet precipitation process. *Mater. Res.* **7,** 625–630 (2004).

73. Padmanabhan, S. K. *et al.* Sol–gel synthesis and characterization of hydroxyapatite nanorods. *Particuology* **7,** 466–470 (2009).

74. Orlovskii, V. P., Komlev, V. S. & Barinov, S. M. Hydroxyapatite and hydroxyapatite-based ceramics. *Inorg. Mater.* **38,** 973–984 (2002).

75. Dorozhkin, S. Calcium Orthophosphate-Based Bioceramics. *Materials* **6,** 3840–3942 (2013).

76. Albrektsson, T. & Johansson, C. Osteoinduction, osteoconduction and osseointegration. *Eur. Spine J.* **10,** S96–S101 (2001).

77. Chuenjitkuntaworn, B. *et al.* Polycaprolactone/hydroxyapatite composite scaffolds: Preparation, characterization, and in vitro and in vivo biological responses of human primary bone cells. *J. Biomed. Mater. Res. A* **94A,** 241–251 (2010).

78. Dalby, M. J., Di Silvio, L., Harper, E. J. & Bonfield, W. Increasing hydroxyapatite incorporation into poly (methylmethacrylate) cement increases osteoblast adhesion and response. *Biomaterials* **23,** 569–576 (2002).

79. Xue, W., Liu, X., Zheng, X. & Ding, C. Effect of hydroxyapatite coating crystallinity on dissolution and osseointegrationin vivo. *J. Biomed. Mater. Res. A* **74A,** 553–561 (2005).

80. Wang, B. C., Chang, E., Yang, C. Y. & Tu, D. A histomorphometric study on osteoconduction and osseointegration of titanium alloy with and without plasma-sprayed hydroxyapatite coating using back-scattered electron images. *J. Mater. Sci. Mater. Med.* **4,** 394–403 (1993).

81. Bertazzo, S. *et al.* Hydroxyapatite surface solubility and effect on cell adhesion. *Colloids Surf. B Biointerfaces* **78,** 177–184 (2010).

82. Laquerriere, P. *et al.* Influence des propriétés physicochimiques d'hydroxyapatites sur le comportement cellulaire. *ITBM-RBM* **26,** 200–205 (2005).

83. Laquerriere, P. *et al.* Importance of hydroxyapatite particles characteristics on cytokines production by human monocytes in vitro. *Biomaterials* **24,** 2739–2747 (2003).

84. Laquerriere, P. *et al.* Influence of hydroxyapatite particle characteristics on the [K]/[Na] ratio: a human monocytes in vitro study. *Colloids Surf. B Biointerfaces* **33,** 39–44 (2004).

85. Malard, O. *et al.* Influence of biphasic calcium phosphate granulometry on bone ingrowth, ceramic resorption, and inflammatory reactions: preliminary in vitro and in vivo study. *J. Biomed. Mater. Res.* **46,** 103–111

86. Hulsart-Billström, G. *et al.* Calcium phosphates compounds in conjunction with hydrogel as carrier for BMP-2: A study on ectopic bone formation in rats. *Acta Biomater.* **7,** 3042–3049 (2011).

87. Asran, A. S., Henning, S. & Michler, G. H. Polyvinyl alcohol–collagen–hydroxyapatite biocomposite nanofibrous scaffold: Mimicking the key features of natural bone at the nanoscale level. *Polymer* **51,** 868–876 (2010).

88. Balgová, Z., Palou, M., Wasserbauer, J., Lutišanová, G. & Kozánkováb, J. Preparation, characterization and in vitro bioactivity of polyvinyl alcohol-hydroxyapatite biphasique membranes. *Acta Chim. Slovaca* **6,** (2013).

89. Chua, C. K., Leong, K. F., Tan, K. H., Wiria, F. E. & Cheah, C. M. Development of tissue scaffolds using selective laser sintering of polyvinyl alcohol/hydroxyapatite biocomposite for craniofacial and joint defects. *J. Mater. Sci. Mater. Med.* **15,** 1113–1121 (2004).

90. Goto, T., Kim, I. Y., Kikuta, K. & Ohtsuki, C. Hydrothermal synthesis of composites of well-crystallized hydroxyapatite and poly(vinyl alcohol) hydrogel. *Mater. Sci. Eng. C* **32,** 397–403 (2012).

91. Chung, Y. S. *et al.* Preparation of hydroxyapatite/poly(vinyl alcohol) composite fibers by wet spinning and their characterization: Hydroxyapatite/Poly(Vinyl Alcohol) Fibers. *J. Appl. Polym. Sci.* **106,** 3423–3429 (2007).

92. Degirmenbasi, N., Kalyon, D. M. & Birinci, E. Biocomposites of nanohydroxyapatite with collagen and poly(vinyl alcohol). *Colloids Surf. B Biointerfaces* **48,** 42–49 (2006).

93. Gonzalez, J. S., Maiolo, A. S., Hoppe, C. E. & Alvarez, V. A. Composite Gels Based on Poly (Vinyl alcohol) for Biomedical Uses. *Procedia Mater. Sci.* **1,** 483–490 (2012).

94. Guha, A. & Sinha, A. Surface Mineralization of Hydrogels Through Octacalcium Phosphate: Surface Mineralization of Hydrogels. *Int. J. Appl. Ceram. Technol.* **8,** 540–546 (2011).

95. Bajpai, A. & Singh, R. Study of biomineralization of poly(vinyl alcohol)-based scaffolds using an alternate soaking approach. *Polym. Int.* **56,** 557–568 (2007).

96. Chang, W. *et al.* Biomimetic composite scaffolds based mineralization of hydroxyapatite on electrospun calcium-containing poly(vinyl alcohol) nanofibers. *Mater. Sci. Eng. C* **33,** 4369–4376 (2013).

97. Thoniyot, P., Tan, M. J., Karim, A. A., Young, D. J. & Loh, X. J. Nanoparticle-Hydrogel Composites: Concept, Design, and Applications of These Promising, Multi-Functional Materials. *Adv. Sci.* **2,** n/a-n/a (2015).

98. Wu, G., Su, B., Zhang, W. & Wang, C. In vitro behaviors of hydroxyapatite reinforced polyvinyl alcohol hydrogel composite. *Mater. Chem. Phys.* **107,** 364–369 (2008).

99. Sinha Ray, S. & Okamoto, M. Polymer/layered silicate nanocomposites: a review from preparation to processing. *Prog. Polym. Sci.* **28,** 1539–1641 (2003).

100. Peak, C. W., Wilker, J. J. & Schmidt, G. A review on tough and sticky hydrogels. *Colloid Polym. Sci.* **291,** 2031–2047 (2013).

101. Matsumura, K., Hayami, T., Hyon, S.-H. & Tsutsumi, S. Control of proliferation and differentiation of osteoblasts on apatite-coated poly(vinyl alcohol) hydrogel as an artificial articular cartilage material. *J. Biomed. Mater. Res. A* **9999A,** NA-NA (2009).

102. Wang, M. *et al.* In vitro andin vivo study to the biocompatibility and biodegradation of hydroxyapatite/poly(vinyl alcohol)/gelatin composite. *J. Biomed. Mater. Res. A* **85A,** 418–426 (2008).

103. Qu, D. *et al.* Ectopic osteochondral formation of biomimetic porous PVA-n-HA/PA6 bilayered scaffold and BMSCs construct in rabbit. *J. Biomed. Mater. Res. B Appl. Biomater.* **96B,** 9–15 (2011).

Section 2. Materials

In this section, the materials used in this thesis are described. In the chapter 4, the different type of poly(vinyl alcohol) substrates are presented. The manufacturing process for films and fibers are described, as well as their morphological and physicochemical characteristics. In the chapter 5, two types of commercial hydroxyapatite powder, namely a non-calcined and a calcined powder, are presented. Based on supplier information, the manufacturing process is briefly described. Then the microstructure and physicochemical characteristics of both powders are given. In the following chapters, a specific Materials section is also given, where additional information are given.

Chapter 4. Poly(vinyl alcohol) (PVA)

Poly(vinyl alcohol) (PVA) was used in all the chapter of the thesis and under various states and shapes depending on the applications. PVA was used as a substrate or as a coating matrix. The substrates were fibers or films.

4.1 Commercial materials

For aqueous solution and film processing, commercial PVA, purchased at Sigma-Aldrich, was used. The molecular weight M_w was 89.000-98.000 $g.mol^{-1}$ and the hydrolysis degree was superior to 99%.

PVA fibers were used in Chapter 6 and 7 and are the same as in reference X.[1] PVA threads were purchased in the form of 15 twisted continuous fibers of 45 dtex[1] (Solvron® MH675, Nitivy Ltd.). PVA fiber bundles were assembled, by a textile manufacturer (Morel-Journel, Lyon, France).

4.2 PVA aqueous solution and substrates processing

PVA aqueous solutions:

Two methods were successively used to produce PVA aqueous solutions. In a first method (principally used in Chapter 6 and 7), PVA powder was dissolved in ultrapure water in a beaker under mechanical stirring using a silicon oil bath heated to 110°C during 15

[1] Tex is a unit of measure for the linear mass density of fibers; 1dtex corresponds to the mass (g) of 10.000 meters of one fiber.

minutes. The weight of the solution was measured after dissolution and water was added to correct from evaporation. The solution was then covered and left to cool down and degas. This method was troublesome due to the formation of a solid skin at the surface of the beaker and due to the continual weight checking in order to keep the correct concentration. In a second method, PVA was dissolved in ultrapure water in a glass bottle partially closed and heated in an oven at 90°C for 1 hour. The bottle was then closed and the solution left to cool down at room temperature.

Film processing:

Dry PVA films were produced by solvent-cast of aqueous PVA solutions.[2] A 10 wt% PVA aqueous solution was poured in Petri dishes and put under vacuum-oven at 700 mbar and 70 °C for 8h. Then it was cooled at room temperature for 12h. Finally the dry PVA film was collected from the Petri dished and stored in zip-bags.

Fibers processing:

Fibers used in this thesis were commercially available fibers produced by dry spinning process[3] according to the information provided on manufacturer website (www.nitivy.co.jp/en/). Figure 49 described the general principle of the dry spinning process. In short, solution of highly hydrolyzed PVA is pumped through a spinneret. Right after the exit of the spinneret, the solvent is evaporated from the fibers by passing in a hot gas stream. Finally, the solidified fibers are collected on take-up rolls.

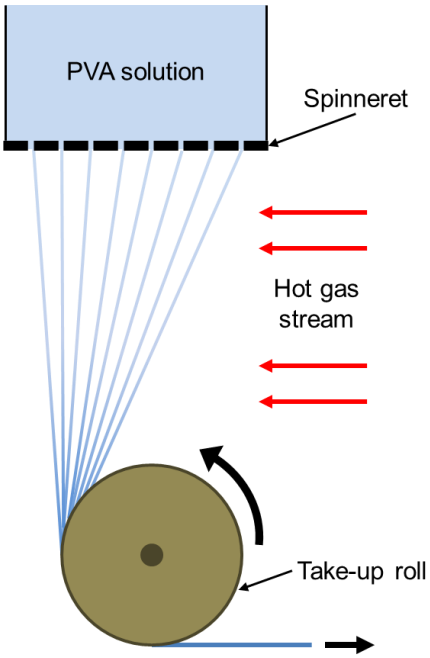

Figure 49 Schematic description of the dry spinning process

4.3 Physicochemical characterization

Morphology

Figure 50a shows a macroscopic observation of the obtained dry PVA films, which have a thickness of 540±170 µm. When soaked in water, PVA hydrogel films were obtained, as shown on Figure 50b.

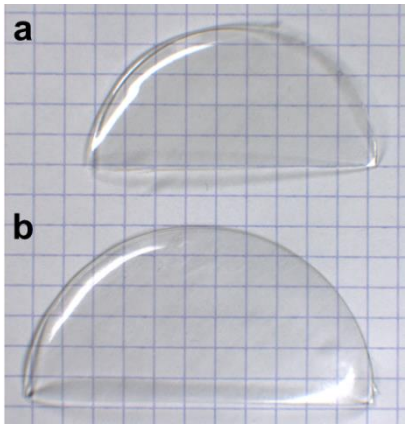

Figure 50 Macroscopic observation of dry (**a**) and swollen (**b**) PVA films, obtained by solvent-cast.

Dry PVA fibers have a diameter of 80±1 µm, as observed on SEM picture in figure 51a. PVA fiber threads were composed of 15 twisted, as shown in Figure 51b. PVA fiber

bundles of about 1.5mm in diameter were assembled by twisting 15 PVA threads together, as shown in Figure 51c.

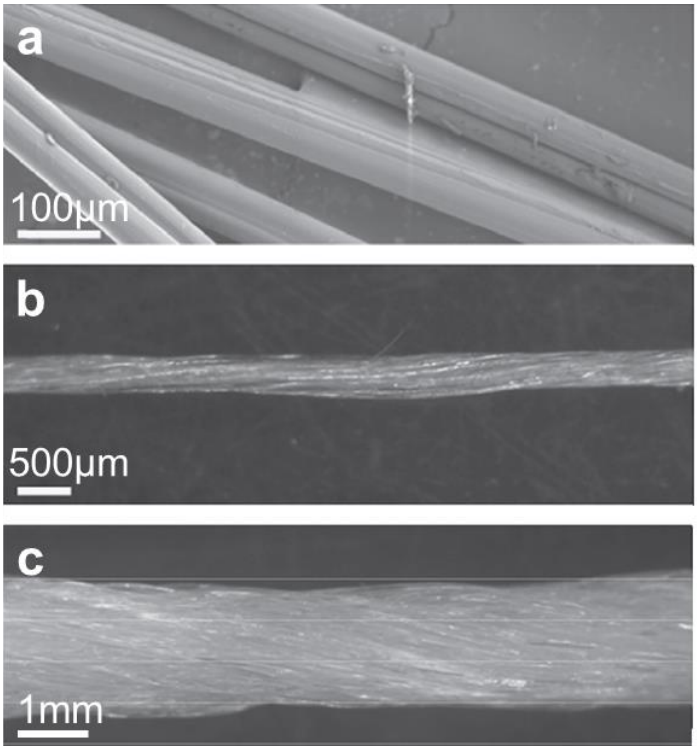

Figure 51 Microscopic observations of dry PVA fiber (**a**), thread (**b**) and bundle (**c**). Reproduced with the authorization of Bach *et al.*[1]

Study of swelling

The swelling equilibrium of the PVA film was reached after 3h of soaking in ultrapure water and the equilibrium water content (WC) was around 57 wt%, as shown in Figure 52a. The water content was estimated from the formula $WC=(M_{eq}-M_i)/M_{eq}$, where M_i is the initial mass and M_{eq} is the mass at swelling equilibrium. The thickness of swollen PVA film at equilibrium was 760±250 µm.

Diameter measurements of dry fibers and upon swelling have been previously realized by Bach *et al.*[1] Swollen fibers have a diameter of 110±10 µm and the swelling equilibrium was reached after 10 minutes of swelling, as shown by Figure 52b. The equilibrium water content was estimated by weighing 3 samples of dry PVA fibers (20 cm long) and comparing

with their weight after 1h of swelling. The equilibrium water content (WC) was around 50 wt%.

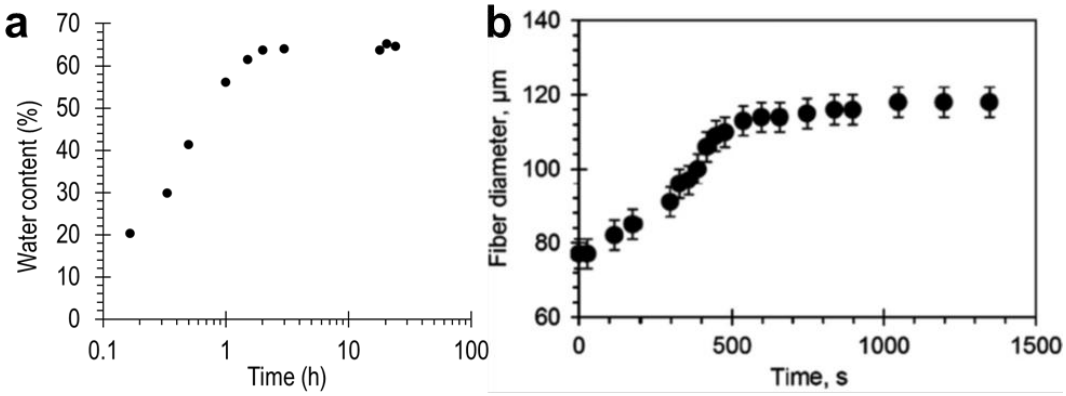

Figure 52 a) Swelling measurements of PVA film in distilled water at room temperature; **b**) Measurement of fiber diameter during swelling in distilled water. Reproduced from Bach *et al.*[1]

Crystallinity measurements

Differential scanning calorimetric (DSC) measurements were performed to measure the melting point and the degree of crystallinity of these PVA films and fibers. Thermograms were obtained on a TA Instrument Q2000 differential scanning calorimeter. Samples for DSC measurements were cut from dry PVA films and fibers and weighed about 3 mg. The temperature ramp was from 0 to 250 °C upon heating at a rate of 10 °C/min. The degree of crystallinity, X_c, was estimated as: $X_c=\Delta H^*/\Delta H_c$, where ΔH^* is the heat of fusion of the PVA sample and ΔH_c is the heat of fusion of a 100% crystalline PVA.[4] The heat of fusion requires to melt a 100% crystalline PVA was chosen to ΔH_c= 138.6 J/g.[4]

Figures 53a and b show the thermograms obtained upon heating for films and fibers respectively. For PVA film, a sharp endothermic peak is noticed at 226°C. The estimated melting temperature is 225±1°C. The area of the peak gave an estimated value the enthalpy of fusion ΔH^*=65.5 J/g. The crystallinity X_c was then calculated to 47.3%. For PVA fibers, a sharp endothermic peak is noticed at 233°C. The estimated melting temperature was 233±1°C. The area of the peak gave an estimated value the enthalpy of fusion ΔH^*=82 J/g. The crystallinity X_c was then calculated to 59%.

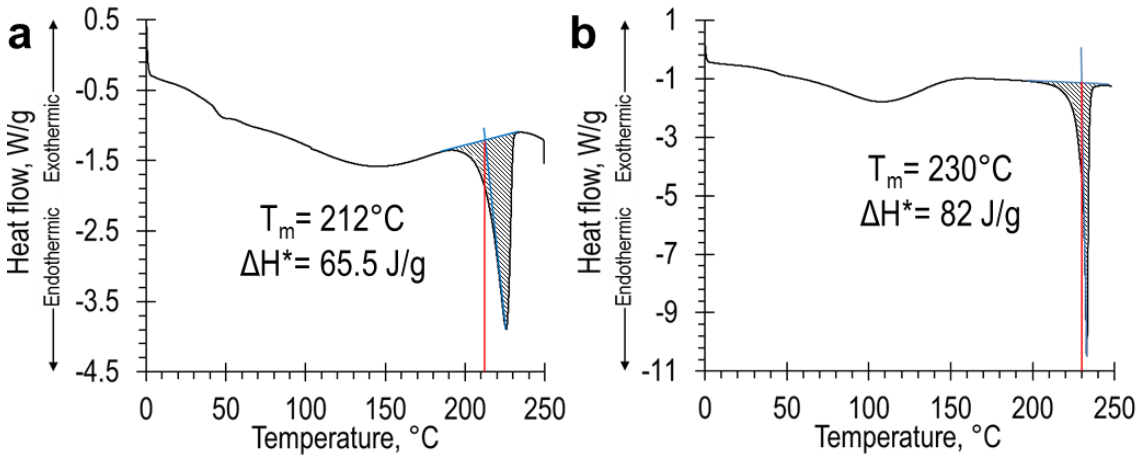

Figure 53 DSC thermogram of dry PVA film (**a**) and fibers (**b**) upon heating from 0 to 250°C at 10°C/min.

Chapter 5. Hydroxyapatite (HA)

In this thesis two types of hydroxyapatite (HA) particles were used. A first powder was a calcined HA powder and was used in all chapters, except the chapter 9 dealing with cell-encapsulation experiments. A second powder was a non-calcined powder and was only used in the chapter 11. In the following, the manufacturing process of HA particles is described and results about their morphological and physical-chemical characteristics are given.

5.1 Manufacturing process of HA particles

The HA calcined and non-calcined particles used are commercial available particles, supplied by Science Applications Industries, Medical Group, France. Based on the supplier information, the HA particles have been produced as follows: the particles were issued from synthetic reaction between diamonium phosphate $(NH_4)_2HPO_4$ and calcium nitrate $Ca(NO_3)_2$ in distilled water, according to the following equation:

$$10\ Ca(NO_3)_2 + 6\ (NH_4)_2HPO_4 + 8\ NH_4OH \rightarrow Ca_{10}(PO_4)_6(OH)_2 + 20\ NH_4NO_3 + 6\ H_2O$$

A solution of ammonium hydroxide NH_4OH was added during the process to catalyze the reaction and to regulate the pH of the solution. Then the solution was filtrated to remove the ammonium components. At the end of this filtration step, a hydroxyapatite slurry was obtained. Finally the slurry was atomized in order to obtain spherical particles. The particles obtained at this stage are referred as “non-calcined particles”. Calcined HA particles were obtained by applying an additional sintering step at 1050 °C under air atmosphere for 40 h,

including a calcination step at 600°C, to eliminate synthesis residues, mostly ammonium nitrates NH_4NO_3. The particles obtained at this stage are referred as “calcined particles”.

5.2 Physicochemical characterization

Granulometry measurements

Granulometry analysis was done by dry dispersion using a Malvern Mastersizer 3000 particle size analyzer. Two different granulometries were used for HA calcined particles, which were 5-25 µm and 25-60µm respectively. A single granulometry was used for non-calcined HA particles, which was 25-60 µm. Table 3 sums up the HA particle granulometry characteristics and Figure 54 shows the overall particle diameter distribution for each particle.

Particles	Mean diameter (µm)	d_{10} (µm)	d_{50} (µm)	d_{90} (µm)
Calcined HA 5-25 µm	13.4	4.4	13.4	23.7
Calcined HA 25-60 µm	41.8	27.6	41.8	61.4
Non-calcined HA 25-60 µm	46.7	8.7	46.7	83.3

Table 3 Particle size distribution of HA particles as measured by dry dispersion granulometry.

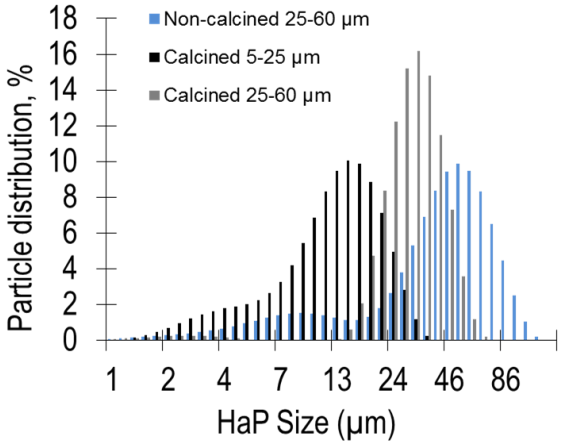

Figure 54 Volume distribution of particle diameter for non-calcined and calcined particles.

5.3 Microstructure and physicochemical characterization

Microstructure analysis

Both HA particles were observed using Nova Nano SEM 450 SEI with secondary electron (S.E.) and backscattered electron (B.S.E.) detectors at 7kV and using Zeiss DSM982 Gemini SEM with secondary electron detector at 5kV. Calcined HA particles have a spherical shape, as shown in Figure 55a and a'. A cross-section of a single particle shows that these particles are porous, as shown in Figure 55b. The porosity level was estimated to 57±7%, after thresholding and binarization of digital images (n=2) with ImageJ software. After further HA particles crushing for fractographic observations, it was obvious that HA particles consist in agglomerates of submicronic HA particles, as shown in Figure 55c. Figure 55d shows a high magnification observation of these submicronic particles, which have a size of 400±200 nm.

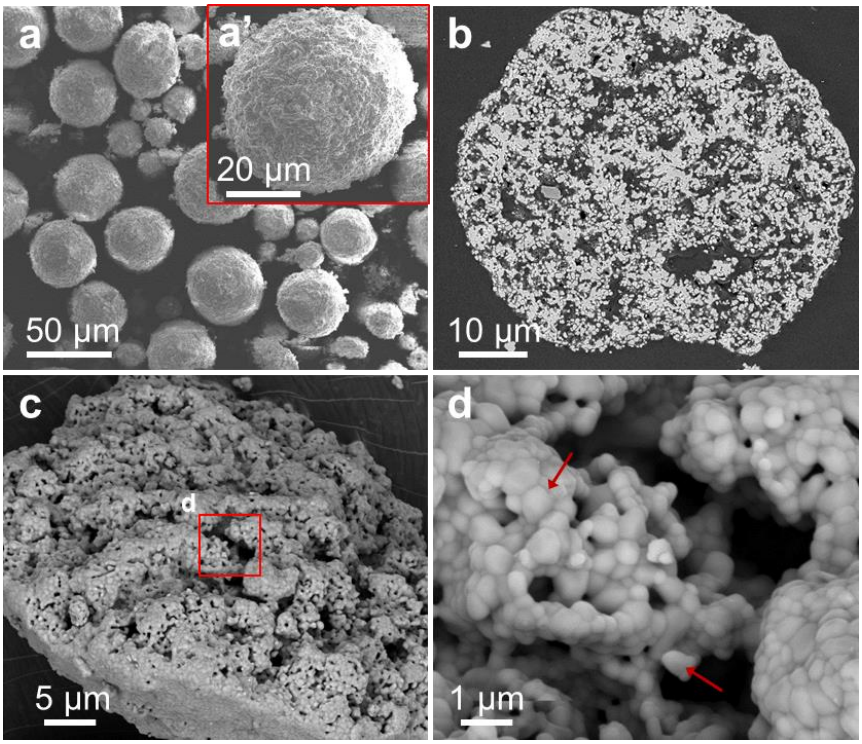

Figure 55 Scanning electronic microscopy imaging of calcined HA particles: **a-a'**) Low magnification observations of the general aspect of the particles; **b**) Cross-section of a single particle observed with B.S.E. detector; **c**) Crushed particle observed with B.S.E. detector; **d**) Zoom of **c**). Red arrow: submicronic particle.

Non-calcined particles also have a spherical shape, as shown in Figure 56a. Cross-section observations of non-calcined HA particles were not possible due to chemical reaction between the HA particles with their synthesis residues and the epoxy resin used to mount sample. Therefore, only fractographic observations of crushed non-calcined HA particles were performed. Figure 56b shows a high magnification observation of a single crushed particle. It shows that these particles are porous agglomerates constituted of submicronic particles. Higher magnification shows that these submicronic particles have an elongated shape with dimensions of hundreds of nanometers long and tenths of nanometers in diameter, as shown in Figure 56c.

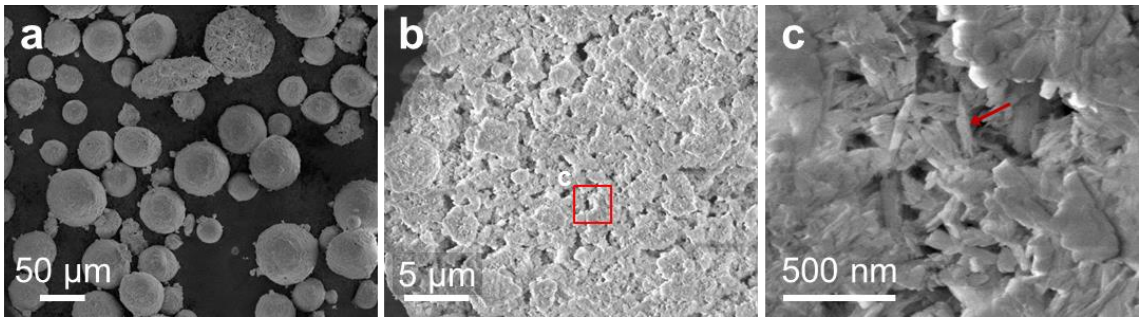

Figure 56 Scanning electronic microscopy imaging of non-calcined HA particles: **a**) Observation of particles morphology; **b**) Observation of crushed particle with S.E. detector; **c**) Zoom of **b**). Red arrow: submicronic particle.

Crystallographic structure and phase identification

The crystallographic structure and phase identification of these particles was investigated by X-ray diffraction (XRD). It was performed with CuKα (Kα1=1.540560 nm; Kα2=1.544390 nm) radiation using a θ/2θ Brucker D-500 diffractometer (40kV, 20 mA, 800 W) at room temperature. Diffraction pattern ranging from 20 to 80° (2θ) were collected using a positional sensitive detector (PSD detector, Elphyse) with scanning step size of 0.032° and counting time of 1 sec. Phases were identified using the International Centre for Diffraction Data powder diffraction files (ICDD-PDF) (#9-432 for hydroxyapatite and #37–1497 for CaO). The mass fraction of each phases and the crystallinity of both particles have been

calculated by comparing the integrated peak intensity areas, which were estimated using Fityk software.[5] The lattice parameters were obtained by Rietveld method using FullProf software.[6]

Figure 57a presents the XRD spectra ranging from 20 to 60° (2θ) of non-calcined and calcined HA particles. For the non-calcined HA particles, a single phase has been identified as pure hydroxyapatite (#9-432). For the HA calcined particles (40h at 1050°C), two phases have been identified: a major hydroxyapatite phase and a minor calcium oxide (CaO) phase. The mass fraction of calcium oxide has been estimated to 1.1% by comparing integrated peak intensity of CaO (200) and $Ca_{10}(PO_4)_6OH_2$ (202).[7] We showed that the CaO phase can be strongly decreased by washing the HA powder ten times in ultra-pure water under magnetic stirring. After these washing cycles, the CaO peaks were no longer obtained, as exhibited in diffraction pattern within the 33-39° range in Figure 57b. The non-calcined HA powder has a crystallinity around 92% and the calcined HA powder crystallinity is superior to 95%. The lattice parameters are listed in Table 4 and are similar to others previous studies.[8,9]

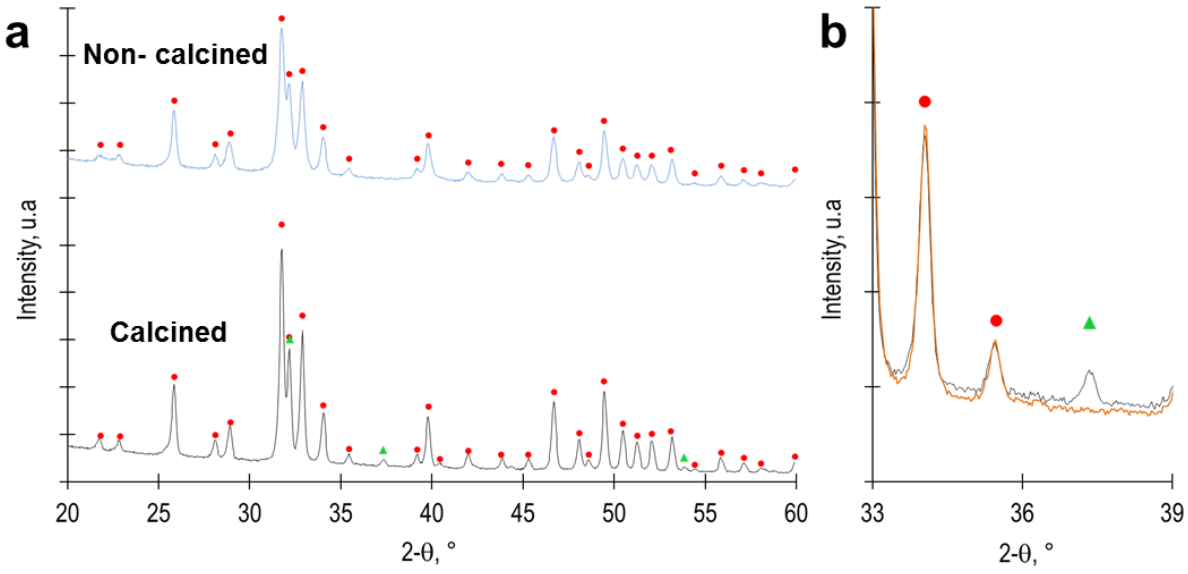

Figure 57 a) XRD spectra of calcined (—) and non-calcined (—) HA particles; **b**) XRD spectra, centered on 33-39°, of calcined (—) and washed calcined HA (—). ICCD-PDF: HA (9-432) (●) and CaO (37–1497) (▲).

Particles	a (Å)	c (Å)	c/a	Ref.
Non-calcined HA	9.419	6.877	0.730	Present work
Calcined (1050°C) HA	9.420	6.882	0.731	Present work
Non-calcined HA	9.419	6.890	0.732	[8]
Calcined (900°C) nano HA	9.419	6.885	0.731	[9]

Table 4 Lattice parameters of the non-calcined and calcined HA and of particles used in other studies.

Fourier transform infrared spectroscopy (FT-IR)

FT-IR spectra were recorded at room temperature using a Bruker TENSOR 37 spectrometer. Spectra were obtained at 4 cm^{-1} resolution averaging 32 scans. Measurements were realized by transmission throughout pellets of compacted HA particles mixed with KBr. Pellets were composed of 25 mg of crushed HA powder and blended with 50 mg of KBr. Pellets were formed by pressing the blends at 1 t of hydraulic pressure.

Figure 58 presents the FT-IR spectra obtained for calcined and non-calcined HA particles. Concerning the non-calcined HA powder, large absorption bands between 3600 and 2800 cm^{-1} corresponds to the absorbed water at the surface of the particles. Bands between 1100 and 900 cm^{-1} and between 700 and 500 cm^{-1} correspond to ν_3PO_4 and ν_4PO_4 modes and are attributed to the phosphate groups of apatite. Bands centered at 1382 and 821 cm^{-1} correspond to NO_3 groups issued from nitrate residues. Concerning the calcined powder, bands at 3647 and 3572 cm^{-1} in the spectra of calcined HA correspond to the OH groups of calcium hydroxide ($Ca(OH)_2$).[10] Another OH group is noticed at 630 cm^{-1}. Bands between 1550 and 1420 cm^{-1} and between 900 and 850 cm^{-1} are ν_3CO_3 and ν_2CO_3 groups issued from apatite carbonates.[11] Bands between 1100 and 900 cm^{-1} and between 700 and 500 cm^{-1} correspond to ν_3PO_4 and ν_4PO_4 modes and are attributed to the phosphate groups of apatite.

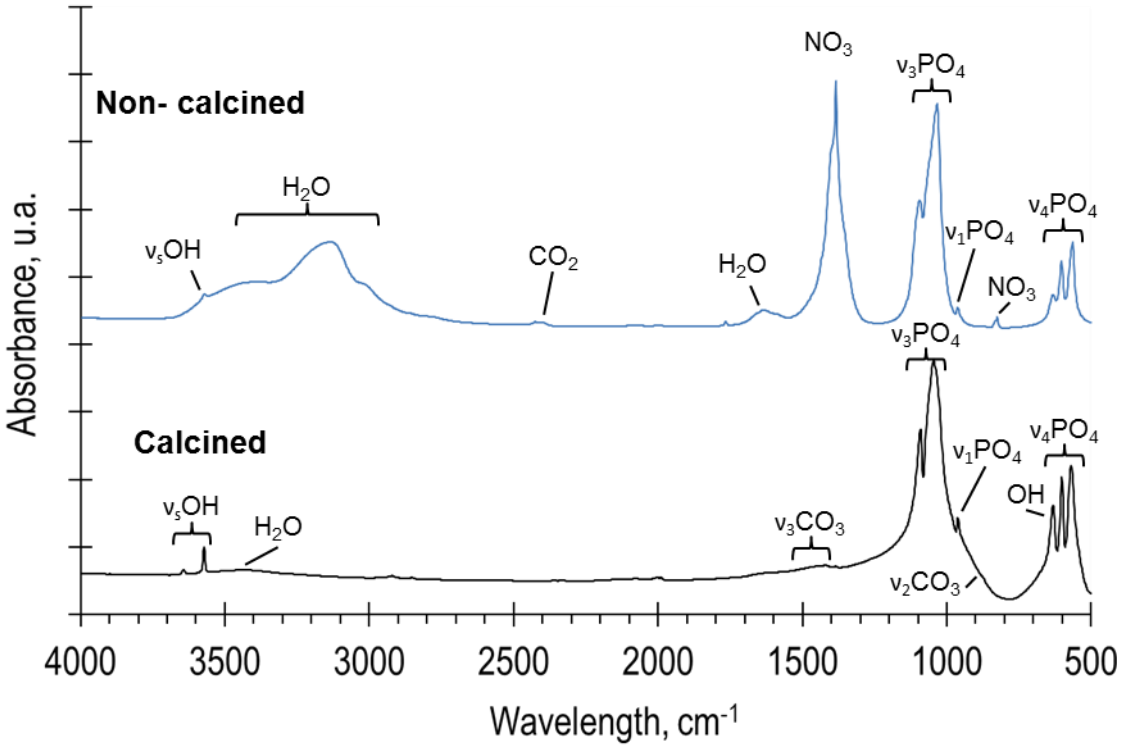

Figure 58 FT-IR spectra of calcined (—) and non-calcined (—) HA particles.

Thermogravimetric analysis (TGA) and differential thermal analysis (DTA)

TGA and DTA curves were simultaneously recorded using a Setaram Instrumentation Ligne 92 TGA/DTA (Caluire, France) apparatus. Measurements were realized under air atmosphere. An amount of 70 mg of each HA particles was placed in alumina crucibles. The heating parameters were 10°C/min to 1550°C.

Figure 59a shows the TGA curve for non-calcined and calcined particles. The mass of the non-calcined powder presents several variations upon heating. Between 30 and 1550°C, the powder has lost about 30% of its initial mass. This is mostly attributed to the elimination of water and nitrate residues from synthesis, as confirmed by exothermic peaks at 200 and 300°C on TDA curve in Figure 59b. On the contrary, the calcined powder does not show any significant mass loss and the measurements indicate a loss inferior to 0.5% of the initial mass. TDA curve shows a large exothermic peak centered at 150°C, probably corresponding to the elimination of water or gaseous releases.

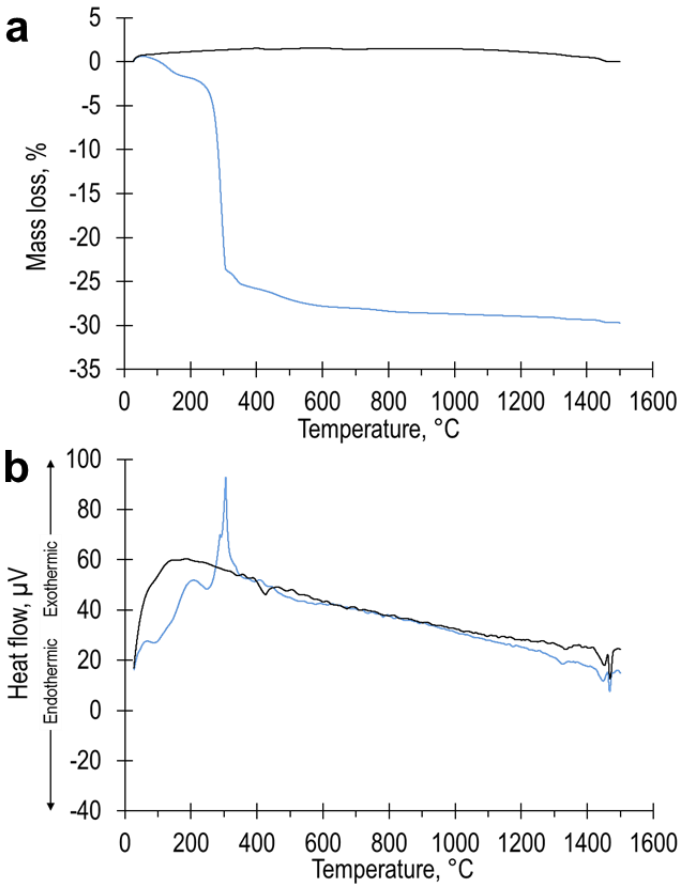

Figure 59 TGA curves (**a**) and TDA curves (**b**) of calcined (—) and non-calcined (—) HA particles.

Reference

1. Bach, J. S. *et al.* Hydrogel fibers for ACL prosthesis: Design and mechanical evaluation of PVA and PVA/UHMWPE fiber constructs. *J. Biomech.* **46,** 1463–1470 (2013).

2. Otsuka, E. & Suzuki, A. A simple method to obtain a swollen PVA gel crosslinked by hydrogen bonds. *J. Appl. Polym. Sci.* **114,** 10–16 (2009).

3. *Handbook of fiber chemistry*. (CRC/Taylor & Francis, 2007).

4. Peppas, N. A. & Merrill, E. W. Differential scanning calorimetry of crystallized PVA hydrogels. *J. Appl. Polym. Sci.* **20,** 1457–1465 (1976).

5. Wojdyr, M. Fityk: a general-purpose peak fitting program. *J. Appl. Crystallogr.* **43,** 1126–1128 (2010).

6. Rodriguez-Carvajal, J. Recent advances in magnetic structure determination neutron powder diffraction. *Phys. B Condens. Matter* **132,** 55–69 (1993).

7. Raynaud, S., Champion, E., Bernache-Assollant, D. & Laval, J.-P. Determination of Calcium/Phosphorus Atomic Ratio of Calcium Phosphate Apatites Using X-ray Diffractometry. *J. Am. Ceram. Soc.* **84,** 359–66 (2001).

8. Murugan, R. & Ramakrishna, S. Crystallographic Study of Hydroxyapatite Bioceramics Derived from Various Sources. *Cryst. Growth Des.* **5,** 111–112 (2005).

9. Zanotto, A., Saladino, M. L., Martino, D. C. & Caponetti, E. Influence of Temperature on Calcium Hydroxyapatite Nanopowders. *Adv. Nanoparticles* **01,** 21–28 (2012).

10. Park, E., Condrate Sr, R. A., Lee, D., Kociba, K. & Gallagher, P. K. Characterization of hydroxyapatite: before and after plasma spraying. *J. Mater. Sci. Mater. Med.* **13,** 211–218 (2002).

11. Lafon, J. P. Synthèse, stabilité thermique et frittage d'hydroxyapatites carbonatées. (Université de Limoges, 2004).

Section 3. Hydrogel-ceramic composite coatings produced by dip-coating for the osteointegration of hydrogel implants

As seen in the bibliographic study, hydroxyapatite poly(vinyl alcohol) hydrogel composites are currently subject of strong researches in the biomedical field. Hydroxyapatite is used as a coating to promote osseoconduction and to secure anchorage of implants to bone. In many cases, composite coatings are composed of different polymers often degradable, making the hydroxyapatite particles accessible to cells. In our system, hydroxyapatite particles are dispersed in a non-degradable poly(vinyl-alcohol) hydrogel matrix, which make difficult for cells to reach hydroxyapatite.

In the chapter 6, we explore a manufacturing process of coatings with tunable surface exposure of hydroxyapatite. This process is based on a combination of dip-coating and physical cross-linking. PVA hydrogel fiber bundles are soaked in PVA aqueous solution, in which HA particles are dispersed. Then a physical cross-linking performed by freezing/thawing method is applied. We observe that it is possible to adjust the surface exposure of hydroxyapatite, the morphology and dimensions and the robustness of the coating by varying the composition of coating solutions. This study will provide a guide to select the suitable coating composition for an in vivo study.

Following the establishment of a suitable manufacturing process of PVA coated hydrogel fibers bundles, we proceeded to an in vivo study of these system in a rabbit animal model. In chapter 3, we will explore the in vivo tolerance and biocompatibility of PVA hydrogel fibers constructs that have been recently developed and shown to reproduce closely the mechanical response of native ligament. We firstly demonstrated that manufactured PVA

coated bundle are easy to handle by surgeon and can be can implanted without complication. Secondly, by means of microCT-scanner and histological investigations we showed that no major osteolysis of bone has been detected and that implants have been well tolerated. This in vivo study has been realized in collaboration with the laboratoire de Bioingénierie et Bioimagerie Ostéo-Articulaire of the Paris-Diderot University. The implantation were supervised by the Pr. H. Petite and Pr. D. Hannouche and realized by the Dr. M. Bachy, a master student A. Villain and myself. Micro-CT and histology analysis were realized and analyzed by H. Petite, A. Villain, M. Bensidhoum and myself.

The chapter 6 has been published in a special issue « The Role of Surfaces and Interfaces for Biomaterials » of the journal Biomatter 2014; 4:e28764.

Chapter 6. Poly(vinyl alcohol) hydrogel coatings with tunable surface exposure of hydroxyapatite

Poly(vinyl alcohol) hydrogel coatings with tunable surface exposure of hydroxyapatite

David Moreau, [1] *Arthur Villain,* [1] *David N. Ku,* [2] *and Laurent Corté*[*1]

[1] Centre des matériaux, UMR 7633 Mines-ParisTech, BP 87, 91003 Evry, France

[2] George W. Woodruff School of Mechanical Engineering, Georgia Institute of Technology Atlanta, GA, 30332, USA.

Published in Biomatter, 4, e28764; April 2014

Abstract

Insufficient bone anchoring is a major limitation of artificial substitutes for connective osteoarticular tissues. The use of coatings containing osseoconductive ceramic particles is one of the actively explored strategies to improve osseointegration and strengthen the bone-implant interface for general tissue engineering. Our hypothesis is that hydroxyapatite (HA) particles can be coated robustly on specific assemblies of PVA hydrogel fibers for the potential anchoring of ligament replacements. A simple dip-coating method is described to produce composite coatings made of microscopic hydroxyapatite (HA) particles dispersed in a poly(vinyl alcohol) (PVA) matrix. The materials are compatible with the requirements for implant Good Manufacturing Practices. They are applied to coat bundles of PVA hydrogel fibers used for the development of ligament implants. By means of optical and electronic microscopy, we show that the coating thickness and surface state can be adjusted by varying

the composition of the dipping solution. Quantitative analysis based on backscattered electron microscopy show that the exposure of HA at the coating surface can be tuned from 0 to over 55% by decreasing the weight ratio of PVA over HA from 0.4 to 0.1. Abrasion experiments simulating bone-implant contact illustrate how the coating cohesion and wear resistance increase by increasing the content of PVA relative to HA. Using pullout experiments, we find that these coatings adhere well to the fiber bundles and detach by propagation of a crack inside the coating. These results provide a guide to select coated implants for anchoring artificial ligaments.

Key words: Hydroxyapatite, Poly(vinyl alcohol), Hydrogel, Dip-coating, Scanning Electron Microscopy.

Abbreviations

ACL: Anterior Cruciate Ligament

HA: Hydroxyapatite

PVA: Poly(vinyl alcohol)

SEM: scanning electron microscopy

SE: secondary electrons

BSE: backscattered electrons

PE: Poly(ethylene)

6.1 Introduction

Injuries of soft connective tissues such as ligaments, tendons, or cartilage do not heal well and often require a reconstruction using natural grafts, durable synthetic implants or degradable tissue-engineered scaffolds.[1–3] To restore proper physiological function, it is crucial that these reconstructed tissues be well anchored to the bone tissues of the treated joint. In particular, for synthetic implants, failures at the bone-implant interface remain a major limitation.[3–5] For bone prosthetics, coating by osseoconductive ceramics has been shown to significantly improve the strength of the anchorage to bone.[6–12] How this approach can be applied to soft tissue substitutes currently motivates strong research efforts.[6–8,13–16] In particular, methods for coatings that contain bioceramics to enhance osseointegration while still adhering properly to the soft implant remains a challenge. Numerous systems have been developed that are composed of osseoconductive or inductive ceramic particles embedded in a biocompatible polymer matrix. [6–8,11,17–19] The exact requirements for the design of such coatings are still not well defined and depend on the implantation site. In particular, it is most likely that a sufficient surface exposure of ceramic particles should be provided to stimulate the activity of neighboring cells and promote growth of bone tissue. The control of this accessibility to bioceramics is central for the osseointegration of permanent coatings but might also play a role for biodegradable coatings at the early stage after implantation. In this article, we investigate a direct approach to make composite hydrogel-hydroxyapatite coatings with a tunable surface exposure of hydroxyapatite created by varying the composition of the coating solution.

The studied coatings are composed of microscopic hydroxyapatite particles embedded in a hydrogel matrix obtained from physically cross-linked poly(vinyl alcohol) (PVA). Such PVA hydrogels form a non-degradable material with excellent biocompatibility.[20–22] PVA hydrogels have already shown promising performances for several soft-tissue replacement

applications including cartilage[15,16,22] and vein valve repair.[23] Besides them being biocompatible, PVA hydrogels do not show strong promotion for secured attachment and proliferation of cells.[6,7] Several studies have shown that PVA hydrogels can be functionalized by the addition of hydroxyapatite (HA) particles, improving cell adhesion, cell proliferation and osteocalcine levels.[12,24–26] Whether these PVA/HA systems can be used as soft tissue implant coatings has been little explored hitherto.

Here, coatings of PVA/HA composite were applied to assemblies of PVA hydrogel fibers, which have recently been shown to reproduce closely the tensile response of native ligaments.[27] By promoting osseointegration, these coatings may enhance the anchoring of these ligament substitutes in bone tunnels. The surface exposure rate of hydroxyapatite was quantified using low vacuum electron microscopy, which allows observations in the hydrated state. Implant-coating adhesion and resistance to wear are also key-issues to ensure that the coating will withstand surgery and physiological loads. Both properties were assessed using pull-out experiments and friction-against-bone experiments, respectively. All these results will serve as design considerations to select an appropriate coating composition and process for *in vivo* studies. In particular, the selected coatings should offer both a large surface exposure of HA particles to ensure accessibility to cells and a cohesion that prevents coating rip-off during and after implantation.

6.2 Materials and methods

Materials

Commercially available PVA threads (Solvron® MH675, Nitivy Ltd.) were purchased in the form of 15 twisted continuous fibers of 45 dtex each. The PVA used to form these fibers was over 95 % hydrolyzed, similar to PVA used in biomedical applications. PVA bundles of

about 1.5 mm in diameter were formed by twisting 15 PVA threads following the same protocol as in ref 27. Embedding and coating of PVA bundles were performed with high molecular weight (89,000-98,000 $kg \cdot mol^{-1}$) and 99 % hydrolyzed PVA (Sigma-Aldrich). A medical grade powder of hydroxyapatite particles (S.A.I, Beligneux, France) was used for the coating with a broad distribution in particle diameter ranging from 5 to 60 µm. Granulometry analysis was done by dry dispersion using a Malvern Mastersizer 3000 particle size analyzer.

Implant fabrication

Preparation of coating solutions

PVA powder was dissolved under mechanical stirring in ultrapure water using a silicon oil bath heated to 110°C for 15 minutes to produce a 10 wt% PVA aqueous solution. The weight of the solution was measured after dissolution and water was added to correct from evaporation. The solution was then covered and let cool down and degas.

HA particles were added to the previously prepared PVA aqueous solution and dispersed by mechanical stirring for 5 minutes. Water content and HA content were adjusted to produce three solutions with different PVA/HA weight ratios as indicated in Table 5. These PVA/HA solutions were then covered and let degas for 3 days.

Coating process

To prevent HA particles from penetrating between fibers, PVA bundles were first embedded in a PVA hydrogel matrix. For that, 10cm PVA bundles were mounted onto stainless steel racks and soaked in the 10 wt% PVA aqueous solution for 1 hour. After this time, the racks were taken out of the solution and let drip for 1 minute. Cross-linking of the PVA solution covering the bundles was obtained by the freezing/thawing method[28] as follows. The racks were placed in a freezer at -20°C for 19 hours and then back to 20°C for 5

hours. This cycle was repeated five times for one of the racks and twice for the rack intended for PVA/HA coating.

The rack of PVA bundles that underwent two freeze/thaw cycles was soaked in the PVA/HA solution for 1 hour, taken out, let drip for 1 minute and submitted to five additional freeze/thaw cycles to cross-link the HA/PVA coating that covered the samples.

Microscopic characterization

The structure of fabricated samples was characterized by optical microscopy and scanning electron microscopy (SEM) using both secondary electron and backscattered electron detection. Optical microscopy was performed with an Axio Scope A1 Zeiss apparatus on fully hydrated samples immersed in water. Observations were made in dark field reflection mode at a 10X magnification. Dimensional uniformity was assessed by measuring the outer diameter in ten different places along the whole bundle length (5cm). An average coating thickness was estimated using Image J Software from cross-section observation in two different places, by measuring the thickness radially in ten directions. SEM was performed on a Nova Nano SEM 450 SEI apparatus in low-vacuum mode at 90 Pascal and 5 kV. In these conditions, no metallization is required and samples can be observed in a semi-hydrated state for the first ten minutes.

Exposure rate estimation

Exposure rate was estimated by image analysis of BSE images using ImageJ software. On these BSE images, exposed hydroxyapatite appears with a brighter contrast than PVA. As a result, images were binarized and the surface exposure rate was estimated by taking the fraction of white pixels. For each type of coating, the measurement was performed on three images corresponding to a total area of about 0.1 mm^2.

Two methods were used to define the threshold for segmentation. In a first method giving a lower bound, a reference threshold was defined on the image having the weakest chemical contrast (R=0.4) and was applied to the others images. In a second method giving an upper bound, the secondary electron image corresponding to each BSE image was used to find a region showing both covered and uncovered surfaces of HA. The threshold was determined as the best value capturing the boundary between covered and uncovered surfaces.

Pull out experiments

Samples for pull-out tests were obtained by embedding the extremity of a thread or a bundle of fibers in a bulk cylinder of PVA or PVA/HA hydrogels. Embedding was obtained in three steps: (i) the thread or bundle were passed through a cylindrical mould, (ii) the mould was filled with a solution of PVA or PVA/HA while holding the thread or bundle in place, (iii) the solution of PVA or PVA/HA was cross-linked by a series of five freezing-thawing cycles. Three different threads or bundles were embedded: threads of polyethylene, threads of 15 twisted PVA fibers and bundles of 15 twisted PVA threads, as described in reference 27.

Pull out experiments were performed on a tensile testing apparatus (Instron 5866) using a 500 N load cell. The embedded end of the threads or bundles was hold in a metal holder while the free extremity was attached to the superior grip using capstan knot. Pulling was performed at 0.5 mm/sec until complete extraction from the bulk cylinder. For bundle pull-out, the deformation of the bundle was measured by following the distance between two markers fixed on each bundle.

Wear characterization

Wear experiments were carried out at room temperature in wet condition using a CETR UMT-3 tester in cylinder-on-cylinder configuration in reciprocating motion. The upper wearing part is a 10 mm long bone cylinder of 5 mm diameter, obtained from cortical bone of

bovine femur. Coated samples are immersed in water and fixed to the lower moving part. Contact between bone and sample is performed by applying an initial normal force of 0.5 N after which normal displacement is fixed. Wear cycles are applied in a reciprocating motion at 1 Hz with a 4 mm amplitude. After 1, 10, 50, 100 and 200 cycles, test was interrupted to create a new contact at 0.5 N and measure the reduction in coating thickness. Surface condition of the sample is also recorded, using Keyence VHX-2000 digital microscope in wet condition.

6.3 Results

The studied coatings were obtained from a medical grade HA powder produced by blending powders with different particle size distributions. Figure 60a shows the overall particle diameter distribution of the HA powder as measured by dry dispersion. This distribution is broad and ranges from about 1 to 70 µm. The number average particle diameter is 27 µm and the diameter ranges between 5 µm and 60 µm for 90 % of the population. The morphology and shape of the particles were investigated by SEM as shown in Figure 60b. Most particles have a spherical shape and observations of particles sprayed over 1 cm^2 show no significant segregation between small and large particles.

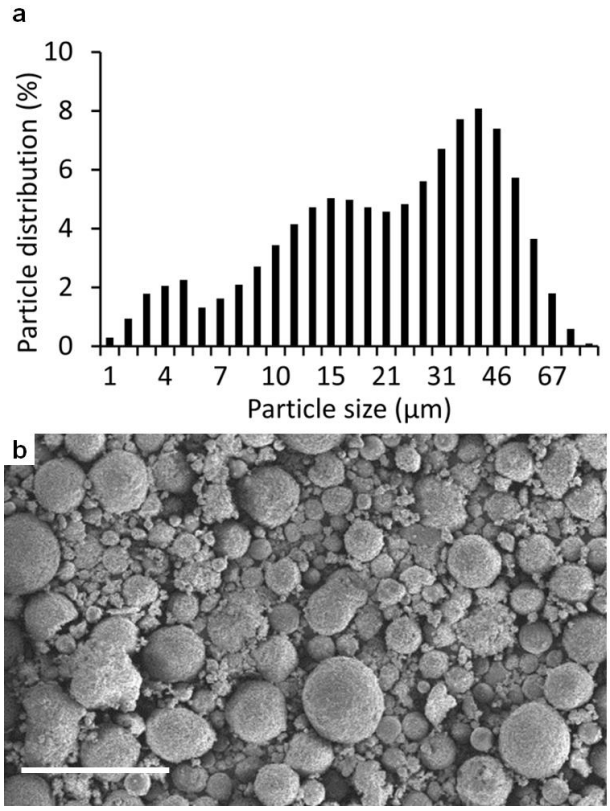

Figure 60 Characterization of HA powder used for coating fabrication: **a**) distribution in particle diameter; **b**) SEM observation of HA powder in secondary electron mode. Scale bar is 100µm.

The studied coating process is based on a dip-coating approach and is composed of several steps as illustrated in Figure 61: i) a bundle of PVA fibers forming the implant was soaked in a PVA aqueous solution; ii) after 1h, it was taken out of the solution and let drip for 1 minute to remove any excess of PVA aqueous solution; iii) the PVA solution coating the fibers was physically cross-linked by a succession of freezing and thawing cycles, as described by Hassan and Peppas[28] ; iv) PVA/HA coating was obtained by soaking these precoated PVA bundles in a PVA/HA aqueous solution; v) after 1h, samples were let drip for 1 minute to remove any excess in PVA/HA solution and vi) were finally cross-linked by repeated freezing-thawing cycles.

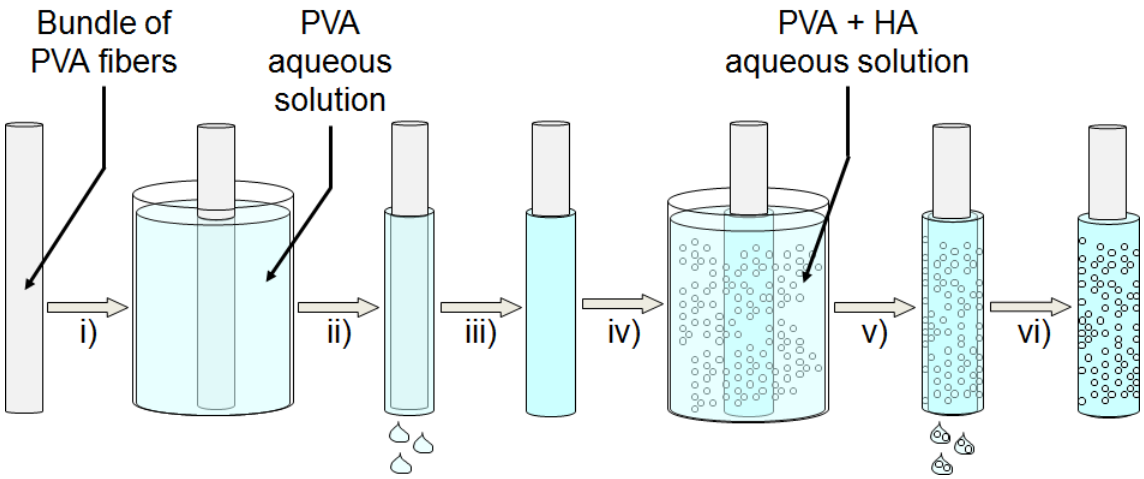

Figure 61 Schematic representation of the coating process.

Several coating compositions were produced by varying the weight ratio of PVA over HA, referred to as R in the following. For that, three different aqueous solutions of PVA and HA were prepared as summarized in Table 5. The corresponding R values are 0.4, 0.2 and 0.1. For each solution, water content was adjusted to produce a uniform coating during step (iv). In particular, the obtained viscosity allowed a homogeneous dispersion of HA particles with our stirring apparatus and a slow sedimentation kinetic during the whole dip-coating step (1h). More details on the compositions and processing steps are given the Materials and Methods section. In the following, the PVA/HA coated samples are compared with PVA coated samples obtained right after step (iii).

H_2O (wt%)	PVA (wt%)	HA (wt%)	R (g/g)
72	8	20	0.4
52	8	40	0.2
45	5	50	0.1

Table 5 Compositions of PVA/HA coating solutions. R gives the weight ratio of PVA over HA.

Both PVA and PVA/HA coated samples were characterized by optical microscopy in dark field reflection mode. In order to remain close to *in vivo* conditions, all observations were made in a hydrated state by fully immersing the samples in water. Figure 62 shows

optical micrographs of the surface and cross-section of various samples. Surface observations indicate that fibers are glued together and aligned along the bundle longitudinal axis for both PVA and PVA/HA coated samples, as shown in Figure 62a and b, respectively. In the case of PVA/HA coated samples, HA particles are uniformly spread with no noticeable difference along the sample length. All samples are fully covered by the PVA/HA coatings and no fibers are visible at the surface, as illustrated in Figure 62b for R=0.4.

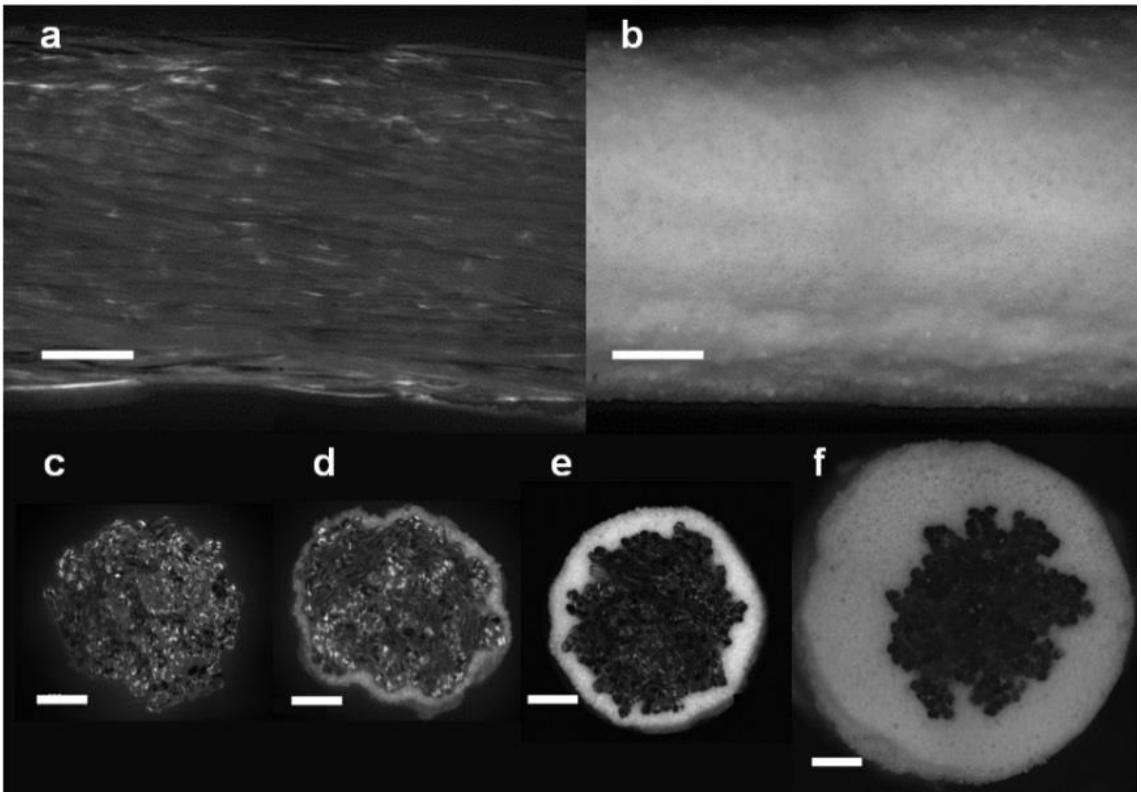

Figure 62 Optical micrographs: surface views of a PVA coated bundle (**a**) and a PVA/HA coated bundle with R=2.5 (**b**); cross-sections of a PVA coated bundle (**c**) and PVA/HA coated bundles with R=0.4, 0.2 and 0.1 (**d-f**). Scale bar is 500µm.

Cross-section observations for PVA coated samples show that fibers have been embedded in a homogeneous PVA matrix. The PVA solution during step (i) has penetrated down to the bundle core. After cross-linking during step (iii), PVA hydrogel is connecting fibers and forms a thin outside layer around the bundle, as shown in Figure 62c. The thickness of this PVA hydrogel layer is about 23±6 µm, and the diameter of the coated bundle is 2080±35 µm. In the case of PVA/HA coated samples, a dense and homogeneous outside layer

is formed around the coating for all values of R, as shown in Figure 62d-f. The coating thickness, and consequently the overall outside diameter of the sample, is increasing with decreasing R, as described in Figure 63. Measurements of the outside diameter in several points show that the coating thickness is uniform with fluctuations of less than 5% along the whole bundle length (5 cm). At one position along the length, cross-section observations show that the coating thickness fluctuates radially as illustrated in Figure 62d-f. These fluctuations represent about 10-20% of the average thickness as indicated by error bars in Figure 63b.

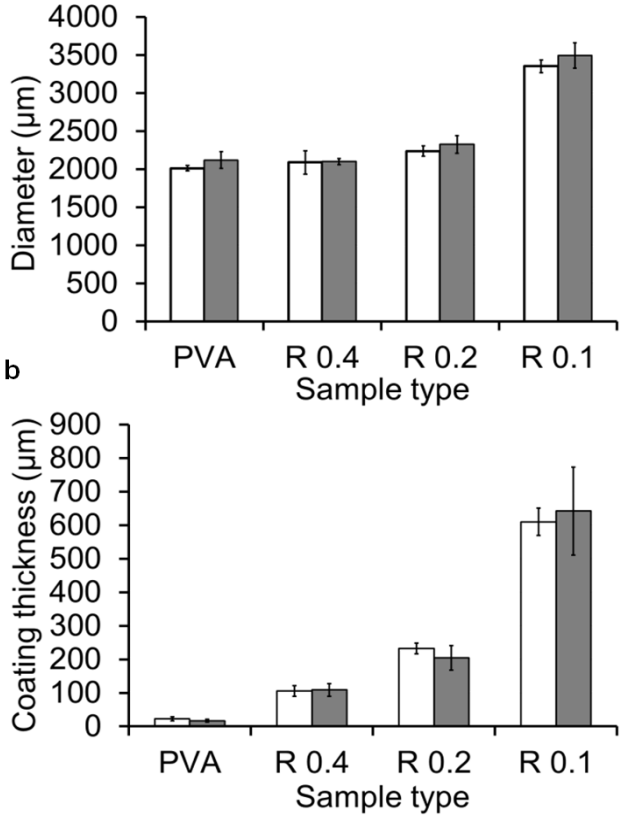

Figure 63 Measurements of diameter (**a**) and coating thickness (**b**) for each type of samples.

Higher magnitude observations were performed using low vacuum SEM, for which hydrated samples can be observed without any metallization and for a few minutes before the effect of water evaporation distorts the microstructure of hydrogel samples. A series of observations in secondary electron mode is given in the first two columns of Figure 64 for

PVA and PVA/HA coated samples. For PVA coated samples, both cross-section (Fig.64a) and surface (Fig.64b) views indicate that the PVA coating fits the bundle closely. At this scale, the coating looks uniform and no cracks are visible at the surface. For PVA/HA coated samples, cross-section observations in Figure 64d, g and j show a homogeneous and dense packing of HA particles along the coating thickness for all values of R. HA particles are glued together by the PVA matrix and no particle has passed through the fibers. Surface observations in Figure 64e, h and k confirm that HA particles are well spread at the surface. All three coatings could withstand drying and no crack was noticed at the surface.

Surface observations of the PVA and PVA/HA coatings were also performed using back-scattered electron (BSE) imaging to estimate the exposure of HA at the surface. BSE images are given in Figure 64c, f, i and l and correspond to the same region of interest as in Figure 64b, e, h and k, respectively. These observations provide a chemical contrast at the sample surface. In particular, HA particles appear much clearer, almost white, than the PVA matrix covering them. For R=0.4 as shown in Figure 64e, the quasi-totality of the area is dark, indicating that no HA is directly exposed at the surface. For R=0.2 and 0.1 as shown in Figure 64i and l, a chemical contrast is observed with white regions corresponding to areas where HA is directly exposed at the surface. For R=0.2, only some of the particles are uncovered while for R=0.1, most of HA is directly exposed and it is difficult to distinguish PVA coated regions from shadows caused by surface topography.

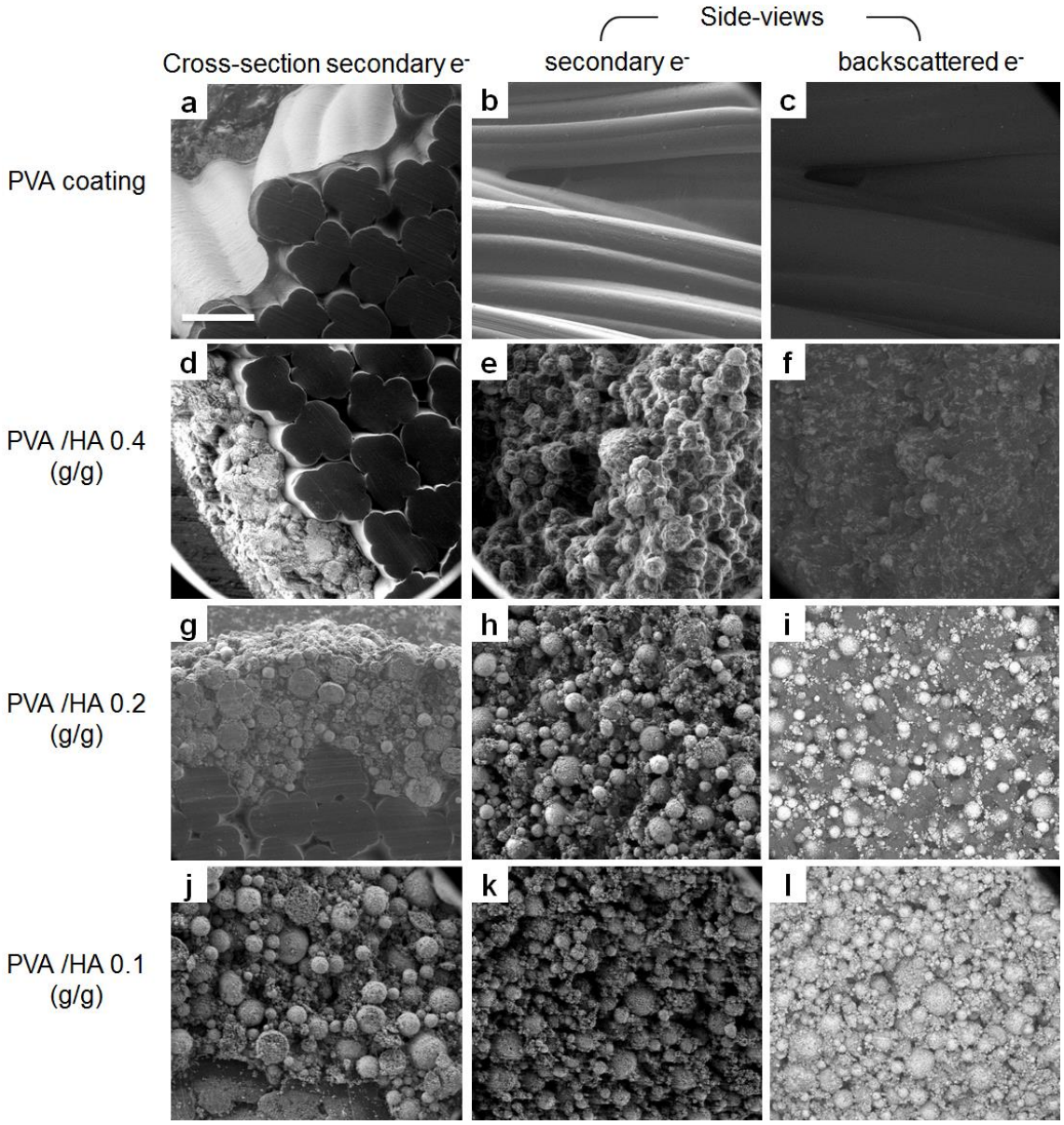

Figure 64 SEM observations of the cross-sections and surfaces of PVA coated (**a-c**) and PVA/HA coated samples with R=0.4 (**d-f**), 0.2 (**g-i**) and 0.1 (**j-l**). Images **c**, f**, i** and **l** show the exact same ROIs as **b**, **e, f** and **k** using backscattered electron imaging. Scale bar is 100µm.

These BSE observations provide a quantitative measure of the HA exposure rate. For that, images have been segmented to provide the percentage of white area, as illustrated in the top picture of Figure 65. Two methods were used to determine the threshold as described in the Materials and Methods section and give an upper and a lower bound for the HA surface exposure rate. Estimations of the exposure rate are plotted in Figure 65 as a function of R. For R=0.4, the percentage of particles exposed at the surface was almost zero. For R=0.2, the exposure rate is about 30±5% and increases to 55±12% for R=0.1. These measurements

suggest that there is a critical PVA to HA ratio below which HA particles are partially covered by PVA hydrogel and therefore, some direct access to HA is possible at the coating surface. With the studied systems, this critical ratio is in the range 0.4-0.2.

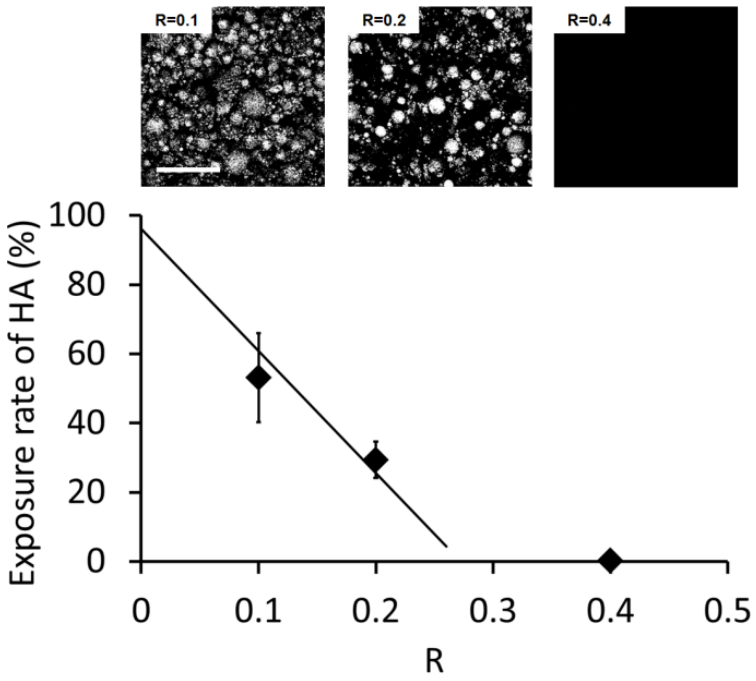

Figure 65 Surface exposure of HA as a function of R. The full line is a linear fit based on data points at R=0.2 and 0.1, going through full exposure for R=0. Top images correspond to binarized BSE images used for image analysis. Scale bar is 100µm.

The stability in water of the coated samples was assessed by storing them in water at room temperature for over 1 year. The implant diameter and the coating thickness remained the same as shown in Figure 63. No microscopic change was observed at the surface. This is consistent with the low solubility of HA and with the stability of physically cross-linked PVA hydrogels, which are known to remain stable in water below 90°C for highly hydrolyzed PVA grades.[29]

Resistance to wear and coating cohesion were assessed by a custom fretting experiment where sample surface is in contact with a cylinder of bovine cortical bone as illustrated in Figure 66a. The bone cylinder had a radius of 2.5 mm and fretting occured by reciprocating motion at 1Hz. Wear was quantified by recording the loss in coating thickness

after 1, 10, 50, 100 and 200 cycles as presented in Figure 66b. A decrease in coating thickness was noticed for all samples, except for PVA coated samples. Resistance to wear increases with increasing ratio R, as shown Figure 66b and c. In particular, after 200 cycles, the loss in coating thickness for the lowest ratio R=0.1 is three and eight times higher than for R=0.2 and for R=0.4 respectively.

The strength of the fiber/coating interface was evaluated using pull-out experiments. Threads or bundles of PVA fibers were embedded in a 2cm-wide bulk cylinder using the same dipping and cross-linking process and the same materials as for the studied coatings. The experiments consisted in measuring the force required to pull these threads or bundles out of the bulk cylinders as illustrated in Figure 67a. A first series of measurements was performed to assess qualitatively the adhesion between the PVA matrix and the PVA fibers. For that, we compared the force required to pull-out a PVA thread and a polyethylene (PE) thread embedded in a bulk PVA cylinder. The corresponding force-displacement curves are given in Figure 67b. For the PVA thread, the thread did not slip immediately out of the cylinder and the force first increased steadily until about 3N. Above 3N, the thread detached abruptly and slipped out of the PVA cylinder. These results strongly suggest that mechanical bonding is formed during the cross-linking process at the interface between the PVA fibers and the PVA coating. For the PE threads, for which no particular bonding with PVA is expected, the thread slipped almost immediately out of the cylinder. The corresponding pull-out force is very weak (<0.5 N) and is most likely caused by friction stresses.

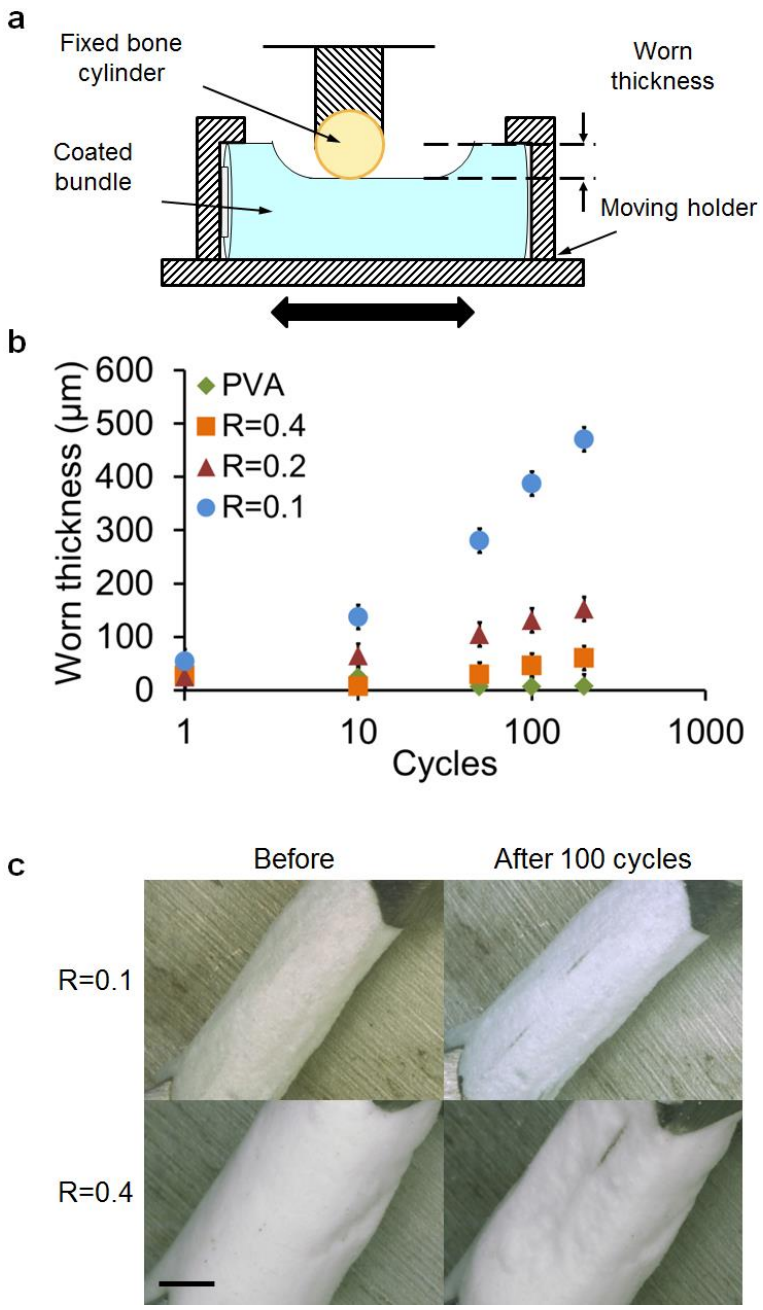

Figure 66 Characterization of the coating resistance to wear: **a)** Schematic representation of the experimental set up; **b)** Worn thickness versus number of cycles for all sample types; **c)** Comparison of surface states before testing and after 100 cycles for R=0.1 and 0.4. Scale bar is 1 mm.

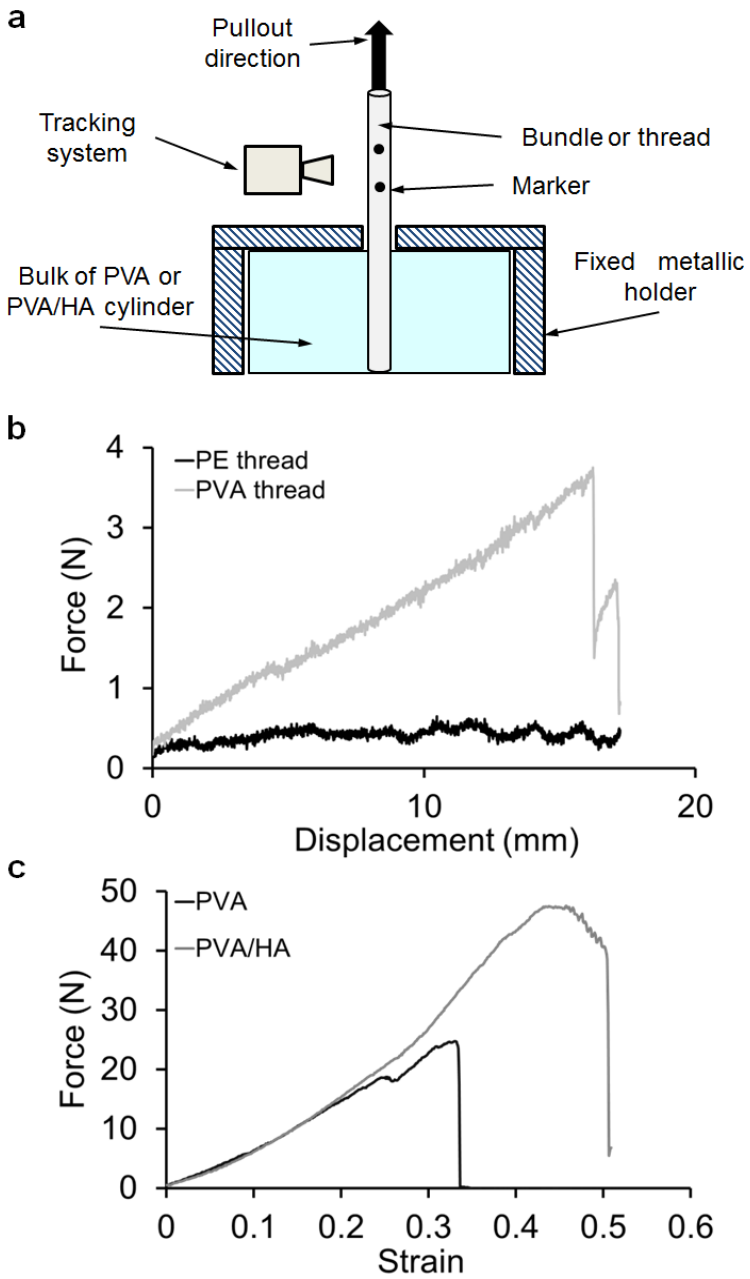

Figure 67 Characterization of the coating adhesion: a) Schematic representation of the pull out test set up. b) Force-displacement curves for PVA and PE threads pulled out of a PVA cross-linked matrix. c) Force-strain curves for PVA pre-coated bundles pulled out of a cross-linked matrix of PVA or PVA/HA (R=0.2)

In a second series, PVA coated samples were embedded in and pulled out of cylinders of PVA or PVA/HA (R=0.2). Corresponding force-strain curves are given in Figure 67c. Like for PVA threads, a strong adhesion was observed: for both PVA and PVA/HA cylinders, the samples first deformed without slipping out of the cylinder and extraction occurred above a critical force. The largest forces were required to pull the samples out of the PVA/HA cylinders. The maximum pull-out forces are 25±2 N and 40±2 N for PVA and PVA/HA cylinders, respectively.

The surfaces of samples after pull-out were examined by SEM in low vacuum mode, as shown in Figure 68 for bundles embedded in a PVA and PVA/HA bulk. In all systems, the surface of the extracted samples was covered with bulk matrix. The surface of fibers was not exposed. Cracking occurred in the bulk PVA or PVA/HA material, but not at the interface with the fibers. In addition, cross-section observations in Figure 68b and d show that an intimate contact was conserved between the fibers and the coating after pull-out, meaning that both PVA and PVA/HA coatings are sufficiently bonded to the fibers to withstand the stresses exerted during pull-out.

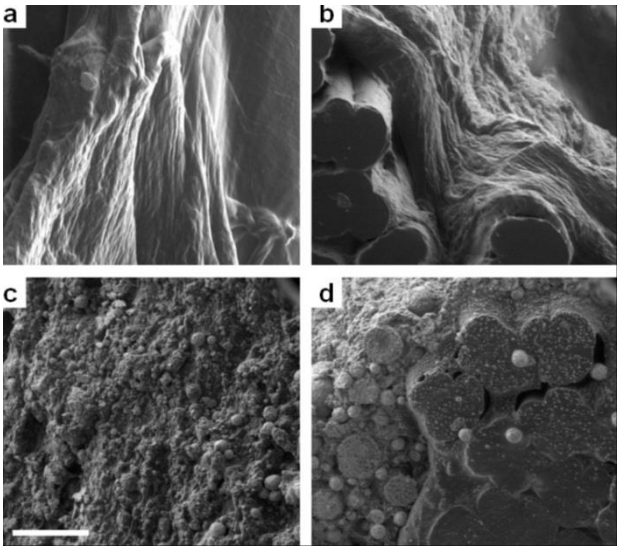

Figure 68 SEM observations of precoated PVA samples pulled out from a matrix of PVA (**a**: surface view, **b**: cross-section) or PVA/HA (**c**: surface view, **d**: cross-section). Scale bar is 100µm.

6.4 Discussion

The results reported in this study show that a simple dip-coating process can be used to produce composite hydrogel-ceramic coatings for which the surface exposure rate of ceramics is tunable from none to almost full exposure. In order to be relevant for *in vivo* use, this process has to fulfil a number of requirements including preservation of the control and repeatability over the coating thickness and surface state.

In the studied systems, spherical HA particles were chosen as they are expected to initiate less inflammatory response than irregular and needle-like particles.[30] A large range in particle size from 1 to 70µm was used. For such a size range, little inflammatory response has been observed in previous works. *In vitro* studies by Laquerriere *et al.* [31,32] have shown that large non-phagocytable particles (10-70 µm) do not provoke a strong inflammatory response. For smaller sizes in the range 1-30 µm, they find that some cellular response and inflammatory activity occur and depend also on the shape of the particles. An *in vitro* and *in vivo* study by Malard *et al.*[33] has shown that small particles with diameters ranging from 10 to 20 µm induce more inflammatory response than larger ones. Here, the proposed process can easily be revised to use a narrower size range if needed.

The microscopic observations presented here show that both the surface state and the thickness of the coatings are strongly dependent on composition. The surface exposure of HA is mostly governed by the relative content of PVA with respect to HA, as quantified by the weight ratio R. BSE observations indicate that the coating composition must remain below a maximum value of R for HA to be exposed. For our systems, this maximum ratio is of the order of 0.30±0.05 as predicted by a linear fit joining the data points for R=0.2 and 0.1 to the full exposure at R=0. This relationship between HA surface exposure and parameter R is most likely related to the wetting of HA particles by hydrated PVA chains, like for the wetting of

granular media by polymer binders.[34,35] For large values of R, full wetting of HA particles by PVA is obtained and only PVA hydrogel is exposed at the coating surface. As R is reduced, the surface of HA particles is partially wetted by PVA which form capillary bridges between particles: a fraction of HA surface becomes directly exposed at the coating surface. As a consequence, the specific surface area of the HA powder and thus the distribution in particle size should be an additional parameter to tune the exposure rate of HA at the surface of coatings.

Major variations in thickness were also obtained with the three studied compositions: a six fold difference was measured between the thinnest (R=0.4) and thickest (R=0.1) coating as shown in Figure 63. From predictions of dip-coating models, it is most likely that these large variations are due to changes in the viscosity of the solutions. In particular, if one neglects gravity effects, the Landau-Levich-Derjaguin theory[36] predicts that the thickness, *e*, of a dip-coated film scales as $e \sim (\eta V)^{2/3}(\rho g)^{-1/2}\gamma^{-1/6}$, where *V* is the substrate extraction velocity, *g* the gravity constant, η and ρ the viscosity and density of the dipping solution, and γ the surface tension of the air-solution interface. In our case, all samples were extracted at the same velocity. Dipping solutions have similar chemical compositions and their density estimated from Table 1 ranges from 1.2 to 1.6. As a result, effects due to changes in ρ and γ can be reasonably neglected. The solution viscosity η remains the only important governing parameter. Accordingly, qualitative observations of the resistance to mixing confirm that the viscosity of the dipping solutions increases noticeably as R decreases from 0.4 to 0.1. Interestingly, this suggests that the thickness of the coating may be adjusted independently from the surface exposure rate of HA by varying the water content alone.

Dimensional measurements show that a uniform coating thickness can be achieved with this process. However, it might be interesting to produce tapered coatings for which the coating thickness decreases with the bone anchoring distance. In particular, for the anchoring

of artificial ligaments, a transition zone from coated to uncoated may be needed at the bone tunnel exit to prevent detachment and migration of HA particles in the intra-articular space. This could be realized here by increasing progressively the extraction velocity or by decreasing the sedimentation speed of HA particles during the dipping step.

The mechanical properties of the composite coatings are also strongly dependent on the relative PVA and HA contents. Fretting experiments on cortical bone reveal strong differences in resistance to wear between the different coating compositions. These differences highlight the mechanical role of the PVA matrix, which is expected to act as a binder providing cohesion to the coating. Accordingly, the results show an eightfold increase in worn thickness when R decreases from 0.4 to 0.1. Pull-out experiments show how strongly these PVA/HA coatings adhere to PVA based implants. The large difference measured between pull-out resistance of PE and PVA threads (Fig. 67b) suggests that some physico-chemical bonding is created at the interface between the PVA fibers and the PVA coating. This bonding may occur during the freezing-thawing steps when PVA crystallites could form and involve chains from both the fibers and the coating. A similar phenomenon could explain the strong adhesion and fractography observations for PVA coated bundles embedded in PVA or PVA/HA bulk as shown in Figures 68b and d.

These mechanical data provide a guide to assess the performance of these coatings in a putative use as the bone tunnel parts of artificial ligament substitutes. For this type of application, rough contacts occur in multiple situations. The most abrasive contacts are most likely created during the surgery, upon insertion in the bone tunnels and fixation with interference screws. Once the device is implanted, physiological loading of the ligament substitute may also induce fretting wear between the coating and cortical or trabecular bone. Such dynamic conditions may cause the detachment of single particles or coating fragments, which in turn may induce inflammatory response after long-term implantation.[37] Coatings

with low PVA content (R=0.1) appear too crumbly to withstand the severe shear caused during bone tunnel insertion.

The *in vivo* stress state at the bone-coating interface is difficult to evaluate because a large fraction of the load is borne by fixation devices, such as interference screws or endobuttons. An upper bound of the *in vivo* strain state applied to the interface can be inferred from the maximum tensile strain undergone by native ligaments. Tensile failure occurs between 9 and 60% of strain for both rabbit[38] and human ACL.[39–41] Pull-out measurements indicate that failure in coated systems with R=0.2 occurs at similar levels of strain, of the order of 40% (Fig 67c). This suggests that no decohesion at the fiber-coating interface is expected upon normal *in vivo* loading. Among the three studied coating compositions, the coating obtained with R=0.2 offers the best compromise between resistance to wear, coating-fiber adhesion and HA exposure, from the perspective of *in vivo* implantation in bone.

As regards biocompatibility, no major issue is expected from the composition of matter. For numbers of applications as implants in the osteo-articular system, both PVA and HA have exhibited good biocompatibility.[15,22,42,43] For PVA/HA composites, previous *in vitro* studies using different processes and particle sizes have shown that these systems do not cause a strong inflammatory response [44–46] and can even induce differentiation and proliferation of osteoblastic cells.[6,8,47] The prior studies do not demonstrate an optimal size, although we suspect grains on the order of 100 microns will leave pores suitable for osteoblast ingrowth. An *in* vivo study using a subcutaneous murine model by Wang *et al.* have also shown a good tolerance with no cytotoxicity for PVA/HA/gelatin systems having a PVA/HA ratio of 2.[13] Full biocompatibility will require evaluation of the component parts together as an assembly. An *in vivo* study with appropriate stress and motion will better evaluate the whole device in the anatomic setting with endpoints of local inflammation and hypertrophy.

6.5 Conclusion

In this work, we report a simple dip-coating process allowing the fabrication of composite surfaces of ceramic (HA) and hydrogel (PVA), for which the surface exposure of ceramic is tunable. The process is reproducible and does not alter the biocompatibility of the coating. By varying the composition of the dipping solution, the geometry and surface state of the coating can be adjusted over a large range. The viscosity of the solution and the relative content of PVA over HA are the main controlling parameters to tune the coating thickness and the HA surface exposure rate, respectively. In addition, these coatings were found to adhere strongly to PVA fibers which may be used as ligament substitutes.

Disclosure of Potential Conflicts of Interest

No potential conflicts of interest were disclosed.

Acknowledgements

The authors are thankful to Y.Auriac and M.Betbeder (Mines-Paristech) for technical support on mechanical testing and SEM observations, as well as H. Proudhon (Mines-Paristech) for fretting experiments. We also thank Dr. H.Petite, Prof. D.Hannouche and Prof. V. Viateau (B2OA, University Paris Diderot) for fruitful discussions. Funding by Mines-ParisTech and Institut Carnot-Mines (Project HAP-Process 2012) is gratefully acknowledged.

References

1. Bray, R. C., Leonard, C. A. & Salo, P. T. Vascular physiology and long-term healing of partial ligament tears. *J. Orthop. Res.* **20,** 984–989 (2002).

2. Woo, S. L.-Y., Abramowitch, S. D., Kilger, R. & Liang, R. Biomechanics of knee ligaments: injury, healing, and repair. *J. Biomech.* **39,** 1–20 (2006).

3. Mascarenhas, R. & MacDonald, P. B. Anterior cruciate ligament reconstruction: a look at prosthetics-past, present and possible future. *McGill J. Med. MJM* **11,** 29 (2008).

4. Guidoin, M.-F. *et al.* Analysis of retrieved polymer fiber based replacements for the ACL. *Biomaterials* **21,** 2461–2474 (2000).

5. Larkin, L. M., Calve, S., Kostrominova, T. Y. & Arruda, E. M. Structure and Functional Evaluation of Tendon–Skeletal Muscle Constructs Engineered *in Vitro*. *Tissue Eng.* **12,** 3149–3158 (2006).

6. Hou, R. *et al.* Magnetic nanohydroxyapatite/PVA composite hydrogels for promoted osteoblast adhesion and proliferation. *Colloids Surf. B Biointerfaces* **103,** 318–325 (2013).

7. Hayami, T., Matsumura, K., Kusunoki, M., Nishikawa, H. & Hontsu, S. Imparting cell adhesion to poly(vinyl alcohol) hydrogel by coating with hydroxyapatite thin film. *Mater. Lett.* **61,** 2667–2670 (2007).

8. Matsumura, K., Hayami, T., Hyon, S.-H. & Tsutsumi, S. Control of proliferation and differentiation of osteoblasts on apatite-coated poly(vinyl alcohol) hydrogel as an artificial articular cartilage material. *J. Biomed. Mater. Res. A* **9999A,** NA–NA (2009).

9. Baxter, F. R. *et al.* Augmentation of Bone Tunnel Healing in Anterior Cruciate Ligament Grafts: Application of Calcium Phosphates and Other Materials. *J. Tissue Eng.* **1,** 712370–712370 (2010).

10. Pan, W., Cao, Z., Li, D. & Zhang, M. Evaluation of the potential application of three different biomaterials combined with bone morphological proteins for enhancing tendon–bone integration. *Injury* **44,** 550–557 (2013).

11. Li, H. *et al.* Composite coating of 58S bioglass and hydroxyapatite on a poly (ethylene terepthalate) artificial ligament graft for the graft osseointegration in a bone tunnel. *Appl. Surf. Sci.* **257,** 9371–9376 (2011).

12. Hirota, M. *et al.* Hydroxyapatite coating for titanium fibre mesh scaffold enhances osteoblast activity and bone tissue formation. *Int. J. Oral Maxillofac. Surg.* **41,** 1304–1309 (2012).

13. Wang, M. *et al.* In vitro andin vivo study to the biocompatibility and biodegradation of hydroxyapatite/poly(vinyl alcohol)/gelatin composite. *J. Biomed. Mater. Res. A* **85A,** 418–426 (2008).

14. Kopeček, J. Hydrogel biomaterials: A smart future? *Biomaterials* **28,** 5185–5192 (2007).

15. Kobayashi, M., Chang, Y.-S. & Oka, M. A two year in vivo study of polyvinyl alcohol-hydrogel (PVA-H) artificial meniscus. *Biomaterials* **26,** 3243–3248 (2005).

16. Maher, S. A. *et al.* Nondegradable hydrogels for the treatment of focal cartilage defects. *J. Biomed. Mater. Res. A* **83A,** 145–155 (2007).

17. Poursamar, S. A., Azami, M. & Mozafari, M. Controllable synthesis and characterization of porous polyvinyl alcohol/hydroxyapatite nanocomposite scaffolds via an in situ colloidal technique. *Colloids Surf. B Biointerfaces* **84,** 310–316 (2011).

18. Sinha, A. & Guha, A. Biomimetic patterning of polymer hydrogels with hydroxyapatite nanoparticles. *Mater. Sci. Eng. C* **29,** 1330–1333 (2009).

19. Suetsugu, Y., Walsh, D., Tanaka, J. & Mann, S. Hydroxyapatite pattern formation in PVA gels. *J. Mater. Sci.* **44,** 5806–5814 (2009).

20. Tadavarthy, S. M., Moller, J. H. & Amplatz, K. Polyvinyl alcohol (Ivalon)--a new embolic material. *Am. J. Roentgenol. Radium Ther. Nucl. Med.* **125,** 609–616 (1975).

21. Hassan, C. M. & Peppas, N. A. in *Biopolymers· PVA Hydrogels, Anionic Polymerisation Nanocomposites* 37–65 (Springer, 2000).

22. Baker, M. I., Walsh, S. P., Schwartz, Z. & Boyan, B. D. A review of polyvinyl alcohol and its uses in cartilage and orthopedic applications. *J. Biomed. Mater. Res. B Appl. Biomater.* **100B,** 1451–1457 (2012).

23. Sathe, R. D. & Ku, D. N. Flexible Prosthetic Vein Valve. *J. Med. Devices* **1,** 105 (2007).

24. Bertazzo, S. *et al.* Hydroxyapatite surface solubility and effect on cell adhesion. *Colloids Surf. B Biointerfaces* **78,** 177–184 (2010).

25. Dalby, M. J., Di Silvio, L., Harper, E. J. & Bonfield, W. Increasing hydroxyapatite incorporation into poly (methylmethacrylate) cement increases osteoblast adhesion and response. *Biomaterials* **23,** 569–576 (2002).

26. Draenert, M., Draenert, A. & Draenert, K. Osseointegration of hydroxyapatite and remodeling-resorption of tricalciumphosphate ceramics: Osseointegration of Calcium phosphate ceramics. *Microsc. Res. Tech.* **76,** 370–380 (2013).

27. Bach, J. S. *et al.* Hydrogel fibers for ACL prosthesis: Design and mechanical evaluation of PVA and PVA/UHMWPE fiber constructs. *J. Biomech.* **46,** 1463–1470 (2013).

28. Hassan, C. M. & Peppas, N. A. Cellular PVA hydrogels produced by freeze/thawing. *J. Appl. Polym. Sci.* **76,** 2075–2079 (2000).

29. Hassan, C. M. & Peppas, N. A. Structure and Morphology of Freeze/Thawed PVA Hydrogels. *Macromolecules* **33,** 2472–2479 (2000).

30. Laquerriere, P. *et al.* Influence des propriétés physicochimiques d'hydroxyapatites sur le comportement cellulaire. *ITBM-RBM* **26,** 200–205 (2005).

31. Laquerriere, P. *et al.* Importance of hydroxyapatite particles characteristics on cytokines production by human monocytes in vitro. *Biomaterials* **24,** 2739–2747 (2003).

32. Laquerriere, P. *et al.* Influence of hydroxyapatite particle characteristics on the [K]/[Na] ratio: a human monocytes in vitro study. *Colloids Surf. B Biointerfaces* **33,** 39–44 (2004).

33. Malard, O. *et al.* Influence of biphasic calcium phosphate granulometry on bone ingrowth, ceramic resorption, and inflammatory reactions: preliminary in vitro and in vivo study. *J. Biomed. Mater. Res.* **46,** 103–111

34. Megias-Alguacil, D. & Gauckler, L. J. Accuracy of the toroidal approximation for the calculus of concave and convex liquid bridges between particles. *Granul. Matter* **13,** 487–492 (2011).

35. Mitarai, N. & Nakanishi, H. Simple model for wet granular materials with liquid clusters. *EPL Europhys. Lett.* **88,** 64001 (2009).

36. Landau, L. & Levich, B. Dragging of a Liquid by a Moving Plate. *Acta Physicochim. URSS* **17,** 42–54 (1942).

37. Morscher, E. W., Hefti, A. & Aebi, U. Severe osteolysis after third-body wear due to hydroxyapatite particles from acetabular cup coating. *J. Bone Joint Surg. Br.* **80,** 267–272 (1998).

38. Yamamoto, S. *et al.* The strain-rate dependence of mechanical properties of rabbit knee ligaments. in *Proceedings of the 18th International Technical Conference on the Enhanced Safety of Vehicles (ESV)* (2003). at <http://www-nrd.nhtsa.dot.gov/pdf/nrd-01/ESV/esv18/CD/proceed/00217.pdf>

39. Butler, D. L., Kay, M. D. & Stouffer, D. C. Comparison of material properties in fascicle-bone units from human patellar tendon and knee ligaments. *J. Biomech.* **19,** 425–432 (1986).

40. Noyes, F. R. & Grood, E. S. The strength of the anterior cruciate ligament in humans and Rhesus monkeys. *J. Bone Jt. Surg.* **58,** 1074–1082 (1976).

41. Takeda, Y., Xerogeanes, J. W., Livesay, G. A., Fu, F. H. & Woo, S. L.-Y. Biomechanical function of the human anterior cruciate ligament. *Arthrosc. J. Arthrosc. Relat. Surg.* **10,** 140–147 (1994).

42. Surmenev, R. A., Surmeneva, M. A. & Ivanova, A. A. Significance of calcium phosphate coatings for the enhancement of new bone osteogenesis – A review. *Acta Biomater.* **10,** 557–579 (2014).

43. Faig-Marti, J. & Gil-Mur, F. J. Hydroxyapatite coatings in prosthetic joints. *Rev. Esp. Cir. Ortopédica Traumatol. Engl. Ed.* **52,** 113–120 (2008).

44. Nie, L. *et al.* Physicochemical characterization and biocompatibility in vitro of biphasic calcium phosphate/polyvinyl alcohol scaffolds prepared by freeze-drying method for bone tissue engineering applications. *Colloids Surf. B Biointerfaces* **100,** 169–176 (2012).

45. Chang, W. *et al.* Biomimetic composite scaffolds based mineralization of hydroxyapatite on electrospun calcium-containing poly(vinyl alcohol) nanofibers. *Mater. Sci. Eng. C* **33,** 4369–4376 (2013).

46. Costa, H. S., Mansur, A. A. P., Barbosa-Stancioli, E. F., Pereira, M. M. & Mansur, H. S. Morphological, mechanical, and biocompatibility characterization of macroporous alumina scaffolds coated with calcium phosphate/PVA. *J. Mater. Sci.* **43,** 510–524 (2008).

47. Wu, G., Su, B., Zhang, W. & Wang, C. In vitro behaviors of hydroxyapatite reinforced polyvinyl alcohol hydrogel composite. *Mater. Chem. Phys.* **107,** 364–369 (2008).

Chapter 7. *In vivo* evaluation of the bone integration of coated poly(vinyl-alcohol) hydrogel fiber implants.

7.1 Introduction

Tearing of ligaments is a debilitating injury that often yields major osteoarticular complications if no suitable care is performed. Because the dense and poorly vascularized architecture of these tissues is not favorable to healing, primary repair is usually not efficient and a full reconstruction is required. In the case of the anterior cruciate ligament (ACL), which is one of the most frequently torn ligaments, the preferred care is based on reconstruction by autograft from tendon tissues. Its clinical outcome is very satisfactory with a success rate close to 95% and a worldwide rate of more than 300,000 reconstructions per year.[1–3] Yet, autograft still exhibits several drawbacks including graft availability, donor site morbidity with long and painful recovery periods.[4] Because of these limitations, there is a persisting and growing demand for an off-the-shelf substitute capable of reproducing the mechanical properties of ligaments while being biocompatible over several decades. Here, we report the first *in-vivo* evaluation of a new artificial system made of synthetic hydrogel fibers using a non-loaded ectopic rabbit model of bone tunnel healing.

Over the last forty years, numerous artificial ligaments have been fabricated from various materials and polymer fibers in particular.[5] Most of them exhibit a tensile stiffness and strength that are similar or superior to those of native ligaments. Nevertheless, in the most demanding case of ACL reconstruction, the majority of these devices have been abandoned due to unacceptable high failure rates resulting from poor anchoring to bone, abrasion of fibers against bone and other fibers or accumulation of wear debris in the synovial cavity.[6,7] Tissue engineering approaches are being explored actively to circumvent these limitations.[8–11]

They still face major challenges including the regeneration of ligament tissues with the proper structure and function, as well as the control of the mechanical properties during the transition from the implanted degradable scaffold to the newly-formed tissue. Other non-degradable materials could provide a more immediate alternate solution for artificial ligament substitutes.[12] The LARS artificial ligament (Ligament Advanced Reinforcement System), made of braided polyethylene terephthalate (PET) fibers, is one of the few available synthetic systems used in clinic for ligament augmentation or reconstruction. Four and eight year follow-up studies have shown satisfying clinical outcomes,[13–15] but there are still unknowns about the long-term behavior. In particular, a decrease in mechanical properties has been reported by Viateau *et al.* in an *in vivo* study performed on a sheep model.[16]

More recently, Bach *et al.* have shown that structures made of hydrogels fibers can exhibit a non-linear tensile response very close to that of native ACL as well as a similar water content of about 50 wt%. The hydrogel forming these fibers is a non-degradable physical hydrogel of poly(vinyl alcohol) (PVA), which has a good history with biocompatibility. Similar PVA hydrogels have already shown promising performances in clinics and in animal *in vivo* studies for the soft osteoarticular tissues replacement, including cartilage,[17] meniscus[18] and intervertebral disc.[19] In the case of PVA hydrogel fibers, little is known about the biological integration and the response of bone tissues after implantation. Furthermore, it is not known whether these PVA hydrogel fibers can be processed, conditioned and manipulated in agreement with clinical requirements.

Although PVA hydrogels were shown to be mostly bio-inert, they do not promote strongly a secured attachment and proliferation of cells.[20,21] As a result, in most cases, a fibrous tissue encapsulation is expected around PVA substitutes *in vivo*. In the case of bone tissue interaction with PVA hydrogels, few studies have been performed.[22,23] For example, Maher *et al.* have reported *in vivo* results of PVA hydrogels used for cartilage defect

treatments.[23] Using a rabbit model, they implanted PVA hydrogels with different compressive modulus in the femoral condyle and observed that implants were surrounded by a fibrous tissue layer after 24 weeks of implantation.

Coating of the implant surface by promoters of bone in-growth could provide a way to control the interface between PVA hydrogels and bone tissues and possibly produce osseoconductive effects. By this mean, the fibrous encapsulation could be reduced or suppressed with direct bone-implant contacts providing a stronger mechanical anchoring. In particular, PVA hydrogels can be functionalized by the addition of hydroxyapatite (HA) particles, improving cell adhesion and proliferation.[20,21,24,25] In this study, we applied this approach to PVA fiber implants and we compared the bone integration of implants with or without a coating of HA particles. This coating was produced by a combination of dip-coating and physical cross-linking, as presented in reference 26.[26] The composition of the coating was selected so as to offer a satisfactory compromise between surface exposure of HA which is then accessible to cells and coating cohesiveness that prevents coating rip-off during implantation.

The *in-vivo* study was designed to assess the quality of the biological response of both uncoated and coated systems. A rabbit model of bone tunnel healing was chosen, where the implants are not submitted to mechanical stress. It is adapted from the study of Li *et al.*,[27] in which they compared the effect of bioceramic coatings on the integration of PET substitutes in bone tunnels.

7.2 Materials and methods

Materials

PVA fibers are the same as in reference 28.[28] PVA threads were purchased in the form of 15 twisted continuous fibers of 45 dtex (Solvron® MH675, Nitivy Ltd.). PVA bundles of about 1.5mm in diameter were assembled, by a textile manufacturer (Morel-Journel, Lyon, France), by twisting 15 PVA threads together. The PVA used in the fiber manufacturing was similar to others PVA grades used in biomedical applications.

The PVA used to fabricate the PVA hydrogel matrix was purchased from Sigma-Aldrich (M_w=89,000-98,000 g/mol, 99% hydrolyzed). Medical grade of hydroxyapatite particles were purchased from S.A.I (Beligneux, France). A blend of two batches with different granulometries was used: a powder with diameter ranging from 5 to 25 µm (50wt%) and a powder with diameters from 25 to 60 µm (50wt%).

Implant fabrication

To ensure a clean environment, each step of the protocol was realized under a chemical hood, thoroughly cleaned with detergent and alcohol. Glassware and steel tools were cleaned with pure ethanol and ultra-pure water and heated at 180°C before being put under the hood. Plastic tools were cleaned with pure ethanol and ultra-pure water. All the steps were realized at room temperature except for the process of cross-linking that implied five cycles of freezing at -20°C and thawing at room temperature.

The solutions to embed and coat the PVA bundles were prepared as follows: A 10wt% PVA aqueous solution was obtained by dissolving PVA in ultrapure water at 110°C during 60 minutes under mechanical stirring. Water was added after dissolution to correct the loss due to evaporation. The PVA aqueous solution was then covered and left to cool down and degas. A composite solution of HA particles and PVA was obtained by dispersing HA particles in the

previously prepared PVA aqueous solution under mechanical stirring for 5 minutes. The HA particles/PVA solution was then covered and left to degas for one day. The composition of the coating solution was 52 wt% of water, 8 wt% of PVA and 40 wt% of HA powder. The weight ratio of PVA over HA was equal to 0.2 (g/g).

The coating procedure is based on the one described in reference 26.[26] It is depicted in Figure 69. 10 cm long dry PVA bundles (i) were mounted on a stainless steel rack. Two identical racks were soaked in the 10% PVA aqueous solution for 1 hour (ii), then taken out, let to drip for 1 minute and placed in sealed polypropylene boxes. The PVA solution remaining around the fibers was physically crosslinked by freezing/thawing (iii)[29,30], the boxes were placed in a freezer at -20°C during 19h and then taken out to thaw at room temperature for 5h. For a first series of 6 implants (PVA implants), this freezing/thawing was repeated five times. For a second series of 6 implants (HA coated implant), freezing/thawing was first repeated twice. Then the rack of PVA bundles was soaked in the PVA/HA solution for 1h (iv), taken out, let to drip for 1 minute and placed in a sealed polypropylene box. Freezing/thawing was finally repeated three times to cross-link the HA coating (v).

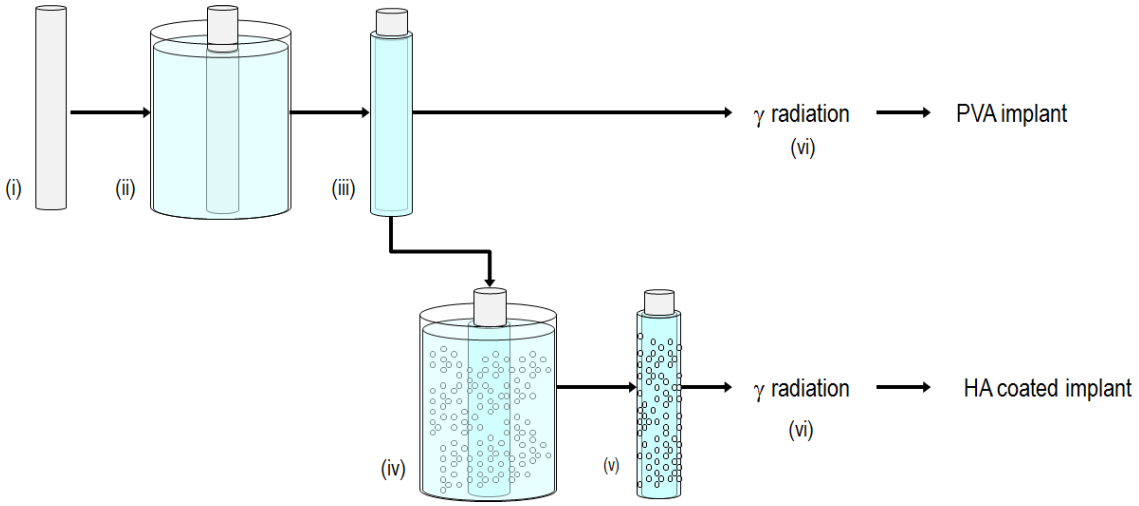

Figure 69 Schematic representation of the implant fabrication process: **(i)** Dry fiber bundle, **(ii)** Soaking in PVA aqueous solution, **(iii)** PVA hydrogel fibres embedded in PVA hydrogel matrix physically cross-linked by freezing-thawing cycles, **(iv)** Soaking of PVA coated bundle in PVA/HA aqueous solution, **(v)** PVA hydrogel fibres coated with HA particles embedded in a PVA hydrogel matrix physically cross-linked by freezing-thawing cycles, **(vi)** Sterilization by gamma-radiation at 25 kGy.

Sterilization of the implants

Each implant was individually packed in a doubled sterile air-tight sample bag (Whirl-Pak, Nasco). The packed samples were submitted to gamma-radiation by a certified provider (Ionisos, Dagneux, France) at a dose of 25 kGy, which is the standard dose for biomedical equipment sterilization (vi).

Animal model

The *in vivo* study was approved by the national ethical committee under the reference N09(CEEALV/2011-02-01). Twelve 17 weeks old male New Zealand White rabbits (Charles River Laboratory) were used, with a mean weight of 3.41±0.2kg. They were randomly divided into two groups, the first group (n=6) received an uncoated implant and the second group (n=6) received a coated implant.

The animal model chosen to study osseointegration consisted in inserting the implant in a bone tunnel drilled through the tibia close to the knee joint, as illustrated in Figure 70. Four month-old New Zealand white rabbits were chosen to provide large enough dimensions

for surgery. The bone tunnel was slanted to enhance the contact surface area between the implant and the host tissue. With this model, a bone-tunnel diameter of 2 mm was selected and implant length was estimated to be of the order of 1 cm.

Implantation

The implantation protocol was adapted from Li *et al.*[27] The surgical procedure was performed on the right leg, under general anesthesia established by intramuscular injection of diazepam (0.5 mg/kg), medetomidine (0.29 mg/kg) and ketamine (0.5 mg/kg). An intra-muscular antibacterial (Cephalexine 75 mg/kg) was also used to prevent any infection. The first incision was made in a medial parapatellar manner. After exposure of the medial and lateral sides of the tibia, an extra-articular bone tunnel of 2mm in diameter was drilled using an orthopedic power tool, as shown in Figure 70a. The implant was passed through the bone tunnel by pulling it with a suture, as observed on Figure 70b. Extremities of the implant were sutured to the periosteum and fascia with prolene 3.0 and cut short so it would not point out under the skin, as shown in Figure 70c. Then, muscles and fascias were closed with vicryl 3.0 and the skin was closed with ethilon 3.0 and an elastoplast bandage was placed on the wound.

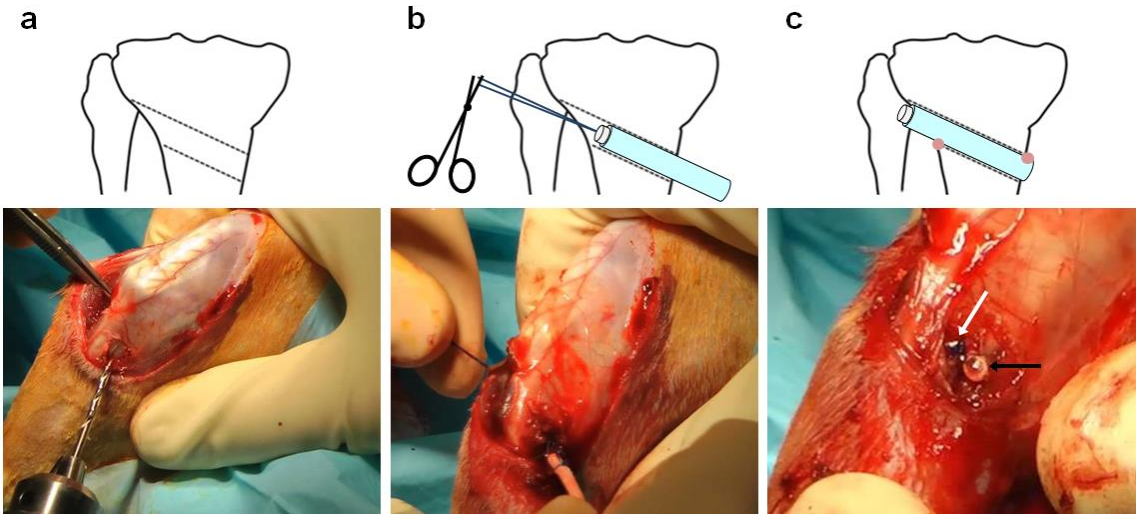

Figure 70 Description and pictures of the implantation protocol, revised from Li et al.23 : **a**) Drilling of a 2 mm slanted bone tunnel in the right tibia, **b**) Insertion of the implant, **c**) Suturing of the implant extremities (black arrow) to the periosteum and fascia with prolene 3.0 suture (white arrow).

Follow-up of the animals

After the procedure the animals were let free of any movement and fed *ad libitum*. They were closely watched and weighted every week. Any sign of complication, nervousness, anorexia or infection of the operated area were carefully looked for. At 6 weeks, the animals were sacrificed for histological examination by an intra-cardiac injection of pentobarbital (1g) after a general anesthesia established as previously mentioned.

Characterization of implant geometry

The implants were observed before and after sterilization with binocular microscopy (M420 Wild-Leitz Leica, Germany) under fully hydrated condition. Dimensional uniformity was assessed by measuring the outer diameter in ten different places along the whole bundle length (5 cm) ($n \geq 2$). An average coating thickness was estimated using ImageJ software from cross-section observation in two different places, by measuring the thickness radially in ten directions evenly distributed. The coating homogeneity was assessed by X-ray microtomography at Laboratoire Navier of Ecole Nationale des Ponts et Chaussées Paristech. HA coated samples were put in glass capillary filled with water and were mounted on the rotation table of an Ultratom (RX solution, France) at 18 mm from the X-ray source (Hamamatsu, Japan) tuned at 80 KeV. During the 360° rotation, 1440 projections (1 sec exposure, resulting in half an hour scans) were recorded by a Paxscan (Varian, USA) flat panel detector (pixel size 127 microns) placed at 460 mm from the source. With this setup, the spatial resolution was 5 µm. 3d reconstruction of the spatial variation of the linear attenuation coefficient µ was achieved using a classical filtered back projection algorithm. Both density and average atomic number of PVA and hydroxyapatite are very different which results in very different values of µ and allows to easily separate both phases. Image analysis and visualization were performed using ImageJ® software and the 3D viewer plugin.[31]

Micro CT scans

At 4 and 6 weeks, the operated area was observed with a micro-computerized tomography scanner (Skyscan 1176, Bruker). The same settings were used for every animal (65kV, 373mA, pixel size: 35mm). Images were reconstructed with softwares furnished by Bruker (NRecon, Dataviewer and CTan). To comply with the 3R's (Replacement-Reduction-Refinement) rules, T_0 were obtained by implanting PVA and HA coated implants in the explanted left (untouched) leg of some of the animals after euthanasia.

Histological study

The explanted knees were fixed in 10% formaldehyde for 7 days, rinsed with water, dehydrated in ethanol (60%, 70%, 80%, 90% and 100%) during 6 days and washed twice with pure xylene for 24 hours. Then the inclusion in poly(methylmethacrylate) (PMMA) was realized in four 48 hours baths as following: Xylene + PMMA; PMMA + dibutyl phtalate; PMMA + 1% catalyser + dibutyl phtalate; PMMA + 2% catalyser + dibutyl phtalate. During the first hour of each bath, they were put under vacuum to prevent air bubbles. The samples were left for 10 days for completion of the inclusion, before being sectioned perpendicular to the longitudinal axis of the bone tunnel with a microtome, mounted on glass slides, ground down to a thickness of 100 µm, polished, and surface-stained with Stevenel blue and van Gieson picrofuchsin. The slides were observed using optical microscopes and scanner (Axio Scope A1, Zeiss, Germany and Aperio, Leica Biosystem, Germany with Calopix software, Tribvn, France).

7.3 Results

Implants characterization

The implants used in this study consisted of 225 continuous PVA fibers. Fibers were assembled into 15 S-twisted threads of 15 Z-twisted fibers. A picture of one bundle is given in Figure 71a. Dry PVA fibers had a diameter of 80±1 µm. Upon immersion in water, they swelled to form PVA hydrogel fibers with an equilibrium water content of 50wt% and a diameter of 110±10 µm.[28] In a first fabrication step, dry bundles were soaked in a 10wt% PVA aqueous solution and subsequently cross-linked to form a bulky cylinder composed of PVA hydrogel fibers embedded in a PVA hydrogel matrix, as shown in Figure 71b. In the following, these pure PVA samples are referred to as PVA implants. In a second step, some of the PVA implants were also coated by dip-coating in a 8wt% PVA aqueous solution containing 40wt% of HA particles. These coated systems were homogenously covered by a layer of HA particles glued together by a PVA hydrogel matrix, as depicted in Figure 71c and d. This coating corresponds to the HA coating with R=0.2 (R=PVA/HA (g/g)) reported in reference 26.[26] In the following, these coated samples are referred to as HA coated implants. More details about the fabrication protocol are given in the Materials&Methods section. The mean diameter is 2.0±0.1 mm for PVA implants and 2.3±0.1 mm for HA coated implants. The sterilization step did not significantly modify the dimensions of the implants, as shown in Figure 71e. In the case of HA coated implants, the thickness of the coating is 230±20 µm.[26]

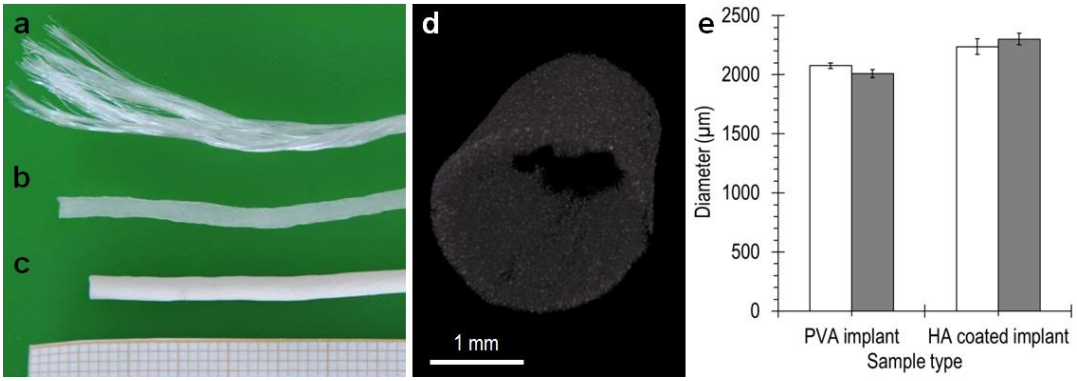

Figure 71 Macroscopic pictures of implants: **a)** dry fiber bundle, **b)** PVA implant, **c)** HA coated implant, **d)** Tomography imaging of HA coated implant, **e)** Outside diameters of PVA implants and HA coated implants before (□) and after (■) sterilization by gamma irradiation.

Implantation and follow-up of the animals

The twelve animals were implanted without major difficulties. Table 6 sums up the animal follow-up.

	PVA implant	**HA coated implant**
Good external healing	5	5
Infectious healing	1	0
Deceased	0	1*
Abnormal behaviour	0	0

(*) Anesthesia issue

Table 6 Follow-up of the animals during 6 weeks post-implantation.

One week after the implantation, six rabbits presented scar splitting without any sign of deep infection, as shown on Figure 72a. This issue was attributed to the rabbits trying to remove their bandages. Rabbits were treated by excision of the wound borders and sutured with ethilon 3.0. After this, bandages were removed from all the animals. During this intervention, one rabbit deceased from the anesthesia and one presented a cutaneous infection that finally healed in four weeks. Animals did not present any sign of abnormal healing and the implanted area regained a healthy aspect five weeks post-implantation, as shown in Figure 72b. In addition, animals had a normal weight gain as compared to the standard weight curve for New Zealand white rabbit, as shown in Figure 72c.

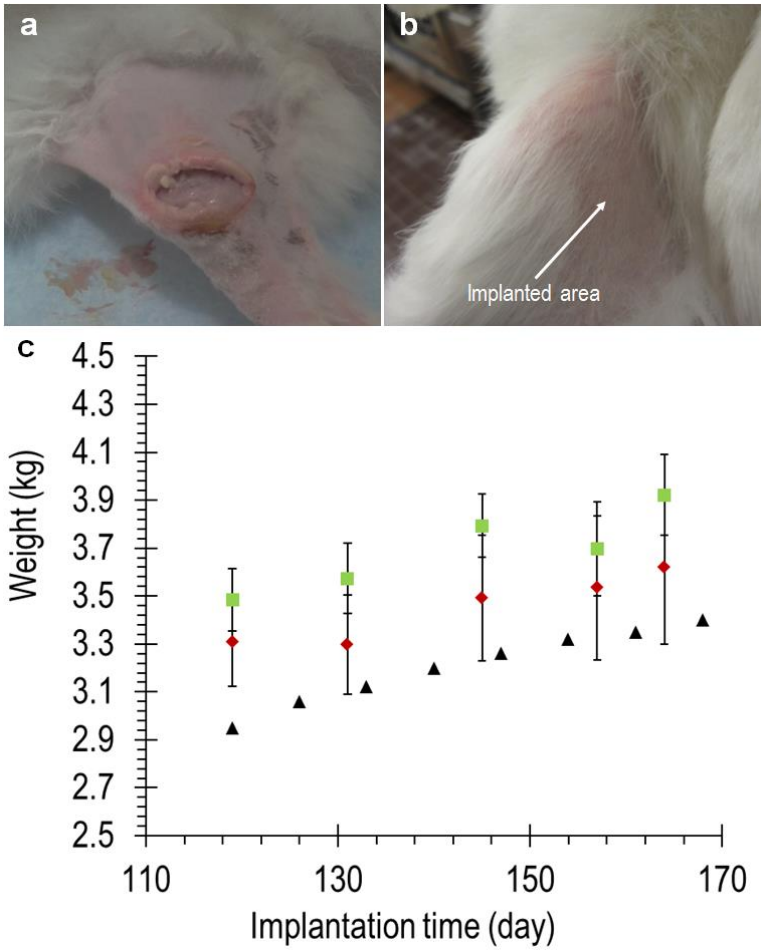

Figure 72 a) Scar splitting after 1 week in 6 rabbits; **b)** Normal healing after 5 weeks; **c)** Evolution of the mean weight during 6 weeks for animals implanted with PVA implant (n=6) (♦), HA coated implants (n=5) (■) and a standard weight curve (▲) of the male New Zealand White rabbit (Harlan Laboratories Inc., USA).

After six weeks, the animals were sacrificed and the implanted area was dissected. The implants had not moved and the sutures were still in place. No macroscopic signs of inflammation or rejection of the implants were noticed. A formation of fibrous tissue was observed at each ends of the bone tunnels. Four rabbits had also their left leg explanted to simulate an initial time point T_0: For that, two PVA and two HA coated implants were inserted in a bone tunnel drilled in these explanted left legs.

Micro-CT scans

Micro-CT scans of the implanted areas were realized on the right leg at four weeks for eight of the rabbits (4 PVA and 4 HA coated implants) and at six weeks for all the rabbits as

well as for the explanted left legs simulating implants at T_0. Figure 73a-b shows sagittal views of the implanted area at T_0 for PVA and HA coated implants, respectively. For both types of implant, the tunnel edges through both cortical walls were clean and sharp, as indicated by white arrows in Figure 73a. A few bone debris caused by drilling were noticed, as pointed by the white star in Figure 73a. PVA hydrogels are radio-transparent and therefore PVA implants could not be seen by micro-CT imaging. On the contrary, for HA coated implant, the HA coating is clearly visible, as pointed by the green arrow on Figure 73b. The contact between HA coated implant and the bone wall was imperfect. Spaces were noticed between the implant surface and the tunnel walls, as pointed by the white dashed arrow in Figure 73b.

Figure 73c-e shows the sagittal views at four and six weeks for PVA and HA coated implants, respectively. No signs of bone resorption were detected and no significant bone tunnels enlargement was noticed. The formation of new bone tissue starting from the internal surface of the cortical bone and progressing toward the middle axis of the tibia along the implant was also observed, as pointed by yellow arrows on Figure 73c-f. This new bone formation was noticed in 4/6 of cases for PVA implants and in 3/5 of cases for HA coated implants. The thickness or length of the newly formed bone tissue was greater in some implants than in others but no correlation was observed with the presence of HA particles.

Due to the radio-transparency of PVA, little information could be obtained about the bone-implant interface for PVA implants. For all HA coated implants, however, a radio-transparent space with a thickness varying between 0 and 200 µm was clearly observed between the bone and the implant surface for all implants, as pointed by the white dashed arrows on Figure 73f. This space suggests the existence of fibrous encapsulation.

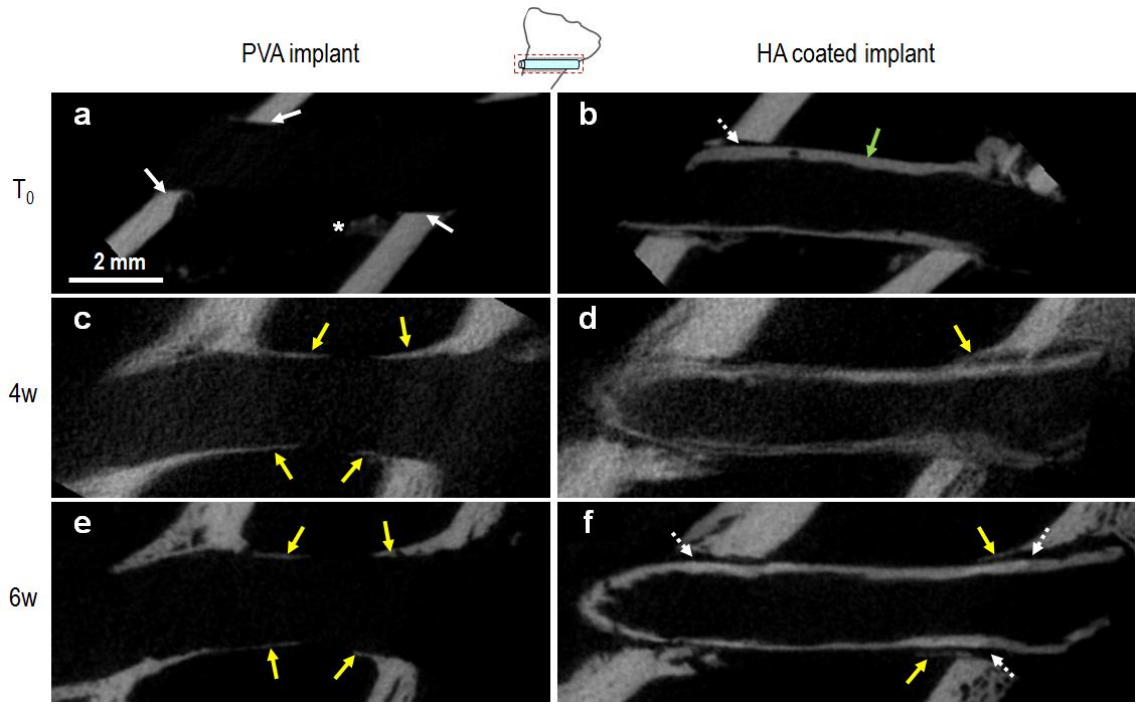

Figure 73 Sagittal views of micro-CT scans of PVA implants (**a**, **c**, **e**) and HA coated implant (**b**, **d**, **f**). Implant at T_0 (**a**, **b**), 4 weeks (**c**, **d**) and 6 weeks (**e**, **f**). White arrow: cortical edge; white star: bone debris; green arrow: HA coating; white dashed arrow: radio-transparent space; yellow arrow: bone formation. Drawings at the top indicate the orientation of the scanned area.

Histology

Figure 74 shows representative histological sections for both PVA and HA coated implants. On these observations, stained host bone (HB) appears pink, PVA implant (PI) is light pink and HA coating (HA) is black, as shown on Figure 74a and d. During the sample preparation, shrinkage of hydrogel implants was induced when replacing water by ethanol, which is not a solvent for PVA. Due to this shrinkage a void was observed between implants and surrounding tissues, as pointed by black dashed arrows on Figure 74b. However, the contour shapes of implants and surrounding tissues match almost perfectly, suggesting that they were in direct contact prior to sample preparation.

For PVA implants, fibers remained together and no debris were found in the surrounding tissues, suggesting that there was no degradation of the implant, as shown in Figure 74a and Figure 74b-c for T_0 and six weeks, respectively. At 6 weeks, implants were

surrounded by a fibrous tissue layer with no direct bone contact, as indicated by black arrows on Figure 74b and c. In some rare places, punctual direct contacts with newly formed bone were noticed, as pointed by yellow arrows in Figure 75a. Based on all observed slices (n=40), the thickness of the fibrous tissue layer was found to be comprised between 0 and 500 µm. In 60% of the observed tissue sections (n=40), newly formed bone tissue was noticed at a remote distance from the implant, as pointed by yellow arrow in Figure 74b. A greater amount of newly formed bone was observed near the cortical edges (Figure 74b) than in the middle of the tibia shaft (Figure 74c).

For HA coated implants, the coatings were mostly intact, as shown in Figure 6d and e for T_0 and 6 weeks, respectively. Nevertheless in four over five explants, detached HA particles were found, as pointed by red stars in Figure 74e and f. These isolated particles were not inflammatory. Similarly to PVA implants, a fibrous tissue layer surrounding the implant was found in all implanted areas, as shown in Figure 74e and f. This fibrous tissue was found to be significantly thinner than with the PVA coated implants. Based on all observed slices (n=33), the thickness has been estimated between 0 and 250 µm. In 76% of tissue sections (n=33), a bone ring surrounding the fibrous tissue was also noticed at a remote distance from the implant. In one explant over five, direct contact with peri-implant new bone was found, as shown in Figure 75b. Similarly to PVA implants, bone formation was more pronounced close to the cortical edges of the bone tunnel (Figure 74e) than in the middle of the tibia shaft (Figure 74f).

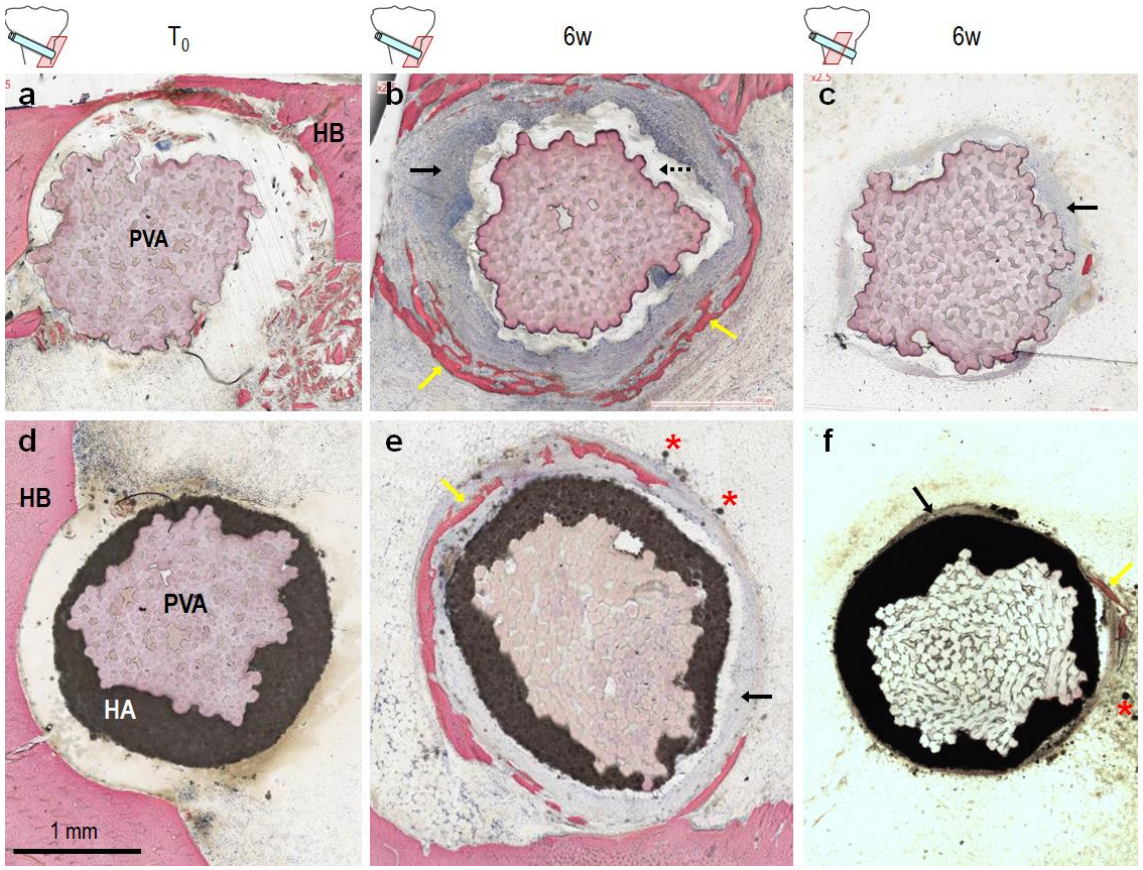

Figure 74 Histological micrographs of implanted area (implant cross-section) for PVA implants(**a**-**c**) and HA coated implants (**d**-**e**). Implant at T_0 (**a**, **d**) and at 6 weeks (**b**,**c**,**e**,**f**). HB: host bone; PVA: PVA implant; HA: HA coating; Black arrows: fibrous tissue; black dashed arrows: void; yellow arrows: neoformed bone; red stars: detached HA particles. Drawings at the top indicate the approximate location of the slice with respect to cortical bone.

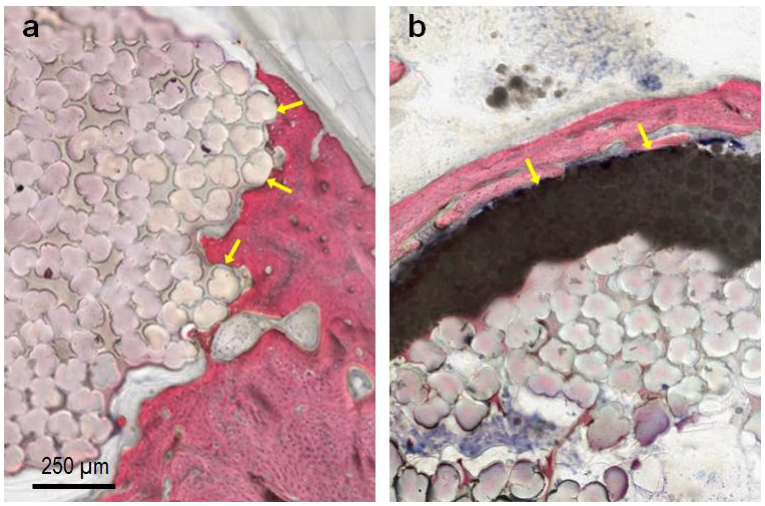

Figure 75 Histological micrographs showing direct contact of PVA implants (**a**) and HA coated implants (**b**) with new bone tissue (yellow arrows).

7.4 Discussion

This study shows that implants based on PVA hydrogel fibers can be assembled in a way that is compatible with implantation requirements. The proposed fabrication process ensured a good repeatability of the shapes and dimensions for both PVA and HA coated implants. All implants were sterilized using gamma-radiation, with a dose (25 kGy) that is used in standard sterilization processes for implant medical devices. The absence of changes in size and colour suggests that this sterilization step has not altered the implants. The sterility of the whole manufacturing process was confirmed by the absence of infection in all the implanted animals.

A good physiological tolerance was reported for both PVA and HA coated implants. The animals did not exhibit behaviour alteration and their weight curves were significantly similar to standard New Zealand White rabbit weight curve (Harlan Laboratories Inc., USA). At a tissue level, micro-CT scans and histological results did not show any sign of bone osteolysis. Between four and six weeks no bone tunnel enlargement has been detected. In all implants, a fibrous tissue layer was surrounding the implants. This fibrous encapsulation looks similar to the one observed by Li *et al.* for PET artificial ligaments after four weeks in exactly the same animal model.[27] Other ligament synthetic substitutes, made of PET, have been implanted by Vaquette *et al.* in sheep.[32] After three months of implantation, the majority of the implants were encapsulated by fibrous tissues layer, with a thickness of around 350 µm.

We compared the bone formation between bare PVA implants and HA coated implants. Observations at T_0, 4, and 6 weeks revealed the formation of new remote bone tissue, as shown by micro-CT scans and histological sections. It was found that the presence of HA particles did not enhance the bone formation, but it seems to have reduced the amount of fibrous tissues around the implants as compared to PVA implants. These results are

consistent with those reported by Li *et al.*.[27] They implanted uncoated, HA, and Bioglass/HA coated PET ligament grafts. At 4 weeks, they did not find any bone formation after addition of HA particles. Conversely, with Bioglass/HA coated implants, new bone tissue was formed in contact with the implant without the formation of a fibrous tissue layer.

The fact that the HA coating had little effects on the osseointegration of the studied implants may be explained by different factors. First of all, the type of ceramic used for the coating might not have been very osseoconductive. In particular, the bioactivity of calcium-phosphate materials is related to their crystallinity, which governs the *in vivo* dissolution and their ability to release ion.[33] In a study by Xue *et al.*,[34] HA coatings with different crystallinities were implanted in the bone marrow and the cortical bone of dog femurs. They showed that the bone formation at short-term (1 month) strongly depends on the crystallinity of HA. HA coatings with low crystallinity (55%) induced higher bone formation than HA coating with high crystallinity (98%). Accordingly, the HA particles used in our study had a high crystallinity greater than 95%, as measured by X-Ray diffraction. The proposed fabrication process could be easily revised to use others particles with lower crystallinity. Another factor may be the insufficient exposure of HA at the surface of the coating. Bioceramic materials, such as HA, are commonly used as pure coating for metallic prosthesis or as pure bulk material for bone substitutes.[35,36] Here, the HA particles are partly embedded in a PVA hydrogel matrix and therefore are not fully exposed at the surface. The HA exposure rate has been previously estimated to 30%.[26] A third factor might be the fact that the initial contact between bone tunnel and implant was not intimate enough. Indeed, the initial affixing of the implant to the host bone is necessary to inhibit micro-motions that prevent formation of peri-implant bone.[37]

7.5 Conclusion

This work reports the first *in vivo* study of PVA hydrogel fiber implants for ligament replacement. The main goal was to assess the *in vivo* tolerance of these implants using a non-loaded and ectopic rabbit model of bone tunnel healing. A second objective was to determine if the quality of the osseointegration of these implants could be improved by an addition of HA particles. Regarding the biocompatibility, a fibrous encapsulation of the implants was observed as it is commonly reported with other PVA substitutes. The absence of bone tunnel osteolysis after 6 weeks and the formation of new bone tissue suggest a good *in vivo* tolerance of PVA implants. The addition of a HA coating did not significantly improved the osseointegration of ligament substitute but has reduced the thickness of the fibrous tissue layer. Based on these results, several modifications could be proposed for an improved design that is more favourable to osseointegration. The relevance of such a system could be explored *in vivo* using a more advanced model that incorporates the cyclic loads applied to ligaments.[38]

Reference

1. Mather, R. C. Societal and Economic Impact of Anterior Cruciate Ligament Tears. *J. Bone Jt. Surg. Am.* **95,** 1751 (2013).

2. Paessler, H. H., Mastrokalos, D. S. & Motsis, E. K. New techniques for anterior cruciate ligament revision surgery. *Acta Clin.* **2,** 48–60 (2002).

3. Renstrom, P. A. Eight clinical conundrums relating to anterior cruciate ligament (ACL) injury in sport: recent evidence and a personal reflection. *Br. J. Sports Med.* **47,** 367–372 (2013).

4. Kartus, J., Movin, T. & Karlsson, J. Donor-site morbidity and anterior knee problems after anterior cruciate ligament reconstruction using autografts. *Arthrosc. J. Arthrosc. Relat. Surg.* **17,** 971–980 (2001).

5. Mascarenhas, R. & MacDonald, P. B. Anterior cruciate ligament reconstruction: a look at prosthetics-past, present and possible future. *McGill J. Med. MJM* **11,** 29 (2008).

6. Legnani, C., Ventura, A., Terzaghi, C., Borgo, E. & Albisetti, W. Anterior cruciate ligament reconstruction with synthetic grafts. A review of literature. *Int. Orthop.* **34,** 465–471 (2010).

7. Guidoin, M.-F. *et al.* Analysis of retrieved polymer fiber based replacements for the ACL. *Biomaterials* **21,** 2461–2474 (2000).

8. Vunjak-Novakovic, G., Altman, G., Horan, R. & Kaplan, D. L. Tissue engineering of ligaments. *Annu. Rev. Biomed. Eng.* **6,** 131–156 (2004).

9. Laurencin, C. T. & Freeman, J. W. Ligament tissue engineering: An evolutionary materials science approach. *Biomaterials* **26,** 7530–7536 (2005).

10. Leong, N. L., Petrigliano, F. A. & McAllister, D. R. Current tissue engineering strategies in anterior cruciate ligament reconstruction: ACL Tissue Engineering. *J. Biomed. Mater. Res. A* **102,** 1614–1624 (2014).

11. Ge, Z., Yang, F., Goh, J. C. H., Ramakrishna, S. & Lee, E. H. Biomaterials and scaffolds for ligament tissue engineering. *J. Biomed. Mater. Res. A* **77A,** 639–652 (2006).

12. Chen, T., Jiang, J. & Chen, S. Status and headway of the clinical application of artificial ligaments. *Asia-Pac. J. Sports Med. Arthrosc. Rehabil. Technol.* **2,** 15–26 (2015).

13. Pan, X., Wen, H., Wang, L. & Ge, T. Bone–patellar tendon–bone autograft versus LARS artificial ligament for anterior cruciate ligament reconstruction. *Eur. J. Orthop. Surg. Traumatol.* **23,** 819–823 (2013).

14. Parchi, P. D. *et al.* Anterior cruciate ligament reconstruction with LARS^{TM} artificial ligament results at a mean follow-up of eight years. *Int. Orthop.* **37,** 1567–1574 (2013).

15. Shen, G., Xu, Y., Dong, Q., Zhou, H. & Yu, C. Arthroscopic Posterior Cruciate Ligament Reconstruction Using LARS Artificial Ligament: A Retrospective Study. *J. Surg. Res.* **173,** 75–82 (2012).

16. Viateau, V. *et al.* Biological and Biomechanical Evaluation of the Ligament Advanced Reinforcement System (LARS AC) in a Sheep Model of Anterior Cruciate Ligament Replacement: A 3-Month and 12-Month Study. *Arthrosc. J. Arthrosc. Relat. Surg.* **29,** 1079–1088 (2013).

17. Sciarretta, F. V. 5 to 8 years follow-up of knee chondral defects treated by PVA-H hydrogel implants. *Eur. Rev. Med. Pharmacol. Sci.* **17,** 3031–3038 (2013).

18. Kobayashi, M., Chang, Y.-S. & Oka, M. A two year in vivo study of polyvinyl alcohol-hydrogel (PVA-H) artificial meniscus. *Biomaterials* **26,** 3243–3248 (2005).

19. Allen, M. J. *et al.* Preclinical evaluation of a poly (vinyl alcohol) hydrogel implant as a replacement for the nucleus pulposus. *Spine* **29,** 515–523 (2004).

20. Hou, R. *et al.* Magnetic nanohydroxyapatite/PVA composite hydrogels for promoted osteoblast adhesion and proliferation. *Colloids Surf. B Biointerfaces* **103,** 318–325 (2013).

21. Hayami, T., Matsumura, K., Kusunoki, M., Nishikawa, H. & Hontsu, S. Imparting cell adhesion to poly(vinyl alcohol) hydrogel by coating with hydroxyapatite thin film. *Mater. Lett.* **61,** 2667–2670 (2007).

22. Rodrigues, A. A. *et al.* In vivo evaluation of hydrogels of polyvinyl alcohol with and without carbon nanoparticles for osteochondral repair. *Carbon* **50,** 2091–2099 (2012).

23. Maher, S. A. *et al.* Nondegradable hydrogels for the treatment of focal cartilage defects. *J. Biomed. Mater. Res. A* **83A,** 145–155 (2007).

24. Wang, M. *et al.* In vitro andin vivo study to the biocompatibility and biodegradation of hydroxyapatite/poly(vinyl alcohol)/gelatin composite. *J. Biomed. Mater. Res. A* **85A,** 418–426 (2008).

25. Song, W., Markel, D. C., Jin, X., Shi, T. & Ren, W. Poly(vinyl alcohol)/collagen/hydroxyapatite hydrogel: Properties and *in vitro* cellular response. *J. Biomed. Mater. Res. A* **100A,** 3071–3079 (2012).

26. Moreau, D., Villain, A., Ku, D. N. & Corté, L. Poly(vinyl alcohol) hydrogel coatings with tunable surface exposure of hydroxyapatite. *Biomatter* **4,** e28764 (2014).

27. Li, H. *et al.* Composite coating of 58S bioglass and hydroxyapatite on a poly (ethylene terepthalate) artificial ligament graft for the graft osseointegration in a bone tunnel. *Appl. Surf. Sci.* **257,** 9371–9376 (2011).

28. Bach, J. S. *et al.* Hydrogel fibers for ACL prosthesis: Design and mechanical evaluation of PVA and PVA/UHMWPE fiber constructs. *J. Biomech.* **46,** 1463–1470 (2013).

29. Peppas, N. A. & Stauffer, S. R. Reinforced uncrosslinked poly (vinyl alcohol) gels produced by cyclic freezing-thawing processes: a short review. *J. Controlled Release* **16,** 305–310 (1991).

30. Stauffer, S. R. & Peppas, N. A. Poly(vinyl alcohol) hydrogels prepared by freezing-thawing cyclic processing. *Polymer* **33,** 3932–3936 (1992).

31. Schmid, B., Schindelin, J., Cardona, A., Longair, M. & Heisenberg, M. A high-level 3D visualization API for Java and ImageJ. *BMC Bioinformatics* **11,** 274 (2010).

32. Vaquette, C. *et al.* The effect of polystyrene sodium sulfonate grafting on polyethylene terephthalate artificial ligaments on in vitro mineralisation and in vivo bone tissue integration. *Biomaterials* **34,** 7048–7063 (2013).

33. Dorozhkin, S. Calcium Orthophosphate-Based Bioceramics. *Materials* **6,** 3840–3942 (2013).

34. Xue, W., Liu, X., Zheng, X. & Ding, C. Effect of hydroxyapatite coating crystallinity on dissolution and osseointegrationin vivo. *J. Biomed. Mater. Res. A* **74A,** 553–561 (2005).

35. Hench, L. L. Bioceramics: from concept to clinic. *J. Am. Ceram. Soc.* **74,** 1487–1510 (1991).

36. Huracek, J. & Spirig, P. The effect of hydroxyapatite coating on the fixation of hip prostheses. *Arch. Orthop. Trauma Surg.* **113,** 72–77 (1994).

37. Mavrogenis, A. F., Dimitriou, R., Parvizi, J. & Babis, G. C. Biology of implant osseointegration. *J Musculoskelet Neuronal Interact* **9,** 61–71 (2009).

38. Bachy, M. *et al.* Anterior cruciate ligament surgery in the rabbit. *J. Orthop. Surg.* **8,** 27 (2013).

Section 4. Hydrogel films by swelling induced gelation

In Chapter 6, we explored a process, based on a combination of dip-coating and physical cross-linking, to produce composite coatings of PVA hydrogel and HA particles on hydrogel substrates. During the study of the process, we noticed that the thickness of the coating depended on the swelling state of the substrate. In this section, we study how to grow a hydrogel film or a composite coating at the surface of a swelling polymer substrate and how to control their quality and thickness.

In chapter 8, we report a new approach to make hydrogel films by inducing the local gelation of a polymer solution at the surface of a swelling polymer substrate. Using a synthetic biocompatible polymer (polyvinyl alcohol), we show how the growth rate and final thickness of these hydrogel films can be finely adjusted by tailoring the solution composition and the swelling dynamics of the substrate.

In collaboration with the Toxicology Pharmacology and Cellular Signaling (INSERM UMR-S 1124) laboratory of the Paris-Descartes University, we devise and test several protocols to encapsulate mammalian cells within PVA hydrogels films. The protocol of swelling induced gelation was adapted to cell manipulation and culture. With these exploratory experiments, we show that cells can be encapsulated in PVA hydrogel films, which remain viable for 48 hours.

Chapter 8. Hydrogel films by swelling induced gelation

8.1 Introduction

In chapter 6, composite coatings of poly(vinyl alcohol) (PVA) hydrogel and hydroxyapatite (HA) particles have been produced by a combination of dip-coating and physical cross-linking. During the study of the process, we noticed an interesting phenomenon: when dry hydrogel substrate was soaked in PVA/HA aqueous solution, a thick coating was obtained around it. Whereas when the substrate was previously swollen, the coating was much thinner. This suggests that the thickness of the coating strongly depends on the swelling state of the substrate. Knowing the peculiar gelation property of PVA, we took advantage of this phenomenon to develop a new gelation method to produce hydrogel films and coatings.

The proposed approach relies on the transport phenomena occurring near the surface of a polymer network swelling in a polymer solution, as illustrated in Figure 76a. Let Φ be the polymer volume fraction of the solution. Upon immersion in this solution, the polymer strands of the network get solvated and the network swells in a diffusive manner. If the chains in solution are much larger than the network mesh size, they are expelled from the volume spanned by the gel. Due to mass conservation, a flux of solvent $\vec{J_S} = -\Phi_p \vec{V}$ is created into the gel, where $\vec{V}$ is the speed of the network-solution interface. For dilute solutions ($\Phi_0 \lesssim 0.01$), chains do not overlap with each other and diffuse like colloidal particles. This random thermal motion is largely dominant and this suction effect at the surface of the swelling network should alter little the solution homogeneity. Different situations are expected for semi-dilute and concentrated solutions ($\Phi_0 \gtrsim 0.01$) where chains are entangled and their collective diffusion is much slower than in the dilute regime. In such situations, thermal diffusion may

not be fast enough to homogenize the solution and the solvent depletion effect should self-amplify: solvent suction creates an increase in polymer concentration at the surface of the swelling network, therefore more chains are expelled upon further swelling, which in turn increases even more the local polymer concentration at the surface.

Such swelling induced process should be particularly strong for semi-dilute solutions of associative polymers, which collective diffusion decreases considerably with increasing concentration. For example, it could explain the results reported by Budtova and Navard where swelling of a polyelectrolyte gels in aqueous solutions of hydroxypropyl cellulose induced a concentration gradient near the swelling surface and a transition in the solution from isotropic to crystal liquid states.[1,2] From birefringency measurements, concentrations as high as 80% were measured in a 5-µm thick layer close to the surface of the gel substrate after 8 min of swelling. Here, we propose to take advantage of this solvent depletion at the surface of swelling substrates to induce the gelation and growth of hydrogel films.

Our approach is based on the simple idea depicted in Figure 76b. It uses the property of some aqueous polymer solutions to form physical gels at high concentration. First, a dry network of hydrophilic polymer is used as a swelling substrate and is immersed into such a solution (step i). As the substrate swells, the concentration in polymer increases at its surface due to the solvent depletion effect described above (step ii). At a given level of swelling, the polymer concentration close to the substrate surface becomes so high that polymer chains associate with each other and form physical cross-links (step iii). As swelling proceeds, cross-linking density increases until the gel point is reached and a hydrogel film is formed at the surface of the substrate (step iv).

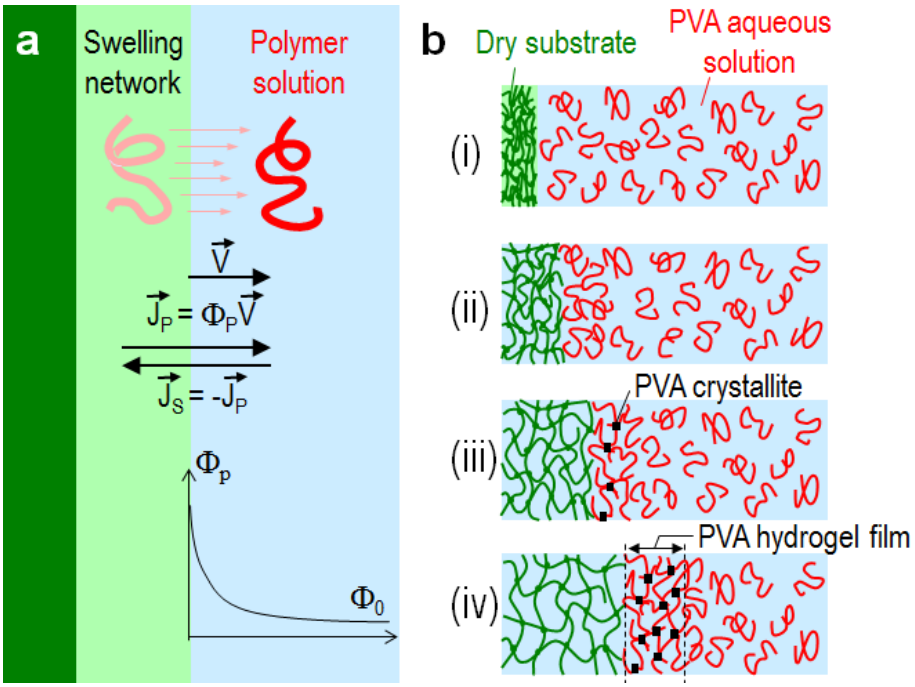

Figure 76 a) Schematic drawing of the mass transport phenomenon of the surface of a swelling substrate in a polymer solution; **b**) Schematic drawing of the swelling induced gelation concept.

Aqueous solutions of PVA were chosen to produce hydrogel films by this process. PVA is one of the few polymers that gel spontaneously at high concentration in aqueous solutions.[3] It is widely used today as a hydrogel forming polymer to make paper coatings,[4] filtration membranes,[5,6] matrices for cell encapsulation,[7,8] phantom tissue for imaging[9] or implants for soft tissue reconstruction.[10,11] At high concentration in water, PVA chains associate through hydrogen bonds between their numerous OH polar groups and eventually form stable PVA crystallites that remain insoluble below 80-90°C.[12] Physical PVA hydrogels are obtained when the cross-linking produced by these crystallites goes beyond reticulation. Various methods have been developed to induce this physical gelation, using solvent evaporation,[13] confinement between ice crystals by freezing-thawing,[14] osmotic pumping in a poor solvent like methanol.[15]

8.2 Materials & Method

Fabrication of polymer solutions:

Poly(vinyl alcohol) (PVA) aqueous solutions were fabricated with high molecular weight (89,000–98,000 g·mol^{-1}) and 99%-hydrolyzed PVA (Sigma-Aldrich). PVA powder was dissolved in ultra-pure water under mechanical stirring and using a silicon oil bath heated to 110°C for 60 min to produce 1, 2.5, 5, 7.5, 10 and 15 wt% PVA aqueous solutions. The weight of the solutions was measured after dissolution and water was added to correct from evaporation. The solutions were then covered, let to cool down and degas.

Poly(vinyl pyrrolidone) (PVP) aqueous solutions were fabricated form PVP with a molecular weight of 40,000 g.mol^{-1}(Sigma-Aldrich). PVP powder was dissolved under mechanical stirring in ultra-pure water using a silicon oil bath heated to 60°C for 60 min to produce 10 wt% PVP aqueous solutions. The weight of the solutions was measured after dissolution and water was added to correct from evaporation. The solution was then covered, let to cool down and degas.

Poly(ethylene glycol) (PEG) aqueous solution were fabricated with high molecular weight (100,000 g·mol^{-1}) PEG (Sigma-Aldrich). PEG powder was dissolved in ultra-pure water at 20°C under mechanical stirring to obtain 10 and 20 wt% PEG aqueous solution.

Gel substrates:

PAAm hydrogels substrates were made from a 40 wt% solution of acrylamide/N,N'-methylene-bisacrylamide (AA/MBA), with a ratio of 37.5:1 (Sigma-Aldrich). Ammonium persulfate (KPS) (Sigma-Aldrich) was used as the initiator. N,N,N′,N′-Tetramethylethylenediamine (TEMED) (Sigma-Aldrich) was used as cross-linking catalyst. A 12 vol% aqueous solution of AA-MBA was first prepared by diluting the 40 wt% solution in ultra-pure water. A 10 wt% aqueous solution of KPS was prepared and added to aqueous

solution of AA-MBA. Then TEMED was added, and the whole solution was stirred and quickly poured in a glass mold of 100 mm x 130 mm x 5 mm. The obtained gel plate was cut in small rectangular pieces and the obtained substrates were dried in air at 20°C under extractor hood for 24 hours.

Spherical substrates were obtained from commercially available gel beads composed of a copolymer of poly(acrylic acid)-poly(acrylamide) (PAAc-PAAm) ("Perles d'eau", Casa, France). They are composed of polyacrylic acid (0.6 wt%), polyacrylamide (0.2 wt%), sodium salt (0.2 wt%) and ultra-pure water (99 wt%). For the experiments, beads were dried at 20°C under extractor hood for 24 hours.

PEG substrates were obtained by solvent cast from a 20wt% aqueous solution. The solution was cast in Petri dishes and dried in a vacuum oven at 700 mbar and 70°C for 12 hours.

Cylinder substrates of PVA were obtained by physical crosslinking of a 10wt% PVA aqueous solution in 4 mm diameter cylindrical molds. Cross-linking of the PVA solution was obtained by the freezing/thawing method[16] as follows. The molds were placed in a freezer at -20°C for 19 h and then back to 20°C for 5 h. This cycle was repeated five times. Then selected PVA cylinders were dried at 20°C under extractor hood for 24 hours.

PVA hydrogel film formation on flat substrate:

PVA films were fabricated by soaking dried rectangular 3 mm-thick PAAm substrates of in 10 and 15 wt% PVA for 3 to 22 hours. Then coated substrates were removed from polymer solution and vigorously rinsed in large amount of ultra-pure water for 15 minutes. Then the films were detached from the substrates, attached to a fishhook and stored in glass tubes filled with ultra-pure water.

Films stability in water was assessed by soaking the films at 20°C or at 90°C in an oil bath. Pictures were taken with a Nikon D300s camera at different times.

The crystallization of PVA films was confirmed by X-ray diffraction measurement performed on the DiffAbs beamline at Synchrotron SOLEIL facility (France). The PVA hydrogel films were mounted in a plastic frame and were maintained between two 25 µm-thick mica windows at a constant distance of 2.7 mm. The samples were illuminated with a monochromatic X-ray beam tuned at 10 keV. The wave length was λ=1.2424 Å. An area detector (MAR345 image plate) was placed at 188 mm downstream of the sample. The exposure time was 30 sec. A Pb beamstop was used to block the intense transmitted beam through the PVA hydrogel samples. A Si diode placed in the centre of the beamstop served to record the transmitted beam intensity through the sample. Synchrotron diffraction images were analyzed using Fit2D software.[17]

Characterization of film growth on spherical beads:

The follow-up of film growth was performed with a macroscope (M420 Wild-Leitz, Leica) at 6.3 and 20 magnifications. Beads were disposed in Petri dishes filled with polymer solutions at different concentrations. Petri dishes were placed on an X-Y moving-stage. Film formation was recorded at various time ranging from 2 min to 24 h. Film thickness was estimated by image analysis done with ImageJ® software,[18] by subtracting the diameter of the gel bead to the diameter of the film around the gel bead. Measurement for each configuration was estimated over 2 to 5 beads.

Fabrication of composite coatings:

Two types of HA particles were used to fabricate composite ceramic-hydrogel coatings: a medical grade powder of HA micro-particles with diameter ranging from 5 to 25 µm (Dv10= 4.4 µm; Dv50=13.5 µm; Dv90= 23.7 µm) (S.A.I., Medical Group, France) and HA nano-particles with diameter smaller than 200 nm (Sigma-Aldrich). For HA micro-particles, granulometry analysis was done by dry dispersion using a Malvern Mastersizer 3000 particle size analyzer. Solutions of HA micro- and nano-particles were prepared by

dispersing 20 wt% of micro- and 5 wt% of nano-particles in 10 wt% PVA aqueous solutions under mechanical stirring for 5 min. The solutions were then covered and put in ultra-sonic bath to remove air bubbles and to refine particle homogenization.

Dry PAAc-PAAm beads were soaked in micro-particles and nano-particles for 30 and 60 min, respectively. Then coated beads were collected and rinsed in ultra-pure water bath under magnetic stirring for 15 min to removed uncrosslinked PVA/HA solution. Immediately after rinsing, coated PAAc-PAAm beads were cut at the equator using a fresh razor blade and observed as described in the following. The structure of composite coatings was characterized by optical microscopy and scanning electron microscopy (SEM) using secondary electron detector. Optical microscopy was performed with an Axio Scope A1 Zeiss apparatus on hydrated samples. Observations were made in dark field reflection mode at a 5x magnification. SEM observation was performed on a Nova Nano SEM 450 SEI apparatus in low-vacuum mode at 90 Pascal and 5 kV. Low-vacuum mode does not require sample metallization and allows observation in semi-hydrated state for the first ten minutes.

Dry and swollen PVA cylinders were soaked for 60 min in the PVA solution containing micro-particles. Then the coated cylinders were collected and vigorously rinsed by hand in an ultra-pure water bath for 5 min to removed uncross-linked PVA/HA solution. Additional cross-linking of the coating was done by one freezing/thawing cycle. The structure of composite coatings was then characterized by X-ray micro-tomography.

Tomography measurement:

PVA hydrogel cylinders coated with PVA/HA films were embedded in quartz capillary filled with water and were observed by X-ray micro-tomography at the Navier laboratory of the Ecole Nationale des Ponts et Chaussées. The specimen was mounted on the rotation table of an Ultratom (RX solution, France) at 18 mm from the X-ray Source (Hamamatsu, Japan) tuned at 80 KeV. During the 360° rotation, 1440 projections (1 sec

exposure, resulting in half an hour scans) were recorded by a Paxscan (Varian, USA) flat panel detector (pixel size 127 microns) placed at 460 mm from the source. With this setup, the spatial resolution was 5 micrometer. 3d reconstruction of the spatial variation of the linear attenuation coefficient μ was achieved using a classical filtered back projection algorithm. Both density and average atomic number of PVA and hydroxyapatite are very different which results in very different values of μ and allows to easily separate both phases. Image analysis visualization was performed using Avizo7 (VSG, FEI group) dedicated software using a combination of isosurfaces and volume rendering techniques.

8.3 Results & Discussion

A simple experiment demonstrates the actual formation of PVA hydrogel films by the proposed swelling induced gelation method. It is described in Figure 77a. 3mm-thick films of chemically cross-linked poly(acrylamide) (PAAm) were used as dry substrates. These PAAm films swell in water within 90 h to form 5.6±0.1 mm-thick hydrogel films containing about 90 wt% water. In this experiment, the dry PAAm films were immersed in 10 and 15 wt% PVA aqueous solutions and left to swell for 3 to 22h. The swollen films were then removed from the solution and rinsed in water under vigorous stirring for 15 min to remove uncrosslinked residual PVA aqueous solution. For all the concentration and immersion time, solid films of PVA hydrogel could be peeled off from the surface of the substrates immediately after rinsing. This is shown in Figure 77b for a soaking time of 3h in a 15 wt% PVA solution. These films remained insoluble in water at 20°C for over a week, as shown in Figure 77c and d for a soaking time of 3h in a 10 wt% PVA solution and of 19h in 15 wt% PVA solution, respectively. However, these films dissolved in less than one hour at 90°C, as shown in Figure 77d for a soaking time of 19h in 15 wt% PVA solution. This confirms the formation of a

physical PVA hydrogel, for which the crystallites acting as cross-links melt in water above 85°C.12

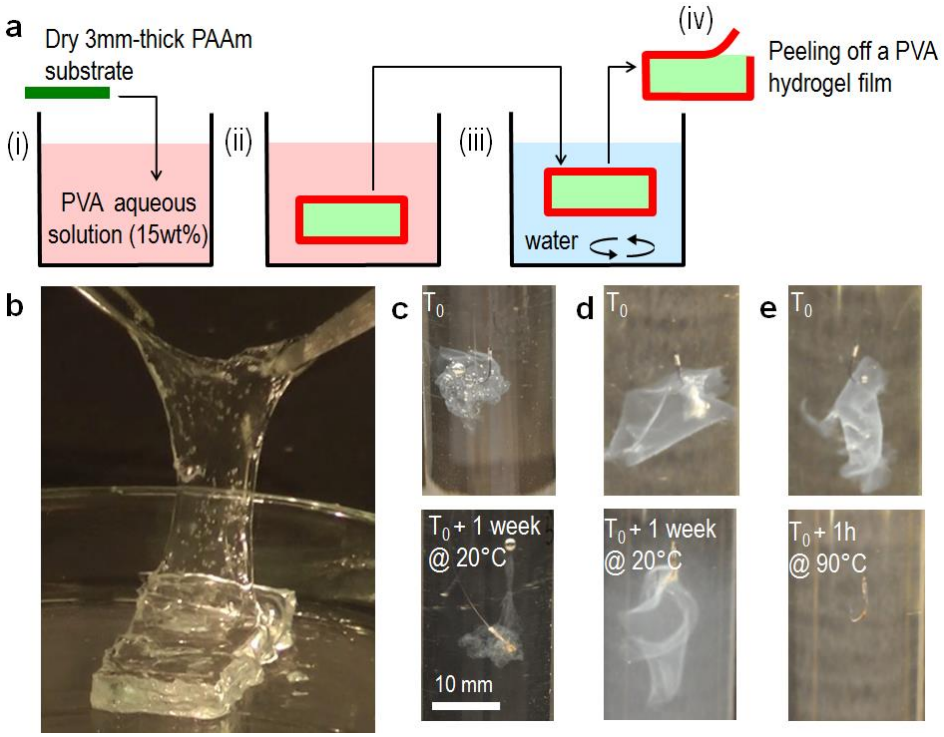

Figure 77 a) Schema of the swelling induced gelation experiment using a PAAm substrate in a 15 wt% PVA aqueous solution; **b**) Peeling off a PVA hydrogel film from a PAAm substrate; **c-d**) Stability experiment done on PVA hydrogel films produced by soaking of PAAm substrates in 10 wt% PVA aqueous solutions for 3h and in 15 wt% PVA aqueous solution for 19h, respectively; **e**) Dissolving of PVA hydrogel films produced by soaking of PAAm substrates in 15 wt% PVA aqueous solution for 19h.

Furthermore, the formation of PVA crystallites in the so-formed films was observed by wide-angle X-ray scattering. This experiment has been performed with PVA hydrogel films obtained by swelling induced gelation using PAAm substrates soaked in 15 wt% PVA solution for 3, 8 and 22 h and with PVA hydrogel films obtained by 5 cycles of freezing/thawing. It revealed the main Bragg peak of PVA crystals, as shown in Figure 78a. The diffraction profile of PVA hydrogel films in the different states exhibits a peak centered at $2\theta \approx 15.7°$ (d=4.55 Å), which corresponds to the $(10\bar{1})$ plan, typical of the PVA crystal structure.[19] This is consistent with the intense $(10\bar{1})$ peak observed with PVA hydrogel films obtained from a 15 wt% PVA solution cross-linked by five freezing/thawing cycles.

Accordingly, no such peak is observed from pure water. The relative intensity of the peaks, given in Figure 78b, was estimated by measuring the colored areas in Figure 78a. It indicates that the crystallinity of the film increases with the soaking time, but it might be also due to the effect of aging and not only the one of swelling induced gelation.

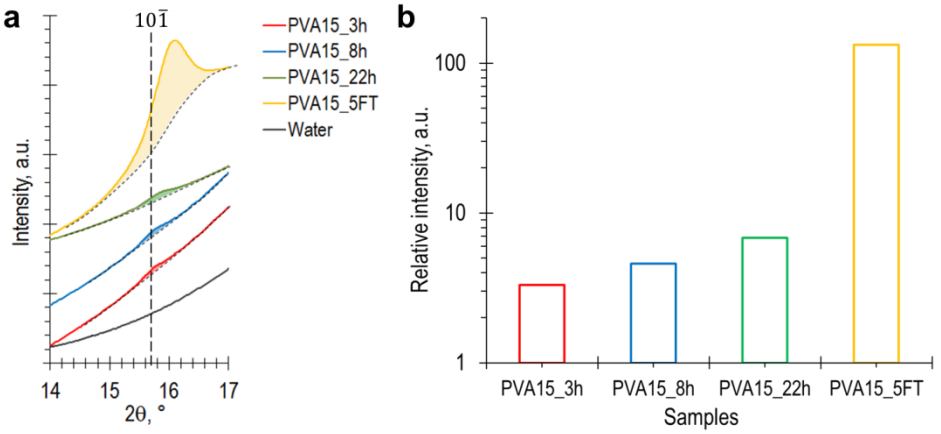

Figure 78 a) X-ray diffraction spectra of PVA hydrogel films produced by swelling induced gelation and compared to film prepared by freezing/thawing (5 cylces) and pure water; **b**) Relative intensity of the peaks underlined in (**a**).

The mechanisms of this hydrogel film formation were characterized quantitatively in other experiments. Spherical substrates were immersed in aqueous solutions and observed from the top by optical microscopy, as depicted in Figure 79a. By this mean, both the swelling process and the formation of a hydrogel film at the substrate-solution interface were continuously monitored. Spheres of poly(acryl amide)-poly(acrylic acid) (PAAm-PAAc) hydrogels containing a green dye were used as the swelling substrates, as shown in Figure 79b. In their dry state, these spheres have a radius of 2.50±0.05 mm. When they were immersed in pure water, they reached equilibrium swelling in about 400 min with a radius of 13.0±0.1 mm, which corresponds to a swelling ratio of 140±15. During swelling, the substrate-solution interface was clearly distinguished as a sharp line at the equator of the swelling spheres. This is shown in Figure 79d after 60 min of immersion (swelling ratio = 73).

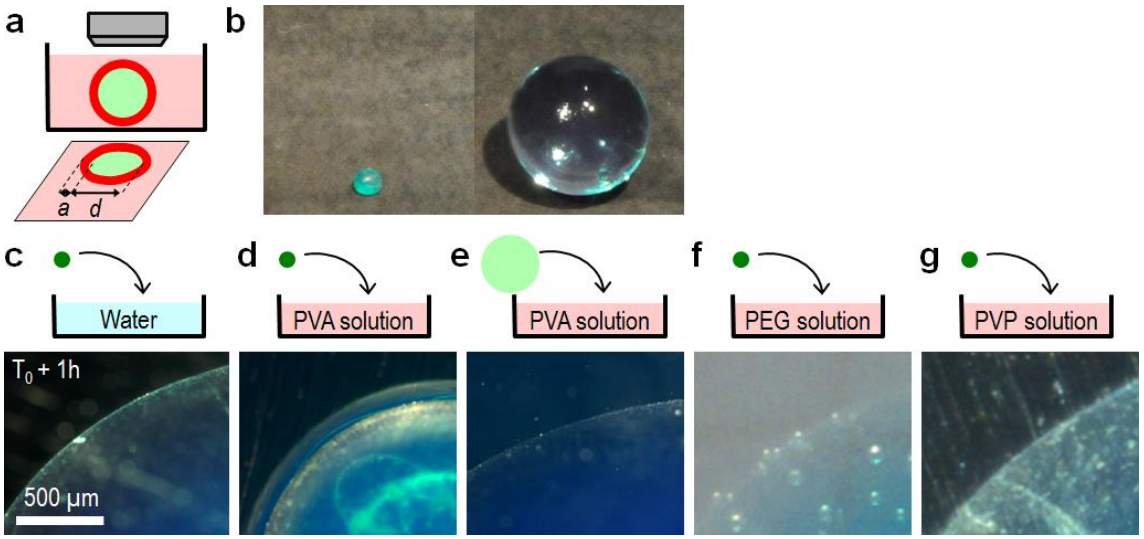

Figure 79 a) Schema of the observation technique to follow the swelling kinetic and the film growth around PAAm bead; **b**) Dry and swollen PAAm beads; Microscopic observation of the equator of dry PAAm beads swollen in pure water (**c**), in 10 wt% PVA aqueous solution (**d**), in 10 wt% PEG aqueous solution (**f**), in 10 wt% PVP aqueous solution (**g**) and swollen PAAm bead soaked in 10 wt% PVA aqueous solution (**e**) after 1 h.

The formation and growth of a PVA hydrogel film was observed when the dry PAAm-PAAc spheres were immersed in PVA solutions. In those cases, a second larger circle appeared concentric with the substrate equator as shown in Figure 79d for a sphere swelling in a 10wt% PVA solution after 60 min of immersion (swelling ratio = 7). This second line corresponds to the interface between a cross-linked PVA hydrogel film and the PVA solution, as seen when detaching the PVA film under the microscope (Figure 80a and b).

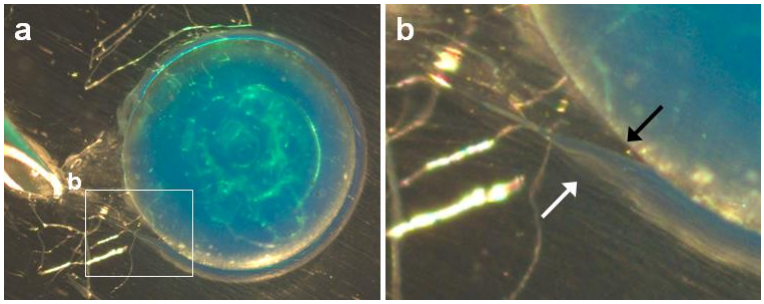

Figure 80 a-b) Microscopic observation of the *in-situ* detachment of a PVA hydrogel film (white arrow) formed at the surface of a PAAm bead (black arrow) swelling in a 10 wt% PVA aqueous solution after 1 h.

Control experiments confirmed that the formation of these PVA hydrogel films was induced by the swelling process and was not the result of some peculiar affinity with the

substrate. For that, PAAm-PAAc spheres were swollen to equilibrium in pure water prior to immersion in the PVA solution. As expected, the sphere diameter decreased due to osmotic deswelling but no hydrogel film was observed at the sphere surface even after 15 hours of immersion, as shown in Figure 79e for a 10wt% PVA solution after 60 min of immersion (swelling ratio = 96). In other control experiments, we verified that no hydrogel films were produced when dry PAAm-PAAc spheres were immersed in 10wt% aqueous solutions of poly(ethylene glycol) (PEG) and poly(vinyl pyrrolidone) (PVP), which do not have the same ability as PVA to gel at high concentration, as shown in Figure 79f and g, respectively.

The swelling of the substrate and thickness of PVA hydrogel films were observed during immersion in PVA solutions with concentrations ranging from 0 to 15wt%, as shown by time-sequences in Figure 81a to e for 1, 2.5, 5, 10 and 15 wt%, respectively. The thickness of the PVA hydrogel film was determined by a specific imaging method, using a macroscope and two methods of lighting used separately in order to distinguish the film and the substrate surface boundaries. The first method was in-lens lighting and was used to reveal the film boundary, as shown in Figure 82a. The second method was achieved by using optical fibers mounted parallel to the Petri dishes, in order to create an oblique incident lighting, as shown in Figure 82b. This second lighting revealed the boundary of the substrate surface.

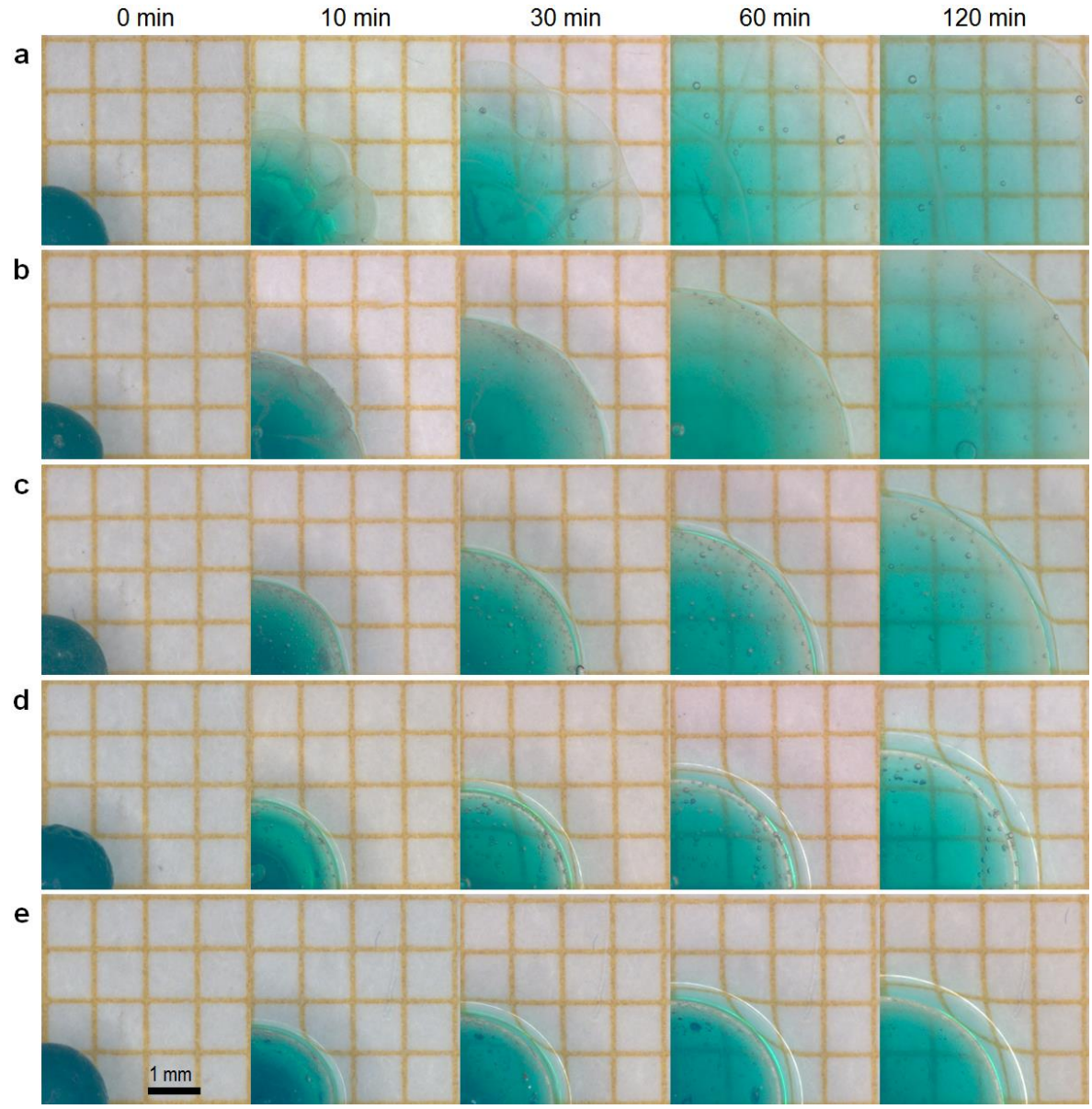

Figure 81 Time sequence observations of the film formation at the surface of PAAm beads swelling in 1 (**a**), 2.5(**b**), 5 (**c**), 10 (**d**) and 15 (**e**) wt% PVA aqueous solution.

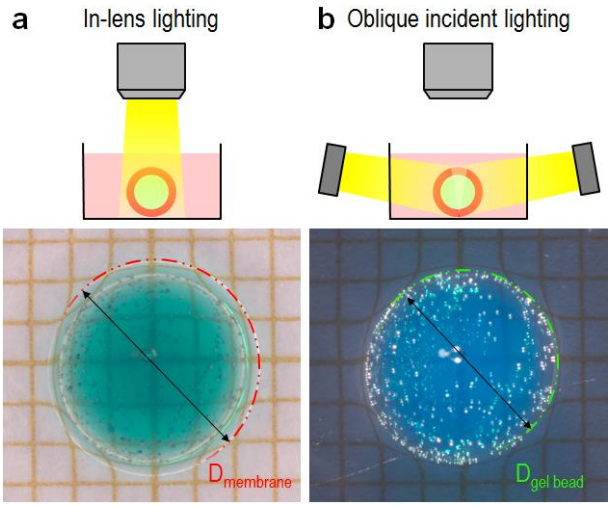

Figure 82 Measurement method: **a**) Film surface observation by in-lens lighting; **b**) Substrate surface observation by oblique incident lighting.

Figure 83a shows the swelling kinetics of dry PAAm-PAAc spheres in PVA solutions with concentrations ranging from 0 to 15wt%. In all the cases, most of the swelling occurred in the first 4 hours and equilibrium was eventually reached after about 15 hours. The extent of swelling decreased with increasing PVA concentration due to the osmotic pressure created by solubilized PVA chains. These swelling curves are well-fitted by the theoretical prediction for gel swelling. Here, the diffusivity equation is given the simpler case of one dimensional swelling (e.g. a thin network film attached to a substrate) and writes:[20,21]

$$R(t) = R_0 + (R_\infty - R_0)\frac{(D_n t)^{1/2}}{R_0} \quad (1)$$

Where, R_0 is the initial radius of the sphere, R_∞ is the equilibrium swelling radius of the sphere and D_n is the diffusivity coefficient of the network. The diffusivity coefficients D_n have been estimated from fits of the experimental curves using Equation 1 and are plotted in Figure 83b (Details about fitting are given in Appendix 2). As concentration increased above the overlap concentration (C* ~ 2.6 wt%),[22] a sharp drop in D_n is observed. This suggests that the swelling of the substrate is constrained by the slow relaxation of the semi-dilute PVA solution, which dictates the flux of water into the substrate.

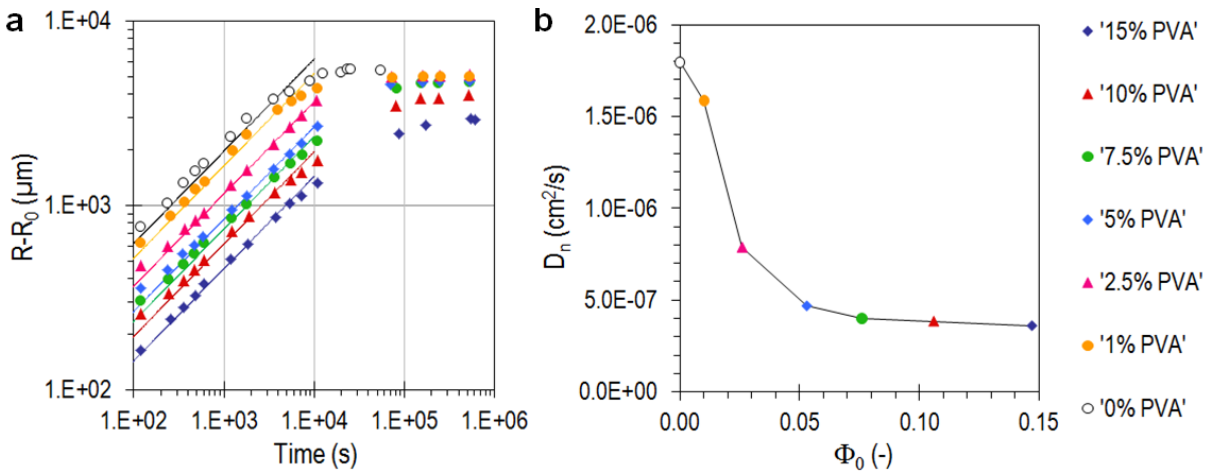

Figure 83 a) Swelling kinetics of the PAAm beads in PVA solutions with different concentration. Solid curves are fits using Eq. 1; **b**) Diffusion coefficients of the PAAm bead in PVA solution of different concentration, obtained from fitting the data in (**a**) with Equation 1.[20,21]

Figure 84a shows the time evolution of the thickness of the PVA films formed at the surface of the same spheres as those in Figure 84d. These results show a strong dependence of the film growth on the concentration of the solution. In the dilute regime (1wt%), no film formation was observed. Close to the overlap concentration (2.5wt%), formation of a film is noticed after 10 min which could correspond to an incubation time or to the time to form a film detectable with our technique (low resolution limit is ~40 µm). In the semi-dilute regime (≥ 5wt%), the formation of a film was observed within the first two minutes. The thickness grew rapidly in the first 10 min and eventually slowed down with a thickening of less than 10µm/min after 30 min of immersion. In all cases, the films stopped growing before the spheres were swollen to equilibrium. In the explored time and concentration ranges, higher PVA concentrations produced thicker films with a three-fold difference between the lowest (2.5wt%) and the highest (15wt%) studied concentrations, as shown in Figure 84b.

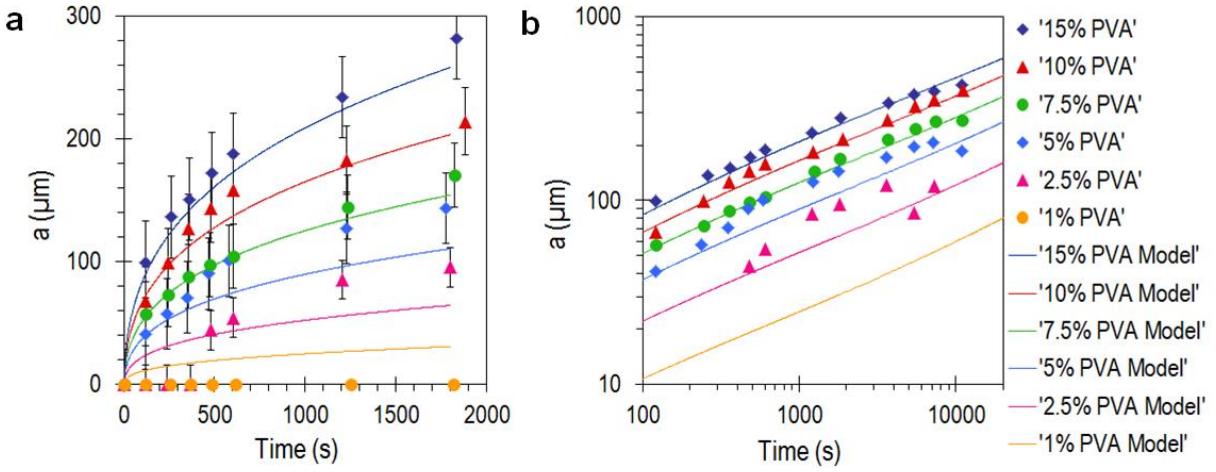

Figure 84 a) Film thickness (a µm) as a function of time (<2000 s); **b**) Log-log chart of the film thickness as a function of time. Solid curves are theoretical prediction using the model given by the Equation 4.

A simple model captures the salient features of the hydrogel film formation observed with these experiments. It is based on the following microscopic picture. Firstly, the solvent depletion process described above induces a local increase in PVA concentration in a layer close to the swelling substrate. At high enough concentrations, the PVA chains in this layer associate and cross-link by crystallization. Above a critical concentration Φ_c, the gel point is reached: the dense PVA liquid layer reticulates to form a PVA hydrogel film. At this stage, a new regime is expected. Transport of water from the newly-formed hydrogel film into the swelling substrate becomes more difficult due to the elastic deformation of the PVA hydrogel network. Instead, it becomes more favourable for water to flow from the solution through the hydrogel film and into the swelling substrate, as already described for gel membrane permeation.[23] As a result, the solvent suction process is displaced at the interface between the PVA hydrogel film and the PVA solution. The hydrogel film builds up until substrate swelling no longer generates a concentration exceeding Φ_c.

At a time t during the growth of the hydrogel film, the swelling substrate has a characteristic thickness R(t) - the radius of PAAm-PAAc spheres in the experiments reported above. It is covered with a PVA hydrogel layer of thickness a(t). To a first approximation, the

PVA concentration profile as a function of the distance from the surface of spherical or flat substrate can be depicted as in Figure 85a and b respectively. We assume that: (i) the PVA solution is in large excess and therefore the PVA concentration far away from the substrate remains constant, equal to $\Phi_{0;}$ (ii) the PVA concentration in the hydrogel layer is homogeneous equal to the critical gelation concentration Φ_c; (iii) the contribution of the transition region at the hydrogel-solution interface is negligible. With such assumptions, mass conservation of PVA simply imposes that the amount of PVA in the volume spanned by the network during swelling is equal to the excess of PVA in the PVA hydrogel film. This writes:

$$\Phi_0 V_s = (\Phi_c - \Phi_0) V_s \quad (2)$$

Where Φ_0 is the concentration of PVA in the solution, Φ_c is the critical gelation concentration, V_s is the volume of the sphere, V_f in the volume of the film. As a function of the dimension of the substrate and of the film, Equation 2 gives:

- For a sphere:

$$\Phi_0\left(\frac{4}{3}\pi R(t)^3 - \frac{4}{3}\pi {R_0}^3\right) = (\Phi_c - \Phi_0)\left(\frac{4}{3}\pi(R(t) + a(t))^3 - \frac{4}{3}\pi R(t)^3\right) \quad (3)$$

$$a(t) = \left[\left(\frac{\Phi_0}{(\Phi_c - \Phi_0)}\right)(R(t)^3 - {R_0}^3) + R(t)^3\right]^{1/3} - R(t) \quad (4)$$

Where a(t) is the thickness of the PVA hydrogel film, R(t) is the radius of the sphere, and R_0 is the initial radius of the sphere.

- For a flat substrate of surface S supposed to be constant:

$$\Phi_0(H(t)S - H_0 S) = (\Phi_c - \Phi_0)((a(t) + H(t))S + H(t)S) \quad (5)$$

$$a(t) = \frac{\Phi_0}{(\Phi_c - \Phi_0)}(H(t) - H_0) \quad (6)$$

Where a(t) is the thickness of the PVA hydrogel film, H(t) is the thickness of the flat substrate, and H_0 is the initial thickness of the flat substrate.

A prediction of film growth as a function of immersion time is then obtained by replacing R(t) or H(t) by diffusion model of swelling given by Equation 1. This prediction for a spherical substrate is applied to the experimental data obtained at various PVA concentrations in the semi-dilute regime (Φ_0 > 2.5wt%). The critical gelation concentration Φ_c is the only adjustable parameter. For a value of Φ_c=0.36, a very good agreement is found between the experimental data and the model, as shown by solid curves in Figure 84a and b. This value Φ_c=0.36 is very close to the value reported in the literature for the gelation concentration of PVA hydrogel.[3]

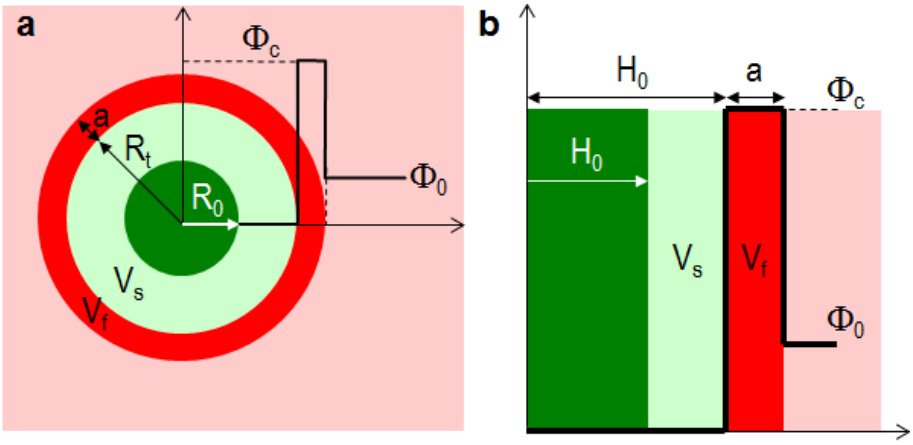

Figure 85 PVA concentration profile as a function of the distance to the substrate interface for a spherical substratre (**a**) and a flat substrate (**b**).

Both the experiments and the model show that this swelling induced process can be well controlled and tuned to form hydrogel films with thicknesses ranging from tens to hundreds of microns. In particular, the kinetics of film growth is fully determined by the solution properties (concentration Φ_0 and gelation concentration Φ_c), the substrate properties

(size R_0 and geometry) as well as by the swelling properties of the system (D_n, R_∞). All of these parameters can be finely tailored by adjusting the solution composition and the chemical nature and topology of the swelling substrate.

The versatility of this fabrication method was verified by producing PVA hydrogel films on a variety of swelling substrates. As long as the swelling speed and extent were large enough, stable films were obtained using dry PAAm, PAAc-PAAm and PEG as substrates. In particular, free standing hydrogel films were produced by using uncrosslinked PEG substrate. In that case, a PVA hydrogel film was formed at the same time as the PEG substrate dissolved, as shown in Figure 86.

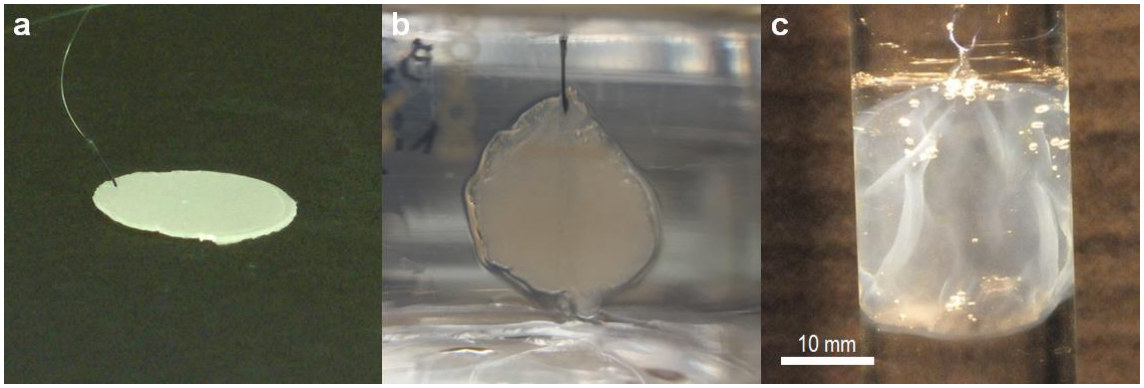

Figure 86 PVA hydrogel film gelation around hydrosoluble PEG substrate. **a**) Uncross-linked PEG substrate; **b**) Soaking in PVA aqueous solution; **c**) PVA film in water.

One particular interest of this approach is for the encapsulation of other solutes or the coating of hydrogel pieces in mild fabrication conditions. We illustrate this potential by producing composite coatings of ceramic particles dispersed in a hydrogel matrix. For that, dry PAAc-PAAm spheres were immersed in 10wt% PVA aqueous solutions containing dispersions of hydroxyapatite micro- or nano-particles having a diameter of between 5 and 25 µm or less than 200 nm, respectively. In all cases, after 60 min of immersion, a dense, homogeneous and solid hydrogel composite film was observed at the surface of the substrate, as illustrated in Figure 87a and b. Microscopic observations by SEM show that particles are

embedded in the PVA matrix and cover homogeneously the substrate. The surface of the PVA/HA nano-particle composite coating and the cross-section of the PVA/HA micro-particle composite coating are shown in Figure 87d, left and right picture respectively. Control experiments were realized by swelling the PAAc-PAAm spheres in water prior to immersion in the PVA-hydroxyapatite solutions for 60 min. Accordingly, no solid films were formed and only a few scattered particles were noticed at the surface of the substrate, as shown in Figure 87c.

Such ceramic-hydrogel coatings can be relevant to improve the bone anchoring of soft osteoarticular implants or scaffolds, which are made of bulk hydrogel pieces. As an example, molded cylinders of physically cross-linked PVA were coated by immersion in an aqueous solution of PVA and hydroxyapatite particles. Two cylinders, one dried and one swollen at the equilibrium, were soaked in PVA/HA aqueous solution for 60 minutes, and vigorously washed for 5 minutes. Then one freezing/thawing cycle[14] was applied to both cylinders, in order to strengthen the coating cross-linking. Tomographic imaging was achieved in order to capture the coating thickness around the substrates. The Z-cut images analysis gave an average thickness of the coatings. In the case of the dried substrate a dense and thick coating was obtained, as depicted in the left picture in Figure 87e. The estimated thickness was 200±100 µm. Whereas the coating achieved with the swollen substrate was much more thinner and scattered. Its thickness was around 30±10 µm, as shown in the right picture in Figure 87e. As the coating was captured with the same height along Z-axis, the volume could be estimated for both coatings. For immersion of the dry cylinder, the volume of the coating was 12.93 mm^3. For the immersion of the previously swollen cylinder, the volume of the coating is ten times smaller (1.76 mm^3). This difference is well illustrated by the tridimensional view of the coatings in Figure 87f.

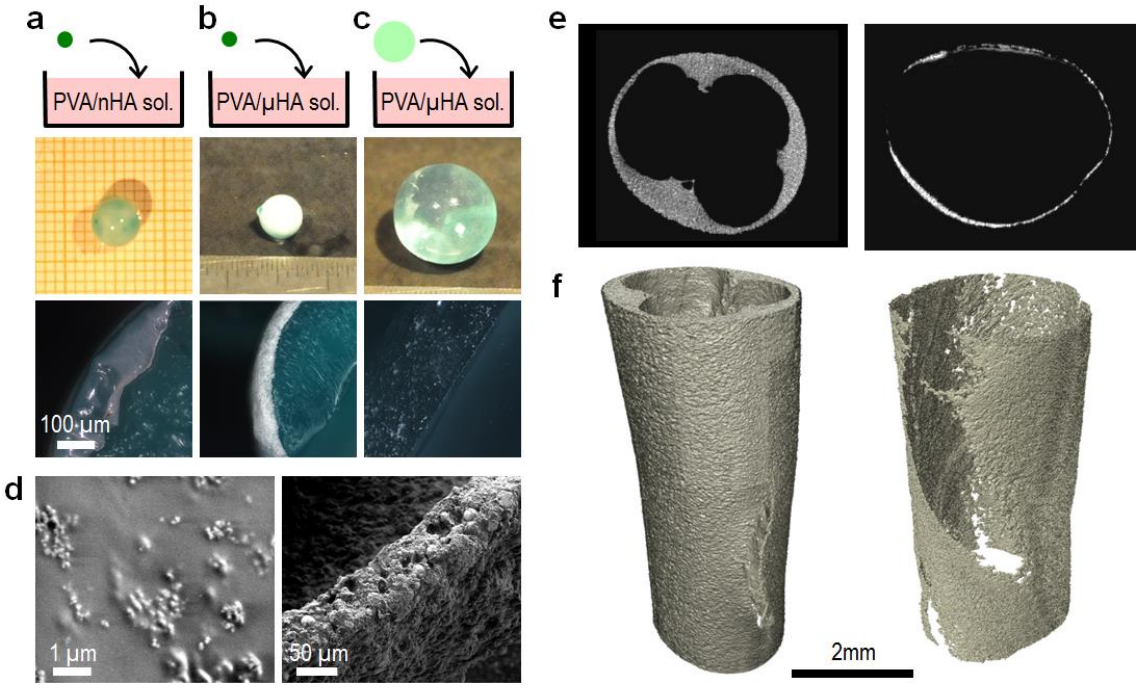

Figure 87 Encapsulation applications: composite coatings. Nano- (**a**) and micro-HA (**b**) particles composite coatings are obtained around dry PAAm beads, whereas no solid coating was obtained on swollen PAAm beads (**c**). SEM observations of the surface of nano-HA coating (**d**-left) and of the cross-section of the micro-HA coating (**d**-right). Coating thickness of PVA implant can be adjusted by varying the swelling state (dry:left - swollen:right) of the substrate as shown by microtomography Z-cut (**e**) and 3D reconstructions (**f**).

8.4 Conclusion

These results suggest that swelling induced gelation provides a new way to produce hydrogel films and coatings in mild conditions. The properties of these films can be tuned by varying soaking time and the composition of the soaking solution. This method can be achieved with multiple polymer substrates. Hybrid coatings with hydroxyapatite particles have been formed around different substrate and shape types. These results open a new way to make composite films or to encapsulate objects. In particular, the softness of this method should be compatible with the manipulation of living matter and could be applied to encapsulate bio-active materials or even cells. This is the object of the next chapter.

References

1. Budtova, T. & Navard, P. Polyelectrolyte hydrogel swelling in a concentrated polymer solution. *Macromolecules* **28,** 1714–1716 (1995).

2. Budtova, T. & Navard, P. Swelling Dynamics of Cross-Linked Poly (acrylic acid) and Neutralized Poly (acrylate-co-acrylic acid) in Aqueous Solutions of (Hydroxypropyl) cellulose. *Macromolecules* **29,** 3931–3936 (1996).

3. Packter, A. & Nerurkar, M. Crystallization in films of polar vinyl polymers-I. Crystallinity of polyvinyl alcohol films prepared by evaporation of aqueous solutions. *Eur. Polym. J.* **4,** 685–693 (1968).

4. Ono, H., Mandai, S. & Edasawa, K. Resin composition and use thereof. (2008).

5. Bessbousse, H., Rhlalou, T., Verchère, J.-F. & Lebrun, L. Removal of heavy metal ions from aqueous solutions by filtration with a novel complexing membrane containing poly(ethyleneimine) in a poly(vinyl alcohol) matrix. *J. Membr. Sci.* **307,** 249–259 (2008).

6. Chuang, W.-Y., Young, T.-H. & Chiu, W.-Y. The effect of acetic acid on the structure and filtration properties of poly (vinyl alcohol) membranes. *J. Membr. Sci.* **172,** 241–251 (2000).

7. Vrana, N. E., O'Grady, A., Kay, E., Cahill, P. A. & McGuinness, G. B. Cell encapsulation within PVA-based hydrogels via freeze-thawing: a one-step scaffold formation and cell storage technique. *J. Tissue Eng. Regen. Med.* **3,** 567–572 (2009).

8. Vrana, N. E. *et al.* Cell encapsulation and cryostorage in PVA-gelatin cryogels: incorporation of carboxylated ε-poly-L-lysine as cryoprotectant. *J. Tissue Eng. Regen. Med.* **6,** 280–290 (2012).

9. Surry, K. J. M., Austin, H. J. B., Fenster, A. & Peters, T. M. Poly(vinyl alcohol) cryogel phantoms for use in ultrasound and MR imaging. *Phys. Med. Biol.* **49,** 5529–5546 (2004).

10. Baker, M. I., Walsh, S. P., Schwartz, Z. & Boyan, B. D. A review of polyvinyl alcohol and its uses in cartilage and orthopedic applications. *J. Biomed. Mater. Res. B Appl. Biomater.* **100B,** 1451–1457 (2012).

11. Sciarretta, F. V. 5 to 8 years follow-up of knee chondral defects treated by PVA-H hydrogel implants. *Eur. Rev. Med. Pharmacol. Sci.* **17,** 3031–3038 (2013).

12. Lozinsky, V. I., Domotenko, L. V., Vainerman, E. S., Mamtsis, A. M. & Rogozhin, S. V. On the possibility of mechanodestruction of poly (vinyl alcohol) molecules under moderate freezing of its concentrated water solutions. *Polym. Bull.* **15,** 333–340 (1986).

13. Otsuka, E. & Suzuki, A. A simple method to obtain a swollen PVA gel crosslinked by hydrogen bonds. *J. Appl. Polym. Sci.* **114,** 10–16 (2009).

14. Hassan, C. M. & Peppas, N. A. in *Biopolymers· PVA Hydrogels, Anionic Polymerisation Nanocomposites* 37–65 (Springer, 2000).

15. Fujiwara, H., Shibayama, M., Chen, J. H. & Nomura, S. Preparation of high-strength poly (vinyl alcohol) fibers by crosslinking wet spinning. *J. Appl. Polym. Sci.* **37,** 1403–1414 (1989).

16. Hassan, C. M. & Peppas, N. A. Cellular PVA hydrogels produced by freeze/thawing. *J. Appl. Polym. Sci.* **76,** 2075–2079 (2000).

17. Hammersley, A. . FIT2D: An Introduction and Overview. *ESRF Intern. Rep.* **ESRF97HA02T,** (1997).

18. Schneider, C. A., Rasband, W. S. & Eliceiri, K. W. NIH Image to ImageJ: 25 years of image analysis. *Nat. Methods* **9,** 671–675 (2012).

19. Ricciardi, R., Auriemma, F., De Rosa, C. & Lauprêtre, F. X-ray Diffraction Analysis of Poly(vinyl alcohol) Hydrogels, Obtained by Freezing and Thawing Techniques. *Macromolecules* **37,** 1921–1927 (2004).

20. Yoon, J., Cai, S., Suo, Z. & Hayward, R. C. Poroelastic swelling kinetics of thin hydrogel layers: comparison of theory and experiment. *Soft Matter* **6,** 6004 (2010).

21. Doi, M. Gel Dynamics. *J. Phys. Soc. Jpn.* **78,** 052001 (2009).

22. Bercea, M., Morariu, S. & Rusu, D. In situ gelation of aqueous solutions of entangled poly(vinyl alcohol). *Soft Matter* **9,** 1244–1253 (2013).

23. Barrière, B. & Leibler, L. Kinetics of solvent absorption and permeation through a highly swellable elastomeric network. *J. Polym. Sci. Part B Polym. Phys.* **41,** 166–182 (2003).

Chapter 9. Cell encapsulation in poly(vinyl alcohol) hydrogel films by swelling induced gelation

9.1 Introduction

Hydrogels are soft polymeric materials that have properties close to the extra-cellular matrix (ECM) of biological tissues. In particular they share with the ECM a high water content, a soft elastic behaviour up to large strains and porosities allowing storage and transport of molecules. Therefore, they have become reference biomaterials to produce artificial matrices to encapsulate bioactive compounds or cells, which can be used in tissue engineering[1]or drug delivery systems.[2] Nevertheless, the design of these systems is greatly constrained by the need to form the hydrogel matrix in mild conditions that do not compromise its biocompatibility and the integrity or viability of the encapsulated components.[3,4] These requirements have hitherto been fulfilled by the use of multi-step processes. Some approaches are based on radical polymerization, including photo-polymerization,[5] thermal activation,[6] or redox reaction,[7] and on step-growth polymerization.[8] These processes allow a control of the hydrogel gelation that can be useful for the *in situ* hydrogel formation[9] or the production of tridimensional hydrogel scaffolds by bioprinting.[10] For some applications, the possibility to produce hydrogel films by a simple method without external action could provide an easier way to store cells in three-dimensional environment or to produce of coatings that contain cells. In this chapter, we show that cells can be encapsulated in poly(vinyl alcohol) (PVA) hydrogel films, using a spontaneous one-step process that does not require any external action.

PVA hydrogels have already been used to store biologic matters, such as drugs or cells.[11–13] Recent studies by Vrana *et al.* have demonstrated that PVA/Gelatine cryogels can

be used as scaffolds to encapsulate vascular arterial smooth muscle cells.[14,15] In their approach, they produced PVA/Gelatine hydrogels crosslinked by the freezing/thawing method. Their encapsulation process involves several steps, including a freezing step at -70°C. This quenching step requires the use of a cryoprotectant, which needs to be properly dosed to avoid cytotoxic effects on cells.[16] In previous chapter (chapter 8), we have shown that hydrogel films of PVA can form spontaneously from an aqueous PVA solution by using the solvent depletion created near the surface of a swelling gel substrate. This approach to produce hydrogel films does not require the use of any harsh physical or chemical treatments. In this chapter, we investigate how this swelling induced gelation approach can be used to encapsulate cells in a PVA hydrogel matrix.

Several questions need to be addressed to use the swelling induced gelation process for cell encapsulation. On the one hand, the process has to be adapted to cell culture conditions and it is not clear how these practical requirements may affect the gelation of a film. Firstly, all the components of the process must be prepared and maintained in sterile conditions. Secondly, cells should remain in a viable environment, which means that the swelling induced gelation process should take place at temperatures close to 37°C and in buffered solution for short periods of times or culture cell media for long term storage. On the other hand, it is also not known how the water transport and concentration variations occurring close to the surface of the swelling substrate may be compatible with the cellular osmolality and do not compromise cell viability.

We have explored these questions using two different approaches based on swelling induced gelation to encapsulate cells in a PVA hydrogel film. They are illustrated in Figure 88. In a first approach (Figure 88a), films of covalently crosslinked poly(acrylamide) (PAAm) were used as the swelling substrate to induce gelation of PVA films. The protocol was as follows: (i) 3-mm thick PAAm films were placed in cell culture wells; (ii) a PVA aqueous

solution containing mouse chondrocyte cells at a concentration of 3.10^4 cells/mL was poured in the wells; (iii) the wells were stored at 37°C for 1h to induce the formation of PVA hydrogel films; (iv) the swollen PAAm substrates covered by PVA hydrogel films were rinsed in large excess of waterand finally (v) they were deposited in new wells and stored with growth medium in an incubator at 37°C. This approach was performed on six wells. The results obtained have not been satisfactory because no stable PVA hydrogel films were formed. We attributed this effect to the fact that within one hour, the swelling rate of PAAm substrates was not large enough to trigger the gelation of PVA hydrogel films at 37°C. Detailed methods and results for this first approach are given in Appendix 2.

In a second approach (Figure 88b), non-crosslinked hydrosoluble poly(ethylene glycol) (PEG) films were used as substrates. With this substrate, we verified that stable PVA hydrogel films with a thickness of a few hundred µm to a few mm are formed at 37°C within a few hours. The protocol was performed as follows: (i) dry PEG films were deposited in glass wells; (ii) mouse fibroblast NH3T3 cells were mixed to a PVA aqueous solution and poured in the wells; (iii) The wells were stored for 3h at 37°C to induce the formation of PVA hydrogel films; (iv) the whole wells were immersed in a large excess of growth medium for 24h to ensure the complete dissolution of the PEG substrates; (v) PVA hydrogel films were then collected and finally (vi) they were deposited in new wells and stored in growth medium in an incubator at 37°C. Using MTT assays and optical microscopy techniques, we assessed the feasibility of this encapsulation approach by characterizing the presence, spatial distribution and viability of encapsulated cells. Based on these observations and on a study of hydrogel film formation in this particular protocol, we propose a picture explaining how the encapsulation and viability of the cells inside the PVA hydrogel films depend on the swelling the PEG substrate and on the thickness of the PVA hydrogel film.

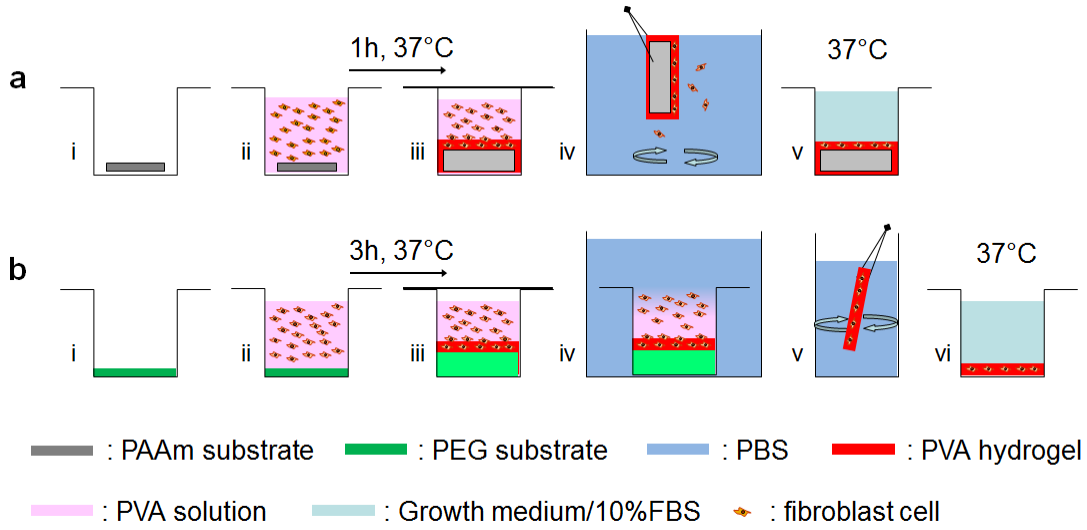

Figure 88 Two studied approaches of encapsulation by swelling induced gelation. a) First approach: gelation of PVA/cell aqueous solution on a cross-linked PAAm substrate; b) Second approach: gelation of PVA/cell aqueous solution on a PEG substrate.

9.2 Materials and methods

Materials

Poly(vinyl alcohol) (PVA) solution was prepared from high molecular weight (89,000–98,000 kg·mol^{-1}) 99%-hydrolyzed PVA powder (Sigma-Aldrich). Poly(ethylene glycol) (PEG) substrates were prepared from high molecular weight (100,000 kg·mol^{-1}) PEG powder (Sigma-Aldrich). Studied cells were mouse fibroblasts NIH-3T3 (ATCC CRL-1658) gratefully given by Suzie Lefebvre, UMR-S 1124, EQ9 (2015/06/19). Growth medium was composed of Dulbecco's Modified Eagle's Medium (DMEM) at 1g/L of glucose (Invitrogen) plus 1mL of Penicillin-Streptomycin PS (Invitrogen) and 10 mL of glutamine 200 mM (Invitrogen) per 500 mL of growth medium. Foetal bovine serum (FBS) was used at 10 % v/v (Lonza). Buffer solution was PBS-1X (Invitrogen). Cells were harvested using a solution of trypsin-EDTA 0,05% (Invitrogen).

Preparation of PVA/growth medium

A 12 wt% PVA solution was prepared by dissolving 12 g of PVA in 88 g of growth medium without FBS. The mixture was autoclaved at 121°C for 1h. Then it was stored at 37°C until use.

Preparation of PEG substrates

PEG substrates were obtained by pressing PEG powder in a manual hydraulic press (15t, Specac, UK). Firstly PEG powder was spread on a sterile plate and exposed to UV light (253.7 nm) for 30 min in order to be sterilized. Substrates were prepared by pressing 1 g of powder into an aluminum mold with a diameter of 22.1±0.1 mm, previously sterilized by dry heat at 180°C for 30 min. The powder was pressed at room temperature under 1 ton of hydraulic pressure for 1 min. The so-obtained substrates were finally packed and stored in sterile bags (Whirl-Pak, Nasco) until experiments. Substrates dimensions were 22 mm in diameter and 2 mm in thickness.

Cell culture

A mouse fibroblast NIH-3T3 (ATCC CRL-1658) cell line was used. Confluent fibroblast cells, cultured in ten T175 culture boxes, were harvested by adding 5 mL of Trypsin/EDTA 0,05% and incubated 5 min in an oven at 37°C. Then 5 mL of growth medium/10%FBS was added to each culture boxes. Suspension solution of cells in growth medium/10%FBS was distributed in four 50 mL tube and was centrifuged at 1500 rpm for 5 min. Supernatant was removed and all residues were put in 5 mL of growth medium/10%FBS. The number of cells and their viability were estimated using automated cell counter (Luna, Logos Biosystems, USA). The total cell concentration was 30.10^6 cells/mL with a viability of 94% and an average cell diameter of 15 µm. For the experiments, a 2 mL cellular suspension at 30.10^6 cells/mL in growth medium/10%FBS and a 2 mL cellular suspension at 2.10^5 cells/mL in growth medium/10%FBS were prepared.

Preparation of PVA/growth medium/FBS with cells

40 mL of the 12wt% PVA/growth medium solution was mixed to 4.2 mL of FBS and placed in ultrasonic bath to degas. 38 mL of the mixture was mixed with 2 mL cellular suspension at 30.10^6 cells/mL. The whole mixture was homogenized by 5 linear up and down motions in a 50 mL syringe.

Encapsulation process

Three protocols were performed: the protocol of cellular encapsulation, as described in Figure 88b, a protocol of positive control of cell viability, as described in Figure 90a, and a protocol of negative control where hydrogel films were formed in the absence of cells, as described in Figure 90b.

In the encapsulation protocol, glass wells of 23 mm in diameter were placed in a 6-well plate and PEG substrates were inserted into the glass wells (Figure 88a(i) and Figure 89a). Then 3mL of PVA/FBS solution, in which cells were dispersed at a concentration of $1.49.10^6$ cell/mL, were poured into the glass wells, as shown in Figure 88a(ii) and Figure 89b. The 6-well plate was covered to prevent evaporation and drying (Figure 88a(iii) and Figure 89c) and was placed for 3 hours in an incubator at 37°C. The wells were then removed from the 6-well plate and dropped into a large excess of growth medium/10% FBS for 24h in an incubator at 37°C (Figure 88a(iv) and Figure 89d). After that, the obtained PVA hydrogel films were detached from the wall of the wells, vigorously rinsed in 10% PBS solution (Figure 88a(v) and Figure 89e) and placed in a new 6-well plate filled with growth medium/10%FBS (Figure 88a(vi) and Figure 89f). Five hydrogel films were obtained: three films were observed 24h after fabrication and two films after 48h.

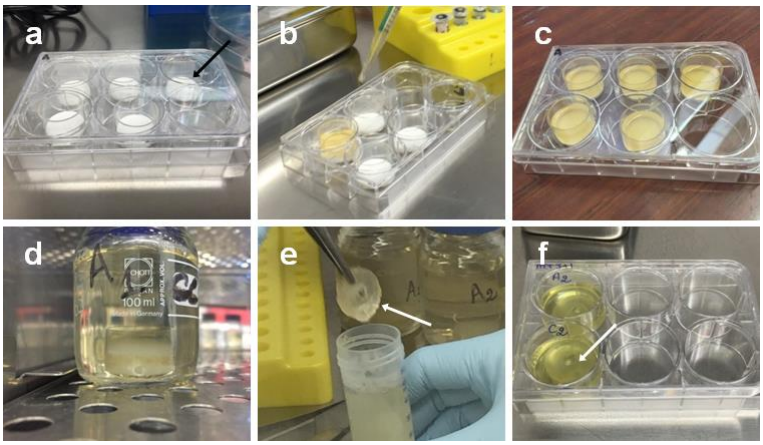

Figure 89 Pictures of the encapsulation process. **a**) PEG substrates in glass wells; **b**) Pouring of PVA/cell solution; **c**) Incubation at 37°C for 3 h; **d**) Soaking in growth medium; **e**) Rinsing in PBS solution; **f**) Incubation in growth medium at 37°C.

In the positive control experiment, cells were dispersed in growth medium/10%FBS and put in a 6-well plate (Figure 90b(ii)) at three different concentrations, 75.10^3, 150.10^3 and 300.10^3 cells/mL. Cells were then let in an incubator at 37°C for 24h (Figure 90b (iii)). After 24h, the growth medium/10%FBS was replaced by a fresh one (Figure 90b(iv)(v)). Three wells were observed 24h after step (v) and three wells 48h after step (v).

The negative control experiment consisted in the exact same procedure as the encapsulation protocol without adding the cells to the PVA solution. PVA hydrogel films were obtained from PVA/PBS solution (Figure 90c(v)) and were placed in a 6-well plate filled with growth medium/10%FBS (Figure 90c(vi)). Four hydrogel films were obtained: two films were observed 24h after fabrication and two films after 48h.

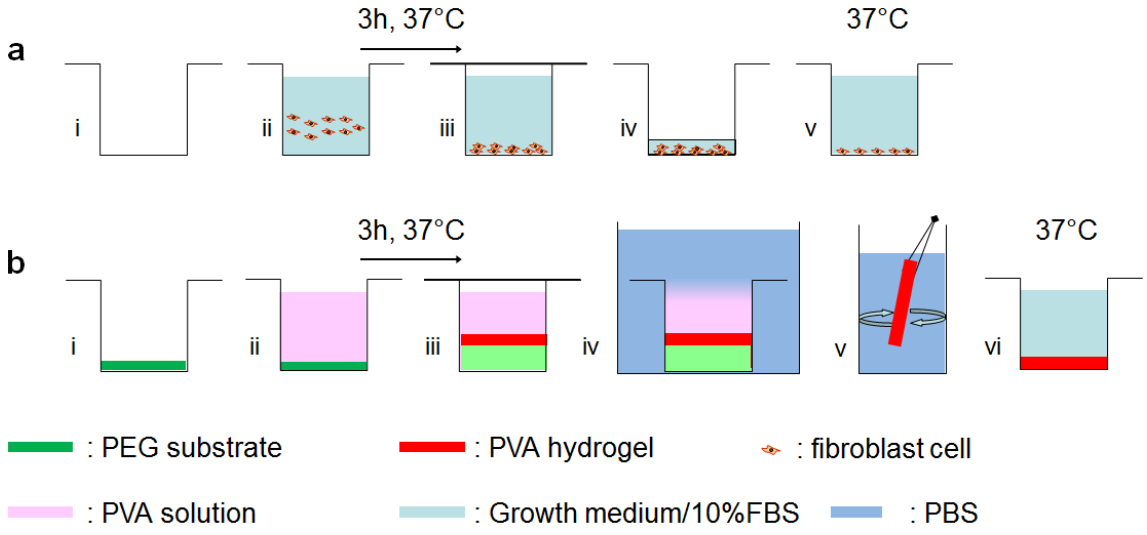

Figure 90 a) Positive control experiment; **b**) Negative control experiment

Cell viability assessment

The viability of the cells was assessed both by fluorescence microscopy and MTT tests. The observations are summarized in the following table:

	Fluorescence microscopy		**MTT test**	
	24h	48h	24h	48h
Encapsulation protocol	2	1	1	1
Positive control	1	1	1	1
Negative control	1	1	1	1

Table 7 Samples reserved for fluorescence microscopy and MTT test.

The microscopic observations were done using an epifluorescence microscope (NIKON Eclipse TE2000E) and a confocal microscope (Zeiss LSM510). Prior to these observations, hydrogel films were stained with fluorophore dyes. Viability assays were performed on unfixed cells. A viability/cytotoxicity kit for mammalian cells (Molecular Probes ref L3224 lot 1657695) was used for the staining. It was composed of two dyes, calcein AM and ethidium homodimer-1. The calcein dye was retained in the cytoplasm of living cells, producing an intense uniform green fluorescence in living cells (excitation/emission 495 nm/515 nm). The ethidium produced a red fluorescence

(excitation/emission 495 nm/635 nm), when binding to nucleic acid of cells with damaged plasma membranes. However ethidium was excluded from the intact plasma membrane of living cells, therefore staining specifically dead cells.

The staining procedure was as follows. Both fluorescence dyes were let to thaw at room temperature in darkness. 60 µL of 2mM EthD-1 and 15 µL of 4mM calcein were added to 30 mL of PBS and the mixture was vortexed. Hydrogel films were rinsed with PBS. 3 mL of the fluorescence solution were added in wells containing the hydrogel films. It was put in an incubator at 37°C for 30 min. Lastly, hydrogel films were rinsed three times with PBS in order to remove unfixed fluorescent dyes.

Living and dead cells were counted using the Cell Counter plugin of the ImageJ® software for each epifluorescence microscopic observations.[17] Viability was estimated as the ratio of the number of living cells over the total number of counted cells. The observed volume, inside which cells were counted, was 0.13±0.07 mm^3. The viability was estimated over 17 images.

MTT tests were performed on hydrogel films both with and without cells. MTT (Sigma 2128) was at 5 mg/mL in DMEM medium (70 mg of MTT + 14 mL of DMEM-L-glutamine-PS). 400 µL of this solution was added to the wells containing hydrogel films in 4 mL of growth medium/10%FBS. Wells were then put in an incubator at 37°C for 2h. After that, the supernatant was removed and 1 mL of DMSO was added. The staining of living cells by MTT was only assessed by macroscopic observations. Indeed, the MTT spectrophotometric test was not possible due to the insolubility of the obtained PVA hydrogel films by DMSO at room temperature.

9.3 Results

Formation of PVA hydrogel films for the cell encapsulation protocol

Before encapsulation experiments, a preliminary experiment was performed to characterize the formation of a PVA film on a PEG substrate. This experiment was exactly like the one described in Figure 88a, except that a pure PVA solution was used instead of a PVA/growth medium solution and film formation was performed at 25°C instead of 37°C. PEG substrates were placed in glass wells and a 12 wt% PVA aqueous solution was poured. After 3h, the glass wells were placed in a large excess of water to dissolve the PEG substrate. Picture of the film formation were taken throughout the process. The following results were very similar to what was observed in the actual encapsulation protocol.

Figure 91 shows a side-view of the glass well during the formation of a PVA hydrogel film at the surface of a dissolving PEG substrate. A 12 wt% PVA solution was poured in the well containing a PEG substrate, as shown in Figure 91a. After 30 min, the formation of a hydrogel film was observed at the surface of the swelling PEG substrate, as shown in Figure 91b. The PEG substrates did not swell uniformly: swelling appeared to be greater in the center than close to the edges. As a result, the PVA hydrogel film formed at the surface of the substrate had a convex shape. The curvature of the interface was amplified as swelling proceeded, as shown after 1 and 3 hours in Figure 91c and d, respectively. Finally, the well containing the PEG substrate and the PVA solution was immersed in a large excess of water or growth medium for 24h. During this step, a leak of PEG through the center of the membrane was systematically observed, as shown in Figure 91e. At the end of this final step, the PEG substrate was completely dissolved. In order to collect the film (Figure 91f), it was necessary to detach the film, which has stuck to the wall during its formation. This sticking has constrained the swelling and induced the shape of the film. We will show that it has consequences on the cell viability. Hydrogels of about 27 mm in diameter were obtained. A

hole was formed in the center with a diameter comprised between 2 and 5 mm. The thickness was not uniform, as shown in Figure 92 showing the cross-section of a PVA hydrogel film from the center to the edge. The film surfaces were curved on the substrate side (bottom-face) and rather flat on the solution side (top-face). A mean thickness of 1.2±0.7 mm was measured, with a minimum thickness of few hundreds µm at the center and a maximum thickness of 2 mm at the edge. The equilibrium water content of the PVA hydrogel film was about 90wt%. The so-obtained hydrogels remained stable and did not dissolve upon immersion in aqueous medium at 37°C for 1 week.

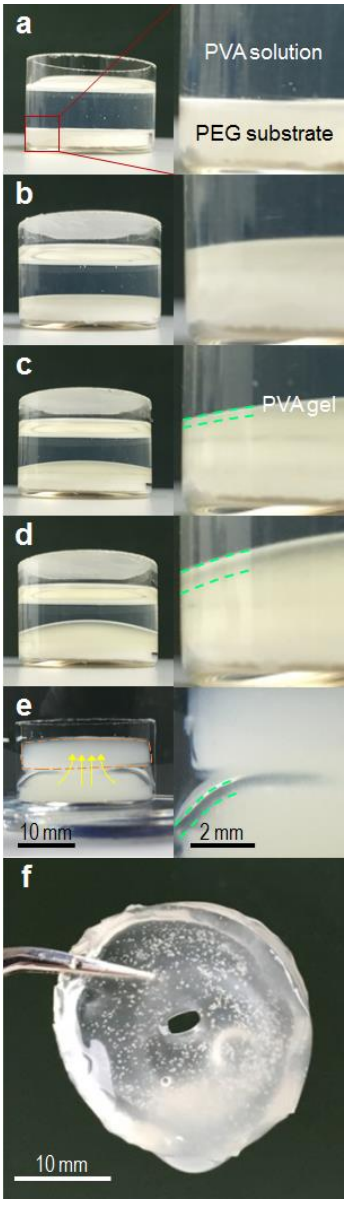

Figure 91 PVA hydrogel film growth. a) PVA solution is poured in well containing PEG substrate; b) After 30 min; c) After 1h; d) After 3h; e) Soaking in water for 24h; f) Obtained PVA hydrogel film. Pictures on the right are magnification of left pictures. Green dashed line: hydrogel film; Yellow arrow: PEG leak; Orange dashed line: PEG solution above the PVA hydrogel film.

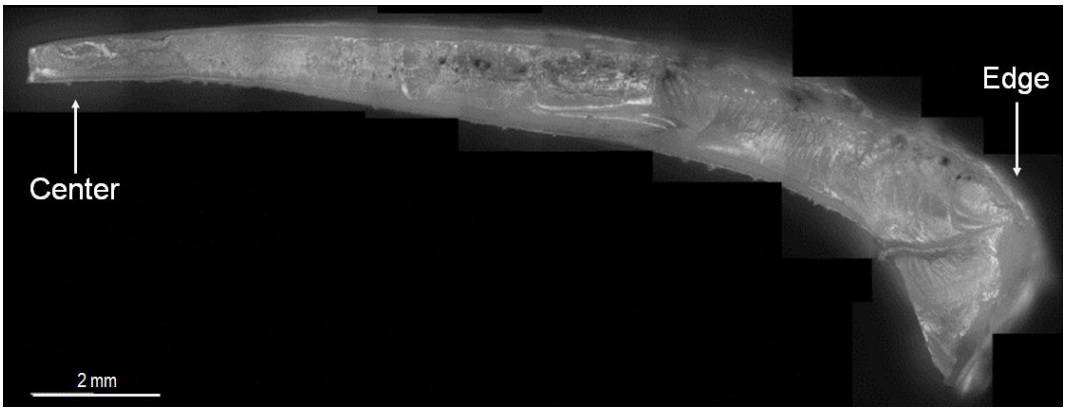

Figure 92 Optical microscopy observation of the cross-section of hydrogel film containing cell after MTT test at 24 h.

MTT tests

The presence of encapsulated living cells was first assessed macroscopically by MTT tests. They were performed on hydrogel films produced by the encapsulation and the negative control protocols. MTT diffused inside the PVA hydrogel films and therefore stained living cells. No quantitative spectrophotometric measurements were made because the hydrogel did not allow a good dissolution of the encapsulated cells by DMSO. The presence of living cells was characterized by studying the presence of dark stains in the hydrogel films. Both top and bottom faces of hydrogel films were observed. "Top-face" refers to the face in contact with the PVA solution and "bottom-face" refers to the face in contact with the PEG substrate.

Figure 93 and 94 shows pictures of the top and bottom-faces of the films with and without cells, after 24h and 48h respectively. After 24h, a large quantity of dark dots were observed, indicating the presence of living cells, as shown in Figure 93a. The absence of stains in the negative control confirms that these dots are not artefacts and corresponds to cells, as shown in Figure 93b and d. This first result demonstrates that living cells have been efficiently encapsulated inside the PVA hydrogel film. The clusters of living cells revealed by these dark dots were heterogeneously distributed in the plane of the film. Living cell clusters were mostly present in a corona at a distance greater than 6 mm from the center. The distribution in living cells through the thickness of the films was observed by looking at

cross-sections, like the one shown in Figure 92. We found that living cells were mostly located at a distance of 700 µm from the bottom-face, in a 450µm-thick layer. This is confirmed by the observation of the bottom-face, where no dark dots are noticed, as shown in Figure 93c.

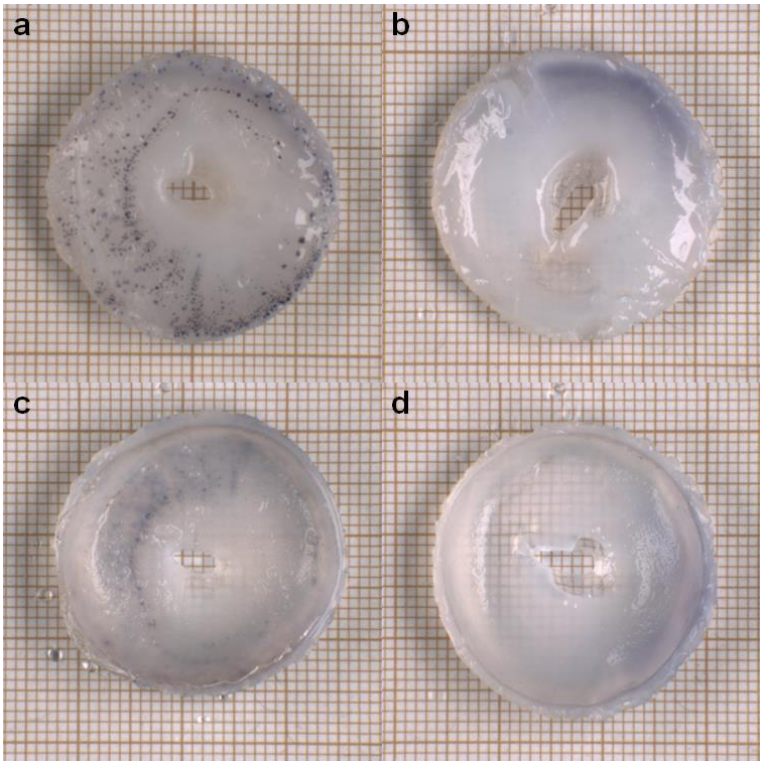

Figure 93 Pictures of the top-face (**a**) and bottom-face (**c**) of cell-encapsulated hydrogel film and of the top-face (**b**) and bottom-face (**d**) of negative control hydrogel film after MTT test at 24h.

After 48h, very similar MTT staining was observed, as shown in Figure 94a and b for the encapsulated film.. Like for the film after 24h, a heterogeneous distribution of living cells into the film was observed and cells were mostly located at a distance greater than 5.5 mm from the center of the film. In addition, no living cells were noticed on the bottom-face of the film (Figure 94b). Comparable to negative control at 24h, no cells were encapsulated in the negative control at 48h, as shown in Figure 94c and d.

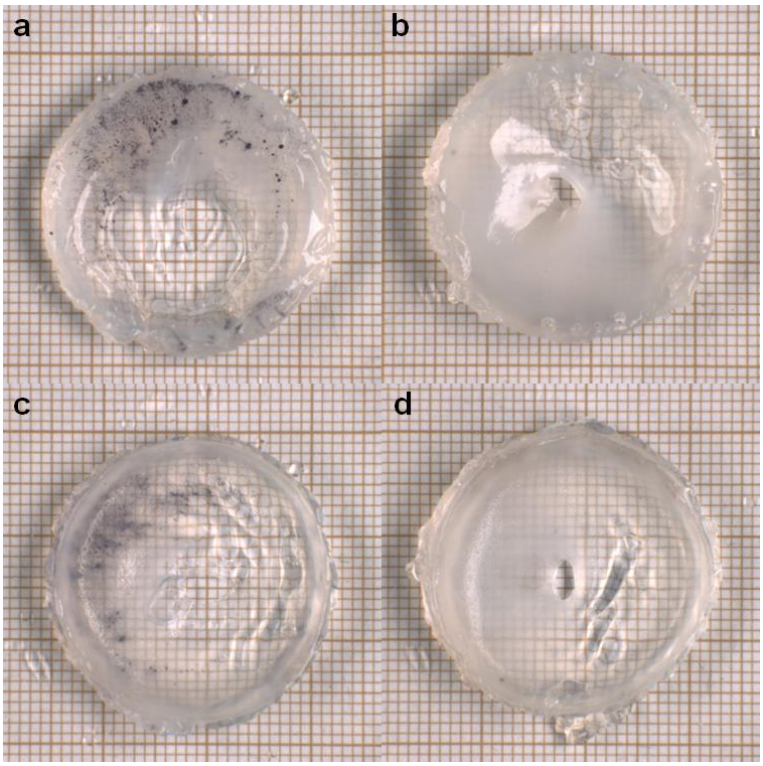

Figure 94 Pictures of the top-face (**a**) and bottom-face (**c**) of cell-encapsulated hydrogel film and of the top-face (**b**) and bottom-face (**d**) of negative control hydrogel film after MTT test at 48h.

Epifluorescence and confocal microscopy

The distribution, the morphology and the viability of the cells inside the hydrogel films were investigated locally using microscopic epifluorescence and confocal microscopy imaging. Figure 95 shows observations of stained cells at 24h (a-d) and at 48h (e-h). Observations were done in a volume of about 0.13±0.07 mm^3 close to the top-face. The positions of each picture in the film are indicated by schemes at the top of Figure 95.

After 24h, close to the center (<6 mm) a strong red fluorescent signal, overlapping a weak green fluorescent signal reveals that cells have been encapsulated during the process but that they were all dead at this time point, as shown in Figure 95a and b. a strong green fluorescent signal was observed with fewer red areas in the positions far from the center (>6 mm). This shows that a significant fraction of the cells were viable. As seen with MTT assays, the cell distribution is heterogeneous with regions of low cell concentration (c=340 cell/mm^3) (Figure 95c) and regions of high cell concentration (c=630 cell/mm^3) (Figure 95d).

After 48h, no strong evolution was noticed as compared to 24h. At distances lower than 6 mm from the center, cells were present but they were all dead, as shown in Figure 95e and f. As the distance from the center increases (>6 mm), the viability strongly increases. Cells were predominantly alive, as indicated by the prevailing green signal on Figure 95g and h, even though some dead cells were noticed.

Based on these observations an attempt was made to quantify the local viability of the cells. It was estimated as the ratio of living cells over the total quantity of cells in the observed volume. Figure 96 shows the plot of the cell viability as a function of the distance from the center of the hydrogel film after 24 and 48h. At a distance greater than 6 mm from the center, the viability increases abruptly and reaches a plateau fluctuating between 50 and 85%.

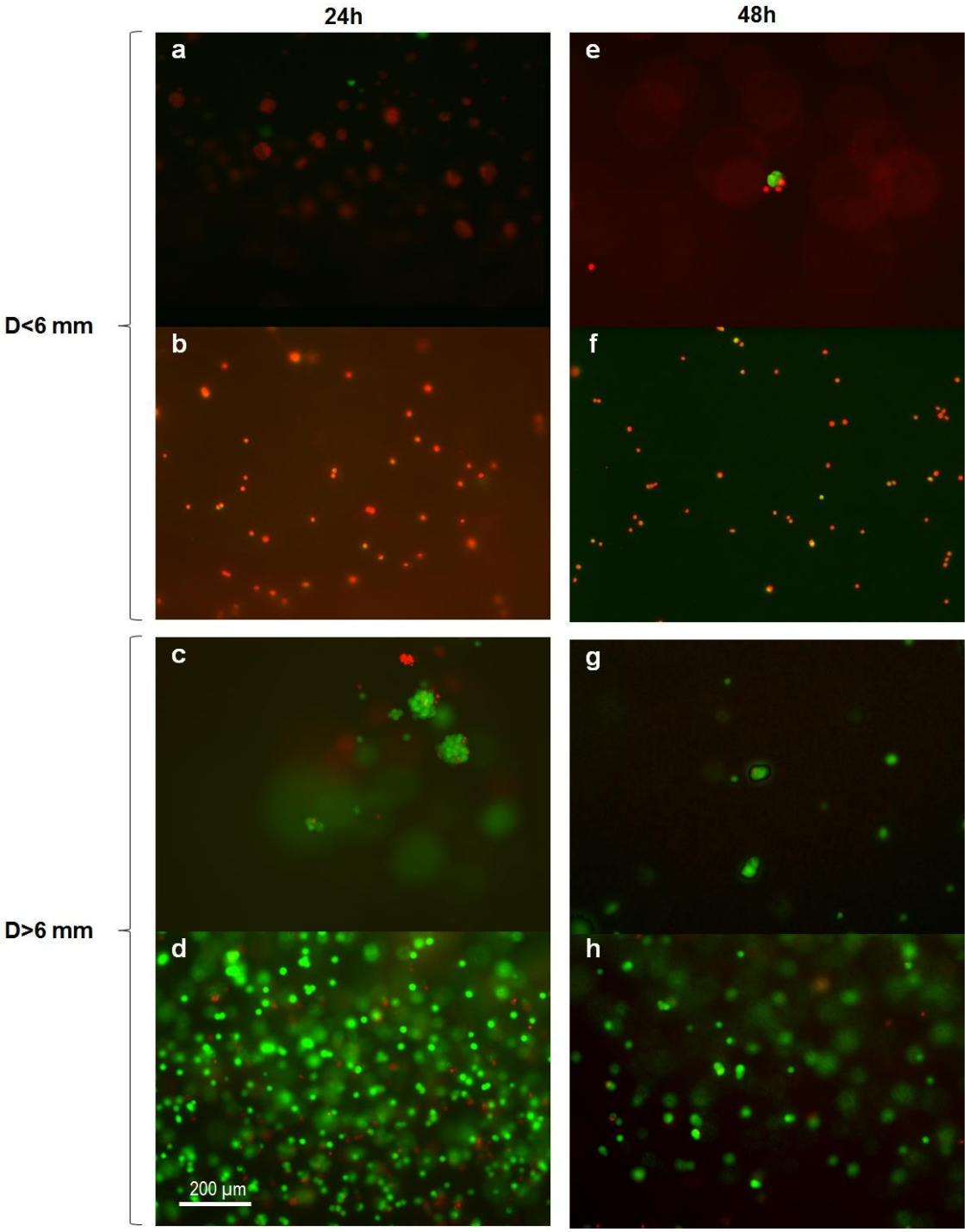

Figure 95 Epifluorescence microscopy observation of the cell-encapsulated hydrogel films for different radial position at 24 and 48h.

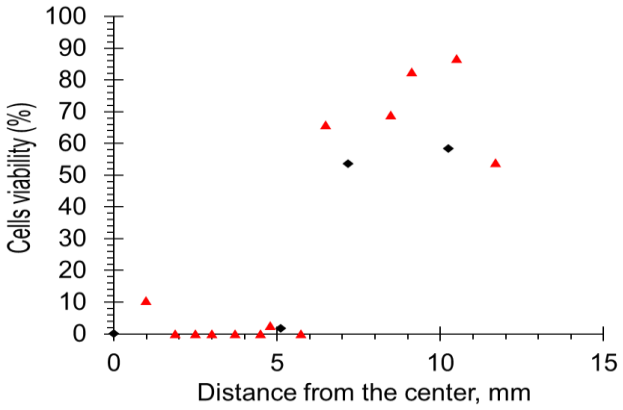

Figure 96 Cell viability as a function of the distance from the center of the hydrogel film, estimated from the epifluorescence microscopy images.

Positive and negative controls were also observed at 24 and 48h. Cells cultured in 6-wells plate, corresponding to positive control, present a viability superior to 95%. All cells were spread on the surface of the well, as shown in Figure 97a and b. This confirmed that no unexpected events other than the swelling induced gelation caused cellular death. Negative controls, corresponding to empty hydrogel films, showed the complete absence of fluorescent signal, as shown in Figure 97c and d. This confirmed that the signal observed in Figure 95 was emitted by stained cells.

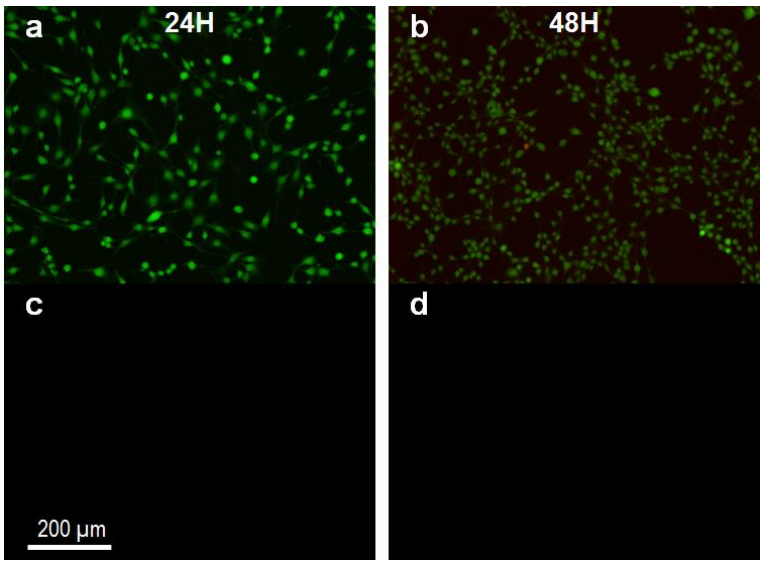

Figure 97 Epifluorescence microscopy observation of the positive control (**a** and **b**) and of the negative control (**c** and **d**) at 24 and 48h.

The morphology and spatial distribution of living cells was also investigated using confocal microscopy. Figure 98 shows observations in a region containing cells in a 450x450x144 μm^3 volume close to the edge of the film after 24 and 48h. No significant differences were seen between the two time points. In these regions a local viability of 73±20 % was measured (n=137 cells). All the living cells had a spherical shape with a mean diameter of 14.5±1.5 µm, which is comparable to the initial size of the cells as measured before encapsulation (15µm).

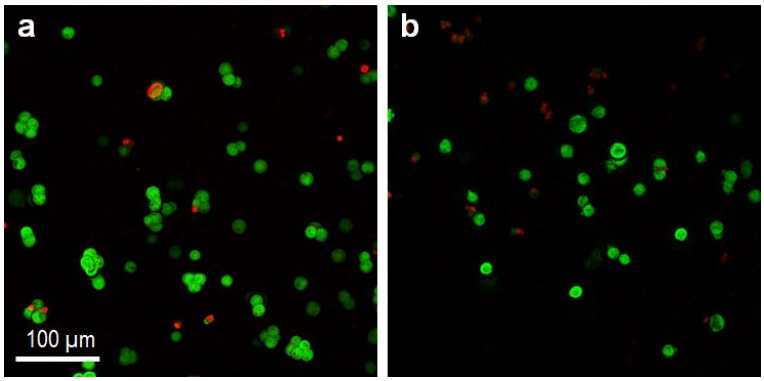

Figure 98 Confocal microscopy imaging of the cells inside the hydrogel film at 24 (**a**) and 48 (**b**) h.

9.4 Discussion

These results show that a protocol based on swelling induced gelation can be devised to encapsulate fibroblastic cells, which remain viable after 48h. Both MTT and fluorescence observations show that the viability of the encapsulated cells strongly depend of the position inside the hydrogel film. In particular, viable cells were encapsulated at distances far from the center (>6 mm) and from the bottom-face (>700 µm). This distribution of living encapsulated cells is possibly related to the process of hydrogel film formation.

During the first 30 minutes, the preliminary experiment (Figure 91) has shown that a thin uniform hydrogel layer was formed at the surface of the swelling PEG substrate. Based on MTT observations, we can say that no living cells have been encapsulated in this layer.

This could be explained by the fact that the solvent flux (J_s) at the surface of the swelling PEG substrate induces a solvent depletion in this region and leads to a strong hypertonic medium, in which the solvent concentration is too low for cellular viability ($<\Phi_v$), as described in Figure 99a. Indeed, it has been shown that in a strong hypertonic medium, cells start to dehydrate and shrink that engenders a decrease of their viability.[18]

After 30min of swelling, we have shown that the film is attached to the wall, inducing a constrained swelling of the substrate starts to bulge (Figure 91c and d) As a consequence, the stretching of the PVA hydrogel film by the swelling PEG substrate imposes a permanent thinning of the film at its center, as indicated by blue arrows in Figure 99b. Although the solvent depletion at the surface of the substrate continues to induce the gelation of additional PVA hydrogel layers, the thickness of the PVA hydrogel film increases much more on the edge than at the center of the film. This might be due to the lower mass transport in the stretched region.

Between 1 and 3 hours and in the edge of the film (Figure 99c), the thickness of the PVA film increase as well as the solvent concentration (Φ_{H2O}) in the PEG substrate. The combination of these two effects leads to a lower concentration gradient of the solvent in the PVA film. If the concentration of cytotoxicity (Φ_v) is lower than the gelation concentration (Φ_c), then there is a zone (purple zone in Figure 99c) of few hundreds of µm in which the solvent concentration is low enough to enable the gelation to occur and high enough to encapsulate living cells.

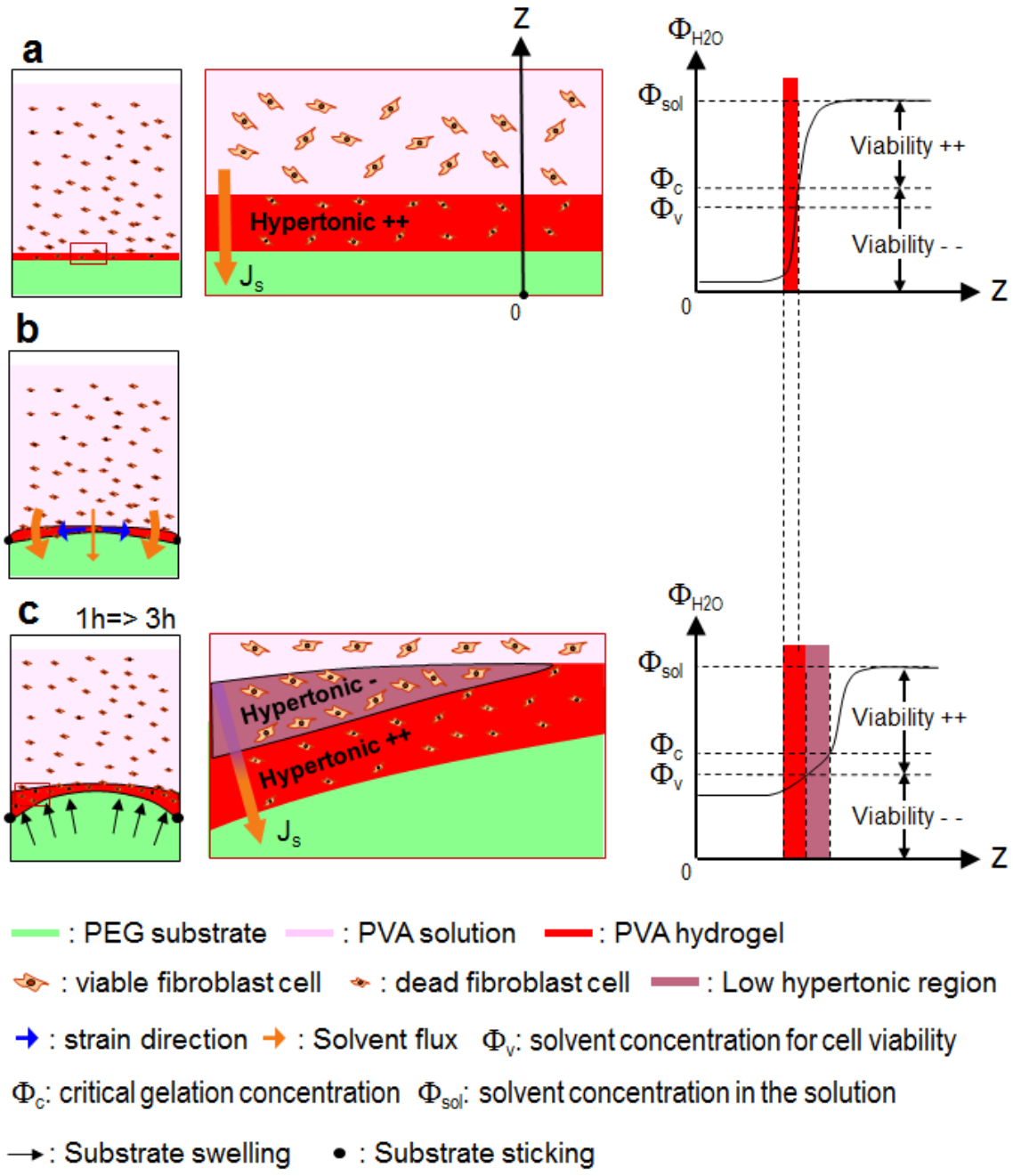

Figure 99 Schematic drawing suggesting the evolution of the cell viability during the film formation.

Another important feature of the films with encapsulated cells is the very heterogeneous distribution of the cells in the films with regions of low and high cell concentration. This might due to the fact that the initial distribution of cells in the PVA/growth medium solution was heterogeneous. During the preparation of the cell/PVA/growth medium solution, a homogenization step was done by 5 linear up and down motions in a 50 mL syringe. This protocol might not have produced a very homogeneous cell

dispersion. Such a mild procedure was chosen on purpose not to damage the cells at this stage of the process. In our process, we calculated the shear rate $\dot{\gamma}$, induced at the tip of the syringe. It has been estimated to $\dot{\gamma}=13\ s^{-1}$, as given by[19] $\dot{\gamma}=4Q/\pi R^3$ with $Q=200\ mm^3/s$ and $R=2.65$ mm. This value can be compared to the one obtained in a study of Canbolat *et al.*, where an electrospinning technique was used to produce 3T3 fibroblast-encapsulated PVA fibers.[20] They showed that the shear rate induced by the needle, used to produce polymer liquid jet in their process has not affected their cell viability. By the same calculation, we found that their shear rate was $\dot{\gamma}=11\ s^{-1}$, with $Q=0.14\ mm^3/s$ and $R=0.254$ mm. This strongly suggest that our process is not harmful for the cells and that additional up and down motions could be reasonably performed to improve the distribution of cells in the solution and thus in the hydrogel films. In addition, the initial PVA solution concentration could be reduced to decrease the solution viscosity in order to facilitate the mixing. Nonetheless, one should be careful not to decrease the solution below the level required to produce a film by swelling induced gelation, as discussed in chapter 8.

9.5 Conclusion

With this study, we demonstrate the possibility to encapsulate mammalian cells in PVA hydrogel films produced by swelling induced gelation. A simple experimental process was devised and adapted to culture requirements. By this process, PVA hydrogel films were formed spontaneously at the surface of swelling PEG substrates and this gelation caused the encapsulation of fibroblasts, which remained viable after 48h in an incubator. Cell viability was heterogeneous inside the gel film and strongly depends on the concentration gradient impose by the swelling of the substrate. Thanks to these first preliminary experiments, several improvements can be envisioned, such as a different shape of the substrate, a less

concentrated PVA solution or a pre-swollen PEG substrate to soften the concentration gradient, in order to enhance the spatial distribution and the yield of the encapsulation process. Furthermore, the PVA used in this study could be modified by blending or grafting other molecular components in order to improve the proliferation and the adhesion of encapsulated cells.[21,22]

References

1. Lee, J. *et al.* Enhanced regeneration of the ligament–bone interface using a poly(l-lactide–co-ε-caprolactone) scaffold with local delivery of cells/BMP-2 using a heparin-based hydrogel. *Acta Biomater.* **7,** 244–257 (2011).

2. Peppas, N. A., Hilt, J. Z., Khademhosseini, A. & Langer, R. Hydrogels in Biology and Medicine: From Molecular Principles to Bionanotechnology. *Adv. Mater.* **18,** 1345–1360 (2006).

3. Hoffman, A. S. Hydrogels for biomedical applications. *Adv. Drug Deliv. Rev.* **64,** 18–23 (2012).

4. Nicodemus, G. D. & Bryant, S. J. Cell Encapsulation in Biodegradable Hydrogels for Tissue Engineering Applications. *Tissue Eng. Part B Rev.* **14,** 149–165 (2008).

5. Bae, K. H., Yoon, J. J. & Park, T. G. Fabrication of Hyaluronic Acid Hydrogel Beads for Cell Encapsulation. *Biotechnol. Prog.* **22,** 297–302 (2006).

6. Temenoff, J. S. *et al.* Thermally Cross-Linked Oligo(poly(ethylene glycol) fumarate) Hydrogels Support Osteogenic Differentiation of Encapsulated Marrow Stromal Cells In Vitro. *Biomacromolecules* **5,** 5–10 (2004).

7. Griffin, D. R. & Kasko, A. M. Photodegradable Macromers and Hydrogels for Live Cell Encapsulation and Release. *J. Am. Chem. Soc.* **134,** 13103–13107 (2012).

8. Zheng Shu, X., Liu, Y., Palumbo, F. S., Luo, Y. & Prestwich, G. D. In situ crosslinkable hyaluronan hydrogels for tissue engineering. *Biomaterials* **25,** 1339–1348 (2004).

9. Trojani, C. *et al.* Three-dimensional culture and differentiation of human osteogenic cells in an injectable hydroxypropylmethylcellulose hydrogel. *Biomaterials* **26,** 5509–5517 (2005).

10. Tasoglu, S. & Demirci, U. Bioprinting for stem cell research. *Trends Biotechnol.* **31,** 10–19 (2013).

11. Schmedlen, R. H., Masters, K. S. & West, J. L. Photocrosslinkable polyvinyl alcohol hydrogels that can be modified with cell adhesion peptides for use in tissue engineering. *Biomaterials* **23,** 4325–4332 (2002).

12. Martens, P. J., Bryant, S. J. & Anseth, K. S. Tailoring the Degradation of Hydrogels Formed from Multivinyl Poly(ethylene glycol) and Poly(vinyl alcohol) Macromers for Cartilage Tissue Engineering. *Biomacromolecules* **4,** 283–292 (2003).

13. Shaheen, S. M. & Yamaura, K. Preparation of theophylline hydrogels of atactic poly(vinyl alcohol)/NaCl/H2O system for drug delivery system. *J. Controlled Release* **81,** 367–377 (2002).

14. Vrana, N. E., O'Grady, A., Kay, E., Cahill, P. A. & McGuinness, G. B. Cell encapsulation within PVA-based hydrogels via freeze-thawing: a one-step scaffold formation and cell storage technique. *J. Tissue Eng. Regen. Med.* **3,** 567–572 (2009).

15. Vrana, N. E. *et al.* Cell encapsulation and cryostorage in PVA-gelatin cryogels: incorporation of carboxylated ε-poly-L-lysine as cryoprotectant. *J. Tissue Eng. Regen. Med.* **6,** 280–290 (2012).

16. Lawson, A., Ahmad, H. & Sambanis, A. Cytotoxicity effects of cryoprotectants as single-component and cocktail vitrification solutions. *Cryobiology* **62,** 115–122 (2011).

17. Schneider, C. A., Rasband, W. S. & Eliceiri, K. W. NIH Image to ImageJ: 25 years of image analysis. *Nat. Methods* **9,** 671–675 (2012).

18. Zawlodzka, S. & Takamatsu, H. Osmotic injury of PC-3 cells by hypertonic NaCl solutions at temperatures above 0°C. *Cryobiology* **50,** 58–70 (2005).

19. Aguado, B. A., Mulyasasmita, W., Su, J., Lampe, K. J. & Heilshorn, S. C. Improving Viability of Stem Cells During Syringe Needle Flow Through the Design of Hydrogel Cell Carriers. *Tissue Eng. Part A* **18,** 806–815 (2012).

20. Fatih Canbolat, M., Tang, C., Bernacki, S. H., Pourdeyhimi, B. & Khan, S. Mammalian Cell Viability in Electrospun Composite Nanofiber Structures. *Macromol. Biosci.* **11,** 1346–1356 (2011).

21. Ino, J. M., Chevallier, P., Letourneur, D., Mantovani, D. & Le Visage, C. Plasma functionalization of poly(vinyl alcohol) hydrogel for cell adhesion enhancement. *Biomatter* **3,** e25414 (2013).

22. Ino, J. M. *et al.* Evaluation of hemocompatibility and endothelialization of hybrid poly(vinyl alcohol) (PVA)/gelatin polymer films: Hemocompatibility And Endothelialization Of Hybrid PVA/Gelatin Polymer Films. *J. Biomed. Mater. Res. B Appl. Biomater.* **101,** 1549–1559 (2013).

Section 5. Hydroxyapatite coatings on PVA hydrogels by cold spray

In this section, we explored a different method, based on thermal spraying technique, to coat a thermo-sensitive polymeric substrates with a bioceramic layer. This process could allow to obtain pure coatings of HA on PVA hydrogel substrates and reach higher density at its surface than using the dip-coating method. At the "Centre des Matériaux", a cold spray apparatus is available and allow to spray HA powders through a jet of compressed heated gas at rather low temperature (~200-600 °C) onto soft and thermo-sensitive PVA substrates. In the literature, there is no study presenting experiments related to the production of HA coating on PVA substrates or other type of hydrogel substrates. Previous works have been done using titanium alloy or polyether ether ketone (PEEK) substrates.

In the chapter 10, the process and the used set-up are firstly presented. Then a systematic study of the spraying parameters is performed to identify appropriate sets of cold spray condition. Then by means of electronic microscopy, we explore the structure of the coating and the interface with the substrate and propose a mechanism of coating formation. Lastly, the behaviour of such a coating in water is characterized by swelling of the substrate.

In the chapter 11, we compare two types of commercial HA powders: a non-calcined and the calcined (used in chapter 10) powders. The composition of these powders strongly affects the formation of the coating and we notice that different coating structures and dimensions can be obtained. In addition, the same systematic study of the spraying parameter is also performed with the non-calcined powder.

Chapter 10. Cold spray coating of submicronic hydroxyapatite on poly(vinyl alcohol) in dry and hydrogel states

10.1 Introduction

Polymer hydrogels have a high potential for osteo-articular soft-tissue replacement. They are composed of a three-dimensional network of hydrophilic macromolecules swollen with water. This kind of structure is very close to that of connective tissues. In particular, poly(vinyl alcohol) (PVA) is a synthetic polymer, that can be physically cross-linked to form non-degradable hydrogels with a good history of biocompatibility.[1] Such PVA hydrogels are already used in clinic for cartilage replacement,[2] and numerous researches are currently carried out to develop artificial meniscus,[3] ligament,[4] and intervertebral disc.[5] One of the main challenges for these substitutes of soft osteo-articular tissues is to ensure sufficient anchorage to hard bone tissues. It has been shown *in vitro* [6,7] and *in vivo* [3,8] that PVA hydrogel is inert and does not adhere to cells or surrounding tissues. It usually gives rise to foreign body reaction: after implantation, an inflammatory response occurs and is followed by the encapsulation of the implant by immune system cells and a loose fibrous tissue. The mechanical properties of the interface between the PVA hydrogel and fibrous tissue are not strong enough to withstand musculoskeletal forces and this may lead to a detachment of the implant. One approach to avoid this fibrous encapsulation and thus strengthen the bone-implant interface consists in functionalizing the implant surface with a bioactive ceramic coating. In this study hydroxyapatite (HA) is used as a coating to promote the adhesion and proliferation of bone cells. Hydroxyapatite is widely used as bone substitute and as coating for metallic prostheses.[9,10] Here we study the cold spray process to achieve HA coating from HA powder propelled at supersonic velocities to form a HA layer at the surface of PVA

substrates. The aim of the work is to obtain a pure crystalline HA coating that can resist immersion in water to form a coating on a PVA hydrogel substrate.

Several methods have been explored to coat PVA hydrogels with calcium-phosphate ceramics including blending of ceramics with PVA solution, [6,11,12] alternate soaking, [13] *in situ* CaP formation in PVA solution.[14] These methods require several steps and are not convenient to coat a specific area of a PVA implant. Recently, Hayami *et al.* have studied a HA coating process based on pulse laser deposition.[15] The laser irradiation of a bulk target under vacuum atmosphere allows the non-thermal deposition of nanometric apatite film on a PVA hydrogel substrate made by freezing/thawing. However, the produced thin film is with amorphous HA. Further crystallization would be needed to restore crystalline HA, but PVA hydrogel substrate cannot stand heat treatment above 85°C.[16] Other spraying techniques using HA powder could be an alternative solution to produce ceramic coating on PVA. Plasma spraying is a well-known technology to apply HA coating on metallic implant.[17] But this process induces the melting of the HA powder above temperature of 1600°C that could lead to PVA degradation. Moreover, the HA thermal decomposition that occurs during plasma spraying promotes the presence of highly soluble amorphous HA.[18] In this context, a solid state spraying process like cold spray technology appears to be an interesting candidate because pure and crystalline HA could be deposited without extensive incoming heat.

Cold spray is a high velocity deposition process of powder without melting of particles. Particles are injected in a jet of compressed heated gas (N_2, He), typically at temperatures ranging between 200-600 °C and pressure between 1-3 MPa in our case, or above in latest generation of cold spray systems. This technology is generally used to achieve coating of ductile metal.[19] Particles are accelerated with the gas by passing through a De Laval type nozzle and are propelled at a supersonic speed onto a substrate. Few realizations of cold spraying hydroxyapatite coatings onto polymer substrates have been reported.[20,21]

Recently Lee *et al.* have produced pure HA coatings of about 100 µm on poly(ether-etherketone) (PEEK) implant cage.[20] *In vivo* evaluation in rabbit model shows a good osteointegration with no fibrous encapsulation. PEEK is a thermoplastic polymer with high melting temperature of 350 °C and high elastic modulus (3.6 GPa).

In this work, two different processing routes were compared to achieve a coating on PVA hydrogel. They are illustrated in Figure 100. For both methods, a dry PVA substrate was produced by solvent casting using the evaporation of water for which physical crosslinking of PVA occurs, as shown by Otsuka et *al.*[22] In a first route (Figure 100a) PVA dry substrates were swollen in water to form PVA hydrogel and then were cold sprayed with HA powder. In a second route (Figure 100b), the dry PVA substrate were first cold sprayed and then swollen. The effects on coating formation of the following cold spray parameters: temperature (T) and pressure (P) of the stagnation gas, stand-off distance (SoD) of the nozzle were investigated to determine a suitable parameters window. By means of microscopic imaging, we characterized the coating and the interface between the deposited particles and the substrate. The morphology and the structure of the PVA/HA interface were investigated by combining optic and scanning electronic microscopy of top-view and cross-section. Based on these observations, also from these of the starting powder, a build-up mechanism is proposed to explain how HA coating was formed by implementing high velocity impacts of HA particles.

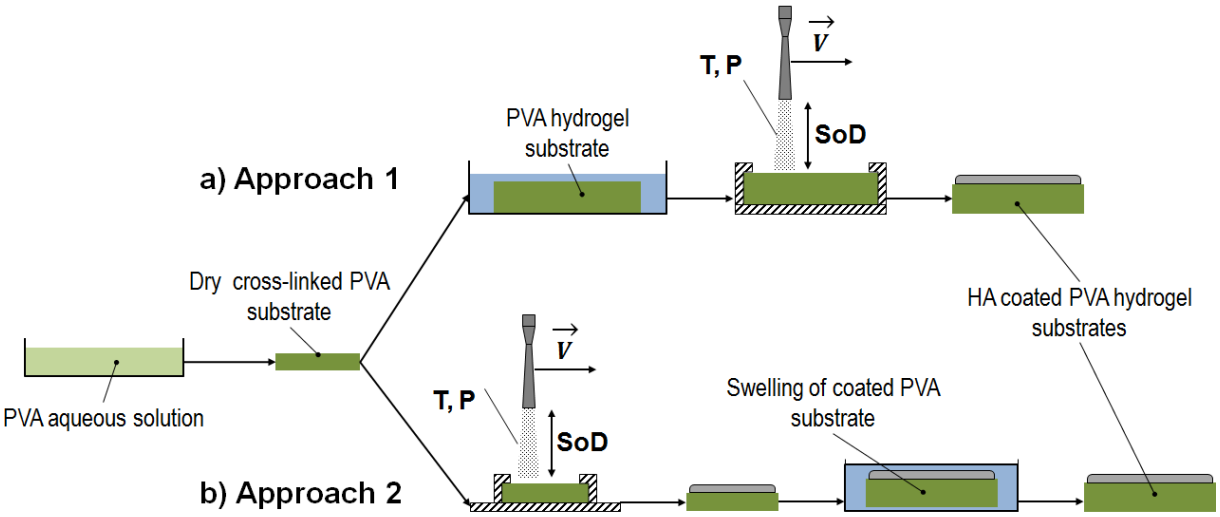

Figure 100 Studied approaches to produce cold-sprayed ceramic coatings on PVA hydrogels: **a)** Approach 1: swelling and spraying. **b)** Approach 2: spraying and swelling.

10.2 Materials & Methods

PVA substrate:

As explained in the Section 2, PVA substrates were produced by solvent casting. A 10 wt% PVA aqueous solution was poured in Petri dishes, put in a vacuum-oven at 700 mbar and 70 °C for 8 h under air and cooled at room temperature for 12h.

Hydroxyapatite particles:

In this study, the calcined HA particles are used and are described in the Section 2. In short, it is a medical grade powder of hydroxyapatite (S.A.I. Medical Group, France) always used for plasma. Particles size analysis was carried out in dry dispersion medium using a Malvern Mastersizer 3000 particle size analyser.

Cold spray apparatus:

The cold spray apparatus used was a cold spray Kinetiks 3000 (Oerlikon Metco, Switzerland). It is composed of several components: a gas tank, a controller, a particle feeder, a gas heating unit and a spraying booth containing the spraying gun and the moving-holder. Figure 101 described the cold spray set-up.

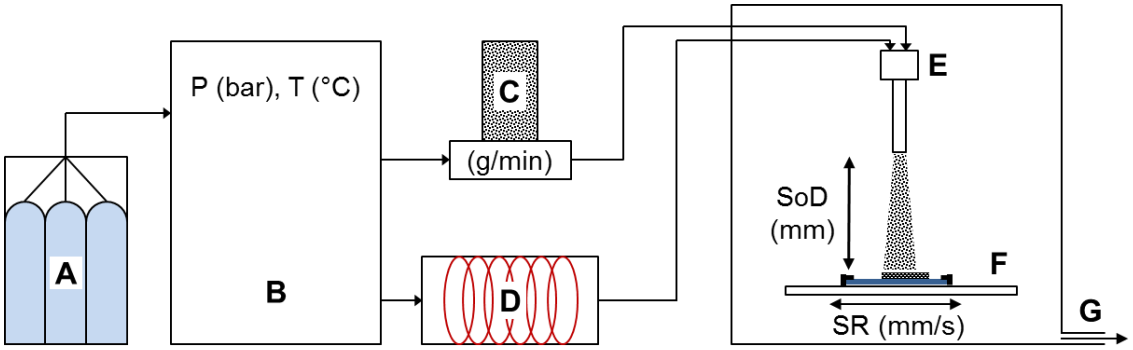

Figure 101 Schematic drawing of the cold spray apparatus: **a**) Gas tank bundle; **b**) Control cabinet **c**) Powder feeder; **d**) Gas heater; **e**) Spray gun; **f**) Moving sample holder; **g**) Dust extractor.

The nitrogen process gas was stored in tanks (**A**) outside the spraying room. The gas temperature and pressure were regulated by the controller (**B**). The gas pressure 'P' could be chosen between 1.0 and 3.0 MPa. Prior passing through the spray gun (**E**), the process gas was heated at given temperature 'T' that could be selected between 200 and 600 °C (**D**). The hydroxyapatite powder was stored in the disk powder feeder (**C**). The particle flow was set at 7±1 g/min for both type of particles. It was estimated by weighing the quantity of particles going out from the nozzle during 1 minute. Figure 102a shows a picture of the spraying booth with the sample holder and the spraying gun. Samples were fixed on a holder, moving straight along X axe (**F**) at a given speed rate 'SR' and at a given stand-off distance 'SoD' from the nozzle. Only one pass coatings were produced. The holder was composed of an aluminium plate on which stainless steel mask were screwed to maintain the samples during spraying, as shown on Figure 102b. Once the samples were fixed on the holder, the spray booth was

locked and dust extractor was turned on (**G**). Prior to start spraying, a stabilization period was required until the process gas has reached the targeted pressure and temperature.

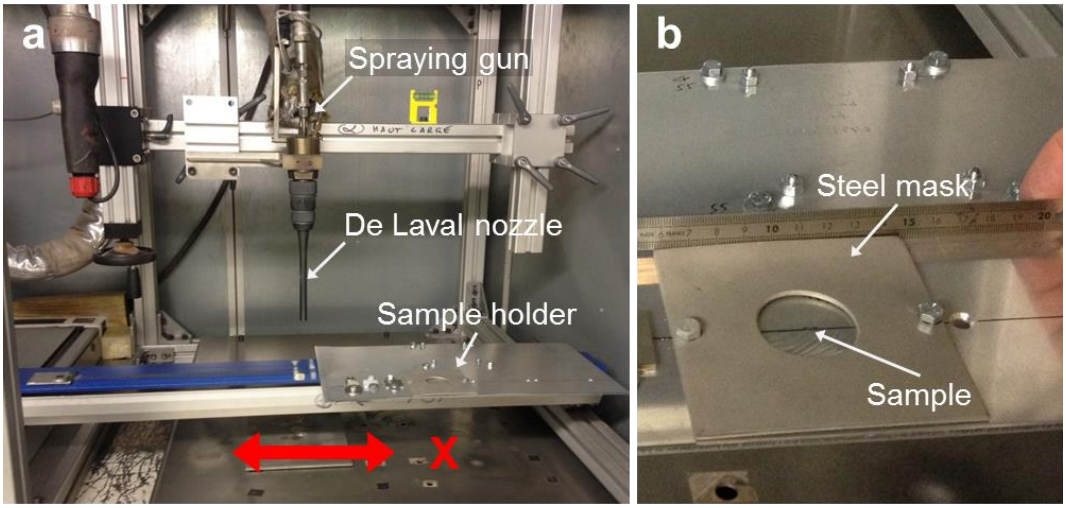

Figure 102 a) Spraying booth; **b**) Sample holder

Cold spray parameters:

The HA powder carried by the process gas was sprayed on dry PVA substrates at different given gas temperatures (T), pressures (P), stand-off distances (SoD) and speed rates (SR). These studied parameters are summarized in Table 8.

P (MPa)	T (°C)	SR(mm/sec)	SoD (mm)
1.0 – 2.0 – 3.0	200 - 300 - 400 - 500 - 600	10	30 - 60 - 100 - 190

Table 8 Cold spray parameters

These experiments were exploratory and the complete range of potential cold spray parameters were envisaged (See Appendix 3). In order to investigate the single effect of each parameter, three parameters were kept constant and only the fourth one was varied.

Differential Scanning Calorimetry measurements:

Thermograms were obtained on a TA Instrument Q2000 differential scanning calorimeter. Sample for DSC measurements were cut from the dry PVA substrate and

weighed about 3 mg. The temperature ramp was 0 to 250 °C upon heating at a rate of 10 °C/min.

Microscopic observations:

Macroscopic observations were performed with a M420 Wild-Leitz Leica macroscope. Microscopic observations were made with an Axio Scope A1 Zeiss microscope in dark field reflection mode at a 5x magnification. SEM observations were performed on a Nova Nano SEM 450 SEI apparatus at 7 kV. Ultra-high magnification images were performed at 5kV with immersion mode. The immersion mode corresponds to an immersion of the sample in a magnetic field, which enhances the electron collection and reduces aberrations. Hydrated PVA samples were observed with low-vacuum mode at 90 Pa and 7 kV. Cross-section of HA coated PVA substrates were realized by cryo-fracturing. Samples were soaked in liquid nitrogen for 2 min and were fractured using pliers.

Temperature measurement:

A thermocouple (2AB, FIM K, Thermocoax) was embedded in a PVA substrate. A 10 wt% PVA solution was poured in a Petri dish where the thermocouple was placed. Then the whole system was put in a vacuum-oven at 700 mbar and 70 °C for 8 h under air and maintained at room temperature for 12h. The thickness of PVA between the thermocouple and the surface of the substrate was less than 500 µm. The embedded thermocouple was placed under holding mask. The spraying parameters for this experiment were T=230°C, P=1 MPa and SoD=30 mm.

Swelling experiments:

PVA substrate was hold in a glass tube filled with ultra-pure water under magnetic stirring. The temperature was kept at 37 °C by a regulation system. The substrate was able to swell freely for a week. Sample weight was measured over time and the PVA hydrogel water

content (wt%) was calculated as follows: $WC=(M_t - M_i)/M_{eq}$, where M_t is the mass at time t, M_i is the mass at t_0 and M_{eq} is the mass at equilibrium.

10.3 Results

Powder characterization:

The HA powder is manufactured industrially by atomization of HA slurry and further calcination at 1050 °C for 40 hours. The microstructure, the chemical composition and the crystallographic structure are described in the Materials chapter. The size of the particles was characterized by dry dispersion and the measured distribution is given in Figure 103a. The powder diameter is comprised between 20 and 70 µm for a mean value of 40 µm and 90 % of the population is under 61 µm. The spherical morphology and microstructure were examined by SEM with BSE mode (Figure 103b). Further observations at higher magnification show that these particles are made up with aggregates of fused submicronic particles having a size of about 500±150 nm, as estimated in Figure 103c. Numerous voids are evidenced in a cross section SEM BSE view of one single particle after mounting in resin and polishing (Figure 103d). It shows that the large spherical particles are highly porous and fully agglomerated. Quantitative image analysis of this image after thresholding and binarization confirmed a high porosity level of 57±7 %.

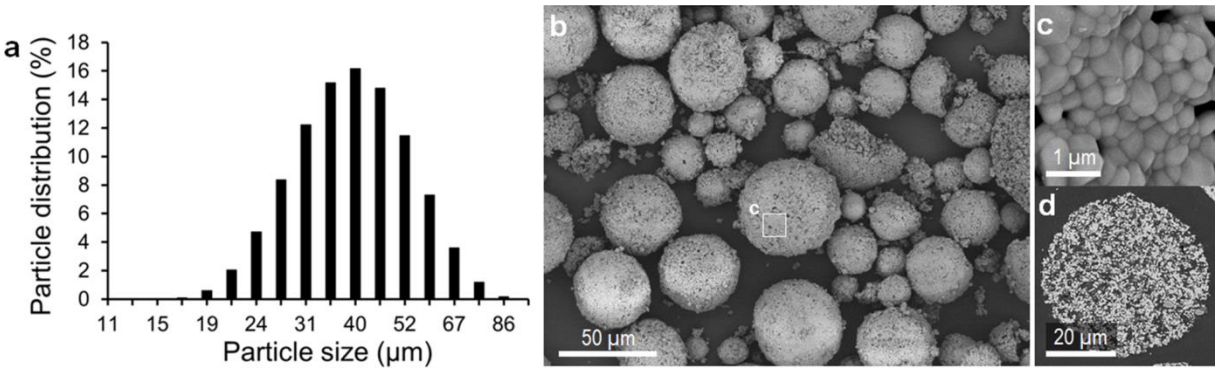

Figure 103 Characterization of HA powder used for cold spray. **a**) Size distribution of HA particles by dry dispersion; Scanning electronic microscopy using backscattered electron detector: **b**) HA particles; **c**) surface of one HA particle showing sintered nanoparticles; **d**) cross-section of one HA particle.

PVA substrates characterization:

Dry PVA substrate and hydrogel PVA (swollen at equilibrium) substrate were studied. Both substrates were obtained by solvent-casting from an aqueous solution of PVA using the same protocol as the one described by Otsuka *et al.*[22] As shown in Figure 104, dry (a) and swollen (b) substrates were cut in the shape of half disc prior to spraying. They have a thickness of about 540±170 µm and 760±250 µm respectively. Dry PVA substrates correspond to the substrates obtained after complete evaporation of water. The physical network that is formed through formation of PVA crystallites was ascertained by using DSC analysis. Figure 104c shows the thermogram obtained upon heating. It clearly shows the existence of an endothermic peak at 225±1°C, which corresponds to the melting of PVA crystals.[23] The estimated melting temperature was 212°C. The degree of crystallinity, Xc, was estimated as: $Xc=\Delta H^*/\Delta Hc$, where ΔH^* is the heat of fusion of the PVA sample and ΔHc is the heat of fusion of a 100% crystalline PVA.[24] The heat of fusion requires to melt a 100% crystalline PVA was chosen to ΔHc= 138.6 J/g. The area of the peak gave an estimated value the enthalpy of fusion ΔH^*=65.5 J/g. The crystallinity Xc was then calculated to 47.3%. Hydrogel PVA substrates were obtained by immersing the dry PVA substrates in water for 24 hours. The substrates do not dissolve and form a stable hydrogel. Figure 104d shows the evolution of the water content over time. The swelling curve indicates that equilibrium is

reached after 3 hours. The water content at equilibrium is 57±1 wt%. Upon heating above 85°C, swollen PVA hydrogel substrates completely dissolves after 1 hour, as it is commonly known.[16]

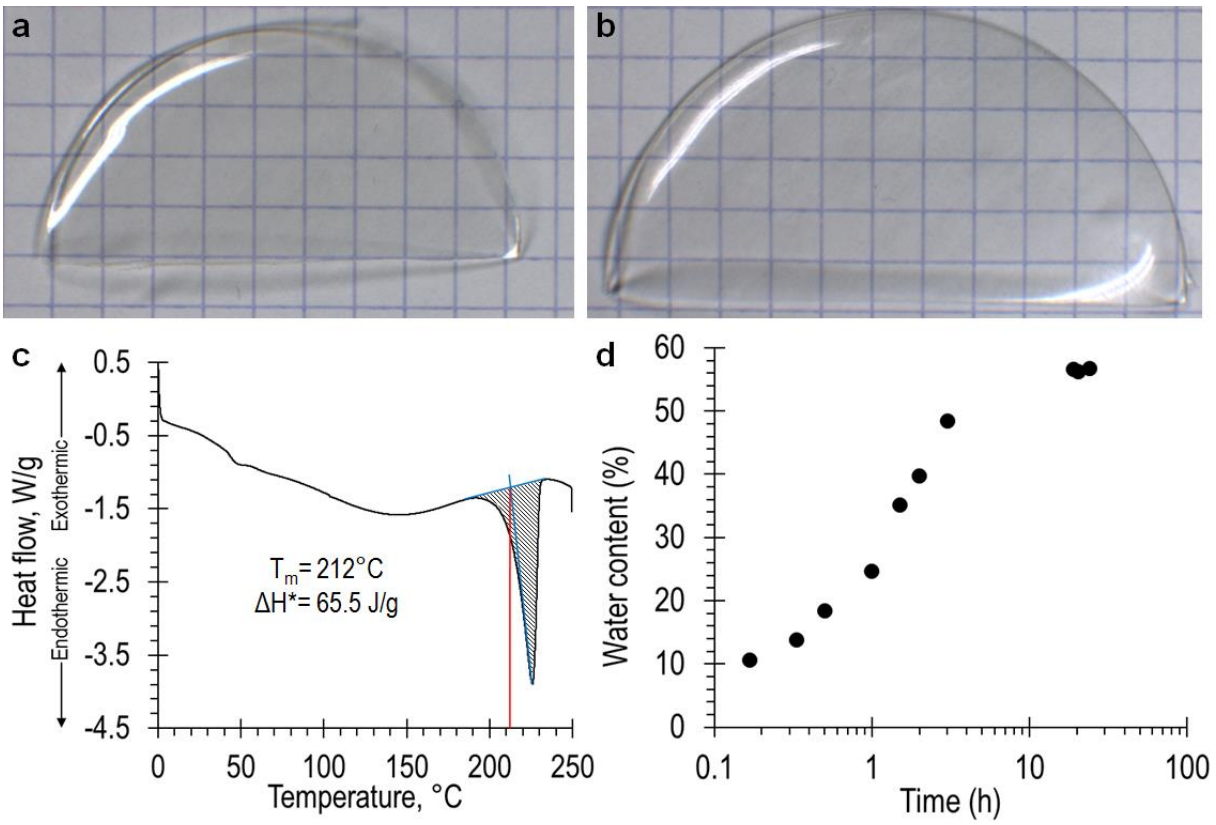

Figure 104 Characterization of PVA substrate used for cold spray: **a**) Dry PVA substrate obtained by solvent casting; **b**) Hydrogel PVA substrate swollen at equilibrium; **c**) DSC thermogram of dry PVA film upon heating from 0 to 250°C at 10°C/min; **d**) Water content of bare PVA hydrogel substrate as a function of time.

<u>HA coating by cold spray on PVA substrates:</u>

In a first series of experiment, we studied the feasibility of routes 1 and 2 described in Figure 100, using the lower temperature and pressure of nitrogen gas for cold spray, respectively T=200 °C, P=1.0 MPa and shorter SoD=30 mm. Figure 105a and b are resulting from processing routes of Figure 100a and b respectively. For route 1, the swollen PVA substrate was fully damage and completely removed by the gas stream during the spraying process. For route 2, it was obvious that the dry substrate could resist to the gas stream. Moreover a rather wide pass of HA (~8 mm) was coated onto the dry PVA substrate without

any macroscopic evidence of degradation. The white HA coating seemed homogeneous and adherent to the substrate. These primary results allowed to conclude that the hot and supersonic gas stream with HA powder prevents the spraying on soft and swollen substrates like PVA hydrogels. Conversely, very encouraging result was obtained to achieve the first step of route 2 because one HA layer could be obtained in case of rigid and dry PVA substrate. Thus, even if processing route 1 could be further investigated to prevent hydrogel PVA degradation. It was chosen to explore further spraying parameters only for route 2 in order to optimize the cold spray parameters.

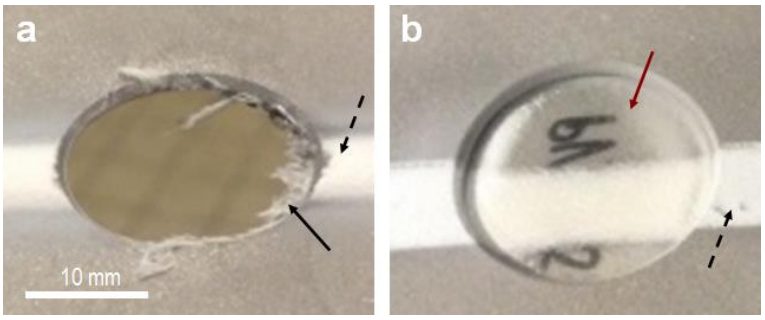

Figure 105 Substrate state after one pass at T=200 °C, P=1 Mpa and D=30 mm: **a**) Cold spraying of hydrogel PVA substrate; **b**) Cold spraying of dry PVA substrate. Black arrow: rest of destroyed PVA hydrogel substrate; black dashed arrow: HA pass; red arrow: dry PVA substrate.

Effects of cold spray parameters (route 2):

The effects of main cold spray parameters (temperature, pressure and stand-off distance) were further investigated in case of route 2. For the shorter stand-off distance (30 mm), the temperature of the stagnation gas was systematically varied between 200 to 270°C for the lower pressure of nitrogen (1.0 MPa). Optical macroscopic top-surface views of the resulting pass of the different HA coatings are given in Figure 106a-d. Neither charring nor physical damage of the substrate was noticed within the 200°C-250°C range of temperature. In general, cold spray coatings are be achieved with gas temperature up to 600°C. In case of dry PVA substrate of route 2, it is obvious that the colour the HA pass turned to brown-yellow at 270°C, as shown in Figure 106d. This evidence of thermal degradation prevents the application of higher temperature of the stagnation gas. Higher nozzle velocity could be

envisaged to limit the time exposure to the heated gas made but wasn't investigated in this work. We focused on the influence of the SoD parameter that would drastically limit the heat and pressure of the gas stream toward the substrate when it is increased. The effect of stagnation gas at highest pressure (P=3.0 MPa) for the lowest temperature (T=200°C) and the shorter spraying distance (SoD=30 mm) was also envisaged to propel HA particles with higher velocities without further thermal input. With such cold spray parameters, a homogeneous coating was realized without evidence of thermal degradation through by the colour modification of the substrate, as depicted in Figure 106e. When the stand-off distance is increased to 60 mm, it is possible to increase the temperature of the propelling gas up to 300°C with the lower pressure as long as the gas pressure is maintained to 1.0 MPa, as shown on Figure 106f. When the pressure is increased to 3 MPa with same other parameters, the substrate is completely charred and burst, as shown on Figure 106g. Using a higher stand-off distance (SoD=150 mm), which is not conventional in cold spray technology, spraying experiments were also achieved with higher temperature (T=400°C) and at a rather high pressure of nitrogen (2.0 MPa). For this latter case, one HA coating with no macroscopic damage was obtained, as shown in Figure 106h. One should notice that increasing the stand-off distance induced an increase of the coating spread with a more diffuse spatial distribution of the HA pass. Width of the HA passes was measured from the macroscopic observations. The measured widths are 7.6±0.1, 8.8±0.2 and 12.6±0.3 mm for stand-off distance of 30, 60, and 150 mm, respectively. With these experiments, we investigated the effect of the different spraying parameters. In the following, we will thoroughly characterize the PVA/HA interface and other HA coating's features for the lowest temperature (T=200°C) and pressure (P=1.0 MPa) condition, corresponding to Figure 106a.

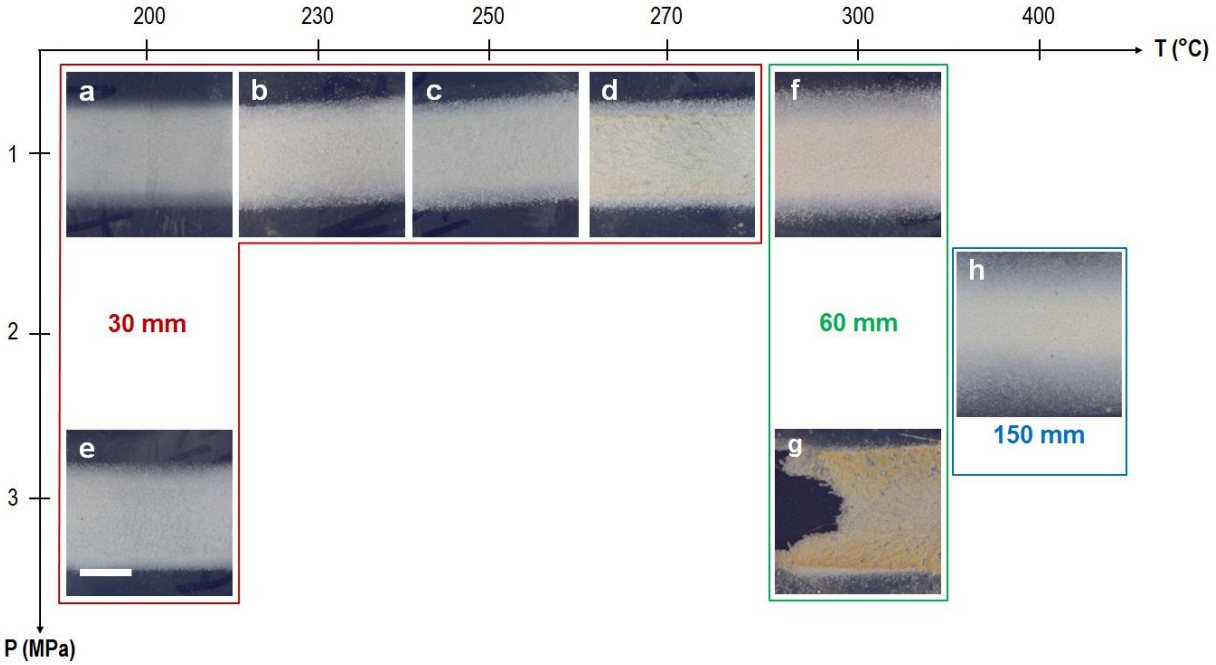

Figure 106 Macroscopic views of the surface of HA coated PVA substrates cold sprayed with different spraying parameters.

Microscopic characterization of the coating structure:

A microscopic observation of the coated specimen was performed for the following spraying parameters: T=200 °C, P=1.0 MPa, SoD=30 mm. Figure 107 shows different areas of the pass surface of the coating observed by SEM. In SE mode, single and isolated spherical impacts (white star) of HA particles can be distinguished at the boundary of the HA pass, i.e. the area where the HA particles were less numerous and without overlapped impact, as shown on Figure 107a. BSE detector gives a chemical contrast of the same boundary area, as given in figure 107b. This observation clearly evidenced the difference between the HA coating (light grey area) and the uncovered PVA substrate (dark grey area). At the centre of the pass, no PVA was detected, as shown in Figure 107c. It ascertained the production of a coating layer that could fully cover the PVA substrate. In this centre region shown in Figure 107c, some spherical HA particles with size similar to the HA starting powder could be detected.

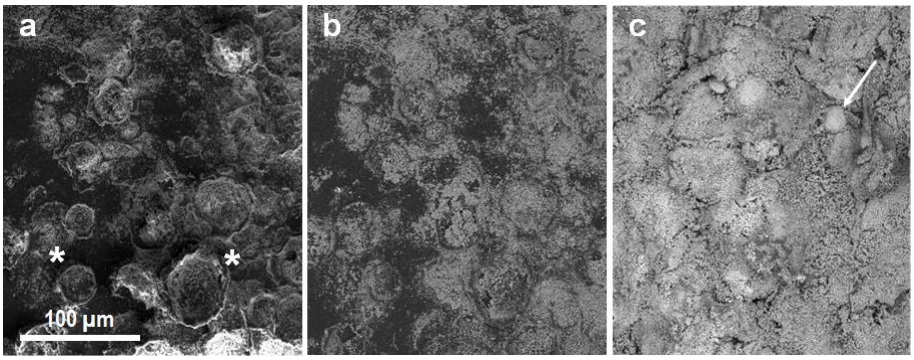

Figure 107 Top surface views of dried PVA substrate coated at T=200 °C, P=10 bar, D=30 mm. Scanning electronic microscopy of the border of the track, in secondary (**a**) and backscattered (**b**) electron mode, white stars highlight crater border; **c**) Scanning electronic microscopy of the middle of the of the track in backscattered electron mode.

Further microscopic observations of the HA/PVA cross-section are given in Figure 108. Optical microscopy observation at low magnification exhibits a continuous white layer with a measured average thickness of 76±12 µm, as shown in Figure 108a. High magnification SEM observations of the interface on cryo-fractured samples are given in Figure 108b and c. It was found that the surface of the PVA substrate has been deformed by the numerous particles to form cavities. Therefore craters have been formed onto the surface, as shown on Figure 108b. It is obvious that initial spherical HA particles have been fragmented into HA submicronic particles and they seem to fully cover the surface cavities, as observed on Figure 108c. Only very few initial particles remain intact, as observed on Figure 108b. The depth of these cavities was similar to the thickness measured by optical microscopy on a coating cross-section (Figure 108a).

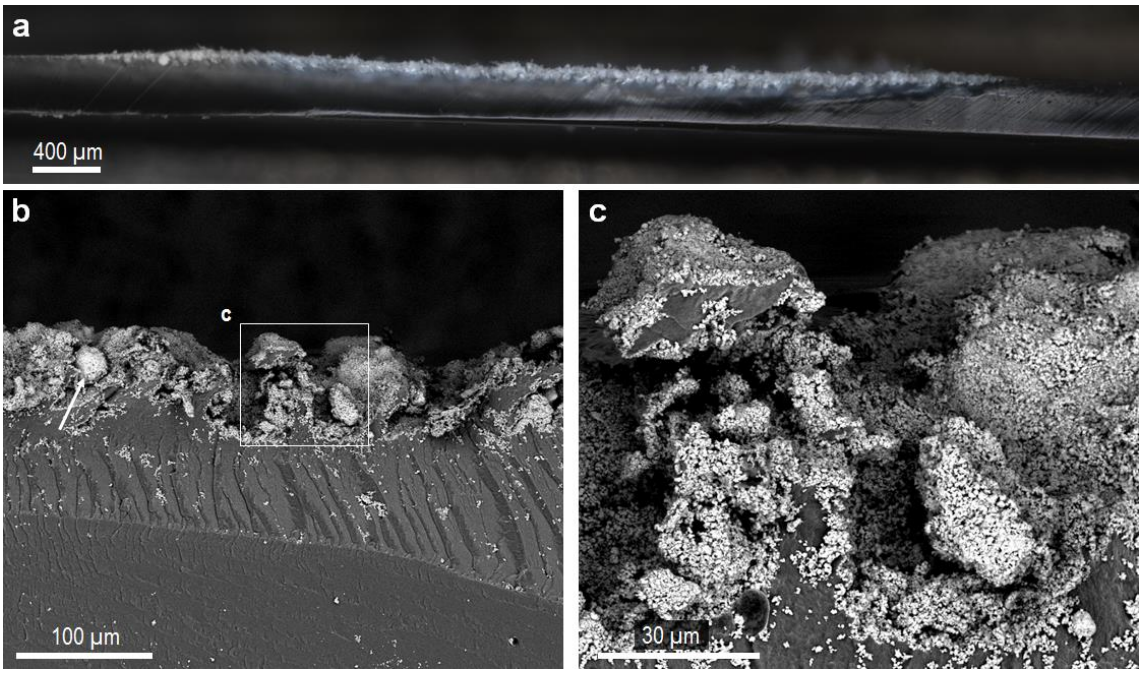

Figure 108 Cross-section views of dried PVA substrate coated at T=200 °C, P=10 bar, D=30 mm. **a**) Optical microscopy of the whole HA coating; **b**) and **c**) Scanning electronic microscopy using backscattered electron detector of the interface between the HA coating and the PVA substrate.

Investigation of the interface between submicronic HA particle and PVA substrate:

The interface between the HA coating and the PVA substrate was observed by ultra-high magnification observations using SEM imaging in immersion mode. As shown Figure 109a, a monolayer of HA submicronic particles was fully covering the surface of one cavity. At higher magnification, in SE mode individual HA submicronic particles (white arrow) are in close contact with the PVA substrate, as shown on Figure 109b. The same area observed with BSE detector on Figure 109c, highlights the close contact between HA submicronic particles (white) and PVA substrate (dark grey). From these observations of the interface it was inferred that the PVA substrate might be locally molten during spraying. Therefore fragmented HA submicronic particles could be better embedded upon cooling of the substrate.

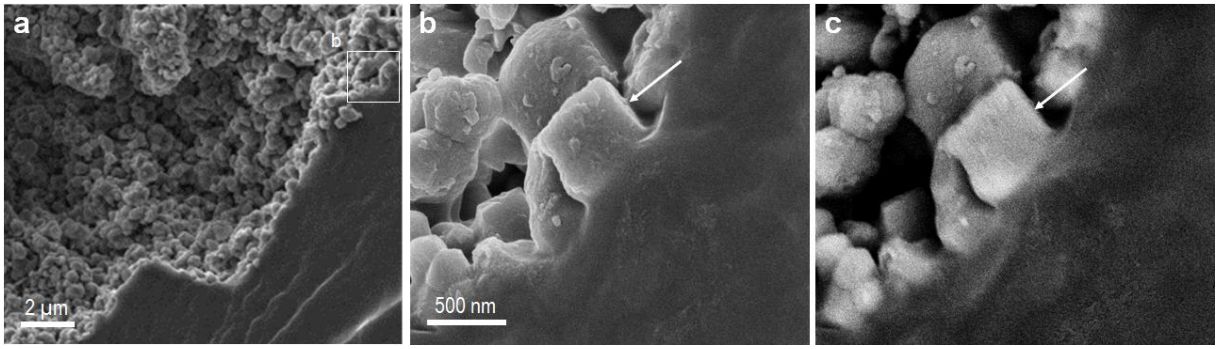

Figure 109 Ultra high magnification scanning electronic microscopy imaging of the interface between HA nano-grains and dry PVA substrate coated at T=200 °C, P=10 bar, D=30 mm. **a**) Interface between HA nano-grains and dry PVA substrate; **b**) View of a single HA nano-grain (white arrow) in secondary electron detection; **c**) Same view in backscattered electron detection.

PVA temperature during cold spraying:

The possible melting of the PVA substrate was explored by measuring the temperature during spraying. This measurement was done thanks to a thermocouple embedded in a PVA substrate. The thermocouple was placed perpendicular to the spraying direction (dashed arrow) and at midway of the holding mask, as shown in Figure 110a. The temperature was recorded in function time as well as the position of the nozzle regarding the thermocouple. Spraying was realized with T=230°C, P=1 MPa and SoD=30 mm. The temperature of 230°C was chosen arbitrarily between 200 and 270°C. The graph on Figure 110b shows that the temperature increased progressively until the nozzle passes right above the thermocouple ($0<t<1$ sec). At this position the temperature recorded is 210±2°C (t=1 s, nozzle position=0 mm). As the traverse speed was set at 10 mm/s, the thermocouple was exposed to this maximum temperature for less than 0.2 s. Then the temperature of the substrate decreases progressively as the nozzle goes away ($1<t<2$ s). These measurements show that a point on the substrate is exposed to a maximum temperature of about 210°C during 0.2 sec. This is consistent with the idea that the PVA can locally melt (T_m=225°C [23]) and the submicronic particles being partially embedded in the PVA substrate.

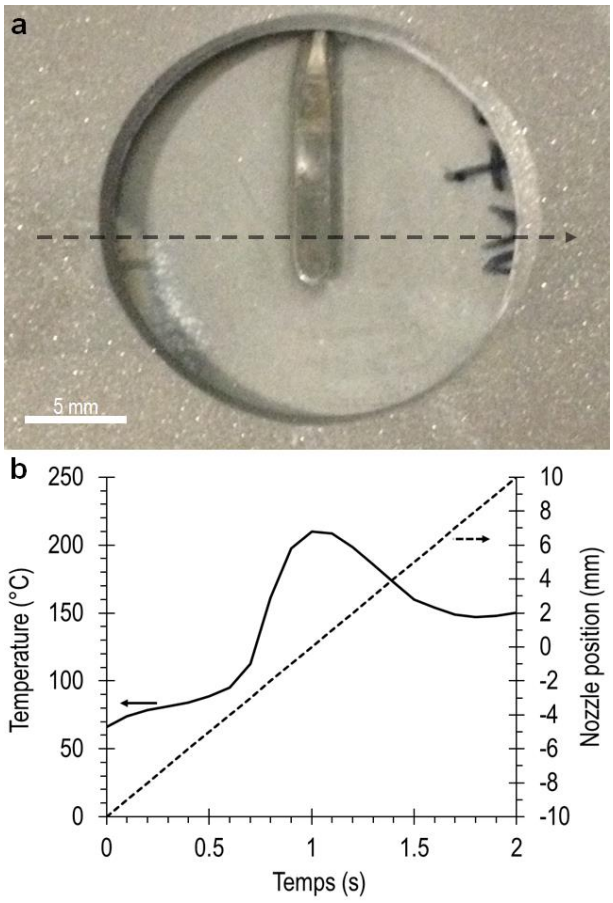

Figure 110 Measurement of temperature during CS process at T= 230 °C P=1MPa and SD=30 mm. **a**) Thermocouple embedded in PVA substrate prior projection; **b**) Temperature and nozzle position relative to the thermocouple in function of time.

Swelling of HA/PVA coating (route 2):

To finalize the route 2, one HA/PVA coating sample was immersed in ultra-pure water for a week at 37 °C under magnetic stirring. Figure 111a and b show the coated substrate before and after swelling, respectively. After this immersion period, it was noticeable that the PVA hydrogel substrate remains fully covered by the HA coating (black arrow). This macroscopic observation was confirmed by SEM observations using BSE detector and low vacuum mode, which allow observations of hydrated samples without sample preparation. On Figure 111c, the surface of the coated hydrogel appears mostly in light grey. This suggests that the substrate (white arrow) is still covered by HA particles (yellow arrow) after swelling. Cross-section view at higher magnification confirmed that craters (white arrow) are still covered by a thin layer of HA submicronic particles (yellow arrow), as observed on Figure

111d. The swelling curve of the coated PVA substrate is reported on Figure 112, the water content of the coated PVA substrate reaches 50±1 wt% after 24 hours of swelling. Its value is 10.7 % less than the swelling of the bare PVA substrate.

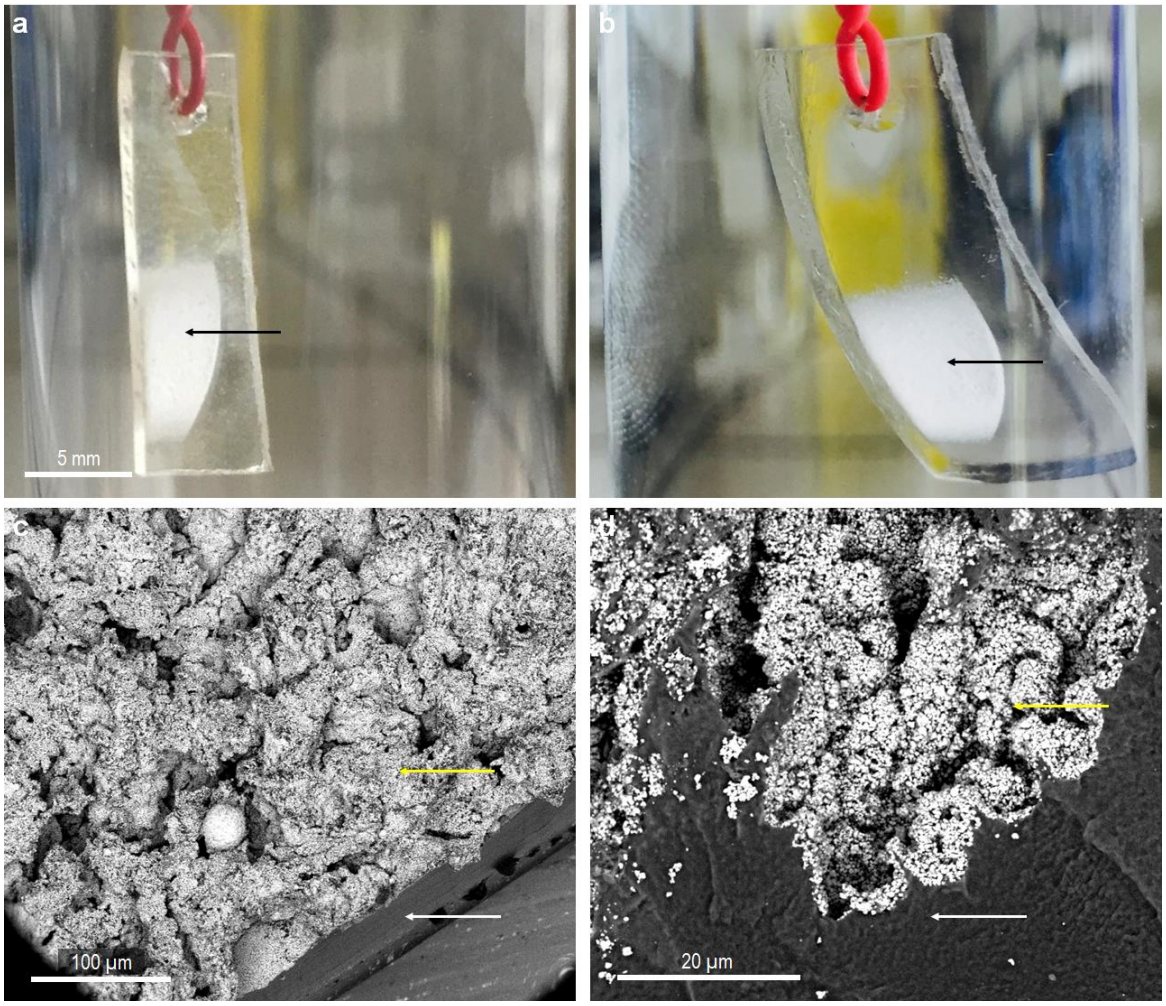

Figure 111 Swelling in water of HA coated PVA substrate (T=200 °C, P=10 bar, D=30 mm) at T_0 (**a**) and after 1 week (**b**) under magnetic stirring at 37°C. Scanning electronic microscopy using backscattered electron detector in low vacuum mode of HA coated PVA hydrogel susbtrate: **c**) Top surface view; **d**) Cross-section view.

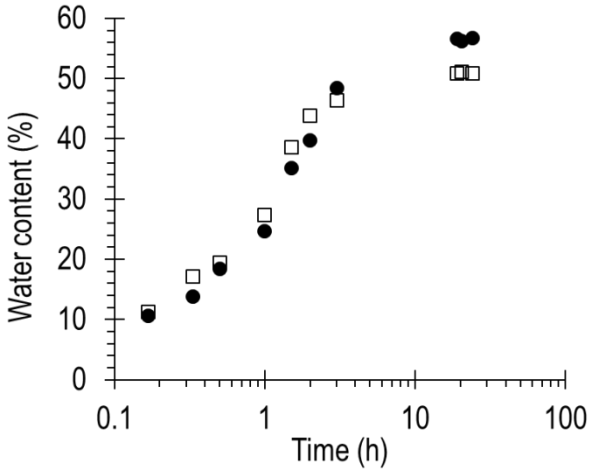

Figure 112 Water content of bare (●) and HA coated (□) PVA hydrogel substrate as a function of time.

10.4 Discussion

The main issue addressed in this work was the assessment of the potential of the cold spray technology to coat hydrogel substrates with a pure and crystalline HA powder to enable bone ingrowth of hydrogel implants. Such HA powder is always used in industry to coat metallic implants by thermal spraying involving the plasma technology to melt the HA particle during coating formation. In our study, we are focusing on a non-thermal coating method, i.e. without melting of HA. Therefore the cold spray technology has been envisaged to spray one HA powder through the supersonic gas stream derived from a heated and compressed propelling gas. However, even if the HA powder is not melted by cold spray, the deposition mechanisms of a brittle material like HA onto a thermo-sensitive and very soft material like PVA has not been clearly understood up to now. The hydrogels of biomedical interest in this work are physical PVA hydrogels with a water content of 55 wt% after swelling that induce a melting temperature of 85°C.[16]We found that a direct spraying onto the hydrogel substrate led to a fully destruction of the hydrogel (route 1). However, with similar cold spray parameters, we found that a coating could be formed on dry PVA substrates and

remained adherent to the so-formed hydrogel substrates after an immersion time of one week. This result made the route 2 successful in order to achieve a bioceramic layer onto hydrophilic polymer substrates like PVA hydrogels.

Pure HA coatings made with submicronic HA particles were produced on dry PVA substrate with various spraying parameters. We noticed that the main limiting factor is thermal degradation of the substrate due to the hot gas stream during spraying. This thermal degradation can be managed by modifying some parameters. For the shorter stand-off distance (SoD=30 mm), the temperature of the stagnation gas can be varied between 200 and 270°C for a pressure of 1 MPa, without macroscopic evidence of substrate degradation. When the pressure is increased to the maximum (P=3.0 MPa), one HA coating can be still obtained for the lowest temperature of 200°C. King *et al.* have used the same ranges of parameters for cold spraying copper powder on thermo-sensitive polymer substrates of polypropylene or high density polyethylene.[25] They did not observe any damages or thermal degradations of these substrates. For bigger stand-off distances (SoD=60 mm), the temperature can be increase to 300°C for low pressures (P≤1.0 MPa). When working at higher pressure (P≥2.0 MPa) or higher temperature (T≥300 °C), stand-off distance has to be increased above 150 mm to avoid charring or bursting of the substrate. In their study, Burlacov *et al.* increase the traverse speed to cold spray thermos-sensitive polymer substrate at high temperatures (T≥400°C), instead of increasing the stand-off distance.[26] The traverse speed was set at 80-100 mm/s, namely ten times higher than in our experiments. In Table 2, we suggest suitable spraying parameter sets suitable for cold spraying on dry PVA substrate, only based on macroscopic observations. Usually, the suitable sets of parameters in cold spray are evaluated by a coefficient of deposition efficiency, K.[27] This coefficient is calculated as follow: $K = \Delta m/Mp$, where Δm is the change of weight of a substrate and Mp is weight of all particles interacting with a

substrate. But due to difficulties of samples weight measurements, it was not possible to calculate this coefficient.

Stand-off distance (mm)	Temperature (°C)	Pressure (MPa)
30	200 -> 270	1
	200	1->3
60	300	1
150	400	1->3

Table 9 Suitable spraying parameters for dry PVA substrates.

Only HA coatings produced with the lowest spraying parameters (T=200°C, P=1.0 MPa, SoD=30 mm) on dry PVA substrates were characterized by optical and electronic microscopy. The microscopic observations revealed that the coating consists in a monolayer of submicronic particles fully covering the PVA surface that was largely deformed by the particle impacts and the hot gas stream, as shown in Figure 108 and 109. Unlike deformable particles, such as ductile metallic particles often used with cold spray process onto metallic substrates or in a less conventional manner onto ceramic or "hard" polymeric substrates, HA particles are brittle material with no plasticity. When impacting the substrate at high velocity, porous HA aggregates are fragmented into smaller submicronic particles, as reported in others cold spray studies using porous ceramic particles.[26,28–30] In particular, Burlacov *et al.* have studied the formation of tungsten dioxide (TiO_2) coatings on various thermoplastic substrates, such as PEEK, poly(ethyleneterephthalate) (PET) or poly(sulfone) (PSU) by cold spray.[26] They observed that TiO_2 particles (Mean diameter: 45 μm) eroded when impacting the substrate. Concerning the surface state of the substrate, SEM observations suggest that the surface is completely riddled by the repeated impacts of particles and the gas stream pressure. Craters and cavities of various depths are formed (Figure 107b and 108b). The formation of

these cavities provides surface roughness, which can be an intended effect, in particular for cellular adhesion.[20,31] In addition, cross-section observations at ultra-high magnifications also indicate that each submicronic particles seem to be embedded into the PVA substrate. Temperature measurement of the substrate during spraying shows that the polymer substrate is softened by heat, as it has almost reached the melting temperature for a few tens of millisecond (Figure 109b). This softening facilitates the bonding of the submicronic particles with the substrate (Figure 108). This phenomenon has been reported in another study,[25] in which copper particles are cold sprayed on various polymer substrates, such as high density poly(ethylene) (HDPE) (T_m=132°C), nylon (T_m=222°C), or Polytetrafluoroethylene (PTFE) (T_m=332°C) with similar spraying parameters. They suggested that the embedment of copper particles in the substrate was related to the high impact velocities and the softening of the polymer substrates. Regarding the thickness of the coatings, thin coatings were obtained and consisted of a monolayer of submicronic HA particles embedded in the PVA substrate. Similar results were reported in a study of Lee *et al.*, where coatings of tungsten trioxide (WO_3) with a thickness of 0.5-1 µm have been produced by cold spray (T=300°C, P=0.7 MPa, SoD=5 mm) on silicone substrates.[32] Conversely, Yamada *et al.* achieved thick coatings (10-100µm) of TiO_2 on steel substrates. Recently, Lee *et al.* have produced pure HA coatings of about 100 µm thick on PEEK substrates. However, they did not give explanation about the building mechanisms. In the study of Burcalov *et al.*, in which 20 µm thick TiO_2 coatings are produced on polymer substrates, they suggested that , the substrate is "squeezed" out of the surface due to impact of particles and acts as a binder between particles and form additional layers.[26]

We suggest propose a coating formation mechanism that could govern the build-up phenomenon, as presented in Figure 113. As previously discussed, several phenomena seem to occur at the same time during impacts of HA micrometric particles. First one concerns

particles fragmentation. Several fragmentation mechanisms can occur: particles can explode at the impact (i) or next particles can crash on previous particles (ii). When particles impact the substrate, they break up in smaller particles. This smaller HA particles have sub-micrometric size and are similar to those composing the initial particles (Figure 103c)). Few particles remain intact after impact (iii). After impact of the first particles, the surface of the substrate is completely riddled and craters and cavities are formed with the a depth between 0 and 50 µm. In the same time, the gas stream is heating the substrate to a temperature close to the melting temperature (T_m) of PVA substrate (iv), which induces a softening of the substrate and allow embedment of submicronic particles into the PVA substrate (v), as shown in Figure 108b) and c). Finally the substrate is cooled down as the gas stream moves away (vi).

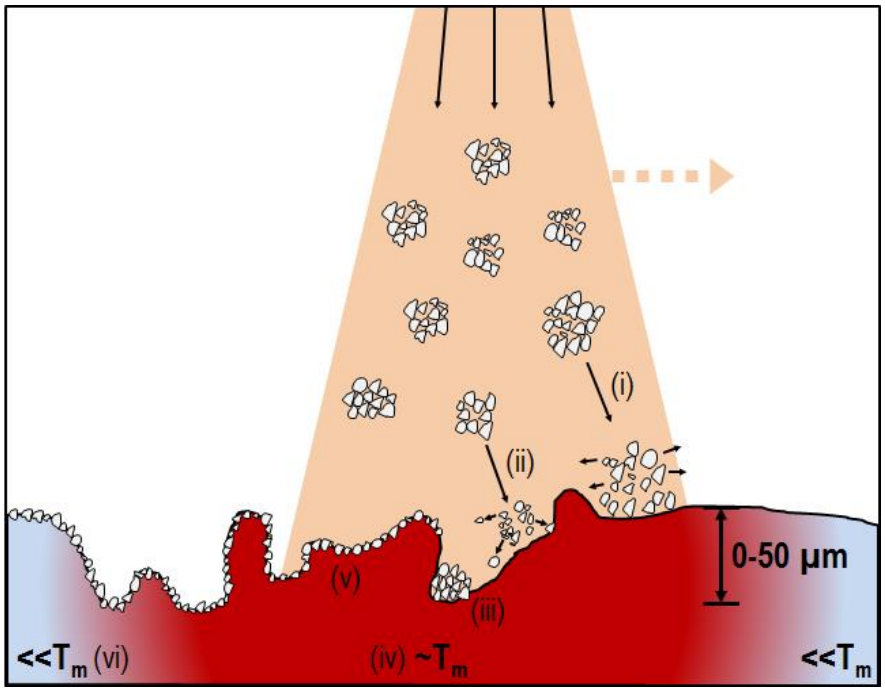

Figure 113 Schematic drawing of the coating formation mechanisms: (i) particle fragmentation at impact, (ii) particle fragmentation by impact of following particles, (iii) few particles remain intact after spraying, (iv) softening of the substrate by gas stream, (v) monolayer coating of submicronic particles, (vi) decrease of substrate temperature.

After spraying, the coated PVA substrates have been allowed to swell in water and the substrate turned into a hydrogel. SEM imaging showed that the HA coating was still adherent to the substrate, even after swelling. This confirms the idea that the submicronic HA particles

are well linked to the PVA substrates. This contact can be explained through the interactions between submicronic particle and the polymer network. As a matter of fact, it has been previously reported that in hydrogel/nanoparticles composites, polymer chains are adsorbed at the surface of the nanoparticles.[33,34] Nanoparticles act as crosslinks and reinforce the hydrogel network. This phenomenon can explain why the submicronic particles are still attached to the substrate even after swelling. A slight difference of 10 % of the equilibrium water content was reported. This difference can be explained by the modification of the PVA substrate crosslinking degree due to the short exposure to high temperature during the spraying process. It has been shown that annealing of PVA hydrogel prior to swelling can modified their swelling properties.[24] Nevertheless, we have no further information on the physico-chemical modifications of the substrate in depth. We do not know if the substrate has been affected on tens or hundreds of micrometers and what is the impact on the initial state of the substrate.

10.5 Conclusion

In this study, we produced pure hydroxyapatite coating onto thermos-sensitive dry PVA substrates by cold spray. Optimal spraying parameters sets were defined for PVA substrate. Dense and homogeneous coatings were obtained on dry PVA substrates. These coated substrates can be swollen and turned into coated PVA hydrogels. A coating formation mechanism was proposed, based on the fragmentation of the highly porous micrometric powder made of aggregated submicronic HA particles, which are embedded into the molten and deformed PVA substrate. Nevertheless, production of thicker coatings (10-100µm) has not been achieved yet.

References

1. Peppas, N. A., Hilt, J. Z., Khademhosseini, A. & Langer, R. Hydrogels in Biology and Medicine: From Molecular Principles to Bionanotechnology. *Adv. Mater.* **18,** 1345–1360 (2006).

2. Sciarretta, F. V. 5 to 8 years follow-up of knee chondral defects treated by PVA-H hydrogel implants. *Eur. Rev. Med. Pharmacol. Sci.* **17,** 3031–3038 (2013).

3. Kobayashi, M., Chang, Y.-S. & Oka, M. A two year in vivo study of polyvinyl alcohol-hydrogel (PVA-H) artificial meniscus. *Biomaterials* **26,** 3243–3248 (2005).

4. Bach, J. S. *et al.* Hydrogel fibers for ACL prosthesis: Design and mechanical evaluation of PVA and PVA/UHMWPE fiber constructs. *J. Biomech.* **46,** 1463–1470 (2013).

5. Darwis, D., Stasica, P., Razzak, M. T. & Rosiak, J. M. Characterization of poly(vinyl alcohol) hydrogel for prosthetic intervertebral disc nucleus. *Radiat. Phys. Chem.* **63,** 539–542 (2002).

6. Hou, R. *et al.* Magnetic nanohydroxyapatite/PVA composite hydrogels for promoted osteoblast adhesion and proliferation. *Colloids Surf. B Biointerfaces* **103,** 318–325 (2013).

7. Matsumura, K., Hayami, T., Hyon, S.-H. & Tsutsumi, S. Control of proliferation and differentiation of osteoblasts on apatite-coated poly(vinyl alcohol) hydrogel as an artificial articular cartilage material. *J. Biomed. Mater. Res. A* **9999A,** NA–NA (2009).

8. Maher, S. A. *et al.* Nondegradable hydrogels for the treatment of focal cartilage defects. *J. Biomed. Mater. Res. A* **83A,** 145–155 (2007).

9. Furlong, R. & Osborn, J. Fixation of hip prostheses by hydroxyapatite ceramic coating. *J. Bone Joint Surg. Br.* **73-B,** 741–745 (1991).

10. Huracek, J. & Spirig, P. The effect of hydroxyapatite coating on the fixation of hip prostheses. *Arch. Orthop. Trauma Surg.* **113,** 72–77 (1994).

11. Asran, A. S., Henning, S. & Michler, G. H. Polyvinyl alcohol–collagen–hydroxyapatite biocomposite nanofibrous scaffold: Mimicking the key features of natural bone at the nanoscale level. *Polymer* **51,** 868–876 (2010).

12. Moreau, D., Villain, A., Ku, D. N. & Corté, L. Poly(vinyl alcohol) hydrogel coatings with tunable surface exposure of hydroxyapatite. *Biomatter* **4,** e28764 (2014).

13. Bajpai, A. & Singh, R. Study of biomineralization of poly(vinyl alcohol)-based scaffolds using an alternate soaking approach. *Polym. Int.* **56,** 557–568 (2007).

14. Gonzalez, J. S., Maiolo, A. S., Hoppe, C. E. & Alvarez, V. A. Composite Gels Based on Poly (Vinyl alcohol) for Biomedical Uses. *Procedia Mater. Sci.* **1,** 483–490 (2012).

15. Hayami, T., Matsumura, K., Kusunoki, M., Nishikawa, H. & Hontsu, S. Imparting cell adhesion to poly(vinyl alcohol) hydrogel by coating with hydroxyapatite thin film. *Mater. Lett.* **61,** 2667–2670 (2007).

16. Lozinsky, V. I., Domotenko, L. V., Vainerman, E. S., Mamtsis, A. M. & Rogozhin, S. V. On the possibility of mechanodestruction of poly (vinyl alcohol) molecules under moderate freezing of its concentrated water solutions. *Polym. Bull.* **15,** 333–340 (1986).

17. Sun, L., Berndt, C. C., Gross, K. A. & Kucuk, A. Material fundamentals and clinical performance of plasma-sprayed hydroxyapatite coatings: a review. *J. Biomed. Mater. Res.* **58,** 570–592 (2001).

18. Prevéy, P. S. X-ray diffraction characterization of crystallinity and phase composition in plasma-sprayed hydroxyapatite coatings. *J. Therm. Spray Technol.* **9,** 369–376 (2000).

19. Papyrin, A. Cold spray technology. *Adv. Mater. Process.* **159,** 49–51 (2001).

20. Lee, J. H. *et al.* In vitro and in vivo evaluation of the bioactivity of hydroxyapatite-coated polyetheretherketone biocomposites created by cold spray technology. *Acta Biomater.* **9,** 6177–6187 (2013).

21. Sanpo, N., Tan, M. L., Cheang, P. & Khor, K. A. Antibacterial Property of Cold-Sprayed HA-Ag/PEEK Coating. *J. Therm. Spray Technol.* **18,** 10–15 (2009).

22. Otsuka, E. & Suzuki, A. A simple method to obtain a swollen PVA gel crosslinked by hydrogen bonds. *J. Appl. Polym. Sci.* **114,** 10–16 (2009).

23. Tubbs, R. K. Melting point and heat of fusion of poly(vinyl Alcohol). *J. Polym. Sci. Part A* **3,** 4181–4189 (1965).

24. Peppas, N. A. & Merrill, E. W. Differential scanning calorimetry of crystallized PVA hydrogels. *J. Appl. Polym. Sci.* **20,** 1457–1465 (1976).

25. King, P. C. *et al.* Embedment of copper particles into polymers by cold spray. *Surf. Coat. Technol.* **216,** 60–67 (2013).

26. Burlacov, I., Jirkovský, J., Kavan, L., Ballhorn, R. & Heimann, R. B. Cold gas dynamic spraying (CGDS) of TiO2 (anatase) powders onto poly(sulfone) substrates: Microstructural characterisation and photocatalytic efficiency. *J. Photochem. Photobiol. Chem.* **187,** 285–292 (2007).

27. Ghelichi, R. & Guagliano, M. Coating by the Cold Spray Process: a state of the art. *Fract. Struct. Integr.* 30–44 (2009).

28. Kliemann, J.-O. *et al.* Formation of Cold-Sprayed Ceramic Titanium Dioxide Layers on Metal Surfaces. *J. Therm. Spray Technol.* **20,** 292–298 (2011).

29. Yang, G.-J., Li, C.-J., Han, F., Li, W.-Y. & Ohmori, A. Low temperature deposition and characterization of TiO2 photocatalytic film through cold spray. *Appl. Surf. Sci.* **254,** 3979–3982 (2008).

30. Seo, D., Sayar, M. & Ogawa, K. SiO2 and MoSi2 formation on Inconel 625 surface via SiC coating deposited by cold spray. *Surf. Coat. Technol.* **206,** 2851–2858 (2012).

31. Deligianni, D. D., Katsala, N. D., Koutsoukos, P. G. & Missirlis, Y. F. Effect of surface roughness of hydroxyapatite on human bone marrow cell adhesion, proliferation, differentiation and detachment strength. *Biomaterials* **22,** 87–96 (2000).

32. Lee, H. Y., Yu, Y. H., Lee, Y. C., Hong, Y. P. & Ko, K. H. Thin Film Coatings of WO3 by Cold Gas Dynamic Spray: A Technical Note. *J. Therm. Spray Technol.* **14,** 183–186 (2005).

33. Zhang, Y. & Ye, L. Structure and property of polyvinyl alcohol/precipitated silica composite hydrogels for microorganism immobilization. *Compos. Part B Eng.* **56,** 749–755 (2014).

34. Carlsson, L., Rose, S., Hourdet, D. & Marcellan, A. Nano-hybrid self-crosslinked PDMA/silica hydrogels. *Soft Matter* **6,** 3619 (2010).

Chapter 11. Influence of the particle composition on the coating formation

11.1 Introduction

In the previous chapter, we showed that coatings of pure HA particles could be produced on PVA hydrogel susbtrates by cold spray. These coatings consist in a layer of submicronic HA particles embedded in the PVA substrate. The thickness of these coatings is similar to the ones obtained in previous studies. Lee *et al.* have produced submicronic coatings of tungsten trioxide (WO_3) of about 2 µm thick on silicon substrates, as shown in Figure 114a.[1] Recently, thicker coatings (~100 µm) of hydroxyapatite were produced on poly(etheretherketone) (PEEK) substrates, as shown in Figure 114b.[2]

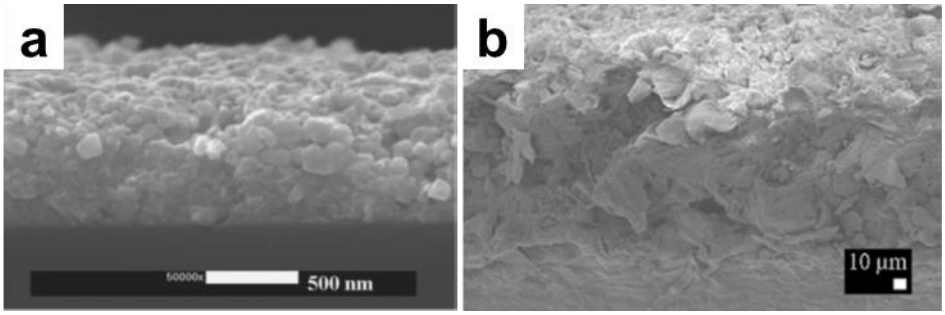

Figure 114 a) Coatings of WO_3 on silicon substrate (300°C, 0.7 MPa);[1] **b**) HA coating on PEEK substrate (400°C, 1.4 MPa).[2]

In this chapter, we investigate the use of another HA powder to produce thicker coatings. This powder is the non-calcined HA powder, which has been previously introduced in the section 2. Here, the main objectives are the identification of the sets of spraying parameters using the non-calcined powder and to compare the two types of powder on the coating formation. Firstly, a systematic study of the spraying parameters (temperature, pressure, stand-off distance and speed-rate) is presented only for non-calcined particles

(thereby being very similar to the study presented in the previous chapter on calcined particles). Then, coatings of both types of HA particles, obtained with a given set of spraying parameters previously identified, are investigated by electronic microscopy and swelling experiments. Lastly, additional physicochemical characterizations of the two types of HA powders will give information about the coating formation.

11.2 Materials and Methods

Hydroxyapatite particles:

Non-calcined and calcined hydroxyapatite powder were used in these experiments. The non-calcined powder has been produced using the same process as calcined powder, except that no calcination treatment at 1050°C for 40 h has been performed. Their physical-chemical characteristics are presented in Section 2.

PVA substrates:

Dry PVA substrates used were the one presented in the Section 2. Briefly, they were formed by solvent-casting method. A 10wt% PVA aqueous solution was poured in Petri dishes and solvent was evaporated in vacuum-oven at 700 mbar and 80°C for 8h. Dry PVA films of 540±170 µm thick and of surface area of about 23 cm^2 were obtained.

Cold spray apparatus:

The cold spray apparatus and set-up used were the same as in the previous chapter.

Cold spray parameters:

The HA powder carried by the process gas was sprayed on dry PVA substrates at different given gas temperatures (T), pressures (P), stand-off distances (SoD) and speed rates (SR). These studied parameters are summarized in Table 1.

P (MPa)	T (°C)	SR(mm/sec)	SoD (mm)
1.0 – 2.0 – 3.0	200 - 300 - 400 - 500 - 600	10	30 - 60 - 100 - 190

Table 10 Cold spray parameters

Microscopic characterization of coatings:

Macroscopic observations were performed under M420 Wild-Leitz Leica macroscope. SEM observations were performed on a Nova Nano SEM 450 (FEI, USA) apparatus at 5 kV with secondary electron detector.

Post-spraying swelling experiment:

After cold spray experiment, both dry PVA films coated with non-calcined HA particles and dry PVA films coated with calcined HA particles were immersed in water at room temperature for 1h to characterize the cohesion of the coating and the adherence between the HA coating and the PVA substrate.

Thermogravimetric analysis (TGA) and differential thermal analysis (DTA) of HA particles after washing:

Non-calcined and calcined particles were vigorously washed separately in an ultra-pure water bath for 2h under magnetic stirring. This washing cycle was repeated 3 times. Then, HA particles were let in an ultra-pure water bath for 96 h. Both types of particle were collected and put in vacuum-oven at 90°C for 72 h.

TGA and DTA curves were simultaneously recorded using a Setaram Instrumentation Ligne 92 TGA/DTA (Caluire, France) apparatus. Measurements were realized under air atmosphere. An amount of 70 mg of each HA particles was placed in alumina crucibles. The heating parameters were 10°C/min to 1550°C.

FT-IR analysis of dissolution salts after HA powder washing:

FT-IR measurements were performed on salts residues of a washing solution from both HA powders. First, non-calcined and calcined HA particles were rinsed separately in water bath under magnetic stirring. Then, particles were let to settle and supernatant waters were collected. These waters were frozen in nitrogen bath and lyophilized using a Freezone 2.5 freeze dry system (Laconco, USA) at T=-84°C and P<0.1 mbar.

FT-IR spectra were recorded at room temperature using a TENSOR 37 spectrometer (Bruker, Germany). Spectra were obtained at 4 cm^{-1} resolution averaging 32 scans. Measurements were realized by transmission throughout pellets of compacted salts mixed with KBr. Pellets were composed of 25 mg of crushed salts and blended with 50 mg of KBr. Pellets were formed by pressing the blends at 1 t of hydraulic pressure.

11.3 Results

Effect of spraying parameters using the non-calcined powder:

The effect of cold spray parameters (temperature, pressure and stand-off distance) were studied systematically with the non-calcined HA particles. For a stand-off distance set at 30 mm, the temperature of the stagnation gas was varied from 200 to 400°C as well as the pressure from 1 to 2 MPa. Figure 115 shows optical macroscopic observations the obtained coatings of non-calcined HA. For 200°C and 1 MPa, translucent PVA and white HA single was obtained, as shown in Figure 115a. When temperature was increased at 300°C, a slight yellowing due to thermal effects appeared and was obviously more pronounced at 400°C, as shown in top-views given in Figure 115b and c respectively. When the pressure was increased to 2 MPa at 30 mm for the lower (and less degrading) temperature of 200°C, no thermal

degradation occurred but the coating was inhomogeneous exhibiting some spalled areas, as shown on Figure 115d.

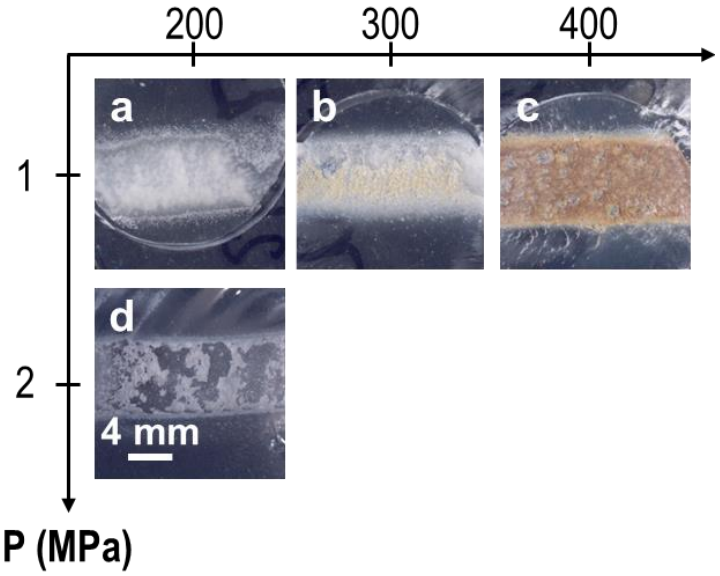

Figure 115 Macroscopic view of the surface of non-calcined HA coated PVA substrates cold sprayed with different temperature and pressure for a stand-off distance of 30 mm.

When the stand-off distance was increased to 60 mm, the temperature of the propelling gas had a lower impact on the substrate. Indeed, at 1.0 MPa and 200 or 300°C, no thermal degradation was observed, as shown on Figure 116a and b. For the lower temperature of 200°C, the pressure could be increased to 3.0 MPa without evidence of thermal degradation, as shown in Figure 116d and f. For temperature above 300°C and pressure above 2 MPa, a higher degree of thermal degradation was obvious according to the yellowing of the substrate, as shown Figure 116e, c and g.

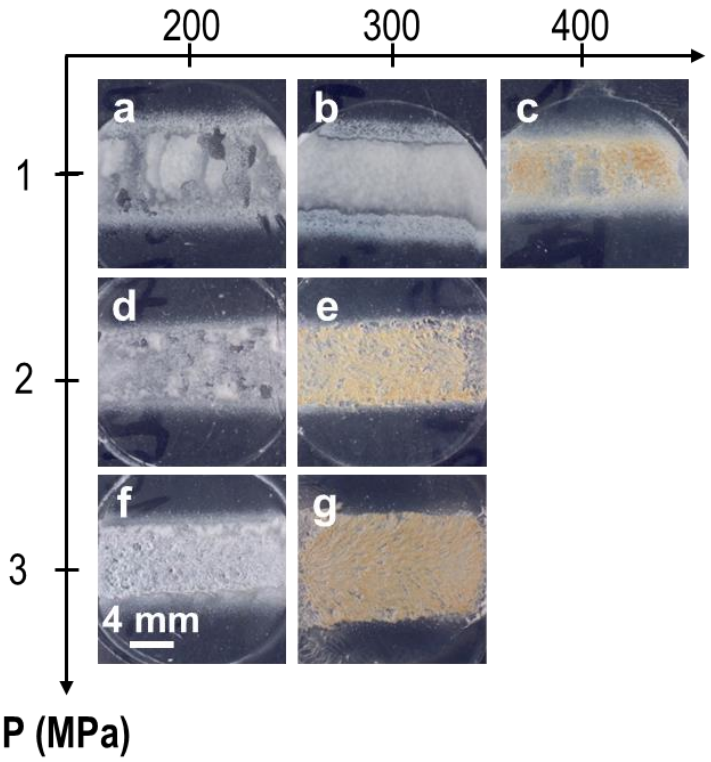

Figure 116 Macroscopic view of the surface of non-calcined HA coated PVA substrates cold sprayed with different temperature and pressure for a stand-off distance of 60 mm.

At stand-off distance above 100 mm, for temperature and pressure superior to 400°C and 2 MPa, thermal degradation was observed, as shown in Figure 117f and h. Below these values, any temperature or pressure could be applied and the substrates were coated homogenously without thermal degradation, as observed in Figure 117a, b, c, d, and e. However the coating produced at 200°C and 3 MPa (Figure 117g) was not fully covering the substrate. This might be due to debonding issue during the spraying.

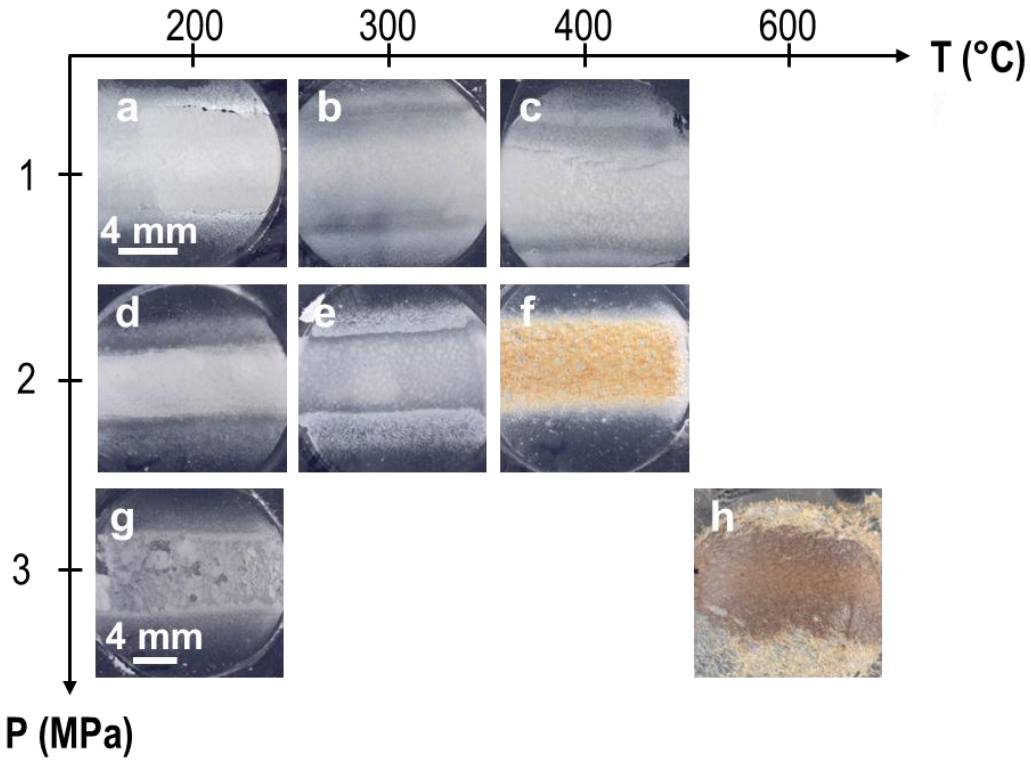

Figure 117 Macroscopic view of the surface of non-calcined HA coated PVA substrates cold sprayed with different temperature and pressure for a stand-off distance of 100 mm.

The widths of the tracks are around 8, 9 and 12mm for stand-off distances of 30, 60, and 100 mm, respectively. With these experiments, we investigated the effect of the different spraying parameters on the coating formation and we identified sets of parameters that could form a deposit on PVA substrates without evidence of thermal degradation.

Effect of HA powder nature:

We also compared the effect of the nature of the HA powder. Non-calcined and calcined HA coatings were produced with the lowest conditions of temperature (200°C), pressure (1 MPa) and stand-off distance (30 mm). These spraying parameters were chosen because they corresponded to the less severe conditions to obtain homogeneous coatings. Figure 118 shows SEM tilted views of non-calcined HA coatings and fractography observations of calcined HA coatings. For non-calcined HA coatings, the fractured cross-section was not achieved because the coating was not adhering enough to the substrate.

Thick and dense coatings were obtained with non-calcined particles, as shown in Figure 118a. The thickness was around 500±100 µm. The initial spherical shape of the porous particles was lost during high velocity impact. Non-calcined HA particles were completely crushed and compacted to form a thick dense layer, as shown at high magnification in Figure 118c. Although the coating itself seemed cohesive, it was not adherent to substrate, as it could be peeled off easily from the substrate and small spaces were visible between the coating and the substrate, as indicated by yellow arrows in Figure 118a. As previously seen in the chapter 10, the calcined particles did not agglomerate to build a thick layer, as shown in Figure 118b. In cross-section views at higher magnification (Figure 118d), we showed that craters have formed in the PVA substrate, in which broken HA particles are embedded. The depth of these craters is about 50±10 µm.

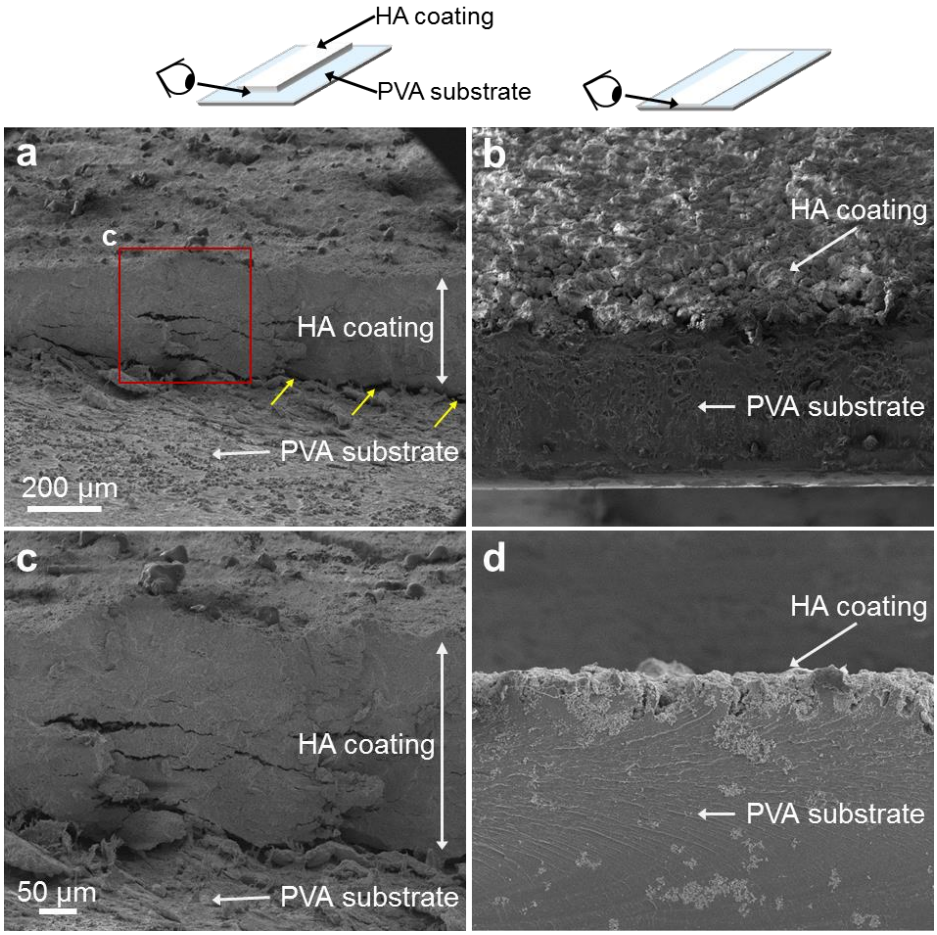

Figure 118 Scanning electronic microscopic observations of the non-calcined HA coating in tilted view (**a**, **c**) and of the calcined HA coating in tilted view (**b**) and in fractography (**d**).

Swelling of coated PVA substrates:

Non-calcined (Figure 119a) and calcined (Figure 119b) HA coated PVA substrates, produced at T=200°C, P=1 MPa and SoD=30 mm, were immersed in water at room temperature. Coatings of non-calcined particles were completely fragmented after 3h of soaking, as shown in Figure 119c. In addition, by scratching gently the surface of the sample, the coating was completely and easily removed, as shown in Figure 119e. Whereas, the coating of calcined particles did not dissolve in water and remained adherent even after gentle scratching, as shown in Figure 119d and f respectively.

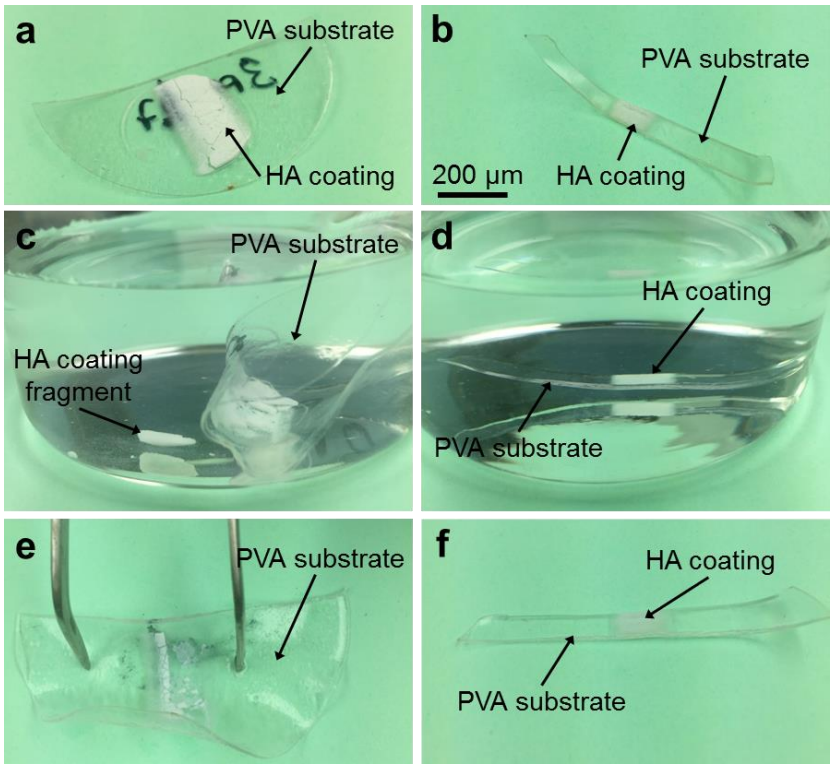

Figure 119 Swelling in water of non-calcined (**a**,**c**,**e**) and calcined (**b**,**d**,**f**) HA coated PVA substrate (T=200 °C, P=10 bar, D=30 mm). After swelling (**a** and **b**); After 3h of swelling(**c** and **d**), After gentle scratching(**e** and **f**).

Thermogravimetric analysis (TGA) and differential thermal analysis (DTA) of HA particles after washing

Figure 120a shows the TGA curve for non-calcined and calcined particles after washing. Compared to non-calcined particles before washing (see Section 2 Chapter 5), the washed non-calcined particles have lost only about 3.5% of their mass. This indicates that a large soluble fraction has been eliminated from these particles during washing. The low mass loss observed on TGA curve of the washed non-calcined particles may be mostly attributed to the elimination of water and few synthesis residues which have not been eliminated during the washing, as confirmed by large exothermic peaks centered at 250 on TDA curve in Figure 120b. On the contrary, the calcined powder does not show any significant mass loss and the measurements indicate a loss inferior to 0.5% of the initial mass. TDA curve shows a large exothermic peak centered at 150°C, probably corresponding to the elimination of water at the

surface of the particles. This indicates that calcined powder did not contain any soluble fraction.

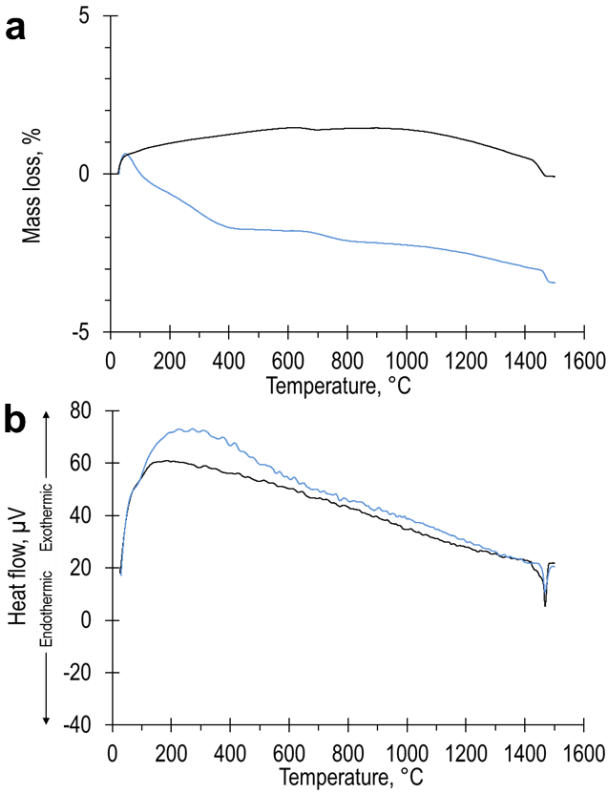

Figure 120 TGA curves (**a**) and TDA curves (**b**) of washed calcined (─) and washed non-calcined (─) HA particles.

FT-IR analysis of salts from HA powders dissolved in water:

To have a better understanding of the behavior of both coatings in water, FT-IR analyses of salts contained in the water after washing the non-calcined and calcined HA particles were carried out. The Figure 121 presents the FT-IR spectra of salts issued from washing waters of calcined and non-calcined HA particles before spraying. Concerning salts issued from non-calcined HA particles, we observed a large and intense band centered at 1398 $cm^{-1}$and a smaller one at 825 cm^{-1}, corresponding to NO_3 groups issued from nitrate residues. A peak at 1049 cm^{-1} was attributed to ν_3PO_4 modes corresponding to phosphate groups of apatite. The large band between 3500 $cm^{-1}$and 2800 cm^{-1} corresponds to water. Spectrum of salts issued from calcined HA particles present absorption bands between 3500 cm^{-1} and 2800 cm^{-1} corresponds to the absorbed water at the surface of the particles. Bands between 1100

cm^{-1} and 900 cm^{-1} and between 700 cm^{-1} and 500 cm^{-1} correspond to ν_3PO_4 and ν_4PO_4 modes are attributed to phosphate groups of apatite. Bands between 1600 and 1400 cm^{-1} and between 900 and 850 cm^{-1} are ν_3CO_3 and ν_2CO_3 modes issued from carbonate groups of apatite.[3] The intense peak at 3643 cm^{-1} and the small peak at 3573 cm^{-1} correspond to OH group of calcium hydroxide ($Ca(OH)_2$).[4]

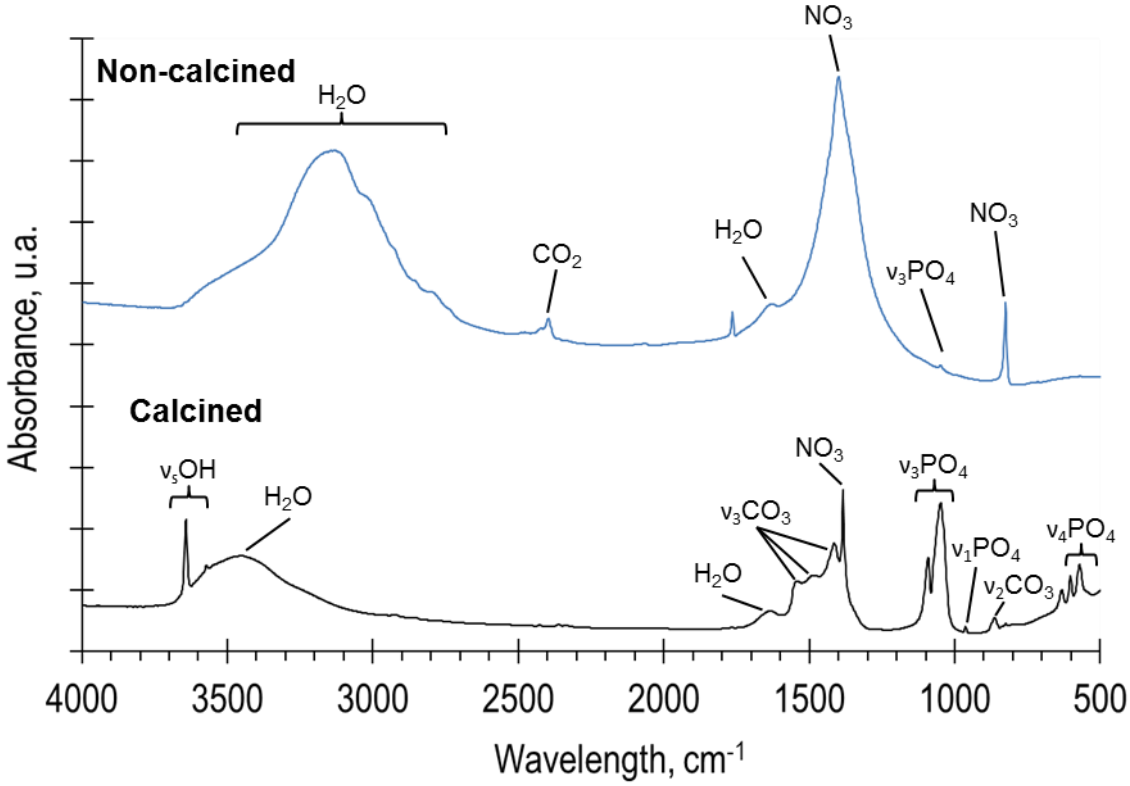

Figure 121 FTIR spectra of salts issued from waters used to wash calcined (—) and non-calcined (—) HA before spraying.

11.4 Discussion

In this chapter, we presented the results of the cold spray experiments using PVA substrates and two types of hydroxyapatite powder. These experiments have allowed to identify the effects of spraying parameters for the non-calcined powder and the influence of the nature of HA powder on the coating formation and on substrate behavior in dry environment or immersed into water.

Sets of spraying parameters were identified for the non-calcined powder. The ranges of spraying condition with the non-calcined powder are similar to the ones with the calcined powder. As previously mentioned in Chapter 10, the deposition efficiency coefficient K has not been calculated due to difficulties to measure the sample weights. Based on macroscopic observations, we proposed a "coating aspect" scale from 1 to 10 for the coatings of non-calcined powder. 1 corresponds to a non-formation of the coating and/or charring of the substrate, 5 corresponds to the formation of a non-uniform coating and/or a yellowing of the substrate and 10 corresponds to the formation of a white and uniform coating and that the substrate is intact. Figure 122 presents a 3-axis chart.

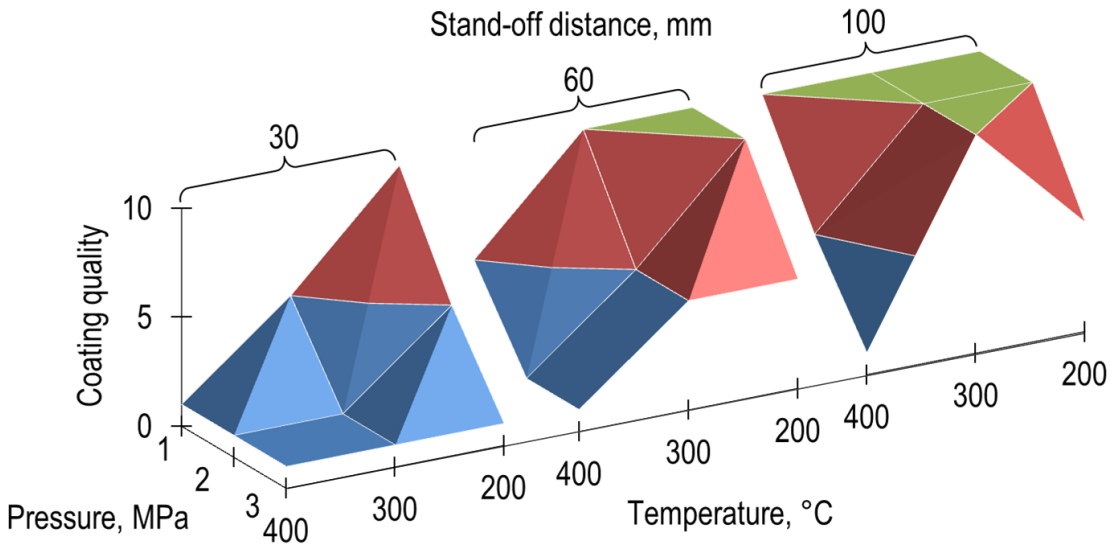

Figure 122 Non-calcined particle coating quality as a function of the temperature, the projection distance, and the pressure.

The limiting factor in cold spray of PVA substrates was the degradation of the substrates. At short stand-off distances (30 mm), only the lowest conditions of temperature and pressure could be applied (200°C and 1MPa). When the stand-off distance was increased to 60 mm, the temperature could be elevated to 300°C for a pressure of 1 MPa and reciprocally and the pressure could be increased to 2 MPa for a temperature of 200°C. For stand-off distances of 100 mm, the temperature and pressure could be increased above 300°C and 2 MPa respectively.

In addition, we showed that the composition of the particles had an effect on the coating formation. The thermal gravimetric analysis of the non-calcined particles before washing (see Section 2, Chapter 5) and after washing confirmed the presence of a soluble fraction, representing 20% of the initial mass of non-calcined particles. In addition the FT-IR analysis of salts showed that this soluble fraction is mostly composed of nitrates, issued from synthesis residues of non-calcined HA particles. This can explained why thick coatings of several hundreds of microns were formed with non-calcined HA powder. Salts contained in the non-particle particles may act as a binder and gives cohesiveness to the coating. This is also why these coatings dissolved completely in water. As a contrary, the absence of soluble fraction in the calcined particles could explain why it has not been possible to build-up thick coatings and explain why these coatings did not dissolve in water.

11.5 Conclusion

In this chapter, we showed that it is possible to produce coatings of HA particles with various thickness on PVA substrates by varying the type of HA powder. Compatible sets of spraying parameters (temperature, pressure, stand-off distance) were identified for the non-calcined HA particles, which are similar to the ones for calcined particles. Dense and homogeneous coatings were obtained with both types of HA particles. Thick coatings of several hundreds of μm were achieved using non-calcined particles, whereas submicronic coatings were obtained with calcined particles. However, we showed that coating of non-calcined HA particles did not adhere firmly to the substrates and did not sustain immersion in water. Conversely, cohesive and adherent coatings of calcined particles were achieved, even when immersed in water. The chemical composition of these non-calcined HA particles could

be modified to allow a better cohesion of the coating, a strongest adhesion to the substrates and prevent dissolution of the coating in water.

References

1. Lee, H. Y., Yu, Y. H., Lee, Y. C., Hong, Y. P. & Ko, K. H. Thin Film Coatings of WO3 by Cold Gas Dynamic Spray: A Technical Note. *J. Therm. Spray Technol.* **14,** 183–186 (2005).

2. Lee, J. H. *et al.* In vitro and in vivo evaluation of the bioactivity of hydroxyapatite-coated polyetheretherketone biocomposites created by cold spray technology. *Acta Biomater.* **9,** 6177–6187 (2013).

3. Rey, C., Collins, B., Goehl, T., Dickson, I. R. & Glimcher, M. J. The carbonate environment in bone mineral: a resolution-enhanced Fourier transform infrared spectroscopy study. *Calcif. Tissue Int.* **45,** 157–164 (1989).

4. Park, E., Condrate Sr, R. A., Lee, D., Kociba, K. & Gallagher, P. K. Characterization of hydroxyapatite: before and after plasma spraying. *J. Mater. Sci. Mater. Med.* **13,** 211–218 (2002).

Appendix 1. Diffusivity coefficients

The diffusivity of the network was estimated from fits of the experimental data. From the theoretical prediction for gel swelling, giving by:

$$R = R_0 + (R_\infty - R_0)\frac{(D_n t)^{1/2}}{R_0} \quad (1)$$

We plotted the Equation 2, as shown in Figure 123 and the diffusion coefficients of the network D_n were calculated from linear functions.

$$\frac{R-R_0}{R_\infty-R_0} = {D_n}^{1/2}\ \frac{t^{1/2}}{R_0} \quad (2)$$

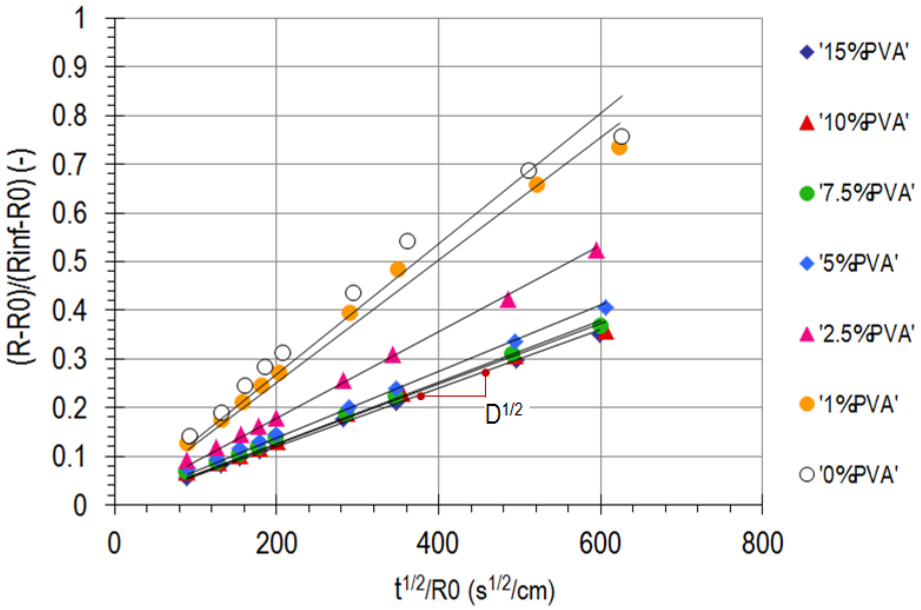

Figure 123 Log-Log plot of the Equation 2. Solid lines are linear curves of slope equals to $D_n^{1/2}$.

The values of the coefficient as a function of the PVA wt% concentration are given in the following table:

PVA concentration (wt%)	D_n (cm^2/s)
0	0.0000017956
1	0.0000015876
2.5	0.000000788544
5	0.000000469225
7	0.000000400689
10	0.000000385641
15	0.000000361201

Table 11 Diffusity coefficient as a function of the concentration of PVA aqueous solutions.

Appendix 2. Encapsulation of chondrocyte cells in poly(vinyl alcohol) hydrogel films gelified at the surface of polyacrylamide swelling substrates.

In this appendix, we present some short results about the preliminary experiment of cell encapsulation, using the swelling induced gelation process. The substrates used in this study were polyacrylamide hydrogels and the cells intended to be encapsulated were chondrocytes.

Materials & Methods

Materials

Poly (vinyl alcohol) (PVA) solution was obtained with high molecular weight (89 000–98 000 $kg{\cdot}mol^{-1}$) and 99% hydrolyzed PVA powder (Sigma-Aldrich). PAAm gel substrates were obtained from a 40% solution of AA-MBA 37,5:1 (Sigma-Aldrich). TEMED (Sigma-Aldrich) and ammonium persulfate (Sigma-Aldrich) were used as initiators to produce PAAm gel substrates. Cells used were mouse chondrocyte. Growth medium was composed of Dulbecco's Modified Eagle's Medium (DMEM) at 1g/L of glucose (Invitrogen) plus 1mL of Penicillin-Streptomycin PS (Invitrogen) and 10 mL of glutamine 200 mM (Invitrogen) per 500 mL of growth medium. Foetal bovine serum (FBS) was used at 10 % v/v (Lonza). Buffer used was PBS-1X (Invitrogen). Cells were harvested using a solution of trypsin-EDTA 0,05% (Invitrogen). Trypan blue (Logo Biosystems) was used for cells counting. Viability/cytotoxicity kit for mammalian cells (Molecular Probes ref L3224 lot 1657695) was used for fluorescent staining. And cell viability was assessed by MTT (Sigma).

Preparation of PAAm gel discs

10.5 mL of PBS1X and 5.5 mL of 40% acrylamide-bis-acrylamide (37,5:1) solution were mixed. Then 300 uL of 10% amonium persulfate and 30 µL of TEMED were added. The whole solution was sterilized by filtration using a 45 µm filter and poured in a glass mold composed of two glass plat spaced of 4.5 mm. After 3h, a gel plate was obtained. Fifteen gel discs of 16 mm were cut off using a punch. Then each disc was attached to a cotton thread and put under sterile hood to dry for 48h. Then dry PAAm discs were stored in Petri dishes.

Cells culture

Mouse chondrocytes were used. For this experiment a large quantity of cells was required. Confluent chondrocytes cells, cultured in 2 T175 culture box, were harvested by adding 5 mL of Trypsin/EDTA 0,05% and incubated 5min in oven at 37°C. Then 5 mL of growth medium/10%FBS was added to culture box.. For the experiments, a 6 mL cellular suspension at $3.7.10^5$ cells/mL in growth medium/10%FBS was prepared.

Preparation of PVA/PBS solution

14 wt% PVA aqueous solution was produced by dissolving 18.35 g of PVA powder in PBS-1X. The mixture was autoclaved at 121°C for 1h. Then it was stored at 37°C until use.

Encapsulation protocole

Three protocols were designed for the first experiment, namely protocol A, B and C. The routine of the different protocol are represented in Figure 124. For protocol A, pictures of the process are also presented in Figure 125.

Protocol A was the protocol of cellular encapsulation. Dry PAAm substrates (Figure 124a) were placed in a 12-wells plate (Figure 124a(i) and Figure 125a). Then 3,3 mL of 14wt% PVA/PBS solution were mixed to 120.000 cells and 0,7 mL of PBS. The whole mixture was homogenized by 5 linear up and down motions in a 50 mL syringe. Then the solution was poured on wells containing PAAm substrates for 1h à 37°C (Figure 124a(ii and iii) and Figure 125b). Then substrates on which gel films have formed were collected, and

rinsed in large excess of PBS under magnetic stirring for 10 min (Figure 124a(iv) and Figure 125c). Then substrates with gel films were placed a new 12-wells plate and 4 mL of grwth medium was added. At the end of the process, hydrogel films were not pilled-off from the surface of the PAAs substrates.

Protocol B was positive control of cell viability. Cells were dispersed in growth medium/10%FBS and put in 6-well plate (Figure 124b(ii)), at concentrations of $30*10^3$ cells/mL. Then cells were let in oven at 37°C for 24h (Figure 124b(iii)). After 24h, the growth medium/10%FBS was replaced by a fresh one (Figure 124b(iv and v).

Protocol C was negative control. Dry PAAm disc were placed in a 12-wells plate (Figure 124c(i)). Then 4,3 mL of 14wt% PVA/PBS solution were mixed to 0,7 mL of PBS. Then 4 mL solution was poured on wells containing PAAm substrates for 1h à 37°C (Figure 124c(ii and iii)). Then substrates on which gel films have formed were collected, and rinsed in large excess of PBS under magnetic stirring (Figure 124c(iv)). Then substrates with gel films were placed a new 12-wells plate and 3,3 mL of PBS plus 0,7 mL of PBS containing 120.000 cells were added. Then substrates were collected, and rinsed in large excess of PBS under magnetic stirring (Figure 124c(vi)) Then substrates with gel films were placed a new 12-wells plate and 4 mL of growth medium was added. At the end of the process, hydrogel films were not pilled-off from the surface of the PAAs substrates.

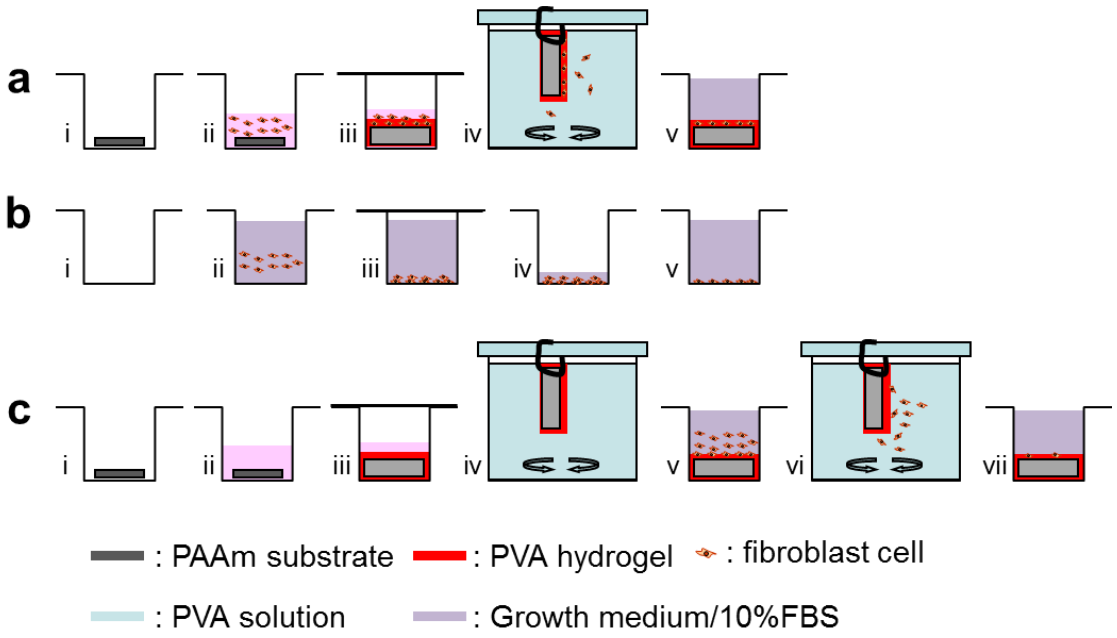

Figure 124 Protocols used in the first encapsulation experiment. **a**) Protocol A: Encapsulation of cells in PVA hydrogel films by swelling induced gelation; **b**) Protocol B: positive control; **c**) Protocol C: negative control: empty PVA hydrogel film.

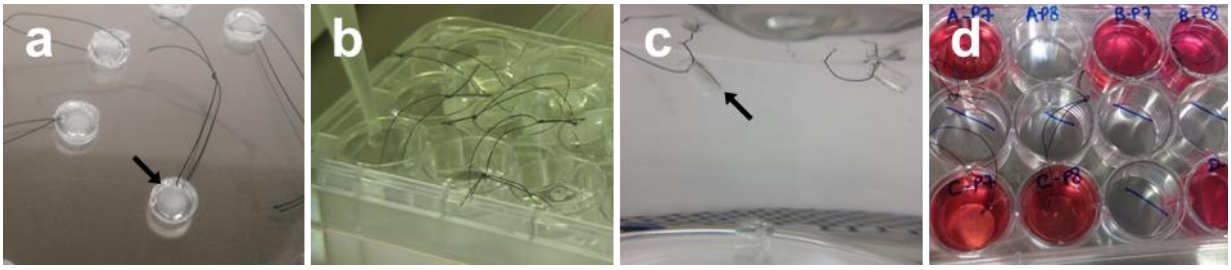

Figure 125 Pictures of protocol A. **a**) PAAm substrates are produced and dried before swelling in PVA/cells solution; **b**) Pouring of PVA/cells solution over PAAm substrates; **c**) PAAm substrates, on which PVA hydrogel films have grown, are rinsed in distilled water for 10 min; **d**) Soaking in large growth medium/10%FBS at 37°C for 24h

Observation and assessment of cell viability

Viability of the cells was qualitatively assessed by optical microscopy and MTT test.

Hydrogel films on PAAm substrates were observed by optical microscopy (Nikon) in transmission. Only the detection of cells in the gel was possible, but no information on their viability.

MTT test was done on hydrogel films. MTT (Sigma 2128) was at 5 mg/mL in DMEM medium (11 mg of MTT + 2.2 mL of DMEM-L-glutamine-PS). 200 µL of this solution was

added to each wells containing hydrogel films in 4 mL of growth medium/10%FBS. Incubation time was 5h at 37°C. Then the supernatant was removed and hydrogels were transferred to a new 12-wells plate. 1 mL of DMSO was added and plate was stirred. Spectrophotometric measurements were done using a spectrophometer at 540 nm.

Results

In this process, cells were intended to be encapsulated in PVA hydrogel films crosslinked by swelling induced gelation at the surface of PAAm substrates. At the end of the process, the films were not pilled-off the substrates.

Optical microscopy

Optical observations of hydrogel films produced with the protocol A did not reveal the presence of encapsulated cells, as shown on Figure 126a. Only rare cells were noticed in all the surface of the hydrogel films, as pointed by white arrow on in Figure 126a. On positive control, cells were numerous and spread at the bottom of the well, as shown in Figure 126b. In hydrogel films of negative control, no cell was observed, except for singular unwashed cells during the second washing step of protocol C (Figure 124c vi), as shown in Figure 126c.

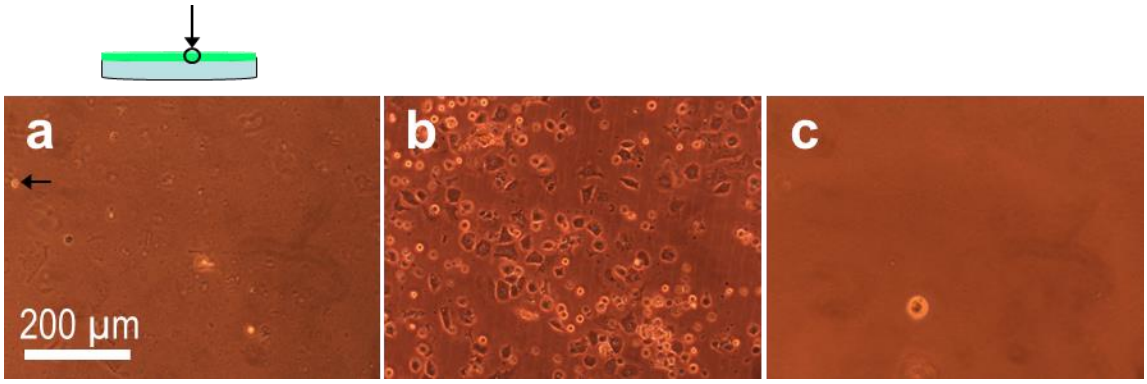

Figure 126 Representative optical microscopy observations after 24h: **a)** Protocol A: Hydrogel with cells; **b)** Positive controle; **c)** Negative controle: empty hydrogel. For (**a**) and (**c**) the focus has been done on the top of the film, as described by drawing. Schema at the top indicates the approximate location of the observation

MTT test of PVA hydrogel film with and without cell

To assess the viability of the cells, MTT test was performed on PVA hydrogel films. MTT measurements show that the viability of cells contained in the gels produced from protocol A is similar as in negative control, as shown in Figure 127. This demonstrates that no living cells are embedded in the hydrogel films.

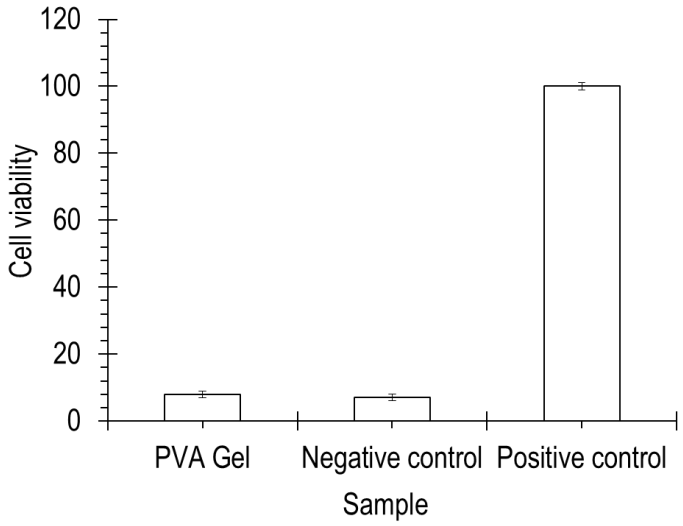

Figure 127 Viability of encapsulated cells measured by MTT assay after 24h.

Discussion & Conclusion

In this series of experiments, the encapsulation process was based on the gelation of PVA hydrogel films at the surface of swelling PAAm substrates. The process was cumbersome to achieve and the preservation of the sterility along the process was inconvenient. Regarding to the cellular encapsulation, the experiment has failed. No cell has been encapsulated in the hydrogel film. MTT assay has shown that viability level of cell-encapsulated hydrogel films was the same as negative control. Furthermore, the existence of a solid hydrogel film after 24h could not been confirmed. When trying to pill-off the films from the substrates, we only collected fragments of hydrogel films and not a solid film, as well as the ones produced in Chapter 8. It is likely that no stable film containing cells were produced.

This is probably due to the swelling time, which was not enough and due to the temperature of the hood during the film formation, which was too high (37°C) to produce PVA hydrogel films that remain stable at 37°C after 24h.

Appendix 3. List of cold spray experiments

The cold spray experiments were exploratory and the list (Table 12) of parameter sets was exhaustive. In order to capture the effect of each parameter three parameters were kept constant and the fourth one was varied.

Experiment #	Particles type	P (MPa)	T (°C)	SoD (mm)	SR(mm/s)
1	Non calcined HA	1	200	30	50
2	Non calcined HA	3	600	30	50
3	Non calcined HA	2	400	30	50
4	Non calcined HA	1	400	30	50
5	Non calcined HA	3	200	30	50
6	Non calcined HA	2	200	30	50
7	Non calcined HA	1	300	30	50
8	Non calcined HA	2	300	30	50
9	Non calcined HA	1	200	30	10
10	Non calcined HA	2	200	30	10
11	Non calcined HA	1	200	100	10
12	Non calcined HA	3	600	100	10
13	Non calcined HA	1	200	100	10
14	Non calcined HA	1	400	100	10
15	Non calcined HA	1	300	100	10
16	Non calcined HA	1	200	60	10
16bis	Non calcined HA	1	200	60	10
17	Non calcined HA	1	300	60	10
18	Non calcined HA	1	400	60	10
19	Non calcined HA	3	600	190	10
20	Non calcined HA	1	400	30	10
21	Non calcined HA	1	300	30	10
22	Non calcined HA	1	200	30	10
23	Non calcined HA	2	200	60	10
24	Non calcined HA	2	300	60	10
25	Non calcined HA	3	200	60	10
26	Non calcined HA	3	300	60	10
27	Non calcined HA	3	300	60	25
28	Non calcined HA	2	200	100	10
29	Non calcined HA	2	300	100	10
30	Non calcined HA	3	200	100	10
31	Non calcined HA	2	400	100	10
32	Non calcined HA	2	300	100	10

33	Non calcined HA	3	600	30	10
34	Non calcined HA	1	200	30	10
35	Non calcined HA	1	300	60	10
36	Non calcined HA	1	300	60	10
37	Non calcined HA	1	300	60	10
38	Non calcined HA	1	200	30	10
39	Non calcined HA	1	200	30	10
40	Non calcined HA	3	300	60	10
41	Non calcined HA	3	300	60	10
42	Calcined HA	3	300	60	10
43	Calcined HA	1	300	60	10
44	Calcined HA	1	200	30	10
45	Calcined HA	1	200	30	10
46	Calcined HA	3	200	30	10
47	Calcined HA	2	500	30	10
48	Calcined HA	2	400	150	10
49	Calcined HA	1	200	30	10
50	Calcined HA	1	270	30	10
51	Calcined HA	1	250	30	10
52	Calcined HA	1	230	30	10
74	Calcined HA	1	200	30	10
75	Calcined HA	1	270	30	10
76	Calcined HA	1	230	30	10
77	Calcined HA	1	250	30	10
78	Calcined HA	3	600	30	10
79	Calcined HA	1	200	30	10

Table 12 Experiments list

Résumé

Le remplacement des tissus mous du système ostéo-articulaire par des implants synthétiques en hydrogel est souvent limité par un faible ancrage avec le tissu osseux. Une approche pour renforcer l'interface os/implant consiste à fonctionnaliser la surface de l'implant par un revêtement biocéramique. Dans cette thèse, nous étudions deux approches pour revêtir des hydrogels d'alcool polyvinylique (APV) avec des particules biocéramiques d'hydroxyapatite (HA). Dans une première approche, basée sur le procédé d'enduction, des substrats d'hydrogel ont été revêtus par des particules d'HA enchâssées dans une matrice d'hydrogel d'APV non-dégradable. Dans ce procédé, le contrôle de la composition de la solution de trempage permet d'ajuster finement l'épaisseur, la cohésion et l'adhérence du revêtement, ainsi que le taux d'exposition d'HA à la surface du revêtement. La biocompatibilité avec la pratique chirurgicale et l'ostéointégration de ces revêtements ont été évaluées par une étude in vivo sur un modèle de cicatrisation de tunnel osseux chez le lapin. Ces premiers travaux nous ont menés à la découverte d'une nouvelle approche pour gélifier des films d'hydrogel par un procédé auto-entretenu, qui consiste à utiliser la déplétion de solvant créée à la surface d'un substrat gonflant dans une solution de polymères pour induire la gélification sans action extérieure. Dans ce procédé, la croissance de ces films dépend de la concentration de la solution, du temps de trempage et de la cinétique de gonflement du substrat. Le caractère doux de ce procédé de gélification a été vérifié en encapsulant des fibroblastes, qui restent viables durant 48h. Avec un second procédé plus énergétique, des substrats en hydrogel d'APV ont été revêtus de couches denses de particules d'HA submicroniques par cold spray. Les paramètres de projection (température, pression, distance de projection) ont été variés systématiquement pour déterminer des conditions de projection appropriées. Un schéma de formation du revêtement est proposé, basé sur les observations microscopiques. Chacun de ces procédés et leur combinaison ouvrent de nouvelles voies dans la conception de systèmes hydrogel-céramique ayant des propriétés microstructurales, mécaniques et biologiques contrôlées.

Mots Clés

Hydrogel, PVA, hydroxyapatite, enduction, gonflement, cold spray

Abstract

The replacement of soft osteoarticular tissues by synthetic hydrogel implants is often limited by a weak anchorage to bone tissues. One approach to strengthen the bone-implant interface consists in functionalizing the surface of the implant by a coating of bioceramics. In this thesis, we investigate two approaches to coat hydrogels of poly(vinyl alcohol) (PVA) with ceramic particles of hydroxyapatite (HA). In a first "soft" process, based on dip-coating, hydrogel substrates were coated with hydroxyapatite particles embedded in a non-degradable PVA hydrogel matrix. In this process, the control of the soaking solution composition allows to finely tune the thickness, the cohesion and the adhesion of the coating, as well as the HA exposure at the coating surface. The biocompatibility with surgical handling and the osteointegration of these systems were assessed by an in vivo study in a rabbit model of bone tunnel healing. This first approach led to the discovery of a new approach to grow physical hydrogel films by a self-sustained process, consisting in using the solvent depletion created at the surface of a swelling polymer substrate immersed in a PVA solution to induce the gelation of hydrogel films without external action. In this process, the growth of these hydrogel films depends on the solution concentration, the soaking time and the swelling kinetics of the substrate. We verified the gentle character of this process by encapsulating fibroblasts, which remain viable for 48h. In a second more "energetic" process, dense coatings of submicronic HA particles were produced on PVA hydrogel by cold spray. Spraying parameters (temperature, pressure and stand-off distance) were varied systematically to determine efficient spraying condition. Based on microscopic observations, a picture explaining the formation of the coating is proposed. Both processes and their combination open new routes for the design of ceramic-hydrogel systems having controlled microstructural, mechanical and biological properties.

Keywords

Hydrogel, PVA, hydroxyapatite, dip-coating, swelling, cold spray